The Molecular Basis of Flowering Time Regulation

David Charles

Department of Molecular and Cellular Biology and Department of Molecular Biosciences

Faculty of Natural Sciences

Imperial College

Submitted in part fulfilment of the requirements for the degree of Doctor of Philosophy

of Imperial College London

Declaration

I, David Charles, declare that this thesis is the result of my work conducted at Imperial College London in the Department of Molecular and Cellular Biology and the Department of Molecular Biosciences. Information and data derived from the published or unpublished work of others has been acknowledged in the text.

Copyright Declaration

The copyright of this thesis rests with the author and is made available under a Creative Commons Attribution Non-Commercial No Derivatives licence. Researchers are free to copy, distribute or transmit the thesis on the condition that they attribute it, that they do not use it for commercial purposes and that they do not alter, transform or build upon it. For any reuse or redistribution, researchers must make clear to others the licence terms of this work and contact the author.

All human wisdom is contained in these two words ...'Wait and Hope'
- The Count of Monte Cristo

Acknowledgements

I would like to thank Colin Turnbull and Xiaodong Zhang for their supervision, advice and for offering me the opportunity to undertake this project. They have provided me with patient guidance, support and motivation throughout my time on this project for which I am eternally thankful.

I would like to thank Andreas Förster, Ciaran McKeown, Kirsten Jensen and Rosa Lopez-Cobollo for teaching me, helping me with experimental design and introducing me to the world of science. Your extensive knowledge has been invaluable and your determination has been a source of inspiration. I have to particularly thank Andreas Förster who spent many hours providing advice and helping me solve problems.

I am extremely grateful to Jan Marchant, Mark Bennett and Mahmoud Ardakani for introducing me to new techniques and to the BBSRC who funded this work.

I am grateful to Ioanna Antoniadi, Zaidah Rahmat, Dan Bose, James Sudlow, Alexander Webb, Sadia Kanvil, Marta Carrara and Siliva Panico for making my time as a PhD student so enjoyable and to my comrade-in-arms, Caroline Ewens, for her constant support.

Finally, I would like to thank my family, who have support and encouraged me throughout this endeavour and without whom none of this would have been possible.

Abbreviations

A	Adenine
APS	Ammonium persulphate
ATP	Adenosine 5'-triphosphate
BSA	Bovine Serum Albumin
C	Cytosine
CO	CONSTANS
CRY	Cryptochrome
DNA	Deoxyribonucleic acid
dsDNA	Double stranded DNA
EDTA	Ethylenediaminetetraacetic acid
FAC	Florigen Activation Complex
FD	FLOWERING LOCUS D
FIC	Floral Inhibitory Complex
FT	FLOWERING LOCUS T
g	Gram
G	Guanine
GFP	Green fluorescent protein
GI	GIGANTEA
HEPES	N-2-Hydroxyethylpiperazine-N'-2-ethanesulfonic acid
HPLC	High performance liquid chromatography
IR	Infrared
IPTG	Isopropyl-β-D-thiogalactopyranoside
LB	Luria Bertani Media
µM	Micromolar
mM	Millimolar
M	Molar
MES	2-(N-morpholino)ethanesulfonic acid
MOPS	3-(N-Morpholino) propanesulfonic acid
ng	Nanogram
nM	Nanomolar
PBS	Phosphate Buffered Saline
PCR	Polymerase chain reaction
PMSF	Phenylmethylsufonyl fluoride
r.p.m	Revolutions per minute
RNA	Ribonucleic acid
SDS	Sodium dodecyl sulphate
SDS PAGE	Sodium dodecyl sulphate polyacrylamide gel electrophoresis
siRNA	Short interfering Ribonucleic acid
SPL	Squamosa Promoter-Binding Protein-Like
T	Thymine
TEMED	N, N', N-Tetramethyl-ethylenediamine
TFL1	Terminal Flowering1
Tris	2-amino-2-(hydroxymethyl)-1,3-propanediol
U.V.	Ultraviolet
X-gal	bromo-chloro-indolyl-galactopyranoside

Abstract

Flowering is controlled by a series of signals integrated to regulate gene expression and coordinate development. The flowering hormone FLOWERING LOCUS T (FT) positively regulates flowering while the highly homologous TERMINAL FLOWERING 1 (TFL1) negatively regulates flowering. FT is recruited to the promoter in a complex with FD, a transcription factor belonging to the bZIP family, and 14-3-3. This complex is called flowering activating complex (FAC). Here TFL1 is shown to form a complex with 14-3-3 proteins and FD that has striking similarity to the FAC. By probing the extended loop of TFL1 a small region was identified towards the N-terminus of the loop that is involved in mediating the interaction with 14-3-3. This TFL1–14-3-3 platform can interact with the C-terminus of FD, and moreover this interaction occurs between FD and 14-3-3 rather than directly between FD and TFL1 as had been previously speculated. Results indicate that the TFL1–14-3-3 complex, but not FT–14-3-3, can interact with the AP1 promoter from *Arabidopsis* and that FD is not required for this interaction. In addition, we have located a region of three residues near the C-terminal portion of the loop that when mutated can convert FT from an activator of flowering into a strong repressor of flowering *in vivo*. Overall, the results suggest that TFL1 can associate with DNA and recruit FD to specific regulatory sites via 14-3-3 proteins, while FT is recruited via FD to a different region within the AP1 promoter region. The data thus provide the basis for a mechanistic model for the antagonistic functions of FT and TFL1 in regulating flowering.

Contents Page

Chapter 1 - General Introduction 19

1.1 The Importance of Flowering in Plant Development 19

1.2 Flowering in Arabidopsis 19

1.3 Initiating Floral Development: An Overview 21

1.4 Flowering Locus T 22

1.4.1 Activity and Action FT 22

1.4.2 Regulation of FT 24

1.4.2.1.1 CONSTANS 24

1.4.2.2 Endogenous Regulation of Flowering Time 25

1.4.2.2.1 The Circadian Clock Associated Genes 25

1.4.2.2.2 GIGANTEA 25

1.4.2.3 Photoperiodic Sensing and Control of Key Regulators 26

1.4.2.3.1 Chromoproteins 26

1.4.2.4 Temperature Sensing in the Regulation of Flowering Time 27

1.4.2.4.1 Cold Sensing: Flowering Locus C (FLC) 27

1.4.2.4.2 Ambient Temperature Sensing: Short Vegetative Phase (SVP) 27

1.5 Terminal Flower 1 28

1.5.1 Activity and Action of TFL1 28

1.5.2 Regulation of TFL1 29

1.6 Biochemical and Structural Comparison of the Floral PEBPs 29

1.6.1 Overall Structure 29

1.6.2 Conserved Residues 30

1.6.2.1 Biochemical Studies of the Extended Loop Structure 30

1.6.2.2 Biochemical Studies of the Binding Pocket 31

1.7 Evolution and Divergence of the Floral PEBPs 33

1.7.1 Paralogs of Floral-Associated PEBPs within Arabidopsis 33

1.7.2 Orthologs of FT and TFL1 35

1.8 Putative Interaction Partners of the Floral PEBPs 36

1.8.1 The 14-3-3 Protein Family 36

1.8.1.1 The Function of 14-3-3 Proteins 36

1.8.1.2 Subcellular Localization of 14-3-3 Proteins 37

1.8.1.3 Structure of 14-3-3 Proteins 38

1.8.1.4 Mechanism of Action of 14-3-3 Proteins 38

1.8.1.5 14-3-3 Proteins in Flowering 39

1.8.2 bZIP Transcription Factors 41

1.8.2.1 Structure and Mechanism of Action of bZIP Transcription Factors 41

1.8.2.2 bZIP Transcription Factors in Flowering 42

1.8.2.2.1 FLOWERING LOCUS D (FD) 42

1.8.2.2.2 FLOWERING LOCUS D PARALOG (FDP) 45
1.9 PEBP associated Floral Complexes 45
1.9.1 Structure and Function 45
1.9.2 Nuclear Localization 46
1.10 Downstream Regulators of Flowering 48
1.10.1 Converting Vegetative Meristem to Floral Meristem 48
1.11 Project Aims, Objectives and Strategies 48
Chapter 2 - Material and Methods 50
2.1 Molecular Biology Methodology 50
2.1.1 Agarose Gel Electrophoresis 50
2.1.2 Polymerase Chain Reaction (PCR) 50
2.1.2.1 PCR Reaction Mix 51
2.1.2.2 PCR Reaction Cycling Parameters 51
2.1.2.3 Site Directed Mutagenesis Mix 51
2.1.2.4 Site Directed Mutagenesis Cycling Parameters 51
2.1.3 Construction of DNA Fragments 52
2.1.4 Plasmids 52
2.1.5 Cloning Strategies 52
2.1.5.1 Sticky End Cloning 52
2.1.5.1.1 Sticky-End Cloning Ligation Mix 54
2.1.5.2 Restriction Digest-Based Cloning 54
2.1.5.2.1 Restriction Digest-Based Cloning Ligation Mix 54
2.1.5.3 Recombination Cloning 54
2.1.6 Transformation of Bacteria 54
2.1.6.1 Transformation of Chemically Competent Cells 54
2.1.6.2 Transformation of Electro-Competent Cells 54
2.1.7 Purification and Verification of Constructs 55
2.2 Protein Production Methodology 55
2.2.1 Protein Expression 55
2.2.2 Autoinduction 56
2.2.2.1 Autoinduction Media 57
2.2.3 Expression of ^{15}N-Labelled Protein 57
2.2.4 Harvesting 57
2.3 Protein Purification Methodology 57
2.3.1 Cell Homogenization and Lysis 58
2.3.2 Ion Exchange Chromatography 59
2.3.3 Affinity Chromatography 59
2.3.3.1 Ni^{2+} Affinity Chromatography 59
2.3.3.1.1 Purification of FT and TFL1 59

2.3.3.1.2 Purification of Untagged TFL1 60
2.3.3.1.3 Purification of 14-3-3 Nu 60
2.3.3.2 GST Affinity Chromatography 60
2.3.4 Size-Exclusion Chromatography 60
2.4 Biochemical Characterization 61
2.4.1 Protein Concentration Determination 61
2.4.2 Polyacrylamide Gel Electrophoresis 61
2.4.2.1 SDS-PAGE 61
2.4.2.2 Native PAGE 62
2.4.3 Mass Spectrometry 63
2.4.3.1 Sample Preparation for Mass Spectrometry 63
2.4.4 Differential Scanning Fluorimetry (DSF) 64
2.4.4.1 Principles of Differential Scanning Fluorimetry (DSF) 64
2.4.4.2 Thermal Shift Assay 64
2.4.4.3 Thermal Shift Assay Analysis 65
2.5 Microscale Thermophoresis 65
2.5.1 Microscale Thermophoresis Principles 65
2.5.2 Microscale Thermophoresis Equipment 66
2.5.3 Microscale Thermophoresis Assay Design 67
2.6 Nuclear Magnetic Resonance (NMR) 67
2.6.1 Nuclear Magnetic Resonance Principles 67
2.6.2 1D NMR 68
2.6.3 2D NMR 68
2.7 Structural Determination by Electron Microscopy (EM) 68
2.7.1 Electron Microscopy Sample Preparation 69
2.7.2 Electron Microscopy Data Processing 69
2.8 X-Ray Crystallography 69
2.8.1 Principles of X-Ray Crystallography 69
2.8.2 Protein Crystallization 70
2.8.2.1 Growing Protein Crystals 70
2.8.2.2 Identifying Protein Crystallization Conditions 71
2.8.2.3 Production of Protein Crystals 72
2.8.2.4 Crystal Freezing and Storage 72
2.8.3 Diffraction 73
2.8.3.1 The Unit Cell 73
2.8.4 Data Acquisition and Processing 74
2.8.4.1 Symmetry and Strategy 74
2.8.4.2 Determining Unit Cell Parameters and Space Groups 74
2.8.4.3 Scaling and Merging 75

2.8.5 Molecular Replacement 75
2.8.5.1 Molecular Replacement Strategy 75
2.8.6 Model Refinement 76
2.8.7 Model Analysis 76
2.9 Plant Cultivation 77
2.9.1 Plant Material 77
2.9.2 Plants Grown on Plates 77
2.9.3 Plants Grown on Soil 77
2.9.4 Confocal Microscopy 77
2.9.5 Plant Transformations 78
2.9.5.1 Preparation of Chemically Competent Agrobacterium 78
2.9.5.2 *Agrobacterium* Transformation 78
2.9.5.3 *Arabidopsis* Transformation 78
2.9.6 Genotyping 79
2.9.6.1 Genomic DNA extraction 79
2.9.7 Physiological Characterisation 79
2.9.7.1 Physiological Characterisation by Light Microscopy 79
2.9.7.2 Physiological Characterisation by Scanning Electron Microscopy 79
2.10 Computational Methodology 79
2.10.1 Protein and DNA Assessment 79
2.10.1.1 Bioinformatics and DNA Translation 79
2.10.1.2 Protein Parameters 80
2.10.1.3 Alignments 80
2.11 Chemical Screens 80
2.11.1 Fragment Library 80
Chapter 3 - Purification and Characterisation of Floral Regulatory Proteins 81
3.1 Introduction 81
3.2 Characterizing Floral PEBPs 81
3.2.1 Bioinformatics Analysis of Floral PEBPs 81
3.2.1.1.1 Divergence of Sequences between FT and TFL1 81
3.2.1.1.2 Comparison of Sequence Conservation within PEBP Clades 84
3.2.2 Expression and Purification of Floral PEBPs 84
3.2.2.1 Purification of untagged TFL1 87
3.2.2.2 Expression and Purification of FT 88
3.2.3 Mass Spectrometry of PEBPs 89
3.2.4 1D NMR of PEBPs 90
3.3 Characterising the 14-3-3 Protein Family 91
3.3.1 Bioinformatics Analysis of the Arabidopsis 14-3-3 Protein Family 91
3.3.1.1 Sequences Similarity between 14-3-3s 91

3.3.1.2 Selection of 14-3-3s 91
3.3.2 Design of 14-3-3 Nu Constructs 93
3.3.3 Purification and Characterisation of 14-3-3 Nu 94
3.3.3.1 Purification of 2xHis 14-3-3 Nu 94
3.3.3.2 Purification of His 14-3-3 Nu 95
3.3.4 Mass Spectrometry of 14-3-3 NU 96
3.4 Purification and Characterisation of FD 97
3.4.1 Bioinformatics Analysis of FD 97
3.4.2 Designing FD Constructs 99
3.4.3 Purification of FD209 T282E 100
3.4.4 Mass Spectrometry of FD209 T282E 101
3.4.5 1D NMR of FD209 T282E 102
3.5 Discussion 103
3.5.1 Expression and Purification of the PEBPs 103
3.5.2 Analysis, Expression and Purification of the 14-3-3s 103
3.5.2.1 Sequence Analysis of 14-3-3s 103
3.5.2.2 Expression and Purification 104
3.5.3 Expression and Purification of the FD 104
3.6 Summary 104
Chapter 4 - Interaction Between TFL1 and 14-3-3s 106
4.1 Introduction 106
4.2 Results 106
4.2.1 Assessment of TFL1 14-3-3 Binding by NMR 106
4.2.2 Quantitative Assessment of TFL1 14-3-3 Binding 110
4.2.2.1 Assessment of TFL1 14-3-3 Binding by EMSA 110
4.2.2.2 Assessment of TFL1 14-3-3 Binding by Thermophoresis 111
4.2.3 Crystallization of the Proto-Floral Inhibitory Complex 112
4.2.3.1 Initial Crystallization Screens and Characterization of initial Hits 112
4.2.3.2 Optimization of Crystals 114
4.2.3.3 Testing, Diffraction and Data Collection 115
4.2.3.4 Crystal Structure of proto-Floral Inhibitory Complex 117
4.2.4 Biochemical Assessment TFL1 14-3-3 Interaction 121
4.2.4.1 Characterisation of the TFL1 Extended Loop Mutants 121
4.2.4.2 Biochemical Assessment of the Role of the Extended Loop in 14-3-3 Interaction 123
4.2.4.3 Biochemical Assessment of the Arg^{133} in 14-3-3 Interaction 125
4.2.4.4 Biochemical Assessment of the Phe^{104} in 14-3-3 Interaction 126
4.3 Discussion 127
4.3.1 The Significance of the TFL1-14-3-3 Complex 127
4.3.1.1 PEBP-14-3-3 Complex Formation 127

4.3.1.2 Structure of TFL1-14-3-3 Complex....127
4.3.2 A Section of the Loop Mediates Binding....128
4.3.3 Interface Mutations....128
4.4 Summary....129
Chapter 5 - The Interaction between FD and 14-3-3s....130
5.1 Introduction....130
5.2 Results....130
5.2.1 Qualitative Assessment of FD 14-3-3 Interaction....130
5.2.2 Initial Quantitative Assessment of FD 14-3-3 Interaction....132
5.2.3 Crystallization of the Floral Inhibitory Complex....133
5.2.3.1 Initial Crystallization Screens....133
5.2.3.2 Replication and Optimization of Crystals....134
5.2.3.3 Testing, Diffraction and Data Collection....135
5.2.3.4 Crystal Structure of Floral Inhibitory Complex....137
5.3 Discussion....139
5.3.1 The Floral Inhibitory Complex....139
5.3.1.1 FD interacts with 14-3-3 Nu....139
5.3.1.2 The Phosphorylation of FD....139
5.4 Summary....140
Chapter 6 - Assessment of the Interaction between DNA and The Floral Complexes....141
6.1 Introduction....141
6.2 Results....141
6.2.1 Bioinformatics and Design of the AP1 Promoter Fragments....141
6.2.2 Assessment of FIC and FAC Interaction with AP1 Promoter DNA....143
6.2.3 Assessment of FIC and FAC Interaction with AP1 Promoter DNA....144
6.2.3.1 Assessment of FIC and FAC Interaction with AP1 Promoter DNA....144
6.2.3.2 Assessment of proto-FIC and proto-FAC Interaction with AP1 Promoter DNA....145
6.2.3.3 Assessment of Complex formation with AP1 Promoter DNA via Native Gel....147
6.2.4 Assessment of FIC and FAC Interaction with C-Box DNA....147
6.2.5 Electron Microscopy of FIC and DNA....149
6.3 Discussion....151
6.3.1 The Interaction of FD with DNA....151
6.3.1.1 FD binds to the Minimal Promoter but not at the C-box....151
6.3.2 The Floral Complexes Differentially Interact with DNA....151
6.3.2.1 The Extended C-box Contains the FIC Binding Site....151
6.3.2.2 The Role of the FIC-DNA Interaction....151
6.3.2.3 The FAC Binding Site....152
6.3.2.4 The FIC and FAC may bind Several Sites....153
6.4 Summary....153

Chapter 7 - Assessment of the Extended Loop *in vivo* 154
7.1 Introduction 154
7.2 Results 154
7.2.1 Construct Design and Transformation of FT-NQQ-GFP 154
7.2.2 Phenotypic Characterisation of FT-NQQ-GFP Plants 157
7.2.3 Assessment of the Early Development of FT-NQQ-GFP Plants 157
7.2.3.1 Assessment of the Late Development of FT-NQQ-GFP Plants 158
7.2.3.2 Assessment of Aberrant Inflorescences by Light Microscopy 159
7.2.3.3 Assessment of Abhorrent Inflorescences by Scanning Electron Microscopy 160
7.2.4 Segregation and Development of FT-NQQ-GFP lines 162
7.2.4.1 Assessment of Bolting 164
7.2.4.2 Assessment of Flowering Time 165
7.3 Discussion 169
7.3.1 TFL1 may be involved in Bolting and the Conversion of Leaves to Flowers 169
7.3.1.1.1 TFL1 involvement in Flowering 169
7.3.1.1.2 TFL1 Involvement in Bolting 169
7.3.1.1.3 TFL1 involvement in the Conversion of Leaves to Flowers 170
7.4 Summary 170
Chapter 8 - Artificial Inhibition of TFL1 Activity 171
8.1 Introduction 171
8.2 Results 171
8.2.1 Molecule Identification 171
8.2.1.1 Screening Small Molecules 171
8.2.1.2 Dose Dependent Effects of Small Molecules *in Vitro* 173
8.2.1.3 Effect of Compounds on TFL1 14-3-3 Interaction 174
8.3 Discussion 175
8.3.1 Small Molecule Inhibition of Protein-Protein Interaction 175
8.3.2 Inhibiting the Interaction between TFL1 and Macromolecules 176
8.4 summary 176
Chapter 9 - Discussion 177
9.1 The Structure of the TFL1-14-3-3 reveals a Common Architecture amongst the Floral Complexes 177
9.2 Structural and Functional Comparison of the FIC and the FAC 177
9.2.1 Structural Comparison 177
9.2.2 The Role of the Extended Loop 181
9.2.2.1 Conformations of the Extended Loop 181
9.2.2.2 The N-terminus of the Loop is involved in the Interaction with 14-3-3s 181
9.2.2.3 The C-terminus of the Loop Plays a Critical Role in Mediating Biological Activity 182
9.2.3 The Role of the Putative Binding Pocket 185
9.2.4 The Role of Other Biological Important Residues 185

9.3 The Indirect Interaction between FD and TFL1 186
9.4 PEBP-14-3-3 Complex is a Universal Platform which may Interact with Several Targets 186
9.5 Floral Complexes as Master Developmental Regulators 187
9.5.1 Floral Complexes Determine the Timing of Bolting and Flowering 187
9.5.2 The Floral Complexes May Determine Morphology 188
9.5.3 PEBP in Other Aspects of Plant Development 188
9.6 DNA binding in Floral Regulation 189
9.6.1 The role of FD in Floral Regulation 189
9.6.1.1 FD may interact with C-box-like elements found across the AP1 Promoter 189
9.6.1.2 Floral Complexes interact with DNA with greater strength than FD Alone 190
9.6.2 DNA Binding may be Important for TFL1 Activity 190
9.6.3 The Floral Inhibitory Complex interacts with the C-box 191
9.6.4 Low Affinity DNA Binding Proteins 191
9.7 The Molecular Basis of Flowering 192
9.7.1 Nuclear localization of the Floral Inhibitory Complex 192
9.7.2 Differential binding as a Key Mechanism for Regulation 193
9.8 Future Work 193
9.8.1 The effect of the FIC upon DNA 193
9.8.2 The effect of FIC upon LFY 194
9.8.3 Identifying Novel Regulators 194
9.8.4 Identifying New Binding Site *in Vivo* 195
9.8.5 Testing the Differential Binding Model 195
9.8.6 Expression of FT-NQQ-GFP in different backgrounds 197
9.8.7 Screening Compounds 197
Chapter 10 - Summary 198

Index of Figures

Figure 1.1: The Regulation and Action of FT. 23
Figure 1.2: A Structural and Biochemical comparison of FT and TFL1. 32
Figure 1.3: Structure of the 14-3-3 Protein. 40
Figure 1.4: Structure of the bZIP region of the transcription factor in complex with DNA. 44
Figure 1.5: Structure of the Florigen Activation Complex. 47
Figure 2.1: Sticky End PCR Cloning Strategy. 53
Figure 2.2: Microscale thermophoresis Schematic. 66
Figure 2.3: Phase diagram of crystallization. 71
Figure 2.4: A Unit Cell Diagram. 73
Figure 3.1: Analysis of Sequence Conservation amongst PEBPs. 82
Figure 3.2: Conservation of residues in plant PEBPs mapped onto the Crystals Structure of FT and TFL1. 83
Figure 3.3: Purification of His tagged TFL1. 86
Figure 3.4: Purification of untagged TFL1. 87
Figure 3.5: Purification of His tagged FT. 88
Figure 3.6: 1D NMR Spectra of TFL1 and FT after purification. Chemical Shift (ppm) is plotted against signal amplitude. 90
Figure 3.7: Analysis of Sequence Conservation amongt 14-3-3 Gene in Arabidosis. 92
Figure 3.8: Design of 14-3-3 Nu Constructs. 93
Figure 3.9: Purification of 2XHis 14-3-3 Nu. 94
Figure 3.10: Purification of His 14-3-3 Nu. 95
Figure 3.11: Peptides indentified by mass spectrometry from samples of 14-3-3 Nu.. 96
Figure 3.12: Analysis of Sequence Conservation amongst FD Homologs. 98
Figure 3.13: Design of FD Constructs. 99
Figure 3.14: Two step purification of FD209 ^{T282E}. 100
Figure 3.15: 1D 1H-NMR of FD209 ^{T282E} 102
Figure 4.1: ^{1}D NMR Spectra of recombinant full-length TFL1 with excess 14-3-3 Nu. 107
Figure 4.2: Interaction of TFL1 with 14-3-3 Nu using NMR. 108
Figure 4.3: Chemical Shift perturbation of TFL1 cause by the interaction with 14-3-3 Nu using NMR. 109
Figure 4.4: Assessment of the Specificity of Binding by Gel Mobility Shift Assay. 110
Figure 4.5: Interaction of TFL1 and FT with 14-3-3 Nu using microscale thermophoresis. 111
Figure 4.6: Putative initial hits in TFL1 - 14-3-3 Nu Crystallization Trials. 112
Figure 4.7: Characterisation of Initial Hits. 113
Figure 4.8: Optimization of TFL1 14-3-3 Nu complex Crystals. 114
Figure 4.9: Diffraction of TFL1 14-3-3 Nu complex grown in 500mM Li_2SO_4, 17.5% PEG 8000 and 5% Glycerol. 115
Figure 4.10: Structure of the Proto-Floral Inhibitory Complex. 118
Figure 4.11: An sulphate moiety bound to 14-3-3 Nu. 119
Figure 4.12: Key residues involved in the interaction between TFL1 (cyan) and 14-3-3 Nu (blue). 120
Figure 4.13: Comparison of TFL1 and a series of TFL1 mutants Gel Filtration Profiles. 121
Figure 4.14: Assessment of the role of the loop in the interaction between TFL1 and 14-3-3 Nu. 122
Figure 4.15: A summary of the assessment of the role of the loop in the interaction between TFL1 and 14-3-3 Nu. 123
Figure 4.16: Assessment of the role of Arg^{133} and Arg^{134} in the interaction between TFL1 and 14-3-3 Nu. 124
Figure 4.17: Assessment of the role of Phe^{104} in the interaction between TFL1 and 14-3-3 Nu. 126
Figure 5.1: Interaction of TFL1 and 14-3-3 Nu with a 7 amino acid C-terminal peptide. 131
Figure 5.2: Interaction of a 7 amino acid C-terminal peptide with14-3-3 Nu using microscale thermophoresis. 132
Figure 5.3: Putative initial hits in TFL1-14-3-3 Nu-FD peptide Crystallization Trials. 133
Figure 5.4: Optimization of Floral Inhibitory Complex Crystals. 134
Figure 5.5: Diffraction of TFL1 14-3-3 Nu complex grown in 500mM Li_2SO_4, 18% PEG 8000 and 8% Glycerol. 135
Figure 5.6: Electron density observed from the structural determination of Floral Inhibitory Complex. 137
Figure 5.7: Structure of the Floral Inhibitory Complex. 138
Figure 6.1: Schematic of the AP1 Core promoter region.. 142
Figure 6.2: The interaction between FD209 T282E and elements of the AP1 promoter. 143
Figure 6.3: The interaction between FIC and FAC with elements of the AP1 promoter. 144
Figure 6.4: The interaction between proto-FIC and proto-FAC with elements of the AP1 promoter. 145
Figure 6.5: Assessment of the interaction between proto-FIC and components by Native gel. 146

Figure 6.6: The interaction between FIC and FAC and elements of the AP1 promoter. 148
Figure 6.7: Images from Micrographs collected for the negative stain structural analysis of the FIC. 149
Figure 6.8: Stuctural Assement of the Particles found on the Micrograph. 150
Figure 7.1: Design, construction and testing of FT-NQQ-GFP. 156
Figure 7.2: Early developmental phenotype of FT-NQQ-GFP plants at approximately 6 weeks. 157
Figure 7.3: Late developmental phenotype of FT-NQQ-GFP plants at approximately 12 weeks. 158
Figure 7.4: Assessment of aberrant inflorescences of FT-NQQ-GFP plants at approximately 12 weeks. 159
Figure 7.5: Assessment of aberrant inflorescences of FT-NQQ-GFP plants at approximately 12 weeks by SEM. 160
Figure 7.6: Assessment of aberrant inflorescences of FT-NQQ-GFP plants at approximately 12 weeks by SEM. 161
Figure 7.7: The Development of T2 Generation FT-NQQ-GFP. 162
Figure 7.8: Genotyping of the early flowering F2 Mutant Plants. 163
Figure 7.9: The time to bolting in T2 transformants over expressing FT-NQQ-GFP. 164
Figure 7.10: Flowering times in T2 transformants over expressing FT-NQQ-GFP. 165
Figure 7.11: Assessment of Flowering Time of Mutant Plants (days-to-flower). 166
Figure 7.12: Phenotypic Characterisation of Mutant Plants at after ~ 4 Weeks. 167
Figure 7.13: Phenotypic Characterisation of Mutant Plants after ~ 5 Weeks of Development. 168
Figure 8.1: Stabilization of TFL1 by Compounds in the fragment library. 172
Figure 8.2: Concentration-dependent stabilization and destabilization of TFL1 by a Series of fragments. 173
Figure 8.3: The change in Affinity between TFL1 and 14-3-3 Nu in the presence of Compound. 174
Figure 9.1: Comparisons of the electrostatic surface of the FIC and the FAC. 179
Figure 9.2: Comparisons of the electrostatic surface of the interior of the FIC and the FAC. 180
Figure 9.3: Crystal structures of FIC and the FAC. 184
Figure 9.4: Model for interaction of floral complexes with AP1. 196

List of Tables

Table 1.1: The Diversity of Flowering Responses in Wild *Arabidopsis thaliana* Strains. 20
Table 2.1: Six vectors were used to created the expression constructs used in this work. 52
Table 2.2: Strains used for protein expression in this study. 56
Table 2.3: The composition of buffers used in this study. 58
Table 2.4: The Composition of SDS-PAGE Gels used in this study. 62
Table 2.5: The Composition of Native PAGE Gels used in this study. 63
Table 3.1: Peptide identified by mass spectrometry from samples of His-TFL1. 89
Table 3.2: Peptides identified by mass spectrometry from samples of His-FT. 89
Table 3.3: Peptides identified by mass spectrometry from samples of His-FD. 101
Table 4.1: Data collection statistics. Values in parentheses are the highest resolution shell. 116
Table 5.1: Data collection statistics. Values in parentheses are the highest resolution shell. 136
Table 7.1: The X^2 test assuming one transgene insertion. 163
Table Appendix 1 : Primer Sequence – Pseudo-Restriction Sites and Restriction Sites Underlined 208

Chapter 1 - General Introduction

1.1 The Importance of Flowering in Plant Development

The transition from vegetative growth to reproductive growth is a pivotal step in the life cycle of plants. The reproductive success of plants is dependent upon a shift between a juvenile state and a reproductively active state. The timing of this transition influences the number of flowers produced and the availability of pollinators (Fenner, 1998). It is regulated by a complex network of interactions which integrate developmental signals to initiate flowering at appropriate times. Agronomically important qualities such as yield and biomass are also tightly linked to these networks and consequently to flowering (Jung and Muller, 2009, Salehi et al., 2005). Increased demand for food staples juxtaposed to the declining rate of yield increases has necessitated the investigation of flowering on a genetic, biochemical and molecular level in order to foster novel strategies for the modulation of flowering (Tilman et al., 2002). This has led to several attempts to modulate flowering to increase the yield of economically and medically important species (Levy et al., 1986, Xue et al., 2008).

1.2 Flowering in Arabidopsis

Flowering is an adaptive trait that is dependent on the microenvironment of the plant. *Arabidopsis thaliana* has been adopted as a major model for the study of adaptive traits partly due to its exposure in nature to a wide array of conditions, which occurs as a consequence of the wide spatial distribution of *Arabidopsis* across Europe, central Asia and parts of Africa. Distinct populations of *Arabidopsis* exist in different locales. Extensive variation in flowering time has been observed amongst these different populations under standard conditions (Table 1.1) (Lempe et al., 2005). Strong correlations have been observed between latitude and flowering under 16 hour long day conditions. This variation is often associated with vernalization, a process which allows plants to predict the onset of warm conditions that are favourable to seed maturation. At least 35% of the variation amongst wild *Arabidopsis* populations can be directly attributed to plant-enviroment interactions including day-length, ambient temperature and vernalization. Importantly, statistically significant differences have been observed amongst the accessions in response to these three traits in isolation (Lempe et al., 2005).

Table 1.1: The Diversity of Flowering Responses in Wild *Arabidopsis thaliana* Strains (Lempe et al., 2005). Response of 40 ecotypes of *Arabidopsis* exposed to long day conditions with 16 hours of light and held at a temperature of 23˚C. Total leafs number alongside days to flowering were measured and compared to the common laboratory strain Col-0.

Ecotype	Stock No	Location	Days To Flowering	Total Leaf Number	Relative to Col-O
Col-0_B	N1093	-	32.18	21.64	N/A
Bay-0	N955	Germany	25.75	16.25	Early
Bd-0	N963	Germany	28.73	20.09	Early
Br-0	N995	Czech Republic	38.67	54.33	Late
Bur-0	N1029	Ireland	47.86	50.29	Late
Cal-0	N1063	UK	24	46.29	Early
Can-0	N1065	Spain	47.67	55.42	Late
Cen-0	N1067	France	24.25	41.78	Early
Chi-0	N1073	Russia	61.67	-	Late
Chi-2	N1077	Russia	52.57	53.25	Late
Cvi-0	N1097	Cape Verde	34.8	16.2	Late
Db-0	N1101	Germany	31.5	22.17	Early
Dr-0	N1115	Germany	30.67	16.58	Early
El-0	N1135	Germany	25.58	14.67	Early
Et-0	N1153	France	55.71	83.38	Late
Fi-0	N1157	Germany	60.5	-	Late
Gre-0	N1211	USA	59	74.25	Late
Gy-0	N1217	France	38.55	26	Late
Hau-0	N1221	Denmark	25.08	15.92	Early
Hs-0	N1237	Germany	28.8	19.5	Early
In-0	N1239	Austria	58.7	67.29	Late
Is-0	N1241	Germany	25	15.55	Early
Kil-0	N1271	UK	26.89	18.78	Early
Kin-0	N1273	USA	38.11	21.11	Late
Kl-0	N1275	Germany	26.44	17.11	Early
Kn-0	N1287	Lithuania	37.3	37.17	Late
Kondara	N6175	Tajikistan	59.6	55	Late
Lip-0	N1337	Poland	28.25	18.5	Early
Ler_C	N6928	-	26.91	14.5	Early
Mir-0	N1379	Italy	54.42	74.92	Late
Mz-0	N1383	Germany	29.22	14.56	Early
Nok-0	N1399	Netherlands	49.27	43.33	Late
Pla-0	N1459	Spain	44.57	52.63	Late
Ra-0	N1481	France	28.22	15.89	Early
Ty-0	N1573	UK	56.2	47.56	Late
Wei-0	N6182	Switzerland	25.5	14.7	Early
WŸ-0	N1615	Germany	28.27	19.27	Early
ZŸ-0	N1627	Switzerland	58.3	94	Late

Conserved processes can be compared amongst plants. There is extensive genomic conservation between *Arabidopsis* and economically important species; 62% of gene sequences from cotton have homologues in *Arabidopsis* (Rong et al., 2005). Genes from agronomically important species have been shown to be functional in *Arabidopsis* (Tieman and Klee, 1999). Consequently, knowledge derived from studies in *Arabidopsis* can been extended to food and fibre crops in order to identify new methods for crop improvement. Because of this and the ease with which it can be grown and manipulated in the laboratory *Arabidopsis* has become an important model system for the study of flowering.

1.3 Initiating Floral Development: An Overview

Flowering can be broken into three biological processes; sensing inductive conditions, transduction of the inductive signal and floral organ development. Initiating flowering at an optimal point in time is dependent upon the success of all three processes (Andres and Coupland, 2012).

The induction of flowering is based upon the perception of environmental stimuli. An abundance of experimental evidence indicates that light plays an important role in initiating flowering. *Arabidopsis* plants exposed to long days flower more quickly than plants exposed to short days, leading to the conclusion that day length triggers a signal that initiates flowering (Reviewed in Mouradov et al., 2002). This signal is known as the florigen, a molecule that is generated after the plant's exposure to an inductive photoperiod and is capable of coordinating the developmental processes associated with the generation of flowers.

Transduction of the floral signal is essential for ensuring synchronicity between plants and the surrounding environment and ensuring that physiological processes are activated at appropriate periods. A variety of macromolecules and small molecules have been implicated in floral signal transduction (Reviewed in Mouradov et al., 2002, Irish, 2010). However, the principle florigen in *Arabidopsis*, is FLOWERING LOCUS T (FT); a protein capable of initiating the developmental programs associated with flowering (Corbesier et al., 2007). FT belongs to the phosphatidyl ethanolamine-binding protein (PEBP) gene family. Other members of the PEBP gene family including TERMINAL FLOWER1 (TFL1), BROTHER OF FT (BFT) and MOTHER OF FT (MFT) have also been implicated in flowering. Consequently, there has been

much research into the role of the PEBP gene family, their interaction partners and their downstream targets.

1.4 Flowering Locus T

1.4.1 Activity and Action FT

The floral integrator FT is a unique signal that plays a critical role in the flowering. *Arabidopsis* mutants deficient in FT flower extremely late relative to wild-type plants when grown under long day conditions, which implicates FT in the transduction of inductive conditions (Corbesier et al., 2007). The overexpression of FT leads to an early flowering phenotype, confirming that FT is a positive regulator of flowering (Kardailsky et al., 1999).

Early discoveries demonstrated that the rate the flowering signal travelled from the leaves to the shoot apical meristem (SAM) was the same as the rate of photosynthetic assimilates travelling through the phloem suggesting that florigen travelled through the phloem (King, 1968). FT is expressed in the vascular tissues in the leaves but acts at the SAM (Takada and Goto, 2003). FT exploits the phloem to translocate from the site of perception to the site of action. Optical imaging via confocal microscopy has been used to track the long distance movement of FT by localising fluorescently tagged FT in aerial organs of FT-deficient plants grafted to the roots of plants expressing GFP-tagged FT. In these plants FT-GFP can be observed in the mature phloem above the graft union and in the apical meristem (Corbesier et al., 2007). Grafting provides unambiguous proof that mobile FT can travel between plant domains. This links leaf-based perception and SAM-based organogenesis. Consequently, whilst FT-GFP restricted to the minor veins of the leaves and unable enter the phloem, is biochemically active within the cells it is restricted to, it has no effect upon flowering because the fusion protein is not mobile (Corbesier et al., 2007). SAM-specific interference of FT expression has no effect on flowering time as FT is transcribed and translated outside of the SAM (Mathieu et al., 2007). This highlights that the presence of *FT* mRNA in SAM either due to expression or transport has little effect on flowering time (Mathieu et al., 2007).

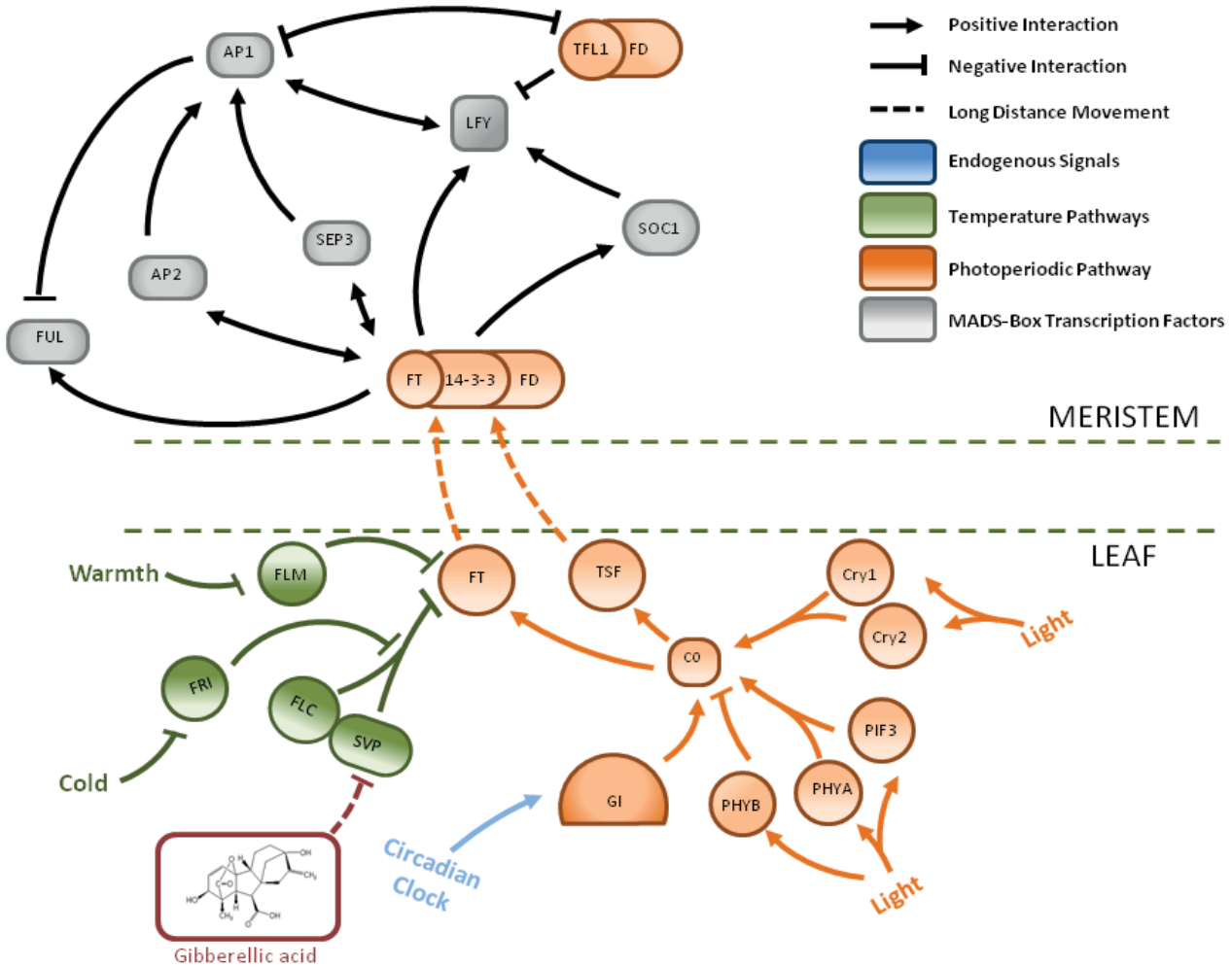


Figure 1.1: The Regulation and Action of FT. FLOWERING LOCUS T (FT) travels through plant vasculature to the meristem and interacts with FLOWERING LOCUS D (FD) via a 14-3-3 proteins initiating flowering. FT is regulated by many pathways. FT is directly regulated by temperature. The onset of cold conditions leads to the repression of FLOWERING LOCUS C (FLC), a negative regulator of flowering which interacts with the first intron of *FT* preventing it from being expressed. It is indirectly regulated by light and endogenous signals derived from the circadian clock. GIGANTEA (GI), a protein controlled by the clock, encodes a transcription factor which regulates CONSTANS (CO). CO is a transcription factor that contains two zing finger motifs and directly acts to upregula FT and TSF. The more CO the earlier flowering occurs, but stability of the protein depends upon the PHYTOCHROMES (PHY) and CHYPTOCHROMES (CRY). FT and FD interact and trigger the activation of a cascade of transcription factor leading to the development of floral organs including *LEAFY* (*LFY)* and *APETALA1* (*AP1).*. TERMINAL FLOWERING 1 (TFL1) and FD work in concert to inhibit several floral identity genes including *LFY* and *AP1.*

At the SAM FT activates a series of floral identity genes including APETALA 1 (AP1), LEAFY (LFY), SEPALLATA 3 (SEP3) and FRUITFULL (FUL). Photoperiodic induction leads to an increase in the expression of LFY and AP1 over a 16 hour period (Hempel et al., 1997). As a result AP1 and the other floral identity genes have been used as markers of the florigen's activity. Overexpression of FT leads to an increase of LFY, AP1, FUL and SEP3 (Yamaguchi et al., 2005, Teper-Bamnolker and Samach, 2005, Schmid et al., 2003). Likewise, *ft-2* mutants have reduced levels of SEP3 and FUL (Teper-Bamnolker and Samach, 2005). These data unambiguously establish that FT plays a major role activating the transcription of genes which are responsible for floral organogenesis.

1.4.2 Regulation of FT

The importance of FT is reflected in the regulation of its expression and activity by a number of pathways. FT plays a pivotal role in integrating different internal and external signals and acting on downstream regulators causing the transition to a reproductively competent state.

1.4.2.1.1 CONSTANS

CONSTANS (*CO*), a strong promoter of flowering is the target of several pathways. CO levels are directly linked to the expression level of FT (Valverde et al., 2004). Plants expressing CO from the strong 35s promoter flower early (Yoo et al., 2005). The levels of CO have been shown to be altered by endogenous signals and several aspects of the *Arabidopsis* microenvironment including light and temperature. The abundance of CO fluctuates: increasing during the day and falling at night (Valverde et al., 2004) The levels of CO protein fluctuate even when CO is expressed constitutively from the strong 35s Cauliflower Mosaic Virus (CaMV) promoter suggesting that many of these sensing pathways regulate CO posttranslationally (Yoo et al., 2005). Importantly, by changing the level of CO, *Arabidopsis* can control the level of FT.

1.4.2.2 Endogenous Regulation of Flowering Time

1.4.2.2.1 The Circadian Clock Associated Genes

The circadian clock is a timekeeper responsible for the rhythmic expression of genes over a 24 hour day and night cycle (Dunlap, 1999). Most biological organisms share a conserved mechanism for generating rhythmic oscillation based on a series of biological feedback loops. The core components of the clock in *Arabidopsis* include a number of transcription factors such as CIRCADIAN CLOCK ASSOCIATED1 (CCA1), LATE ELONGATED HYPOCOTYL (LHY) and TIMING OF CAB EXPRESSION1 (TOC1) (Ding et al., 2007). These components are thought to function with other components to form two interlocking feedback loops. The central loop is formed by the three core genes (Locke et al., 2005). *lhy* and *cca1* encode transcription factors that inhibits the expression of TOC1. LHY and CCA1 are degraded over time leading to the activation of TOC1. TOC1 enhances the expression of CCA1 and LHY (Wang and Tobin, 1998, Alabadi et al., 2002). TOC1 and other genes feed back into the central control loop as well as causing downstream effects. Mutations in cca1, lhy and toc1 result in early flowering suggesting that the circadian clock plays an important role in the control of flowering (Mizoguchi et al., 2005).

1.4.2.2.2 GIGANTEA

GIGANTEA is transcription factor that works in concert with numerous proteins to regulate flowering (Huq et al., 2000). Deletion of *Gi* and its homologs in *Arabidopsis* and other plant species like *Pisum sativum* results in a late-flowering phenotype (Hecht et al., 2007). In continuous light and darkness levels of *GIGANTEA* fluctuate in a circadian manner even in the absence of exogenous signals; suggesting that internal signals like the circadian clock regulate the levels of GI (Hecht et al., 2007). GI mutants are unable to fully express CO, which may explain their late flowering phenotype (Suarez-Lopez et al., 2001, Hecht et al., 2007).

1.4.2.3 Photoperiodic Sensing and Control of Key Regulators

1.4.2.3.1 Chromoproteins

The expression of FT is indirectly regulated by light through proteins like CO. CO is regulated by a series of light sensing proteins. The phytochrome family of chromoproteins respond to red and far-red light, and enable *Arabidopsis* to sense inductive conditions (Essen et al., 2008). In *Arabidopsis*, five genes have been identified *PHYTOCHROME A* (*PHYA*), *PHYTOCHROME B* (*PHYB*), *PHYTOCHROME C* (*PHYC*), *PHYTOCHROME D* (*PHYD*) and *PHYTOCHROME E* (*PHYE*). These proteins share a modular architecture with an N-terminal photosensing domain and a C-terminal histidine kinase region (Essen et al., 2008, Castillon et al., 2007). Within the context of flowering *PHYA* and *PHYB* act antagonistically (Reviewed in Boss et al., 2004). *PHYB* deficient plants flower early whereas mutations to *PHYA* are associated with a late flowering phenotype (Johnson et al., 1994, Miyata et al., 2011). This is partly mediated by influencing the level of CO. In far-red light PHYA stabilizes CONSTANS (Valverde et al., 2004). PHYB acts to reduce CO through ubiquitination and targeted proteolysis (Valverde et al., 2004). As such PHYA is as a positive regulator of flowering whilst PHYB is as a negative regulator, affecting the level of CO.

In *Arabidopsis*, blue and ultraviolet light is perceived by the cryptochrome family of photoreceptors. The cryptochrome protein family also regulate flowering through CO. CRYPTOCHROME 1 (CRY1) and CRYPTOCHROME 2 (CRY2) act to stabilize CO protein indirectly by inhibiting its degradation (Valverde et al., 2004). Plants with mutations in these two light receptors have lower levels of *ft* and have a delayed flowering phenotype (Bagnall et al., 1996, Guo et al., 1998). This phenotype is also observed in *CRY* mutant plants that over-express CO under the 35s promoter (Valverde et al., 2004). The absence of CRYPTOCHROMES causes higher turnover of CO preventing it from promoting *FT* expression (Valverde et al., 2004)

1.4.2.4 Temperature Sensing in the Regulation of Flowering Time

1.4.2.4.1 Cold Sensing: Flowering Locus C (FLC)

Certain ecotypes of *Arabidopsis* need to experience a period of low temperature in order to flower, a process is known as vernalization, which causes the de-repression of floral activators. In *Arabidopsis*, exposure to extended periods of low temperature causes the de-repression of flowering locus C (FLC) and frigida (FRI) which inhibit flowering. FRI inhibits flowering by promoting the expression of FLC (Risk et al., 2010). FLC is unusual in that it directly affects the expression of *ft*. Overexpression of FLC, a member of the MADS-box transcription factor family causes the reduction in expression of flowering activators including SOC1 and FT mRNA levels in the leaves (Searle et al., 2006). Mechanistically this is mediated by the direct interaction of FLC with soc1 promoter and to the first intron of ft (Hepworth et al., 2002, Searle et al., 2006). The overexpression of *FT* from a non-native promoter can compensate for the ectopic overexpression of FLC suggesting that the repression of *FT* is a major mechanism by which FLC mediates the repression of flowering (Searle et al., 2006).

1.4.2.4.2 Ambient Temperature Sensing: Short Vegetative Phase (SVP)

In addition to being able to sense cold conditions, ecotypes of *Arabidopsis* have developed pathways to detect and respond to changes in ambient temperature. SVP, a MADS-box transcription factor, plays a critical role in the control of flowering in response to fluctuations of ambient temperature. Wild-type plants grown at 16° C flower later than plants grown at 23° C; *svp* mutants however, flower at the same time in either temperature (Lee et al., 2007). Simply, SVP provides a means by which *Arabidopsis* can inhibit floral development in response to slight decreases in temperature. Overexpression of SVP causes a delay in flowering relative to wild-type plants at either 16° C or 23° C. This late flowering phenotype corresponds to reduced levels of *FT* expression (Lee et al., 2007). SVP is capable of reducing FT levels by binding to FT promoter and inhibiting transcription (Lee et al., 2007). Interestingly, mutations to SVP partially suppress the late flowering phenotype associated with overexpression of FLC suggesting that FLC requires SVP to suppress FT which is plausible as an association between the two proteins has been demonstrated by yeast-two hybrid assays (Fujiwara et al., 2008, Lee et al., 2007).

1.5 Terminal Flower 1

1.5.1 Activity and Action of TFL1

Inhibition is an essential feature of robust developmental pathways. Negative signalling enables the creation of an internal equilibrium state. A homolog of *FT*, *TERMINAL FLOWERING 1* (*TFL1*) has been shown to play an antagonistic role in flowering in *Arabidopsis.* Mutations within *TFL1* can lead to shorter vegetative stages and premature flowering (Bradley et al., 1996, Shannon and Meeks-Wagner, 1991). Mutant plants deficient in TFL1 require less exposure to inductive conditions than wild-type plants. On average wild-type plants require seven long days before they are committed to flowering whilst *tfl1* mutant plants on average require five long days (Bradley et al., 1997). Morphologically, there is no difference between vegetative TFL1 mutant and wild type plants (Shannon and Meeks-Wagner, 1991). Neither the shape of leaves, nor the early stages of inflorescence development, have been shown to be affected by TFL1 mutation, which suggests that TFL1 does not play a direct role in organogenesis (Shannon and Meeks-Wagner, 1991). However, tfl1 mutations are associated with the production of a terminal flower, a floral primordia initiated at the summit of an inflorescence, suggesting that TFL1 may acts as an inhibitory element influencing the determination of meristems (Shannon and Meeks-Wagner, 1991).

TFL1 has been shown to repress the transcription of genes involved in flowering. Mutant plants deficient in *TFL1* show increased transcription of *AP1*, *FUL*, *LFY*, *SEP1* and *SEP3* relative to wild type plants (Hanano and Goto, 2011, Gustafson-Brown et al., 1994). Constitutive expression of TFL1 fused to the transcriptional repressor domain SRDX (derived from the ethylene response element family of general transcriptional repressors) results in decreased levels of these genes and plants are phenotypically indistinguishable to those plant expressing TFL1 (Hanano and Goto, 2011). The ability of TFL1 to repress floral genes when ectopically over-expressed is negated when TFL1 is fused to the transcriptional activator domain VP16 and these plants are also early flowering (Hanano and Goto, 2011). The repression of *ap1* may be a critical function of TFL1 (Hanano and Goto, 2011). 35S:AP1 and loss-of-function mutations to TFL1 have similar physiological phenotypes indicating that *ap1* may be an important target

of TFL1 (Liljegren et al., 1999). AP1 expression has been shown to rise after the photoperiodic induction of floral development (Hempel et al., 1997). Consequently, AP1 can be used as a marker of floral determination and also as indicator of TFL1 activity.

TFL1 is expressed within the SAM, restricted to the inner cells under the apical dome but has also been shown to be expressed throughout the stem of inflorescences (Bradley et al., 1997, Ratcliffe et al., 1999). TFL1 however has been shown to move across the shoot apical meristem. TFL1 is found at similar levels across cell groups rather than as a gradient suggesting some form of selective transport (Conti and Bradley, 2007). It has been suggested that TFL1 may modulate target genes differentially within the inner cells of the shoot apical meristem relative to the outer cells allowing controlled meristem development (Conti and Bradley, 2007).

1.5.2 Regulation of TFL1

The regulation of TFL1 remains largely enigmatic but there is a strong body of evidence to suggest that it may be partly controlled by hormones. TFL1 has been linked to several plant hormones including auxin and members of the cytokinin family in the regeneration of inflorescence (Guan et al., 2006). Hormonal manipulation with thiadiazuron (TDZ), a synthetic cytokinin and 2,4-Di-chlorophenoxyacetic acid, a synthetic auxin, has been associated with strong expression of TFL1 (Guan et al., 2006). Indeed, loss-of-function mutations to the cytokinin receptors AHK2, AHK3 and AHK4 are associated with delayed flowering in *Arabidopsis* (Riefler et al., 2006). Thus plants may be able to control the inhibition of flowering through a variety of networks.

1.6 Biochemical and Structural Comparison of the Floral PEBPs

1.6.1 Overall Structure

The crystal structures of FT and TFL1 have been determined (Ahn et al., 2006). FT and TFL1 have one large central five-stranded β-sheet flanked on either side by short α-helices and are similar to previously characterise PEBPs like CENTRORADIALIS (CEN) (Banfield and Brady, 2000). The two structures vary slightly; with 1.22 Å root mean square of deviation (r.m.s.d) over 156 equivalent Cα positions. A

prominent feature shared by the two structures is the extended loop (residues 129 - 146) originating from the fourth β-sheet. Both the sequence and structural variation in the loop is much greater than variation over the whole protein; within this region equivalent Cα deviate from one another by 3Å. The C-terminal extension of FT and TFL1 is not visible in either of the crystal structures and is thought to be flexible (Ahn et al., 2006).

1.6.2 Conserved Residues

1.6.2.1 Biochemical Studies of the Extended Loop Structure

The extended loops of TFL1 and FT were identified as functionally critical by biochemical experiments involving 'exon swaps'. Both *FT* and *TFL1* have four exons. Transgenic chimeric proteins containing combinations of exons from *FT* and *TFL1* were created and overexpressed in plants devoid of FT and TFL1. In almost all cases plants overexpressing chimeras with the fourth exon of *FT* flowered earlier than control plants and almost as early as plants overexpressing *FT*. Conversely, plants expressing chimeras containing the fourth exon of *TFL1* appeared to flower later than the negative controls. This fourth exon contains the extended loop structures found on FT and TFL1 (Ahn et al., 2006). Swapping sections within the fourth segment has provided a more detailed understanding of activity. TFL1-like activity can be conferred upon FT by replacing a 14 amino acid section (referred to as segment B) from this loop (Ahn et al., 2006). However, TFL1 cannot be converted to FT by a reciprocal exchange (Ahn et al., 2006). Given that the loop of TFL1 is enough to confer TFL1 activity then critical residues responsible for the delayed flowering phenotype associated with TFL1 may lie within the loop. In order to confer FT activity a 38 amino acid section of the fourth exon containing both the loop (Segment B) and an adjacent region (Segment C) must be substituted (Ahn et al., 2006). Neither Segment B nor Segment C alone was sufficient to impart FT-like activity. In conclusion, the loop contains residues responsible for the activity of TFL1 but only partly contributes to the activity of FT.

1.6.2.2 Biochemical Studies of the Binding Pocket

A discrete pocket found on the surface of the PEBP family of proteins is present FT and TFL1. Amino acids at the surface of the pocket have been shown to affect function. One residue in particular, Tyr^{85} in FT (His^{88} in TFL1) has been shown to be crucial for the opposing activities of FT and TFL1 (Hanzawa et al., 2005). Converting Tyr^{85} in FT into a histidine significantly delays flowering when compared to mutants overexpressing TFL1. Conversely, wild-type flowering was observed in plants expressing modified TFL1 where tyrosine replaced His^{88}. When these proteins were overexpressed in *ft;tfl1* double mutants TFL1 ^{H88Y} flowered significantly earlier than plants overexpressing wild-type TFL1 and *ft;tfl1* double mutants. Likewise, plants expressing FT ^{Y88H} flowered much later than those overexpressing FT. Simply, mutant FT appears to act like a repressor of flowering whilst mutant TFL1 acts as an activator of flowering. However, plants overexpressing TFL1 ^{H88Y} flower later than plants overexpressing FT. Moreover, plants expressing FT ^{Y88H} flower much earlier than plants overexpressing TFL1 and double mutants lacking FT and TFL1. This is crucial because it infers that despite single amino acid swap the mutations FT and TFL1 still retain some wild type activity.

Changes to the architecture of the binding site have been shown to be important in determining the activity of homologs of TFL1. Studies of the tomato homolog SP show that a single mutation converting one amino acid in the conserved, binding-pocket related DPDxP motif (P76L) was able to abrogate the phenotype associated with SP overexpression (Pnueli et al., 1998). The binding pocket of the PEBP family of proteins is highly homologous. Phosphotyrosine has been shown to bind within the human PEBP binding pocket (Simister et al., 2011). Given the homology between the PEBPs in this region the evidence suggests that PEBPs might bind phosphorylated proteins and that the mechanism of interaction involves the binding pocket (Simister et al., 2011).

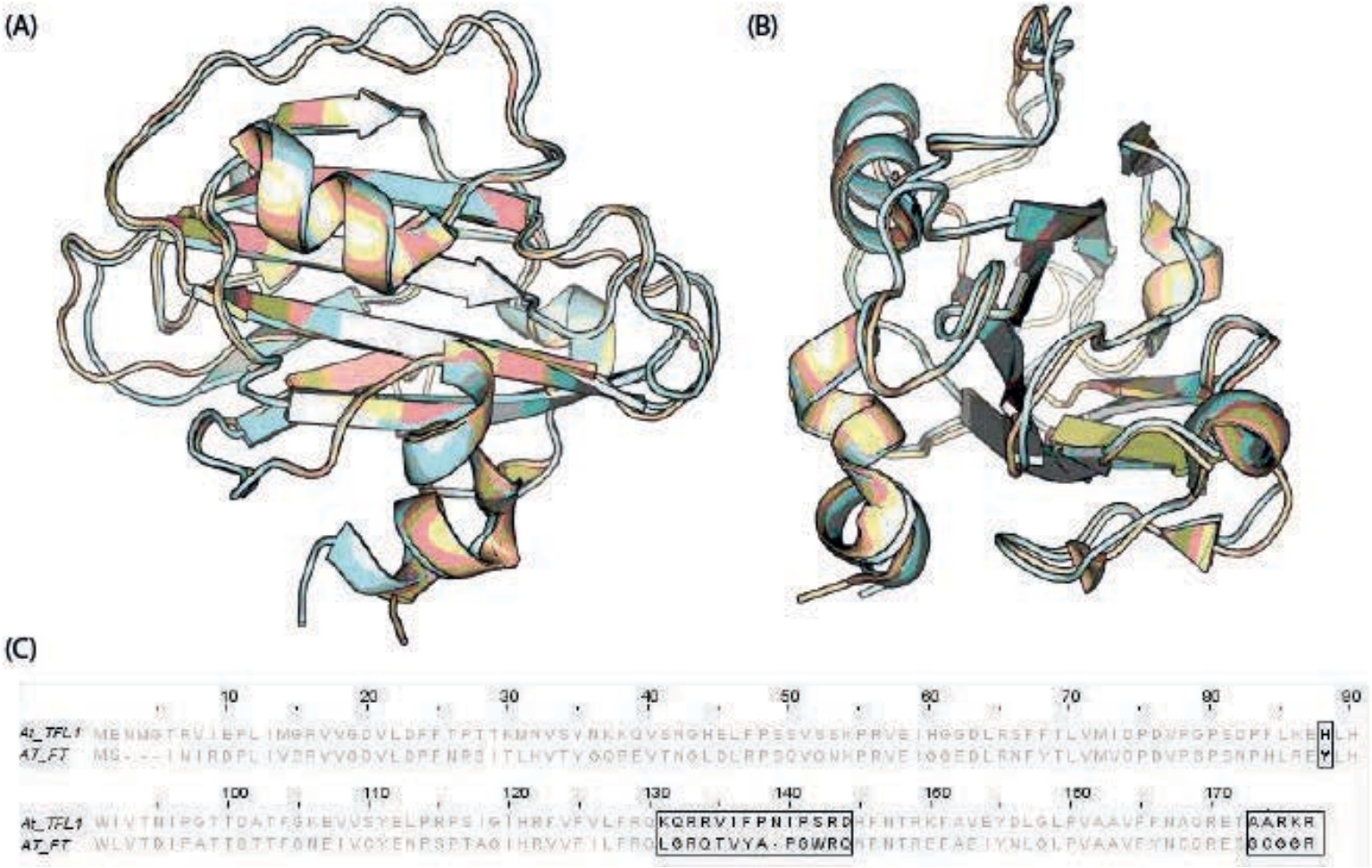


Figure 1.2: A Structural and Biochemical comparison of FT and TFL1. (A-B) The crystal structure of FT (Wheat) and TFL1 (Cyan). FT and TFL1 have a typical PEBP structure with a central β-sheet flanked by an alpha helix. **(C)** Sequence alignment of FT and TFL1. FT and TFL share more than 60% sequence identity. The greatest region of divergence is found around the extended loop: from amino acids 128 to 142. Key divergent residues boxed.

1.7 Evolution and Divergence of the Floral PEBPs

1.7.1 Paralogs of Floral-Associated PEBPs within Arabidopsis

Critical signalling systems often have functional redundancies (Cutler and McCourt, 2005). The sequenced *Arabidopsis* genome has revealed the presence of a number of FT-like proteins that may act redundantly to FT and TFL1. TWIN SISTER OF FT (TSF) is a closely related PEBP that shares 82% sequence identity with FT (Yamaguchi et al., 2005). TSF and FT share functional characteristics. The overexpression of *TSF* from the 35s promoter leads to an early flowering phenotype, demonstrating that TSF is a positive regulator of flowering (Kobayashi et al., 1999). Like FT the photoperiodic induction of TSF has been observed under long day conditions. Shifting short day plants into long day conditions results in higher levels of TSF, which suggests that TSF is under the influence of circadian clock related elements like CO (Yamaguchi et al., 2005). This notion is supported by the fact that mutations to critical upstream down-regulators like *phyB* lead to higher levels of FT and TSF (Yamaguchi et al., 2005). In fact, TSF appears to act upon the same targets as FT. The overexpression of TSF and FT also leads to expression of downstream MADS-box transcription factors (Yamaguchi et al., 2005). Collectively, this evidence demonstrates that TSF is an activator of flowering. However, mutations to FT delay flowering even though TSF is present. Moreover, *tsf* null mutants grown under inductive conditions do not have phenotype suggesting that *TSF* is redundant to *FT* (Yamaguchi et al., 2005). tsf ft double mutants flower later than tsf mutants alone suggesting that tsf makes an active contribution to flowering (Yamaguchi et al., 2005). *tsf* mutants flower later than wild-type control under short-day conditions suggesting that it makes a contribution to flowering under short-day conditions (Yamaguchi et al., 2005).

Redundancy mechanisms have also been identified within the inhibitory pathways. *BROTHER OF FT* (*BFT*) is may play an inhibitory role (Yoo et al., 2010). When *BFT* is overexpressed plants show a distinct late flowering phenotype. Both *35s::TFL1* plants and *35s::BFT* plants flower late and have floral defects; first-formed flowers had leaf-like petals with visible trichomes. Plants unable to express *BFT* are not associated with a distinct phenotype suggesting that the action of *BFT* is masked by the action of another gene (Yoo et al., 2010).

The ligand binding pocket appears to play a central role in the action of BFT. Sequence comparison has revealed that in key areas *BFT* is more closely related to *FT* than to *TFL1*. Amino acids identified as playing a critical role in FT/TFL1 activity have been examined. BFT and FT both have a tyrosine in position 85 at the opening of the anion binding pocket. Converting this tyrosine into a histidine reduces the late flowering phenotype supporting the idea that this residue has a role in mediating the action of FT but also suggesting that other residues are essential (Hanzawa et al., 2005). BFT is more similar to TFL1 at positions 140/144 (FT/TFL1), where TFL1 contains an aspartic acid and BFT contains a glutamic acid residue. Biochemically, aspartic acid and glutamic acid are similar as both have negatively charged carboxylic acid functional groups. In TFL1 this amino acid is thought to form a hydrogen bond with a conserved his^{88} linking the binding pocket and the extended loop (Ahn et al., 2006). Collectively this highlights the importance of the binding pocket in mediating the action of BFT.

MOTHER OF FT (*MFT*), a homolog which shares 68% sequence identity with FT, may also play a role in flowering. However, key residues in the binding pocket differ from the FT-like PEBPs. The key tyrosine at position 88 is replaced with a tryptophan. Experimental evidence suggests that *MFT* is a positive regulator of flowering; overexpression of *MFT* leads to an early flowering phenotype (Yoo et al., 2004). However, mutations to *MFT* that abrogate gene expression do not result in any phenotype (Yoo et al., 2004). This suggests that *MFT* may act redundantly in flowering. *MFT* may also play a role in seed germination. *MFT* is expressed in the radicle-hypocotyl transition zone in embryos in response to abscisic acid, which indicates it may play a role in seed development (Xi et al., 2010).

ARABIDOPSIS THALIANA CENTRORADIALIS (ATC), is a homolog of TFL1 which shares high sequence similarity to CENTRORADIALIS (CEN) for *Antirrhinum* (Mimida et al., 2001). Overexpression of ATC results in a late flowering phenotype though no phenotype is observed in *atc* mutants (Mimida et al., 2001). However, the effects of ATC are possibly pleiotropic as ATC is expressed in the hypocotyl of seedlings rather that in the meristem of inflorescences (Mimida et al., 2001).

1.7.2 Orthologs of FT and TFL1

Duplication and divergence of PEBPs have been observed in several crop plants. In maize (*Zea mays*) 24 PEBP genes have been identified. In Pea (*Pisum sativum*) at least 7 PEBP genes have been identified. Numerous PEBPs have also been identified in Rice (*Oryza sativa*) (Nakagawa et al., 2002, Ishikawa et al., 2005, Komiya et al., 2008). Although these PEBPs share significant sequence similarity, their unique expression profiles indicate distinct biological functions.

Across all plants flowering is largely dependent on the action of FT homologs. In Rice, there is genetic and molecular evidence that Hd3a is the florigen (Ishikawa et al., 2005). Overexpression of Hd3a leads to an early flowering phenotype (Tamaki et al., 2007). The most likely candidate for the Maize florigen is ZCN8 which is closely related to other FT-like PEBPs from monocots like rice. Like *Arabidopsis* FT and the rice counterpart Hd3a, ZCN8 is predominantly expressed in the leaf blades, a feature that is well conserved across plant species (Corbesier et al., 2007, Danilevskaya et al., 2008, Tamaki et al., 2007). Moreover expression of ZCN8 induces early flowering (Meng et al., 2011).

TFL1-like genes control inflorescence architecture. In tomato, mutations to SELF-PRUNING (SP) cause an accelerated flowering, a phenotype also observed in plants overexpressing of antisense SP RNA (Pnueli et al., 1998). In Rice, RCN1 and RCN2 overexpression leads to delays in flowering and atypical panicles (Nakagawa et al., 2002). Indeed, the expression of RCN1 or RCN2 in *Arabidopsis* can also delay flowering indicating that the mechanisms behind the inhibition of flowering are conserved between species.

One exception to the FT and TFL1 mediated regulation of flowering time is found in Sugar Beet. In Sugar Beet, a pair of PEBP homologs related to FT regulate the transition to flowering. BvFT2, has been shown to play a positive role in the regulation of flowering. BvFT2 shares 77% sequence identity with FT and 82% sequence identity with its antagonistic partner, BvFT1 which mediates negative regulation of flowering. BvFT1 in terms of protein sequence is more closely related to FT (74% sequence identity) than to TFL1 (56% sequence identity) (Pin et al., 2010). However, despite the low sequence similarity, BvFT1 acts like a homolog of TFL1 *in vivo*. BvFT1 has been shown to repress flowering in Sugar Beet and *Arabidopsis*. Like FT, BvFT1 has been shown to be expressed in the leaves rather than in the shoot apical meristem

suggesting it may also be mobile. The difference between the actions of the two Sugar Beet proteins has been shown to be associated with the external loop of BvFT1 and BvFT2. Chimeric proteins where the loops of BvFT1 and BvFT2 were switched have been shown to mediate opposite effects when overexpressed in *Arabidopsis*. Within this section of external loop BvFT1 and BvFT2 differ by three amino acids. This suggests that these three amino acids are critical for the action of BvFT1 and BvFT2 (Pin et al., 2010).

1.8 Putative Interaction Partners of the Floral PEBPs

1.8.1 The 14-3-3 Protein Family

The 14-3-3 family is a well characterised group of proteins involved in transcription, signalling and regulation. In *Arabidopsis* 14 family members exists. Each member is designated by a Greek letter. Although homologous, isoforms within *Arabidopsis* are differentially regulated spatially and temporally (Rosenquist et al., 2001). Some 14-3-3 proteins appear to be expressed widely across a number of tissues; 14-3-3 lambda, kappa and omega have been shown to be expressed in flowers, leaves and stem (Sorrell et al., 2003). The expression of 14-3-3 Chi has been observed in roots of seedlings and mature plants, and immature flowers (Daugherty et al., 1996). 14-3-3 Omicron has been shown to be expressed in leaves, roots and flowers (Rosenquist et al., 2001). This suggests that the 14-3-3 family may play a role in processes that are ubiquitous across all cell types. However, the tissue specific expression of some members suggest that they may play a part in specific developmental events; 14-3-3 Iota is expressed only in flowers (Rosenquist et al., 2001).

1.8.1.1 The Function of 14-3-3 Proteins

The 14-3-3 family of proteins have emerged as key facilitators of a variety of biological processes. 14-3-3 proteins have been directly linked to primary metabolism, development and stress responses. Ectopic over-expression of *Arabidopsis* 14-3-3 Lambda in cotton resulted in crops with increased tolerance to water stress and higher photosynthetic rates under drought conditions (Yan et al., 2004). Reducing the expression of 14-3-3 Epsilon and Mu via the overexpression of antisense RNA lead to a increase in starch

accumulation suggesting a possible role of 14-3-3 protein in the inhibition of starch biosynthesis (Sehnke et al., 2001). 14-3-3 proteins have also been linked to aspects of plant development including seed maturation (Schoonheim et al., 2007).

Plant 14-3-3 proteins play a role in transcriptional regulation. One member of the 14-3-3 family, GRF14, regulates the expression of the alcohol dehydrogenase gene in *Arabidopsis*. In this case a 14-3-3 protein forms a multi-protein transcriptional complex where it assists in the interaction with regulatory motifs found in the promoter (Lu et al., 1992). It is speculated that in plants they play a role in regulation of kinases (Lu et al., 1992). Thus the physiological and genetic evidence suggests that 14-3-3 regulate a wide range of plant processes.

14-3-3 proteins demonstrate biological redundancy which complicates their functional annotation. Knockout lines of single 14-3-3 proteins are often aphenotypic possibly because of the high level of sequence and structural homology amongst 14-3-3s (Rosenquist et al., 2000, Krysan et al., 1996). The high level of similarity can even ensure biological activity when expressed in other species. *Arabidopsis* 14-3-3 proteins have been shown to be capable of complementing yeast lacking 14-3-3 proteins. The lethal phenotype caused by mutations to *bmh1* and *bmh2* in yeast can be prevented by the expression of one of four 14-3-3s from *Arabidopsis* (van Heusden et al., 1996). Within *Arabidopsis*, the sequence similarity between 14-3-3 proteins is thought to enable functional redundancy.

1.8.1.2 Subcellular Localization of 14-3-3 Proteins

The specialised function of 14-3-3 proteins is partly dependent upon their subcellular localization. The location of a 14-3-3 determines which processes they can be involved in. In plants, 14-3-3 protein have been located by immunofluorescence in both the cytosol and in the nucleus, which is consistent with the notion that 14-3-3 protein may act as cellular shuttles for proteins, targeting them to specific locations (Bihn et al., 1997). 14-3-3 proteins have been shown to promote nuclear localization under some circumstances and to mediate nuclear exclusion in others (Kumagai and Dunphy, 1999, Seimiya et al., 2000). These actions can have a significant biological impact; 14-3-3 proteins in humans, can inhibit programmed cell death by excluding apoptosis enhancing factors from the nucleus whilst other 14-3-3

proteins change cell progression by shuttling cyclin dependent protein kinases (Wu and Wolgemuth, 1995, Zha et al., 1996).

1.8.1.3 Structure of 14-3-3 Proteins

14-3-3 proteins have been structurally characterised via X-ray crystallography. They form cup-shaped dimers where each protomer is composed of several α-helices (Liu et al., 1995) (Figure 1.3). Collectively, these helices form a L-shape around a central channel. Three long helices form the floor of the structure whilst stacks of shorter helices make the walls (Liu et al., 1995, Benzinger et al., 2005). The dimer formed is approximately 35Å in length, 35Å in width and 20Å deep (Yaffe et al., 1997). The protomers of the dimer are related by a 2-fold rotational axis through the dimer interface (Yaffe et al., 1997).

Within the same species, 14-3-3 proteins tend to be highly conserved (Aitken et al., 1992). The most variable residues in 14-3-3 proteins are found towards the surface of the protein while more conserved are residues involved in the packing of the α-helices and around the central channel (Reviewed in Wu et al., 1997). Within *Arabidopsis* 14-3-3 proteins, the most variable residues are towards C-terminus of the protein (Reviewed in Wu et al., 1997). Protomers interact via their largely hydrophobic N-termini (Xiao et al., 1995). Residues that make up the dimer interface determine the extent to which homo and hetero-dimerization can occur (Xiao et al., 1995, Jones et al., 1995). 14-3-3 have been shown to hetero-dimerize *in vitro* and *in vivo* (Paul et al., 2005).

1.8.1.4 Mechanism of Action of 14-3-3 Proteins

14-3-3 proteins regulate biochemical pathways often by interacting with phosphorylated target proteins (Obsil et al., 2001). Phosphorylation is a common post-translational modification that is known to affect the activity and stability of proteins as well as the assembly and disassembly of macromolecular complexes (Cohen, 2002). By binding to modified proteins, 14-3-3 proteins enable parts of the regulatory machinery to assemble around targets. Several hundreds of proteins have been shown to interact with 14-3-3 proteins including those involved in metabolism, signal transduction and trafficking.

Protein interactions involving 14-3-3 proteins fall into two categories whose recognition motifs are RSXpSXP and RX[SYFWTQAD]Xp(S/T)X[PLM] (where p indicates a phosphorylated amino acids) (Munoz-Fontela et al., 2007). Peptides containing the binding motifs have been crystallized with 14-3-3 proteins. These peptides bind to a discrete cleft within the central channel in the 14-3-3 dimer (Yaffe et al., 1997). The arginine found at the beginning of the binding motif interacts with acidic residues found in the cleft whereas the phosphate group in the binding motif interacts with conserved arginines found at the central core of the binding cleft (Figure 1.3) (Yaffe et al., 1997).

1.8.1.5 14-3-3 Proteins in Flowering

Only small phenotypic differences have been observed between wild-type plants and mutants. In rice, GF14c (a 14-3-3 protein) acts as an inhibitor of flowering; plants overexpressing GF14c have been shown to have a slightly delayed flowering phenotype whilst mutants lacking GF14c are slightly early flowering (Purwestri et al., 2009). Rice plants overexpressing GF14b and GF14e flower at 61.9 and 63.5 days respectively, whereas wild-type plants flower at 65.0 days after sowing (Taoka et al., 2011). *Arabidopsis* plants unable to express 14-3-3 upsilon or expressing reduced levels of 14-3-3 mu flower slightly later than wild-type controls in long-day conditions. Lines without 14-3-3 upsilon had one additional leaf relative to wild-type plants (Mayfield et al., 2007). Lines without 14-3-3 mu had two extra leaves relative to wild-type plants (Mayfield et al., 2007). In contrast, plants deficient in *ft* on average have 26 more leaves than wild-type plants under long day conditions (Yoo et al., 2005). The relatively small effect of mutating a single 14-3-3 may be partly due to redundancy; several 14-3-3 proteins may be able to assist in flowering. In mutants plants lacking expression of a single 14-3-3 flowering is not delayed under short-day conditions (Mayfield et al., 2007). This indicates that 14-3-3 are involved in flowering via the photoperiodic pathway which induces flowering under long-day.

Figure 1.3: Structure of the 14-3-3 Protein. (A) Each monomer is composed of α-helices. Monomers dimerize in opposite orientations. **(B-C)** Peptides derived from the binding site of target proteins are localise in the amphipathic groove of 14-3-3 proteins. **(B)** A Mode I interaction between the 14-3-3 and the target peptide. Mode I interactions use the optimal sequence RSXpSXP (where p is a phosphorylated serine). **(C)** A Mode II interaction between the 14-3-3 and the target peptide. Mode II interactions use the consensus sequence RX[SYFWTQAD]Xp(S/T)X[PLM]. PDB IDs: 1YWT (yellow) and 2C1N (blue).

In rice, HD3a a homolog of FT, has been shown to interact with members of the rice 14-3-3 proteins. This interaction has been characterised *in vitro* by NMR, yeast-two hybrid and pull-down assays and *in vivo* by bimolecular fluorescence complementation (Taoka et al., 2011). Mutants of HD3a that are unable to bind to 14-3-3 protein *in vitro* are also unable to accelerate flowering when overexpressed *in vivo*. FT and HD3a share sequence 73%, and key residues involved in binding are highly conserved thus it is likely that this represents a conserved mechanism of action (Taoka et al., 2011).

1.8.2 bZIP Transcription Factors

Transcription factors play an essential role in the coordination of biological processes. In plants, basic leucine zipper (bZIP) transcription factors are critical regulators of development and the responses to biotic and abiotic stress. In *Arabidopsis*, there are at least 75 bZIP transcription factors (Reviewed in Jakoby et al., 2002, Riechmann et al., 2000). This complexity enables sessile plants to deal with a variety of adverse conditions.

1.8.2.1 Structure and Mechanism of Action of bZIP Transcription Factors

The bZIP motif found on these transcription factors can be divided into a basic region 16 amino acids in length, a distinct DNA binding region with an N-x_7-R/K sequence, and a leucine zipper composed of heptad repeats of leucine (L-x_6-L-x_6-L). Collectively, these domains are located on an amphipathic α-helix. bZIP transcription factors form dimers via electrostatic interactions between polar residues in the helices (Reviewed in Jakoby et al., 2002). These transcription factors are capable of activating and repressing gene transcription (Reviewed in Jakoby et al., 2002).

bZIP transcription factors initiate changes in biological processes by binding to cis-acting elements in the promoter of genes and altering their expression. BZIPs typically bind to sections on DNA with the sequence XACGTX (where X is any nucleotide). Three main groups have been observed; the C-box (GACGTC), the G-box (CACGTG) and the A-box (TACGTA) (Izawa et al., 1993). The nucleotides that flank these sequences regulate binding specificity. Gel mobility shift assays have shown that groups of bZIP transcription factors can bind preferentially to a single element or to multiple elements with equal

affinity (Izawa et al., 1993). Other binding motifs have been identified; Opaque (O2), in Pea interacts with high affinity with an unusual motif (ATGAGTCAT) despite the presence of a C-box in the promoter, which does not contribute to binding (de Pater et al., 1994).

1.8.2.2 bZIP Transcription Factors in Flowering

Recognition elements for bZIP transcription factors have been identified in the promoter sequences of a number of floral meristem-identity genes. In AP1, a C-box motif has been identified within a 500bp region that is sufficient to mediate transcription (Wigge et al., 2005). To understand the mechanism of action of the floral regulators, several interactions studies have been conducted to elucidate possible transcription factors that can facilitate floral development (Abe et al., 2005).

1.8.2.2.1 FLOWERING LOCUS D (FD)

The precocious-flowering phenotype caused by the overexpression of FT is partially suppressed in mutants with reduced levels of a bZIP transcription factor designated *FLOWERING LOCUS D* (*FD*) (Pockros et al., 2007, Abe et al., 2005). Plants unable to express *FD* flower significantly later than wild-type controls (Abe et al., 2005). Unlike upstream regulators, FD-EGFP fusion proteins have been localized to the nucleus of cells within the shoot apical meristem (Abe et al, 2005). This suggests a role in initiating the morphological changes in the shoot apical meristem via transcription.

The C-terminus of FD contains a number of functionally relevant features including the basic region/leucine zipper (bZIP) domain, responsible for DNA binding and a putative C-terminal Ser/Thr phosphorylation site (Abe et al., 2005). These features are thought to play a critical role in the action of FD as they are also present in homologs of FD in different species (Muszynski et al., 2006). In Maize, the equivalent protein DFL1 has been shown to contain a typical bZIP consensus sequence L_{160}-x_6-L_{167}-x_6-L_{174}-x_6-L_{181}. Phosphorylation may play an important role as *FD* is part of the 'Group A' family of bZIP transcription factors many of which are regulated by phosphorylation (Jakoby et al., 2002). A total of nine serine and one Serine/Threonine phosphorylation sites were predicted in FD, suggesting that phosphorylation plays an important role in FD regulation (Muszynski et al., 2006).

It has been demonstrated that FT and TFL1 can interact with FD *in vitro* by yeast-two hybrid assays and *in planta* via bi-molecular fluorescence complementation (Abe et al., 2005). These assays provided clear evidence that FD interacts with FT and TFL1 (Abe et al., 2005). In tomato, yeast-two hybrid assays have demonstrated that tomato FT (SFT) and tomato TFL1 (SP) are capable of interacting with a bZIP transcription factor designated SPBG (Lifschitz et al., 2006, Pnueli et al., 2001a). Bioinformatics studies have shown that SPBG is part of a group of G-box binding proteins and that it is related to two *Arabidopsis* proteins, FD and FLOWERING LOCUS D PARALOG (FDP) (Lifschitz et al., 2006, Pnueli et al., 2001a). Likewise, in maize the FT-like protein ZCN8 and DFL1, a bZIP transcription factor, have been shown to interact in yeast two-hybrid assays (Danilevskaya et al., 2008). Collectively, this indicates that an association between plant floral PEBPs and bZIP transcription factors is universally important.

The interaction between plant floral PEBPs and bZIP transcription factors has not been shown unambiguously *in vitro*. Pull-down assays initially suggested that *Arabidopsis* FD and FT directly interact (Abe et al., 2005). However, this direct interaction has not been observed between rice HD3a and OsFD in pull-down assays, isothermal titration calorimetry or NMR (Taoka et al., 2011). In fact, it has been suggested that 14-3-3 proteins are required to bridge the interaction and that the association observed in yeast-two hybrid studies was the effect of ternary complex formation, where yeast 14-3-3 protein were recruited to FT and FD (Taoka et al., 2011). Regardless, FD's association with proteins from the photoperiodic pathway has prompted further investigation about its role.

A number of genes have been shown to be upregulated by the FT-FD complex. Plants deficient in *FT* or *FD* were deficient in expression of important flowering genes including *AP1* (Abe et al., 2005). The abolition or reduction of *FT* signalling in plants overexpressing FD in an ectopic manner also caused the reduction in *AP1* induction, demonstrating the importance of FD in the transduction of floral signalling (Abe et al., 2005).

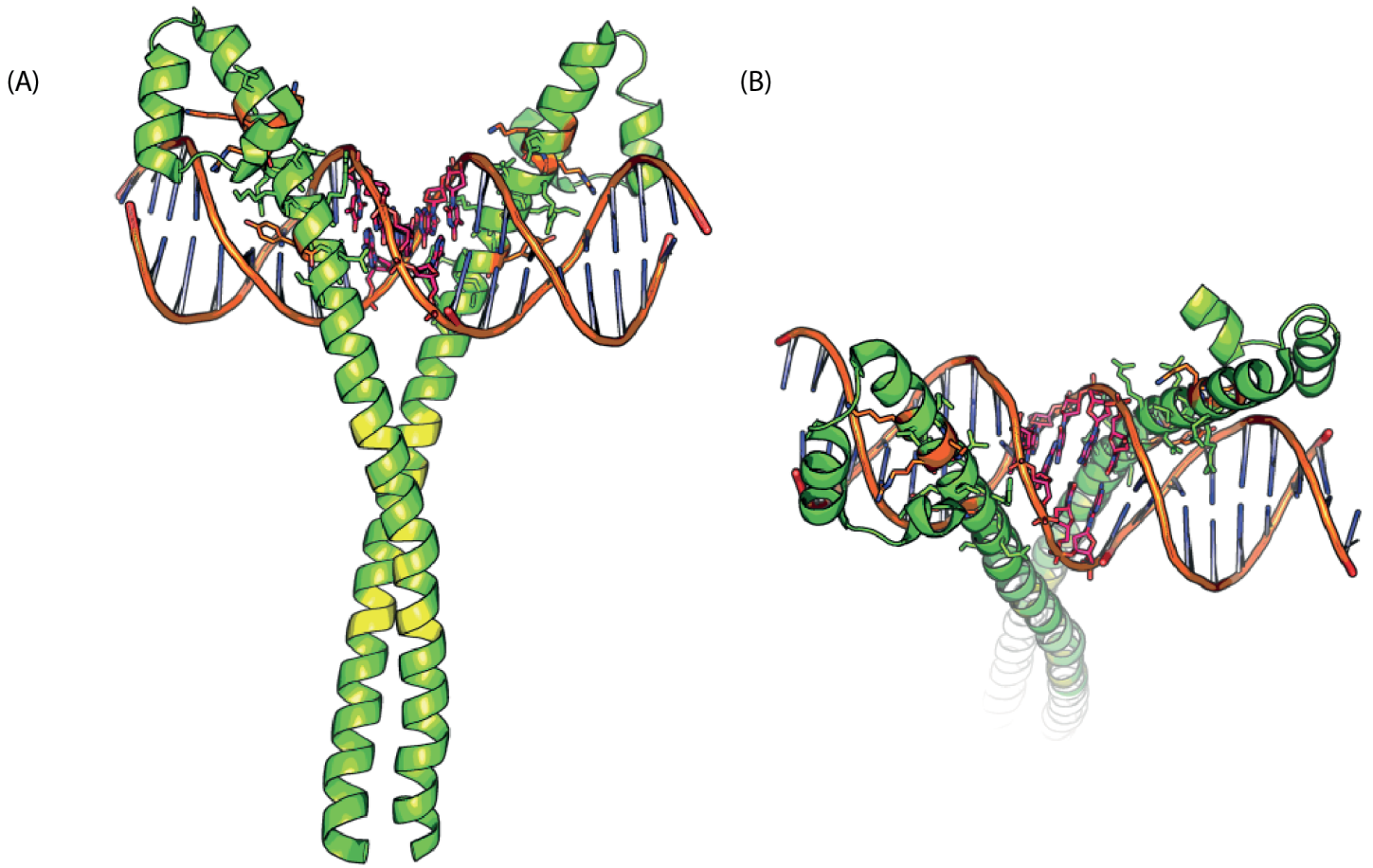


Figure 1.4: Structure of the bZIP region of the transcription factor in complex with DNA (PDB ID: 4AUW). (A) bZIP bind to DNA as dimers, the two protomers adhere to one another via the hydrophobic residues. **(B)** bZIP transcription factors often bind to DNA sequences with ACGT motifs (purple) though some have been found to bind to non-canonical non-palindromic motifs. The interaction often occurs through basic residues found in the DNA binding domain (residues within this region with similarity to FD highlighted orange). Residues that share identity with FD with the dimerization interface are highlighted in yellow.

1.8.2.2.2 FLOWERING LOCUS D PARALOG (FDP)

Both FT and TFL1 interact with a paralog of FD (Abe et al., 2005). In *Arabidopsis*, FDP is located on chromosome two in a region of segmental duplication (Abe et al., 2005). FDP shares 54% sequence identity with FD, with particularly high similarity in the C-terminus. However, the role in the regulation of FDP in flowering time is unclear. No significant difference in the onset of flowering between populations of lines carrying the FDP mutation and wild-type plants has been observed (Hanano and Goto, 2011). However the tested mutations may have little effect on function or FDP could act redundantly to FD.

1.9 PEBP associated Floral Complexes

1.9.1 Structure and Function

The crystal structure of a complex formed from HD3a, a 14-3-3 protein and a 9 amino acid peptide of the OsFD C-terminus shows a hetero-hexameric structure complex where two HD3a molecules interact with a 14-3-3 dimer (Taoka et al., 2011). The complex is W-shaped, approximately 95Å in width and 70Å in diameter. The HD3a binding surface of the 14-3-3 protein is composed of two α-helices, near the C-terminus. The HD3a binding region can be divided into two regions, an acidic lobe and a hydrophobic cavity. The acidic lobe is centred about four residues within the loop between E206, E208, E212 and E213 and contains tyrosine 215 which forms salt bridges with HD3a via arginine 132 (R132) and arginine 64 (R64). Mutations to residues R64 or R132 reduce but do not abolish the interactions between HD3a and 14-3-3, highlighting their importance.

Several interactions between the HD3a and 14-3-3 proteins occur within the hydrophobic cavity. The hydrophobic cavity is formed by the cleft between the two α-helices at the C-terminus of 14-3-3. The cavity contains the side chains from several residues including F200, M222, I204 and L22. Several residues from HD3a (M63, P96, T98, T99 and F103) are buried within the cavity. Given that the residues are conserved across species, it is likely that FTs from one species could interact with another species 14-3-3 proteins, which may partly explain cross-species activity of FTs.

The C-terminus of OsFD interacts with HD3a via 14-3-3. The C-terminus interacts with a positively charged cleft in the 14-3-3 protomer via a series of side-chain/main-chain interactions. The phosphorylated serine (S192) forms several interactions with the side chains of R58, R131 and Y132. The phosphorylation of residues is thought to be critical for interaction (Abe et al., 2005). Moreover, the R-X-X-(S/T)-A-P-F motif is conserved across species (Taoka et al., 2011). Mutating phosphorylated threonine in the C-terminus of FD prevents the interaction of binding partners (Abe et al., 2005). Given the conservation of the motif, phosphorylation may be an essential feature in the activation of flowering.

Importantly, the OsFD and the HD3a components of the complex are spatially separated at the point of expression. The 14-3-3 protein acts as a bridge connecting the C-terminus of OsFD with HD3a (Taoka et al., 2011). Despite this it is unclear what the functional and biological role of HD3a is within the complex. Likewise, it is unclear how TFL1-like homologs could possibly inhibit the activity of HD3a. However, SP, a TFL1 homolog in tomato, has been shown to interact with 14-3-3 in yeast two-hybrid assays, raising the possibility that an FD/14-3-3/TFL1 complex could also exist (Pnueli et al., 1998).

1.9.2 Nuclear Localization

The components of the floral activation complex exist in distinct cellular domains (Taoka et al., 2011). In vivo, HD3a tagged with mCherry can be detected in both the cytoplasm and the nucleus. Fluorescently tagged 14-3-3 proteins in Rice are found within in the cytoplasm confined via an exposed nuclear export signal (NES) found at C-terminus. It has been proposed that the interaction with HD3a occludes the NES inhibiting the specific exclusion. Fluorescently tagged OsFD is found exclusively within the nucleus and interaction between OsFD with complexes of HD3a and 14-3-3s occur in the nucleus. As a result it has been proposed that upon binding of HD3a and 14-3-3, the 14-3-3-HD3a complex can enter the nucleus and interact with OsFD.

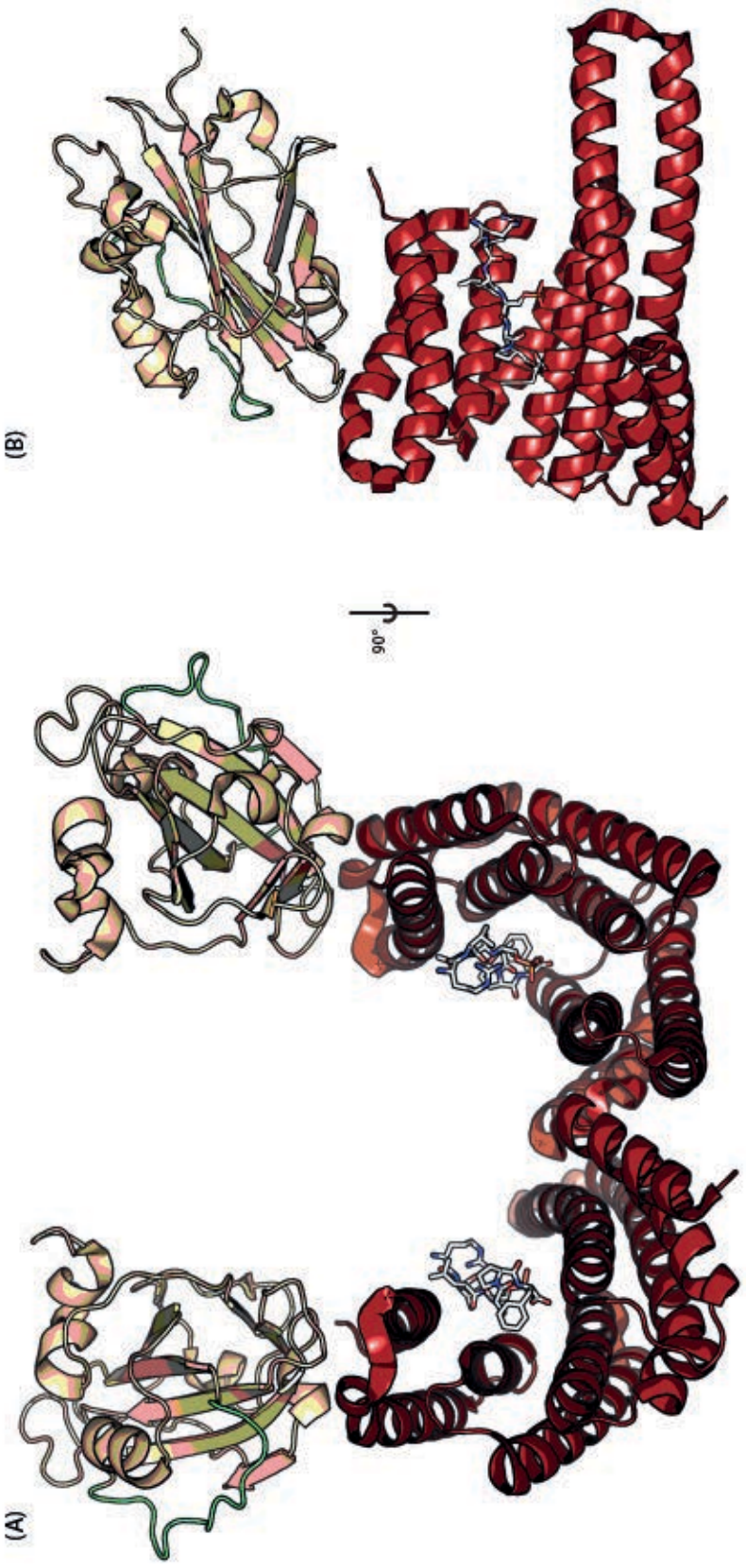


Figure 1.5: Structure of the Florigen Activation Complex. (A) The FAC in rice is heterohexamer composed of a 14-3-3 dimer (red), two HD3a (wheat) and two peptides derived from the C-terminus of FD. **(B)** Structure rotated by 90°. FD binds to a positively charged cleft within the 14-3-3 protomer. The extended loop structures in the Rice FAC are found towards the exterior of the structure (Green).

1.10 Downstream Regulators of Flowering

The shoot apical meristem transitions to a reproductively active state after plants perceive appropriate environmental cues. The formation of flowers occurs in distinct steps, the first of these is converting the vegetative meristem to a floral meristem (Reviewed in Krizek and Fletcher, 2005).

1.10.1 Converting Vegetative Meristem to Floral Meristem

The expression of floral identity genes including *LFY* and *AP1* cause the conversion of vegetative shoots into inflorescences and then flowers. Overexpression of LFY has been shown to be sufficient to convert lateral shoots and main shoots to single flowers (Weigel and Nilsson, 1995). *lfy* mutations cause floral meristems to become inflorescence meristem (Weigel et al., 1992). The phenotype is enhanced in double mutants of *ap1* and *lfy*. *AP1* and *LFY* encode transcription factors that are responsible for the signalling cascade that leads to floral patterning (Riechmann et al., 1996, Parcy et al., 1998). FT and TFL1 act upstream of *ap1* and *lfy*; inducing or repressing their expression respectively (Hanano and Goto, 2011, Wigge et al., 2005). However, the mechanism by which TFL1 inhibits these processes, given the high sequence similarity between TFL1 and FT, has yet to be elucidated.

1.11 Project Aims, Objectives and Strategies

The principle aims of this project were to investigate the mechanisms of regulating flowering time by TFL1 using a combination of biochemistry, structural biology and *in vivo* methodologies. Specifically, this project intended to investigate TFL1's interactions with various binding partners and subsequently to utilise this knowledge to convert an FT into a TFL1-like repressor of flowering, *in vivo*. To this end several objective were established:

1. **To develop a method for the production of TFL1, FT and FD recombinantly.**

A key objective was to develop methodologies to express, purify and characterise proteins known to be involved in the regulation of flowering time.

2. **Investigate the interaction between TFL1 and 14-3-3 Proteins**

This study aimed to identify and select a model 14-3-3 protein in *Arabidopsis* and to assess whether any interaction between TFL1 and the model 14-3-3 protein existed.

3. **Investigate the interaction between TFL1 and FD**

In this study, one aim was to biochemically probe the interaction between FD and TFL1 to assess whether a direct interaction existed. In case of a lack of direct interaction, work could be conducted to identify if 14-3-3 proteins act as intermediate and to structurally characterise and resulting complex.

4. **Investigate the interaction between the AP1 core promoter and TFL1 alongside associated proteins**

One aim was to establish if FD and/or the activator or repressor complexes could directly interact with AP1 promoter.

5. **Create a TFL1-like proteins, *in vivo*, via mutagenesis of FT**

A key objective was to modify FT and convert it into a repressor of flowering *in vivo*. Flowering time could be assessed by the number of days the mutant and wild-type plants take to flower.

6. **Investigate novel methodologies to artificially inhibit the biological activity of TFL1**

This project aimed to establish biochemically whether it is possible to artificially inhibit TFL1 using biologically relevant molecule via medium-throughput binding assays and thermal profile perturbation.

These objectives were systematically evaluated to provide information about the activity and mode of action of TFL1 as well as to provide resources for future investigations to understand the molecular basis of flowering time regulation.

Chapter 2 - Material and Methods

2.1 Molecular Biology Methodology

2.1.1 Agarose Gel Electrophoresis

Gels composed of 0.9% (w/v) agarose were used throughout the project. Agarose was weighed and dissolved in 1x Tris-Acetate-EDTA (TAE) derived from a 50x stock TAE buffer (Qiagen). The solution was heated by microwaving at 850 watts. 3 µl of Gel Red (Biotium) was added per 100 ml of the gel mixture and mixed by agitation. Gels formed by allowing the mixture to cool within appropriate gel moulds. Samples of DNA were mixed with appropriate volumes of loading buffer (50% glycerol and 0.05 bromophenol blue) and loaded into moulded wells. 5 µl of 1kb molecular marker mix (3 µl 1Kb plus marker (Invitrogen), 22 DNA loading dye and 125 µl water) was added to enable estimation of size. Gels were run at 100 volts for 30 minutes. Bands were visualised by ultraviolet transillumination (Gene Genius, Synoptics). Images were processed with Gene Snap version 6.08 (Synoptics).

2.1.2 Polymerase Chain Reaction (PCR)

DNA was amplified using the polymerase chain reaction (Saiki et al., 1985). Oligonucleotides primers used for cloning were acquired from Eurofins MWG (Appendix 1). Oligonucleotides for analytical PCR were acquired from Invitrogen (Appendix 1). Primers were used to amplify genes, add mutations, incorporate restriction sites and add stop codons. Reactions were conducted using a Robocycler gradient 40 (Stratagene) thermal cycle with a heated lid to prevent condensation of the reaction on the lids of PCR tubes. Reactions were conducted in the presence of DMSO (dimethyl sulfoxide) to minimize secondary structure formation within primers and improve specificity (Varadaraj and Skinner, 1994). The melting temperature of each of the primers was used to determine the correct annealing temperature. PCR products were purified either using a QIAquick Gel Extraction Kit when undesired fragments were also present or QIAquick PCR purification kit when the amplification returned only specific products, as judged by agarose gel electrophoresis.

2.1.2.1 PCR Reaction Mix

PCR reactions were created by mixing two components: a DNA mix and a polymerase mix. The DNA mix contained 3 µl of PfuUltraII buffer (10x stock), 2 µl of the forward primer (125ng), 2 µl of the reverse primer (125ng), 1 µl DMSO, 0.3 µl of the DNA template and 21.7 µl of water. One AmpliWax PCR Gem wax bead (Applied Biosystems) was then added to this mixture which was then heated to 95˚C in a heat block for a period of 90 seconds. The mixture was then cooled on ice until the wax bead had resolidified creating a layer of wax on top of the solution. The polymerase mix contained 2 µl of PfuUltraII Buffer (10x), 1 µl of dNTP mix, 0.8 µl of PfuUltraII (Stratagene) and 16.2 µl of H_20. This 20 µl solution was added on top of the wax layer. Analytical PCRs were conducted with GoTAQ (Promega) following the manufacturer's protocol.

2.1.2.2 PCR Reaction Cycling Parameters

PCR reaction cycles began with an initial denaturation step of 95°C for 90 seconds minute as outlined above. This was followed by an amplification step involving a denaturing stage at 95°C for 30 seconds, an annealing stage conducted at the predetermined annealing temperature for 30 seconds and an extension stage at 72°C for 30 seconds per Kb of DNA. The amplification step was repeated 25 times and was followed by an elongation step at 72°C lasting for 10 minutes. All complete reactions were held at 6°C until processing.

2.1.2.3 Site Directed Mutagenesis Mix

Site directed mutagenesis reaction were prepared by mixing 5 µl of PfuUltraII 10x buffer, 2 µl of each oligonucleotide primer (62.5ng), 1 µl of dNTP mix, 1 µl DMSO, 0.3 µl of the DNA template, 1 µl of PfuUltraII and 37.7 µl of water.

2.1.2.4 Site Directed Mutagenesis Cycling Parameters

PCR was initiated with a denaturation step of 95°C for 30 seconds. This was followed by an amplification step involving a denaturation stage 95°C for 30 seconds, an annealing stage at 55°C for 30 seconds and an extension stage at 72°C for 30 seconds per kb of plasmid length. The amplification step was repeated for

18 cycles. After the cycling reaction, 1 µl of DpnI was added to the reaction mixture to remove the original template. The reaction mixture was incubated at 37°C for 16 hours.

2.1.3 Construction of DNA Fragments

Chimeric PCR fragments were created by PCR. Primers were designed to contain: a region from the product to be amplified and a region capable of complementary interaction with a second PCR fragment. Products were then amplified (as in Section 2.1.2) extracted from agarose gels and mixed in a 1:1 molar ratio. Primers for the entire template were added and PCR was conducted as in Section 2.1.2.

2.1.4 Plasmids

Several vectors were used to create cloning and expression constructs. Details for the vectors are listed in Table 2.1.

Table 2.1: Six vectors were used to created the expression constructs used in this work. Listed are the names, resistance marker and affinity tags where relevant.

Vector	Resistant	TAG	Location	Map
pET26b	Kanamycin	HIS_6	C-terminus	Appendix
pET28b	Kanamycin	HIS_6	N- and C- terminus	Appendix
pET53	Ampicillin	$HIS_{6\ and\ STREP}$	N- and C- terminus	Appendix
pGEX-6-P1	Ampicillin	GST	N- terminus	Appendix
PCR8	Spectinomycin	-	-	Appendix
pGWB5	Ampicillin and Hygromycin	GFP	C- terminus	Appendix

2.1.5 Cloning Strategies

2.1.5.1 Sticky End Cloning

The sticky-end PCR cloning strategy (Walker et al, 2008) was deployed to create expression constructs involving the pET vectors (Novagen) (Appendix 2). To simulate the overhangs produced by restriction enzymes like NdeI and XhoI two inserts were created using primers ending in sequences corresponding to the cleaved restriction site. These primers were designated "long" if they contained the overhang from a digested piece of DNA or "short" if they contained the shorter complementary region. Target genes were

amplified with a long forward primer and a short reverse primer or with a short forward primer and a long reverse primer (Figure 2.1).

An *Nde1* site, which contains an ATG start codon if used in frame, was integrated into the PCR product before gene of interest. Nde1 (NEB) cuts the restriction site CATATG between the second and third bases, leaving a 5' TA overhang. An *Xho1* site, was integrated after the gene. Xho1 (NEB) cuts DNA with the sequence CTCGAG after the first C leaving a 5' TCG overhang.

The sizes of the two long/short and short/long (see above) PCR products were checked using gel electrophoresis. Correctly amplified PCR products were mixed and heated to 95˚C for ten minutes to separate strands, followed by a 5 minute incubation step at 65˚C. DNA was allowed to cool to room temperature. Cooling allows re-annealing; which produces four products: the two parent PCR products and two hybrids, one of which contains an overhang mimicking and Nde1 cut as the 5' end and a overhang mimicking the XhoI site at the 3' end and correspond to the desired insert with sticky end on both sides. Thus 25% of the PCR mix is able to ligate into vector opened with NdeI and XhoI.

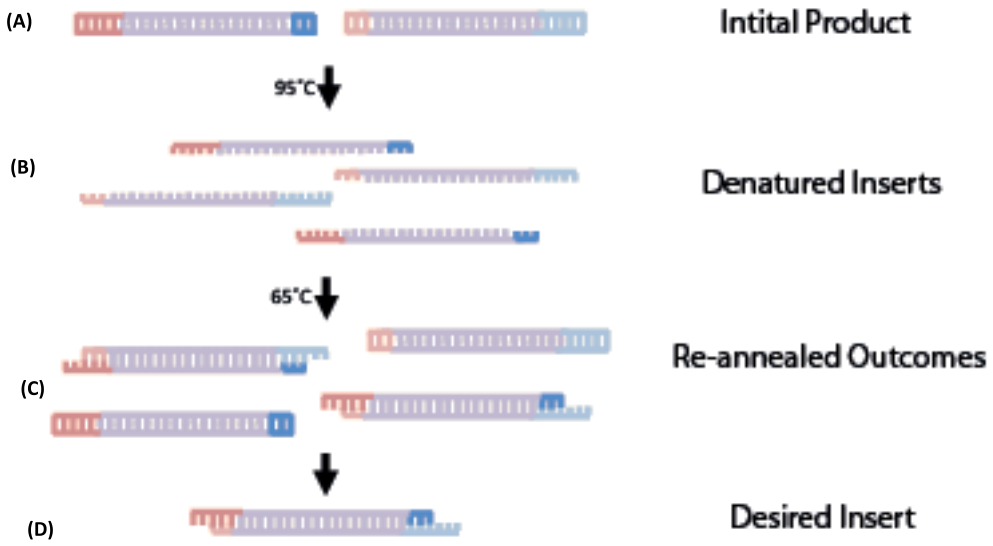


Figure 2.1: Sticky End PCR Cloning Strategy. Target genes were amplified with four primers designed to replicate the sense or antisense strands of a stretch of DNA cut with restriction enzymes. **(A)** Genes of interest were amplified with long forward primer and short reverse primers or with short forward primers and long reverse primers. **(B)** Correctly amplified PCR products were mixed and heated to 95°C for ten minutes. **(C)** This pseudo-denaturation step was followed by 65°C step lasting 5 minutes before DNA was allowed to cool to room temperature. Cooling allows re-annealing which causes four products: two parent PCR products and two hybrids, one of which is the desired insert **(D)**.

2.1.5.1.1 Sticky-End Cloning Ligation Mix

Ligations were performed with T4 DNA Ligase (NEB). A 1:12 molar ratio of digested plasmid to insert was mixed with 2 µl of T4 DNA Ligase buffer and 0.5µl of Ligase. All ligation reactions were brought to a total volume of 20 µl with water.

2.1.5.2 Restriction Digest-Based Cloning

Vectors and insert were digested with matching restriction enzymes over a period of 16 hours. Products were purified using gel extractions (vectors) and PCR cleanup (insert) prior to ligation.

2.1.5.2.1 Restriction Digest-Based Cloning Ligation Mix

Ligations were conducted using T4 DNA Ligase (NEB). A 1:3 molar ratio of digested plasmid to insert was mixed with 2 µl of T4 DNA Ligase buffer and 0.5 µl of Ligase. All ligation reactions were brought to a total volume of 20 µl with water. Ligations were incubated at 16°C overnight.

2.1.5.3 Recombination Cloning

PCR products were directly incorporated into plasmids via recombination. PCR products were initial cloned into PCR8 via the TOPO cloning reaction according to the manufacturer's instructions (Invitrogen). Products were then transferred into destination vectors using an LR recombination reaction (Invitrogen).

2.1.6 Transformation of Bacteria

2.1.6.1 Transformation of Chemically Competent Cells

Freshly thawed competent XL1-Blue cells (Stratagene) were transformed with 5µl of the purified ligation reaction. Transformation was conducted according to the manufacturer's instructions.

2.1.6.2 Transformation of Electro-Competent Cells

50 µl of electro-competent cells were thawed on ice. 0.2 µl - 5 µl of plasmid DNA was added to the cell suspension, which was then transferred to an electroporation cuvette (Biorad). Cells were electroporated at 1.67kV, 25µF, and 200δ then placed on ice for 2-3 minutes. Cells were resuspended in 0.7 ml of LB and

transferred to an Eppendorf tube and incubated for 1 hour at 37˚C with shaking at 225 r.p.m. For transformation with known purified plasmids, between 5 and 10 µl of cell suspension was spread onto LB-Agar plates containing the appropriate antibiotic and incubated overnight at 37˚C. For the transformation with ligations products, the cell suspension was pelleted in a tabletop centrifuge for 10 seconds at 13,400 r.p.m. The supernatant was reduced to 100 µl and the pellet was resuspended before being spread on to LB-Agar containing the appropriate antibiotic and incubated overnight at 37˚C.

2.1.7 Purification and Verification of Constructs

A number of colonies were taken from plates and used to initiate small cultures in 4ml LB with the appropriate antibiotic. After growth overnight at 37°C these cultures were pelleted and the plasmid purified using QIAprep Spin Miniprep Kit (Qiagen) according to the manufacturer's instructions. The DNA was eluted in 50 µl of buffer EB. Purified plasmid was assessed using by restriction digest before being sent for dye-terminator sequencing (Eurofins MWG-Operon).

2.2 Protein Production Methodology

2.2.1 Protein Expression

Recombinant protein expression was performed in *Escherichia coli* (*E. coli*) in strains (Table 2.2) compatible with the T7 expression system. In this system, the host has a chromosomal copy of the T7 polymerase gene under the control of the lacUV5 promoter. Protein expression is induced by allolactose or isopropyl-β-D-thiogalactopyranoside (IPTG), a molecular mimic of allolactose. The presence of either compound leads to the de-repression of the lacUV5 promoter and the expression of the T7 polymerase.

Table 2.2: Strains used for protein expression in this study. Listed are the strain names, genotype and notes regarding the strain.

Strain	Genotype and Characteristics	Notes
Escherichia coli Rosetta II	*E.coli* B, F-, *dcm, ompT, hsdS,* (*rB-mB-*) *gal*, λ(DE3)	Rosetta II strains are BL21 (DE3) derivatives. They contain genes for rarely used tRNAs (including AGG, AGA, AUA, CUA, CCC and GGA) on a plasmid that confers chloramphenicol resistance. The strain is deficient in ompT, a protease that may degrade some recombinant proteins.
Escherichia coli BL21 (DE3)	F-, ompT, gal, dcm Ion, HsdSB (rB-mB-) λ(DE3) {LacL, LacUV5-t7, ind1, sam7, nin5)])	Protein expression cells that do not have the requirement for chloramphenicol.

Bacterial strains transformed with a T7 compatible plasmid produce LacI, a protein which binds to the lacUV5 promoter preventing expression of genomically integrated T7 polymerase. LacI also binds to a lac operon element found upstream of the gene of interest inhibiting expression. Allolactose and IPTG bind to LacI causing a conformational change, which prevents it from interacting with the lacUV5 promoter (Taraban et al., 2008, Lin et al., 2000). This conformational change is the basis of induction and leads to the derepression of the lacUV5 promoter, which triggers the expression of the T7 polymerase and the gene of interest.

Expression constructs were transformed into BL21 (DE3) cells. Colonies from an agar plate were used to start 25 ml overnight cultures. 5 ml of culture was then used to inoculate 1 L of LB in a 2 L conical flask. Cultures were grown at 37°C in a shaking incubator. Periodically, the optical density of the culture at 600 nm (OD_{600}) was taken to monitor growth. Samples of culture were placed in a cuvette, with a 1 cm path length, and measured spectrophotometrically. At an OD_{600} of 0.6 to 0.8 the cultures were induced with 1 mM IPTG. After induction cultures were grown overnight at 22°C in a shaking incubator.

2.2.2 Autoinduction

Autoinduction was used to produce high yields of soluble TFL1. In autoinduction media (in this case either LB or minimal media) is modified to include glucose, lactose and glycerol. As glucose inhibits the uptake of lactose, *E. coli* use glucose in preference to lactose allowing the culture to reach a high optical density. As glucose is depleted, lactose is taken up and can be converted to allolactose an inducer of expression.

In later phases of growth, glycerol is used as a carbon source (Studier, 2005). This leads to gradual induction allowing greater time for the folding of expressed proteins.

2.2.2.1 Autoinduction Media

500 ml of LB or minimal media was modified by the addition of 0.5ml of 1 M MgSO4, 10 ml of 50x 5052 solution (containing 0.5% glycerol, 0.05% glucose and 0.2% α-lactose) and 25 ml of NPS (containing 0.5 M $(NH_4)_2SO_4$, 1 M KH_2PO_4 and 1 M Na_2HPO_4) and ~10 µl of antifoam.

Expression constructs were transformed into BL21 (DE3) cells. 10 ml of an overnight culture was used to inoculate 1 L of auto induction media. Cultures were grown for 5 hours at 37°C and then overnight at 22°C.

2.2.3 Expression of ^{15}N-Labelled Protein

Labelled proteins were produced by autoinduction using M9 minimal media. 200 ml of a 5x stock M9 salts (239 mM Na_2HPO_4-$7H_2O$, 110 mM KH_2PO_4, 43 mM NaCl, 93 mM NH_4Cl) was diluted with 2 ml of 1M MgSO4, 20 ml of 20% glucose and 100 ul of 1M $CaCl_2$ and adjusted with water to 1 litre. The autoinduction media was made as described previously.$^{15}NH_4Cl$ and $^{15}(NH_4)_2SO_4$ were used to provide a source of ^{15}N. A small overnight culture grown in LB was harvested by centrifugation at 4000 RCF and resuspended in 20 ml of M9 minimal media. 5 ml of resuspended culture was used to inoculate 1 L of Autoinducation minimal media. Cultures were grown at 37°C for 5 hours and left overnight at 22°C.

2.2.4 Harvesting

Cells were harvested by centrifugation for 15 minutes at 8829 RCF. After centrifugation the supernatant was removed and the pellet stored at -80°C.

2.3 Protein Purification Methodology

Recombinant proteins were extracted from *E.coli* and purified with methods depending upon the protein's biochemical characteristics, including the presence of an affinity tag, overall charge and size. Crude protein extracts were subjected to a series of separations which gradually enriched the abundance

of the target protein. To ensure reproducibility purifications were conducted on an Äkta purifier, Äkta prime or Äkta FPLC (GE Healthcare) using filtered buffers outlined in Table 2.3. All buffers were filtered through a 0.45 nitrocellulose membrane (Thermo Scientific) prior to use. The preparations were assayed after each purification step to determine the effectiveness of each step.

Table 2.3: The composition of buffers used in this study.

Buffer Name	Protein	Buffer	pH	Salt	Reducing Agent	Other Components
PEBP Ion Exchange Wash Buffer	FT and TFL1	50mM KH_2PO_4	6.8	50mM KCl	1mM DTT	-
PEBP Ion Exchange Elution Buffer	FT and TFL1	50mM KH_2PO_4	6.8	1M KCl	1mM DTT	-
PEBP His Wash Buffer	FT and TFL1	50mM KH_2PO_4	6.8	50mM KCl	2mM BME	50 mM Imidazole
PEBP His Elution Buffer	FT and TFL1	50mM KH_2PO_4	6.8	50mM KCl	2mM BME	500 mM Imidazole
PEBP Gel Filtration Buffer	FT and TFL1	50mM KH_2PO_4	6.8	200mM KCl	1mM DTT	-
14-3-3 His Wash Buffer	14-3-3 Nu	50mM Tris-HCl	7.4	200mM NaCl	2mM BME	50 mM Imidazole
14-3-3 His Elution Buffer	14-3-3 Nu	50mM Tris-HCl	7.4	200mM NaCl	2mM BME	500 mM Imidazole
14-3-3 Gel Filtration Buffer	14-3-3 Nu	50mM Tris-HCl	7.4	200mM NaCl	1mM DTT	-
GST Lysis Buffer	FD	50mM HEPES	7.4	200mM KCl	2mM BME	-
GST Elution Buffer	FD	50mM HEPES	7.4	200mM KCl	2mM BME	10mM reduced glutathione
FD Gel Filtration Buffer	FD	50mM $NaH_2C_6H_5O_7$	5.5	200mM KCL	2mM BME	-
Assay Buffer	All	50mM KH_2PO_4	6.8	150mM KCL	-	-

2.3.1 Cell Homogenization and Lysis

Cell pellets, harvested by centrifugation were resuspended in lysis buffer. Protease inhibitors, including 0.17 mg/ml PMSF (phenylmethanesulfonylfluoride), 0.01mg/ml aprotinin, 0.005 mg/ml leupeptin and 0.001 mg/ml pepstatin A were added to prevent degradation of the target protein. To remove DNA, 100 µM $MgCL_2$ and 0.001 mg/ml DNAse 1 were also added. Cells were disrupted via sonication. Cell debris was removed by centrifugation at ~40,000g for 45 minutes. The cleared supernatant was passed through the appropriate purification column by peristaltic pump overnight at 4°C.

2.3.2 Ion Exchange Chromatography

Ion exchange chromatography is the separation of molecules based upon difference in charge. Ion exchange was chosen as the first step in the purification of FT and TFL1 from bacterial lysate. FT has a PI of 7.75. TFL1 has a PI of 9.69. At pH 6.8 both FT and TFL1 have a net positive charge. As a result proteins were purified by cation exchange chromatography using SP HP columns (GE Healthcare). Pre-loaded columns were transferred over to an Åkta purification system (GE Healthcare). The absorbance at 280nm was measured throughout the experiment to detect the elution of protein. The column was washed for 5 column volumes. Proteins were eluted over a salt gradient between 0% and 40% elution buffer lasting 8 column volumes. The concentration of elution B was held at 40% for 3 column volumes. After this additional proteins were eluted over a gradient from 40% and 80% of buffer B lasting 8 column volumes. Throughout fractions of 8 ml were taken for analysis fractions containing the protein of interest were pooled for further purification.

2.3.3 Affinity Chromatography

Affinity chromatography is based on the interaction of an affinity tag with specific chemical groups coupled to a resin. Purification with polyhistidine tags and with glutathione S-transferase are among the most cost effective strategies (Lichty et al., 2005).

2.3.3.1 Ni^{2+} Affinity Chromatography

2.3.3.1.1Purification of FT and TFL1

His-tagged proteins were purified using a Hi-Trap chelating column (GE Healthcare). The column was equilibrated with 3 column volumes of PEBP His Wash Buffer. Protein purified by ion exchange chromatography was loaded onto the column using a superloop. The column was washed with 12 column volumes of PEBP His Wash Buffer. Protein was then eluted by washing the column with 3 column volumes of PEBP His Elution Buffer. Fractions were collected and pooled for further purification.

2.3.3.1.2 Purification of Untagged TFL1

Purified his-tagged TFL1 with a thrombin cleavage site incorporated between the affinity tag and the protein (acquired as describe in section 2.3.3.1.1) was incubated with thrombin for 24 hours in dialysis tubing with a 3500 molecular weight cut-off. TFL1 was dialysed into His Wash Buffer with 0% imidazole. The protein sample was loaded into the superloop. The sample was loaded onto a Hi-Trap chelating column (GE Healthcare). The column was washed with 12 column volumes of PEBP His Wash Buffer. Cleaved protein was eluted during the wash phase. Tagged protein was then eluted by washing the column with 3 column volumes of PEBP His Elution Buffer. Fractions were collected and pooled for further purification.

2.3.3.1.3 Purification of 14-3-3 Nu

Ni^{2+} affinity purification was used to purify 14-3-3 Nu from lysate. Cleared lysate was loaded onto the column using a peristaltic pump. The column was transferred to a pre-prepared HPLC system. The column was washed with 3 column volumes of 14-3-3 His Wash Buffer before bound protein was eluted with stepped increases in the concentration of imidazole. The column was washed sequentially with 3 column volumes of 10%, 20%, 60% and 100% 14-3-3 His Elution Buffer. Fractions of 8 ml were collected analysed and pooled for further purification.

2.3.3.2 GST Affinity Chromatography

GST-tagged proteins were purified directly from crude lysate using a 5 ml GST-Trap column (GE Healthcare). Cleared lysate was loaded onto the column using a peristaltic pump pre-prepared columns were transferred onto Äkta purification system. 14 column volumes of GST lysis buffer was used to remove untagged proteins. GST-tagged proteins were eluted with GST elution buffer (Table 2.3).

2.3.4 Size-Exclusion Chromatography

Size-exclusion chromatography was used as a final purification step for all proteins. Size-exclusion chromatography separates proteins by size. Size-exclusion columns are made of a porous matrix which smaller proteins can enter. Large proteins are unable to enter the matrix and so travel through the

columns faster as a smaller volume is accessible to them. FT, TFL1 and FD[209] samples were purified using a Superdex™ 75 column (GE Healthcare). 14-3-3 Nu was purified using a Superdex™ 200 column (GE Healthcare). Protein was concentrated to 2 ml using an Amicon Ultra Filter Spin Concentrator (Millipore) and injected onto a pre-equilibrated column. Fractions were taken, analysed and used for biochemical assays.

2.4 Biochemical Characterization

2.4.1 Protein Concentration Determination

The concentration of protein samples was determined via absorbance measurements at 280 nM (A) using a NanoDrop UV spectrophotometer (Fisher Scientific) which had been blanked against sample buffer. The concentration (c) was calculated using the following formula:

$$c = {}^{A}/_{\in l}$$

In this equation, l is the path length and ε is the extinction coefficient of the protein, which was estimated using the ProtPram server (ExPASy).

2.4.2 Polyacrylamide Gel Electrophoresis

2.4.2.1 SDS-PAGE

Protein quality and quantity was assessed by SDS-PAGE (Sodium Dodecyl Sulphate - Polyacrylamide Gel Electrophoresis). 5 ul of loading buffer (50 mM Tris, 25% glycerol (v/v), 4% SDS (v/v), 1% βME, 20 µg/l bromophenol blue) was added to 30 ul of sample. Samples were denatured at 95°C for three minutes. Samples were then loaded onto 15% gels (Table 2.4) prepared in 6ml casts (Invitrogen).

Table 2.4: The composition of SDS-PAGE Gels used in this study. Table details the components and stocks used to create SDS-PAGE gels.

	Component	Stock Concentration	Volume (ml)
Resolving Gel	Water	-	2.3
	Acrylamide	30%	5.0
	Tris pH8.8	1.5 M	2.5
	SDS	10%	0.1
	APS	10%	0.1
	TEMED	-	0.004
	Total		**10**
Stacking Gel	Water	-	0.7
	Acrylamide	30%	0.1
	Tris pH6.8	1 M	o.13
	SDS	10%	0.01
	APS	10%	0.01
	TEMED	-	0.001
	Water		**1.0**

Electrophoresis was then conducted at 180 V for 45 minutes in running buffer (7.4 g Glycine, 1.51 g Tris Base, 0.5% SDS in 1 L of H_2O). Gels were washed with water, briefly microwaved with a fixing agent (50% ethanol, 5% acetic acid) and stained for 15 minutes (50% Ethanol, 8% Acetic acid, Brilliant Blue R-205). Gels were left to destain overnight (5% Ethanol, 6% Acetic Acid).

2.4.2.2 Native PAGE

Native PAGE was used to assess the propensity of proteins to form complexes with other proteins and with DNA. Protein and protein-DNA samples were mixed with native gel loading dye (50% Glycerol, 0.25% Bromophenol Blue) and were run on native gels (Table 2.5).

Table 2.5: The composition of Native PAGE Gels used in this study. Table details the components and stocks used to create a Native PAGE gel.

	Component	Stock Concentration	Volume (ml)
Native Gel	Water	-	7.0
	Acrylamide	30%	2.0
	10xTris Running Buffer	-	1.0
	APS	10%	0.1
	TEMED	-	0.010

Gels were run at 100 V for 75 minutes in native running buffer (7.4 g Glycine, 1.51 g Tris Base in 1 L of H_2O). Protein-protein native gel here stained as described in section 2.4.2.1. Protein-DNA native gels were stained in 50 ml of running buffer with Gel Red (Biotium).

2.4.3 Mass Spectrometry

Mass spectrometry is an indispensible analytical technique used in molecular and cellular biology to identify a variety of molecules. A mass spectrometer is composed of an ion source, an analysis unit that can measure the mass-to-charge ratio of the ionized sample and sort molecules, and a detector. Complex mixtures of proteins, peptides and small molecules can be separated before analysis by liquid-chromatography. This allows measurement of several molecules within a sample to be analysed in a single run. An enzymatically digested protein can produce a set of unique peptides which can be used to provide an identity. In this study, mass spectrometry was used to confirm the identity of proteins in solution.

2.4.3.1 Sample Preparation for Mass Spectrometry

Samples containing approximately 30 µg of protein were diluted to 100 µl with 50 mM NH_4HCO_3 and 5 µl of 200 mM DTT in 100mM NH_4HCO_3. The sample was boiled on a heat block for 10 minutes and then incubated at room temperature for 45-60 minutes. 4 µl 1 M iodoacetamide was added, the protein samples were vortexed briefly, spun and incubated at room temperature for 45 minutes. The iodoacetamide was neutralized by the addition of 20 µl 200 mM DTT. Subsequently, protein samples

were vortexed briefly, spun and incubated at room temperature for 45 minutes. Trypsin was added in a 1:50 ratio of trypsin to sample. The pH of the sample altered with formic acid to pH 6. Samples were run on a QTRAP mass spectrometer (AB Sciex Instruments) using a multiple reaction monitoring (MRM) method for the identification of defined peptides. Mass spectrometry was conducted by Mr Mark Bennett, Mass Spectrometry Facility Manager.

2.4.4 Differential Scanning Fluorimetry (DSF)

2.4.4.1 Principles of Differential Scanning Fluorimetry (DSF)

DSF is a technique to measure the thermal unfolding of a protein. The unfolding is monitored indirectly by measuring the fluorescence of a dye that is quenched in aqueous solution. As a protein the unfolds, the dye binds to exposed hydrophobic stretches and fluoresces. The intensity of fluorescence can be plotted against temperature; typically a folded protein has a sigmoidal unfolding profile which can be modelled using the equation:

$$Y = LL + \frac{UL - LL}{1 + \exp(\frac{Tm - x}{a})}$$

In the equation, LL is the value of the minimum intensity, UL is the maximum intensity, *a* is the slope of the curve and T_m is the inflection point of the of the curve (also known as the melting temperature) (Niesen et al., 2007).

2.4.4.2 Thermal Shift Assay

Small molecules, peptides and nucleic acids that interact with a protein are likely to increase a its stability. This can be assessed by DSF. Proteins dialysed into assay buffer were diluted down to 4 µM. Compounds and peptides were added to this at molar equivalents. The stock solution of SYPRO ORANGE (Invitrogen) was diluted 1000-fold and was added to each reaction. Protein behaviour was monitored over a 1K/min temperature gradient from 20°C to 95°C with fluorescence measurements taken every 0.2°C in an Eppendorf RT-PCR machine.

2.4.4.3 Thermal Shift Assay Analysis

Thermal shift data were analysed in Microsoft Excel with the solver plugin (Frontline Systems Inc) (Kemmer and Keller, 2010) using the equation in section 2.4.4.1. Curves were produced by normalizing data and plotting them in Microsoft Excel.

2.5 Microscale Thermophoresis

Thermophoresis is the movement of molecules in solution across a temperature gradient. Changes in thermophoresis of a protein caused by interaction with ligand can be detected. The change can be measured as a function of concentration allowing determination of the dissociation constant (Kd). In this study thermophoresis was used to assess protein-protein and protein-DNA interactions.

2.5.1 Microscale Thermophoresis Principles

Movement of molecules according to heat it is known as thermodiffusion. When a molecule moves from hot-to-cold it is described as having undergone positive thermodiffusion whereas when a molecule moves from cold-to-hot it is described as having undergone negative thermodiffusion. The steady state depletion of a molecule in an area, in liquid, for a given temperature is described by the equation:

$$C_{hot}/c_{cold} = \exp(-S_T \, \Delta T)$$

In the equation, C is the concentration of a molecule, C_{hot}/C_{cold} is the ratio of the molecule present when a heat source is applied, ΔT is a change in temperature and S_T is the Soret coefficient. Though a full theoretical understanding of thermodiffusion has yet to be obtained, the major determinants of a molecule's movement across a temperature gradient appear to be size, hydration shell and charge (Duhr and Braun, 2006). This relationship can be described with the equation:

$$S_T = \frac{A}{kT}\left(-\Delta S_{hyd}(T) + \frac{\beta\sigma_{eff^2}}{4\varepsilon\varepsilon_0 T}\, x\, \lambda_{DH}\right)$$

In this equation, A is the size of the particle, λ_{DH} is the Debye length (the length particles can be separated by charge due to electrical field dampening by electrons), T is temperature, $S_{hyd}(T)$ refers to the hydration shell (where S_{hyd} is the hydration enthalpy), σ_{eff} is the charge of the molecule, k is Boltzmann constant, ε is the permittivity of a medium, ε_0 is the permittivity of free space, β is the temperature effects of the dielectric constant of water (Duhr, personal communication). Changes in size, hydration shell and charge can be detected experimentally by measuring the thermodiffusion.

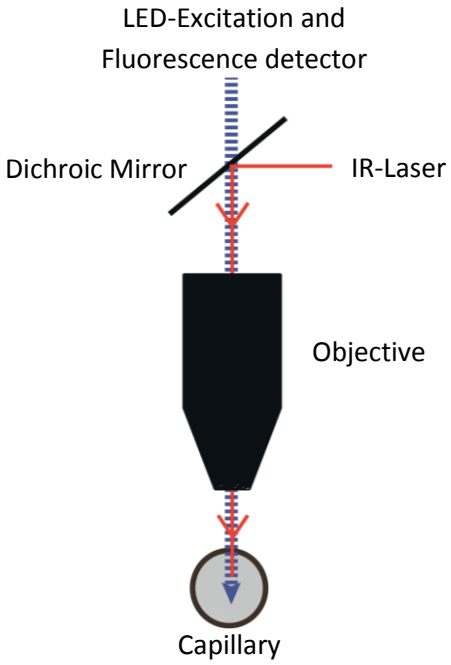


Figure 2.2: Microscale thermophoresis schematic. A microscale thermophoresis machine has an LED and an infra-red laser. The laser is used to heat the solution in the capillary and create the temperature gradient. LED-excitation enables excitation of the fluorophores attached to the bait protein. Both are channelled to the same location by a dichroic mirror and an objective.

2.5.2 Microscale Thermophoresis Equipment

All thermophoresis experiments were conducted in a Nanotemper Monolith NT.115 (Nanotemper Technologies GmbH). Thermophoresis can be monitored via a fluorescence signal associated with the bait molecule which can be either from a fluorescent protein fused to the bait protein or from a fluorescent dye chemically cross-linked to the bait molecule. These fluorophores are excited by a LED and the

fluorescence intensity can be measured. The sample is heated in particular area using a infrared laser with a wavelength 1430 nm (Seidel et al., 2013). This laser light is focused to a particular area in the capillary where the fluorescent intensity measurement is taken (Figure 2.2). Samples are placed in capillaries which are then subjected to thermophoresis.

2.5.3 Microscale Thermophoresis Assay Design

In microscale thermophoresis prey protein is titrated into fluorescently tagged bait protein which is kept at a constant concentration. The bait is kept at low concentrations (50 nM in this work). The prey protein is concentrated to approximately 20 times the Kd and serially diluted across 16 samples. Purified protein was dialysed into assay buffer whilst DNA oligos (Sigma) were diluted in assay buffer prior to use. Samples were transferred into capillaries according to manufacturer's instruction. Capillaries of known thickness and diameter were used to ensure reproducible temperature gradients. All experiments were conducted at 25°C. A Hill coefficient or a one site binding model was fitted to the data with Origin 8.6.

2.6 Nuclear Magnetic Resonance (NMR)

NMR was used to determine whether proteins were folded and to determine if interactions were occurring.

2.6.1 Nuclear Magnetic Resonance Principles

In NMR, the activity in atomic nuclei in a magnetic field is monitored. In quantum mechanics, the nucleus of an atom has an associated spin. The spin is determined by the overall charge of the nucleus and is described with the nuclear spin angular quantum number, I. Different atomic nuclei have different spin values. ^{1}H and ^{15}N both have spin values of $^{1}/_{2}$ whilst deuterium ^{2}H has a spin value of 1. The presence of a magnetic field causes the nuclei to align to the magnetic field or against it, either in a low energy state (+I) or a high energy state (-I). A radio pulse at a specific frequency can be used to make the nuclei transition from the low state to the high state and cause nuclei in the high state to transition to the low state. The difference in energy absorbed by nuclei that transition to a higher state versus the energy emitted by nuclei transitioning from a high to a low state is recorded as signal. Spin can be affected by

the local chemical environment which means that the transitioning events provide information about the environment around atoms. Electron shielding by covalent bonded electronegative atoms like nitrogen is greater than the shielding provided by carbon. As a result amide and methyl nuclei signals can be distinguished. Aromatic rings which in folded proteins typically are placed inside the core of the protein can affect other neighbouring residues. Aromatic rings act as small magnetic fields which can cause an effect known as ring current shifts where methyl associated nuclei close to aromatic rings resonated differently to methyl nuclei alone. This can be used as a reliable indicator of proper folding.

2.6.2 1D NMR

1D NMR can be used as a screening tool to differentiate between structured and unstructured protein. In this study 1D NMR was used to identify proteins that are amenable to further biochemical and structural studies. In 1D experiments 500 µl of protein at between 50 and 150 µM was dialysed into assay buffer (Table 2.3) and transferred into an NMR tube. 1D NMR experiments were conducted on a Bruker Avance III 600 spectrometer at 303 K. 1D NMR experiments were conducted with the kind assistance of Dr Jan Marchant, NMR facility manager at Imperial College London.

2.6.3 2D NMR

Multi-dimensional NMR was used analyse the interaction of proteins. This involves correlating nuclei from ^{1}H and ^{15}N nuclei using Transverse Relaxation Optimized Spectroscopy (TROSY) experiments. This technique is appropriate for the analysis of large complexes. In NMR experiments 300 µl of protein in assay buffer was transferred into shigami NMR tubes. 2D NMR experiments were conducted upon a Bruker Avance II 800 spectrometer at 303 K. 2D NMR experiments were conducted with the kind assistance of Dr Jan Marchant, NMR facility manager at Imperial College London.

2.7 Structural Determination by Electron Microscopy (EM)

Electron microscopy can provide structural information for macromolecules and supramolecular assemblies greater than 100 KDa and has been used as an approach for investigating the interaction

between protein-DNA complex (Czarnota et al., 1997). Sets of particles at random orientations can be used to construct a three-dimensional structure (Van Heel, 1987).

2.7.1 Electron Microscopy Sample Preparation

Purified protein and DNA samples were mixed in equimolar concentrations and diluted to a concentration of 0.1 mg/ml. Grids were prepared by glow-discharge, a process that causes grids to become hydrophilic. Samples then were applied to a grid, washed and stained in an acidified 2% uranyl acetate solution (pH4.5). The excess liquid was removed and the grid were left to dry. Grids were placed in a specimen holder and then imaged in a CM200 (Philips) transmission electron microscope.

2.7.2 Electron Microscopy Data Processing

Several were taken micrographs of each grid and used in the acquisition of partial images. Partials were manually picked using Boxer. Particles were placed into boxes approximately twice the size of the protein complex.

2.8 X-Ray Crystallography

2.8.1 Principles of X-Ray Crystallography

All electromagnetic radiation can be described in terms of three properties; the wavelength, the amplitude and the phase. The wavelength is the distance between two wave maxima whilst the amplitude is the height of the maxima. The phase of the wave is the angle at the origin. Waves typically interact with matter in three ways. They can be absorbed, reflected or refracted. Waves can also affect one another; this phenomenon is known as interference. Interference is a change of amplitude when two waves of equal wavelength are incident upon a locale. Constructive interference is the increase in amplitude that occurs when two waves are in phase. Destructive interference is the decrease in amplitude that occurs when two waves are out of phase.

X-rays are a form of electromagnetic radiation with a wavelength between 0.1-100 Å. As bond lengths are in the Ångström range X-rays can be used to visualise molecules to the atomic level. Usually, crystals are

used as specimens because data from single molecules are too weak to be measured Crystals act as diffraction grids. The positive interference of scattered X-rays can be measured on a detector as diffraction spots.

2.8.2 Protein Crystallization

Crystallization is a special case of precipitation. Crystals are three-dimensional arrangements of molecules in a periodic arrangement. Layers within these crystals can be considered as planes. Molecules within a crystal attempt reach the lowest free energy.

2.8.2.1 Growing Protein Crystals

Growth of crystals is dependent upon a number of factors. Two of the experimentally most important ones are the concentration of precipitant and the concentration of protein. The effects of these two variables can be visualised by a phase diagram (Figure 2.3a). At low protein concentration and low precipitant concentration, the protein remains soluble and crystallization does not occur. At high protein and precipitant concentrations, proteins nucleate, forming microscopic clusters. Nucleation can lead to either the formation of microcrystals or amorphous aggregate. At protein and precipitant concentration that are neither too low or too high crystals can grow. Crystallization strategies aim to take a protein solution from the unsaturated region, cause it to undergo nucleation and then take it to the metastable zone where crystal growth is sustained (Figure 2.3b).

In this study, protein crystals were grown using the vapour diffusion methodology. This involves setting up a small volume of concentrated protein solution alongside a much larger reservoir of a crystallization solution containing high concentrations of precipitants. Before closing the system the protein solution is mixed with a small volume of crystallization solution. The protein drop thus contains precipitant at a lower concentration than the reservoir. During incubation, diffusion of water vapour increases the precipitant and protein concentrations in the drop until equilibrium is reached. If the starting protein and precipitant concentrations and the volume of drop and reservoir have been chosen correctly, nucleation

will occur. Nucleation decreases the effective protein concentration, which brings the solution towards conditions where growth is possible (Figure 2.3b).

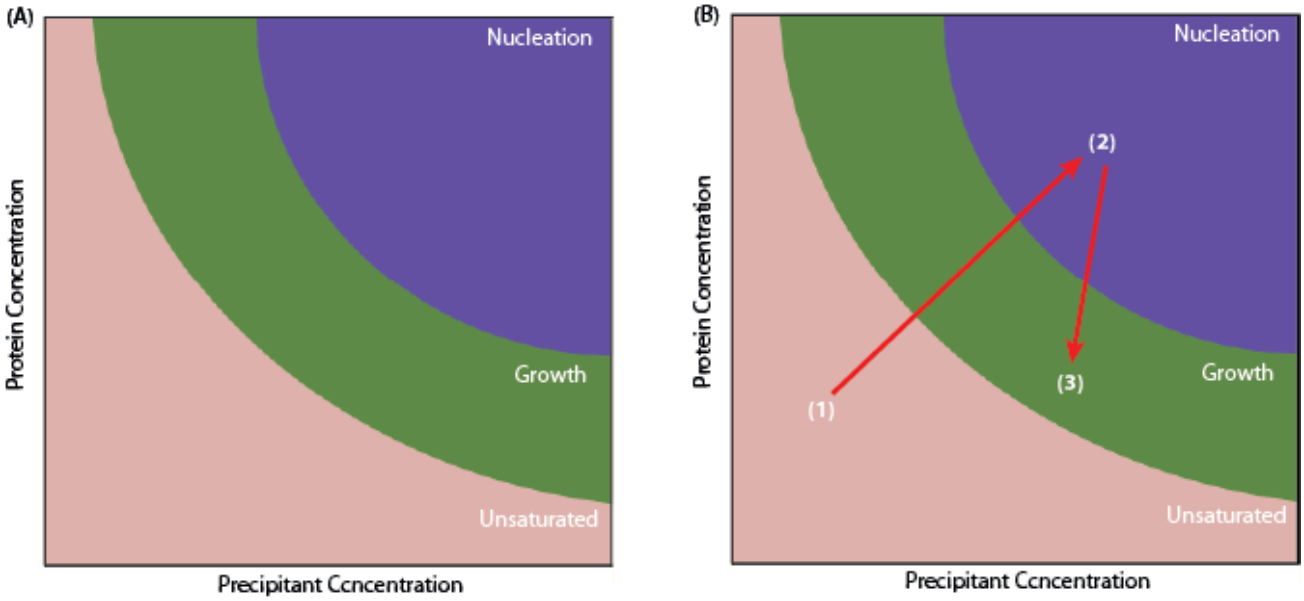


Figure 2.3: Phase diagram of crystallization. (A) Regions coloured red represent conditions that lack the protein or precipitant concentrations to initiate crystallization. Conditions in the blue section (supersaturated region) are capable of initiating nucleation. Conditions in the green section (metastable region) are capable of sustaining growth alone. **(B)** Strategy for crystallization. Protein to be crystallized must move from unsaturated conditions, to conditions were nucleation can occur and then to conditions where growth can occurs.

2.8.2.2 Identifying Protein Crystallization Conditions

Besides protein and precipitant concentrations, several other chemical parameters influence protein crystallization including, pH, the nature of the precipitant and the presence of salts and additives. To sample as many factors as possible, sparse matrix crystallization screens containing a large number of diverse reservoir solutions based on previously acquired crystallization conditions were used in this work. Conditions can be arranged into arrays compatible with robotic approaches, allowing for medium-throughput automated screening.

For nucleation to occur the protein solution must be of sufficient concentration. Protein samples to be trialled were concentrated to approximately 12 mg/ml. Peptide was added at this stage at a 5:1 molar ratio of peptide to complex. Samples were then spun at 4°C for 30 minutes and the supernatant used for trials. This ensured the removal of exogenous nucleants like dust particles, and enhanced the

reproducibility of crystallization. Protein solution was distributed into several 96-well sparse-matrix sitting drop plates with a Mosquito crystallization robot (TTP LabTech). Trays were set up with 140 nl of protein solution per drop, mixed with 140 nl of reservoir solution. Plates were sealed manually with CrystalClear tape (Hampton). Trays were left in a crystallization incubator at 4°C and observed periodically under a microscope.

2.8.2.3 Production of Protein Crystals

After the identification of initial hits, replication and optimization screens were designed around conditions that produced crystalline precipitate or microcrystals. Typically precipitant concentrations and buffer pH were varied systematically within replication screen. Protein was concentrated and spun as described previously. 250 µl of crystallization solution was placed in the reservoir of 48-well sitting drop plates. 2 µl of protein solution was added to the well and mixed with 2 µl of reservoir solution. Plates were sealed and stored for 10 days at 4°C.

2.8.2.4 Crystal Freezing and Storage

Large crystal with regular shapes and smooth faces were screened for their diffraction properties either in-house or at Diamond Light Source. During the process of data collection protein crystals can suffer radiation damage. The extent of radiation damage is reduced at low temperatures. To permit the acquisition of complete datasets from a single crystal (Hope et al., 1989) all crystals in this study were flash frozen in liquid nitrogen. To prevent the formation of ice which could compromise data quality, all crystals were grown in solutions containing cryoprotectant (Reviewed in Hope, 1990). Crystals were extracted from wells using a mounted CryoLoop (Hamptons Research) and transferred directly into liquid nitrogen. Crystals to be assessed at the in house X-ray source were stored in vials; crystals to be assessed at the synchrotron were stored in universal pucks.

2.8.3 Diffraction

To acquire information about the three-dimensional structure of a macromolecule, a crystal is mounted between an X-ray source and an X-ray detector. Crystals diffract the source beam, which creates a spot on the detector. Rotation of crystals during data collection permitted the acquisitions of complete datasets. The diffraction pattern provides information about the path travelled by the diffracted beam. The spacing between reflections within the diffraction pattern enables the calculation of the parameters of the crystal lattice. The intensity of each spot in the diffraction pattern provides information about the contents of the unit cell. Together with their phases, the electron density throughout the unit cell can be calculated from the intensities of the diffraction spots. Crucially, however, the phase of the wave is not recorded during data collection

2.8.3.1 The Unit Cell

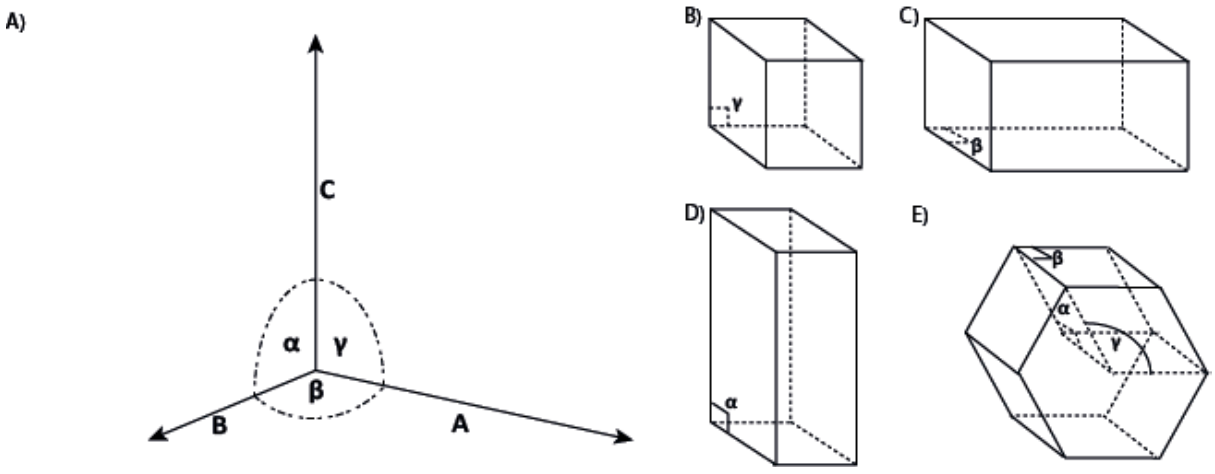


Figure 2.4: A Unit Cell Diagram. (A) Depiction of axis and angles within a unit cell. **(B)** Cubic crystal system with the angle γ indicated. **(C)** Tetragonal crystal system with the angle β indicated. **(D)** Orthorhombic crystal system with the angle α indicated and **(E)** Hexagonal crystal system all angles indicated.

The unit cell is the basic building block of a protein crystal. Crystals can be described as series of unit cells; the crystal can be generated from the unit cell by serial translation along the three axes. Unit cells exist in three dimensions and are defined by the lengths of three unique edges (a, b and c) and the angles between them (α, β and γ) (Figure 2.4a). The angles and lengths found in different units cells are

important features. In a simple cubic system a, b and c are equal and α, β and γ all equal to 90° (Figure 2.4b). In a simple hexagonal crystal system a and b are equal whilst c can be different and γ is 120° whilst α and β are 90° (Figure 2.4e). In a simple tetragonal crystal system α, β and γ all equal to 90°, A and B are equal but C does not have to be.

2.8.4 Data Acquisition and Processing

To collect data crystals were exposed to a beam of coherent monochromatic X-rays. In this project data were initially acquired using X-rays from an in-house rotating copper anode source (Rigaku MicroMax 007 HF) X-ray source fitted with a Saturn 944+ charged couple device (CCD) detector. Acquired data can be read out to a computer. High-resolution data were later acquired using X-rays from a synchrotron radiation source (Diamond Light Source). Advanced PILATUS detectors (DECTRIS) were used to collect data at the synchrotron. All data acquisition, processing and refinement were conducted with the kind assistance of Dr. Andreas Förster.

2.8.4.1 Symmetry and Strategy

To reduce the effects of radiation damage to crystals the data collection strategy was optimised to acquire the most data with the least exposure of crystals to X-rays. In a crystal with symmetry elements, multiple orientations produce exactly the same reflections, reducing the range of rotation over which data has to be collected to acquire all unique reflections. To develop an appropriate strategy all crystals were screened and the size of the unit cell, the space group and their orientation in the beam calculated. With these parameters, scripts in data acquisition software packages calculate the most efficient data collection strategies.

2.8.4.2 Determining Unit Cell Parameters and Space Groups

Data were processed in iMOSFLM, a program containing tools for indexing reflections, determining the cell parameters, space group and integrating relections. This process yields unmerged reflections, a list containing the index of each individually measured reflection, its intensity and the associated error.

2.8.4.3 Scaling and Merging

Data were scaled and merged using aimless, which is associated with the iMOSFLM data processing package. Scaling ensures that the intensities of spots from different images are consistent by giving each image within a data set a scaling factor. Merging is the process of replacing intensity data of equivalent spots (which are typically multiply measured spot and symmetry-related reflections) measured sp with average intensities.

2.8.5 Molecular Replacement

The phases of the diffracted beams are not recorded but are necessary to solve the structure of a protein, which is calculated from the amplitudes and phases of all reflections (defined in section 2.8.1). One strategy to estimate the phase is using a known protein. This structure, known as the phasing model, is typically a related protein that shares at least 30% sequence identity. The process involves placing the known model into the calculated unit cell. Placement within the unit cell requires both rotation and translation of the selected model within the cell. The rotation of the step determines the orientation of the phasing model with regards to the unknown molecules. The translation step determines the translation required to superimpose the target upon the unknown molecules. The unit cell size and the symmetry of molecules places constraints on the location and orientation of molecules within the unit cell, reducing the computational power required. The number of molecules within the unit cell also places significant restrains upon possible solutions. Given the molecular weight, the dimensions of the unit cell and space group, it is possible to calculate the likelihood of a number of molecules fitting within in the unit cell (Kantardjieff and Rupp, 2003). This allows the calculation of theoretical structure factors which can then be compared with intensity values for reflections.

2.8.5.1 Molecular Replacement Strategy

In this project suitable phasing models were identified and downloaded from the Protein Data Bank. Signal-to-noise was increased by removing all water molecules from the phasing molecule. In addition, non conserved side-chains were pruned with the program, Chainsaw. Molecular replacement was

conducted with Phaser, a software package which uses a probabilistic methodology for assessing the agreement between model and data. Phaser was chosen as it allows combinations of known structures to be used as a search model. Outputs from Phaser were assessed by the Log likelihood gain and Z-scores before being assessed visually.

2.8.6 Model Refinement

After molecular replacement the solution was refined. Refinement is the process of maximizing the agreement between the model and the data. In a model each atom is given a coordinate position, a temperature factor (B factor), which is related to the thermal motion of an atom and an occupancy (Q) score, which related to the fraction of that atom in that position. Refinement optimizes the atomic coordinates and other parameters in the model so that the model fits the data. In this project REFMAC5 (Murshudov et al., 2011) in the CCP4 environment (Winn et al., 2011) and Phenix (Adams et al., 2010) were used to refine models. Three types of refinement were used. Ridged-body optimization, jelly-body refinement and group B factor refinement. In ridged-body refinement sub-units are treated as one body and are adjusted within the unit cell to maximise agreement. In jelly-body refinement rigid bodies are allowed to deform to maximise agreement between the model and the data. Group B-factor refinement optimises the B-factors of entire residues instead of individual atoms.

2.8.7 Model Analysis

Protein models were initially visualised and assessed using Coot; a program that can display electron density maps and models (Emsley et al., 2010). Coot contains numerous validation tools, including tools for the assessment of torsion angles. Backbone torsion angles Phi (Cn-1-Nn-Cαn-Cn) and Psi (Nn-Cαn-Cn-Nn+1) are restricted by energetic and steric factors. The Ramachandran plot provides a visual overview of favoured angle pairs and was used to identify outliers, which were then either explained by convincing density or adjusted to shift the angles to preferred values. Side chain torsion angles (Chi) are also restricted, but their preferred values are amino acid-dependent. Coot contains a library of preferred rotamers (Lovell et al., 2000) that facilitates the modelling of side chain conformations in preferred geometries. Because of the low resolution of the data, extensive use was made of this feature.

2.9 Plant Cultivation

2.9.1 Plant Material

Seeds of *Arabidopsis thaliana* including the Colombia (Col-0) accession (N1092), Ler ecotype (NW20), tfl1-1 (N6167) and *ft-10* mutants (N9869) were obtained from the Nottingham Arabidopsis Stock Centre. 35s::FT-GFP plants and *ft-7* plants were kindly provided by Prof. George Coupland.

2.9.2 Plants Grown on Plates

Plants were grown on half Murashige-Skoog (MS) media (0.21% Murashige-Skoog media, 1% sucrose, 0.05% MES pH5.7-5.8 and 0.8% of phytagel). Seeds of *Arabidopsis thaliana* were surface sterilized in 70% ethanol for a period of one minute. The ethanol was removed and seeds were immersed in a sodium hypochlorite solution for 15 minutes. This was followed by repeated washing in sterilised deionised water. Seeds were sown onto plates with MS-Phytagel (Murashige and Skoog, 1962). Plates were kept in vertical racks, which were stored at 4°C for 48 hours before being transferred to a controlled growth room with long day growth conditions (16 hours light/8 hours dark) with light at 120 µmol m^{-2} sec^{-1} provided by florescent lamps. Plants were kept at 23°C during the day and 20°C at night with a relative humidity of 65%.

2.9.3 Plants Grown on Soil

Plant seeds were transplanted into P24 trays (5 cm square pots, 24 pots per tray, one seed per pot) containing moist F2 modular compost and sand (Scotts) and vermiculite (Sinclair). Trays were stored at 4°C for a period of 48 hours. Plants were transferred to a controlled growth environment with either long day or short day conditions (10 hours light/14 hours dark). Light was provided by florescent lamps set to provide light at 120 µmol m^{-2} sec^{-1} plates were kept at 65% humidity and at 23°C during the day and 20°C at night.

2.9.4 Confocal Microscopy

Confocal microscopy was conducted upon *Arabidopsis* seedlings and leaves. Roots and leaves were imaged *in situ* using a confocal laser scanning microscope (CLSM, Leica TCS SP II; Leica Microsystems).

Fluorophores were excited by laser. GFP was excited by light at 488 nm and emissions were observed using a detection window between 495 and 570 nm. Background autofluorescence was excited using a 405 nm laser with a 420 - 500 nm detection window. Chlorophyll was excited by using a 633 laser with a detection window between 640 - 715 nm. Images were obtained using a 20x lens. Images were processed using the Channel Dye Separation feature of the Leica Confocal Software.

2.9.5 Plant Transformations

2.9.5.1 Preparation of Chemically Competent Agrobacterium

Stocks of chemically competent *Agrobacterium* were prepared. *Agrobacterium* (Agl1 strain) were grown on LB agar plates with rifampicin. A single colony was picked and grown for ~24 hours at 28°C in 10 ml of LB with rifampicin. 2 ml of the overnight culture was used to inoculate 100 ml of LB which was grown to an $O.D_{600}$ of 0.5. Cultures were chilled on ice for 2 minutes then spun for 5 minutes at 5000 RCF at 4°C. The pellet was dissolved in 20 ml cold, sterile 0.15M NaCl and centrifuged for 5 minutes at 5000 RCF at 4°C. This pellet was dissolved in 2 ml of cold, sterile $CaCl_2$ and frozen as 200 µl aliquots in liquid nitrogen.

2.9.5.2 *Agrobacterium* Transformation

100 ng of plasmid was added to an aliquot of *Agrobacterium*. This was kept on ice for 30 minutes before being frozen in liquid nitrogen for 1 minute. Cells were thawed in a 37°C water bath for approximately 1 minute. 600 µl of LB was added the cell incubated at 38°C for 4 hours. After recovery cells were spun down at 3000 RCF for 3 minutes, 400 µl of the supernatant was removed and the remaining pellet was resuspended in the supernatant before being transferred onto LB agar with rifampicin and other appropriate antibiotics. Bacteria were cultured for 3 days at 28°C.

2.9.5.3 *Arabidopsis* Transformation

A single transformants *Agrobacterium* colony was used to inoculate a 10 ml culture of LB with rifampicin with appropriate antibiotics. The culture was grown overnight in a shaker at 28°C. This culture was used to inoculate 500 ml of LB which contained rifampicin and other appropriate antibiotics. These were then grown to an $O.D_{600}$ of 2. The cells were spun down at 3000 RCF for 10 minutes at 28°C, the supernatant

was removed and the bacteria resuspended in infiltration media (4.2% MS, 5% Sucrose adjusted pH 5.7). 10 µl of SILWET (Momentive) and 2 µl of Benzylaminopurine was added to the infiltration media. Plants were held in the bacterial culture for 5 minutes. Plants were then placed inside a plastic container to dry.

2.9.6 Genotyping

2.9.6.1 Genomic DNA extraction

Approximately 100 mg of plant tissues was flash frozen in liquid nitrogen. Tissue was ground into a fine powder using a micropestle and processed using a gDNA plant mini kit (Qiagen).

2.9.7 Physiological Characterisation

2.9.7.1 Physiological Characterisation by Light Microscopy

Plant structures were examined using a LEICA MZ 16 F dissecting microscope. Visible light was provided by a using a LEICA CLS 150 XE light source whilst broad spectrum UV excitation was provided by a mercury lamp (HBO 50). Images were taken on a LEICA DFC300 FX.

2.9.7.2 Physiological Characterisation by Scanning Electron Microscopy

Plant structures were assessed at high resolution using a JSM5610LV (Variable Pressure) Scanning Electron Microscopy. Images were taken by Dr Mahmoud Ardakani, Research Officer, Electron Microscopy facility in the Department of Materials.

2.10 Computational Methodology

2.10.1 Protein and DNA Assessment

2.10.1.1 Bioinformatics and DNA Translation

Basic Local Alignment Search Tool (BLAST) searches were carried out to identify orthologs of genes of interest (Altschul et al., 1990). DNA was translated into amino acid sequence using the ExPASy Protein Translate server.

2.10.1.2 Protein Parameters

Theoretical molecular weights and extinction coefficients were estimated using ExPASy ProtPram Server using protein sequences.

2.10.1.3 Alignments

Amino acid and DNA sequences were aligned using the CLUSTALW server and visualised using JALVIEW (Waterhouse et al., 2009). Secondary structure predictions were conducted using PSIPRED (Bryson et al., 1999, Jones, 1999). Models of proteins were created using the Protein Homology/analogY Recognition Engine Version 2.0 (Phyre 2.0) (Kelley and Sternberg, 2009).

2.11 Chemical Screens

2.11.1 Fragment Library

Compounds were derived from a Maybridge Fragment Library was kindly provided by Dr. Ed Tate (Zartler and Shapiro, 2005).

Chapter 3 Purification and Characterisation of Floral Regulatory Proteins

3.1 Introduction

In plants, TFL1 and FT regulate the onset of flowering. They modulate signalling pathways through FD, a transcription factor. In this study, an optimized protocol for the high yield production of several proteins involved in the floral regulatory pathway has been developed that will facilitate future biochemical and structural characterization.

3.2 Characterizing Floral PEBPs

3.2.1 Bioinformatics Analysis of Floral PEBPs

3.2.1.1.1 Divergence of Sequences between FT and TFL1

FT-like and TFL1-like PEBPs have opposing functions in the regulation of flowering time. To establish sequence motifs that may be functionally important, a selection of PEBP-like protein sequences were aligned and organised phylogenetically. FT-like and TFL1-like clades, groups derived from a single ancestral gene, were identified. Comparisons of sequences were then made between clades to identify regions of strong divergence between FT and TFL1 that could impart specialised function. Sequence analysis highlighted several regions of divergence between the FT-like and the TFL-like clade (Figure 3.1). In agreement with previous analyses the FT-like subgroup of PEBPs was distinguished by a conserved tyrosine at position 85 whilst the TFL1 subgroup contained a histidine at the equivalent position (Ahn et al., 2006). Despite an overall sequence identity of 55% between FT and TFL1, the loop regions only share 18% sequence similarity, which supports the hypothesis that this region is important for imparting antagonistic functions. In TFL1 homologs, a highly conserved positively charged residue, typically lysine, was found at position 150 whereas the equivalent residue in FT was always negatively charged. The C-termini of the FT and TFL1 may also be important for functional differences given the similarity within groups but significant difference between clades.

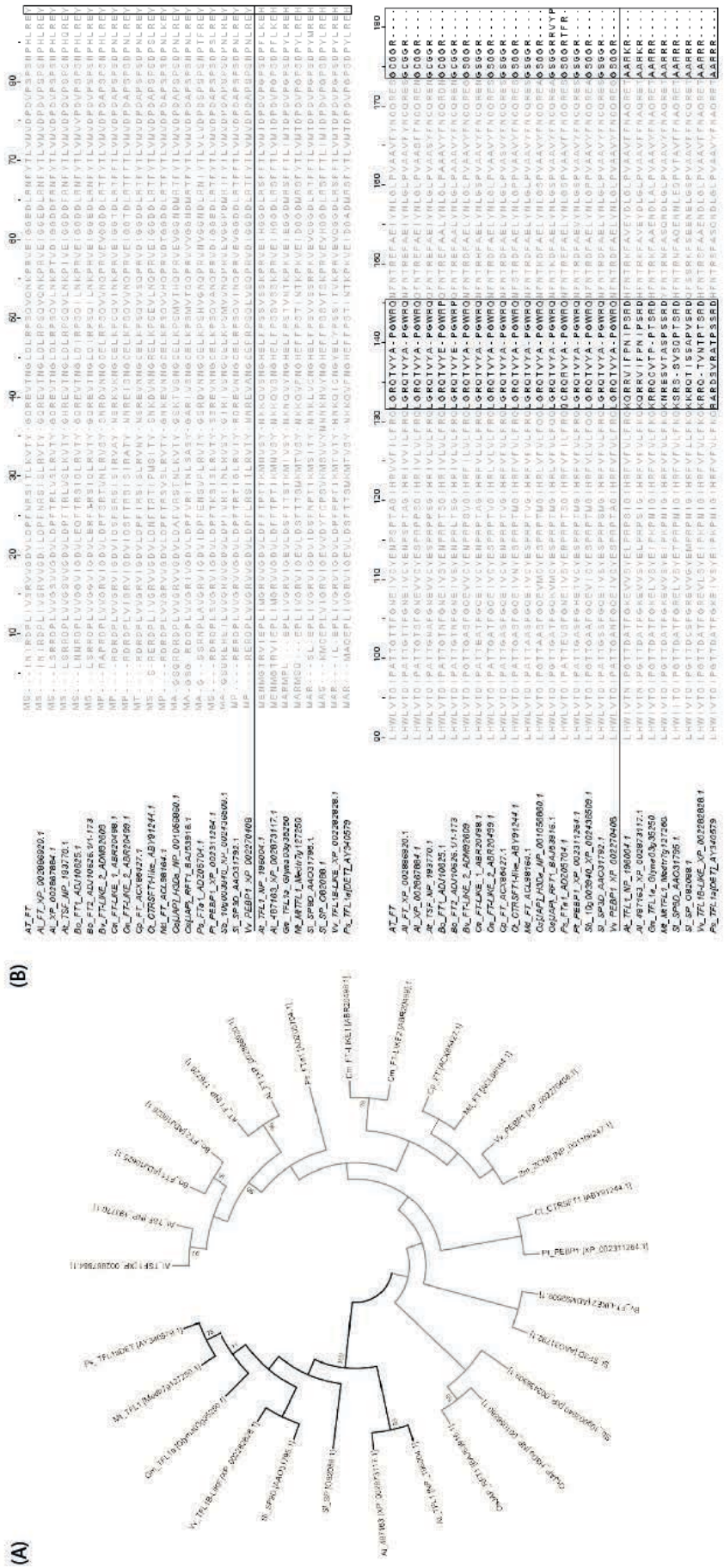


Figure 3.1: Analysis of Sequence Conservation amongst PEBPs. (A) Inferred phylogeny of PEBP genes using the maximum likelihood method. There were a total 27 sequences in the final dataset. Phylogenetic analyses were conducted in MEGA4 (Tamura et al., 2007). (B) Multiple sequence alignment of Plant PEBPs aligned using the clustalW algorithm. Sequences are divided into FT-like and TFL1-like groups. Key sequence elements are boxed.

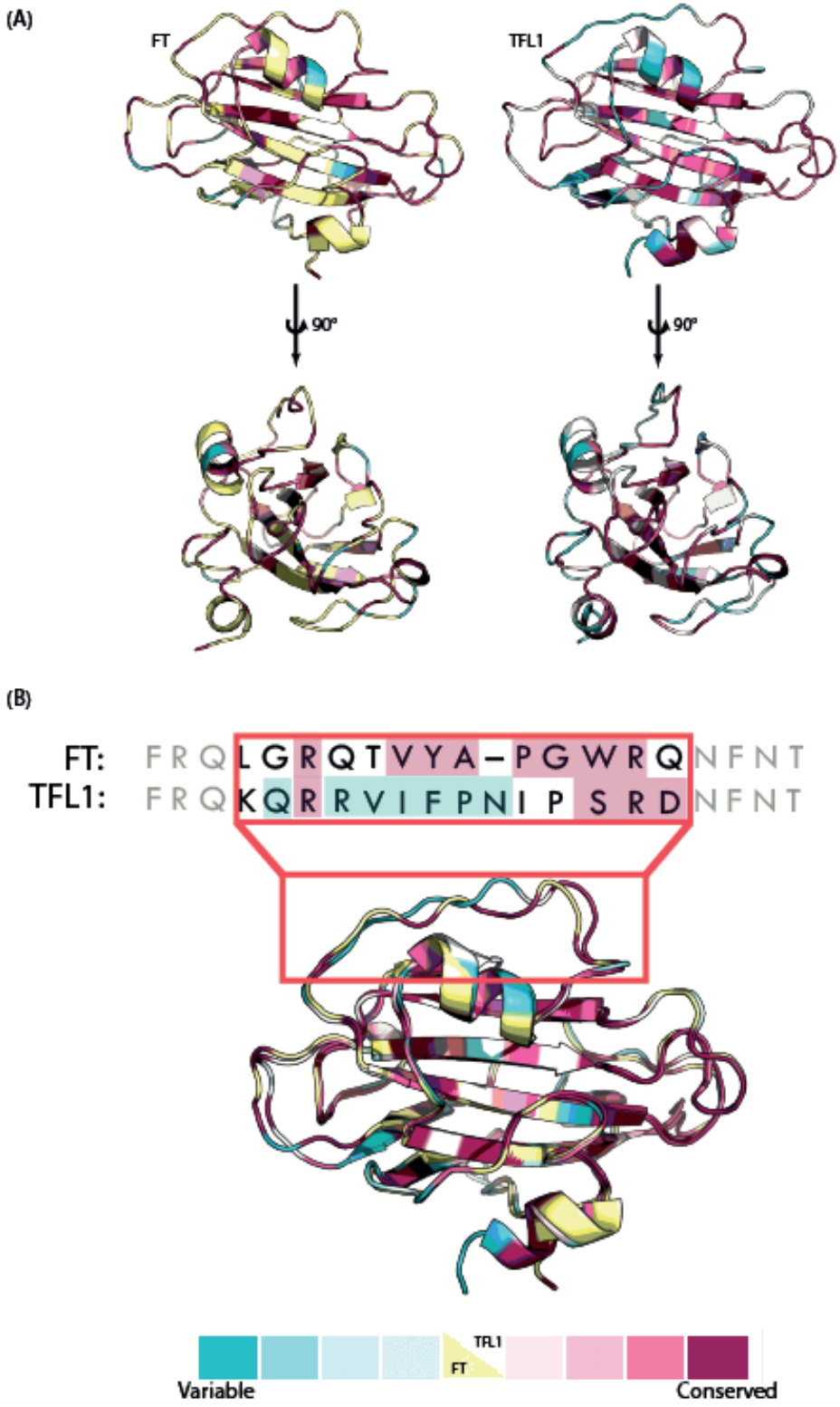


Figure 3.2: Conservation of residues in plant PEBPs mapped onto the Crystal Structures of FT and TFL1. Conservation was separately assessed within the FT and TFL1 clades. **(A)** Structures of FT and TFL1. Highly conserved are coloured red whilst variable residues are coloured blue. Residues with average scores are coloured in white (TFL1) or in Yellow (FT). **(B)** Assessment of the extended loop structure of FT and TFL1.

3.2.1.1.2 Comparison of Sequence Conservation within PEBP Clades

Highly conserved residues are often important for structure and function. Comparing homology between family members can establish the extent to which an amino acid is evolutionarily conserved. To identify hotspots of conservation amongst the FT-Like and TFL1-Like family members, PEBPs were analysed using the CONSURF server based upon the multiple sequence alignment (Figure 3.1). The conservation scores were mapped onto the structures to identify important functional regions in the proteins. Several highly conserved regions were identified (Figure 3.2a).

The large extended loop structures on the surface of FT and TFL1 differ dramatically. The loop of TFL1 is highly variable, particularly between residues 134-139. Several well conserved residues were identified including Arg^{133}, Ser^{141}, Arg^{142} and Asp^{143} (Figure 3.2b). In FT, the loop is largely conserved. Between residues 133 and 139 several residues are either absolutely conserved or share biochemical properties. Arg^{133}, Ala^{135}, Pro^{136} and Arg^{139} are absolutely conserved amongst the FT-like clade (Figure 3.2b). Arg^{130} in FT and Arg^{133} in TFL1 may play similar roles. The equivalent residue in HD3a is involved in the interaction with binding partners (Taoka et al., 2011). Arg^{139} In FT and the equivalent residue in TFL1, Arg^{143} are also absolutely conserved suggesting that they play a structural or functional role in PEBPs.

Residues at the C-terminus, between residues 174 and 177 in TFL1 (170 and 175 in FT), are highly conserved within the FT and TFL1 clades but divergent between them. In TFL1 the C-terminus is highly charged containing several arginines and lysines. In FT, the C-terminus contains numerous glycine residues and a single arginine. The C-termini of FT and TFL1 are not present in the crystal structures and consequently conserved residues could not be mapped, but it is known that disordered loops and termini are often involved in binding interactions and this may be the case with the floral PEBPs (May et al., 2010).

3.2.2 Expression and Purification of Floral PEBPs

To characterise TFL1 biochemically and structurally, a robust protocol for overexpressing and purifying TFL1 was developed. TFL1 was cloned into the vectors pET28 and pET26, enabling the expression of N-

terminally his-tagged TFL1 and untagged TFL1, respectively. The his-tagged TFL1 construct contained a thrombin cleavage site between the his-tag and TFL1 allowing removal of the his-tag. In this project, the construct expressing his-tagged TFL1 was used predominantly. Protein expression and purification methodology is detailed in section 2.5. TFL1 was purified over three steps involving ion exchange, Ni-affinity and gel filtration. Ion exchange yielded significant amounts of protein but owing to impurities further purification was required (Figure 3.3a; Figure 3.3b). Purification of the pooled fractions of his-TFL1 via Ni-affinity resulted in extremely pure his-TFL1 eluting from the column in a single, sharp peak (Figure 3.3c; Figure 3.3d). This was then further purified by gel filtration using an SD75 column which separated a small amount of aggregated protein from the rest of the sample resulting in a small void volume peak at approximately 40 ml and a sharp peak at approximately 65 ml which contained pure his-tagged monomeric TFL1 (Figure 3.3e; Figure 3.3f).

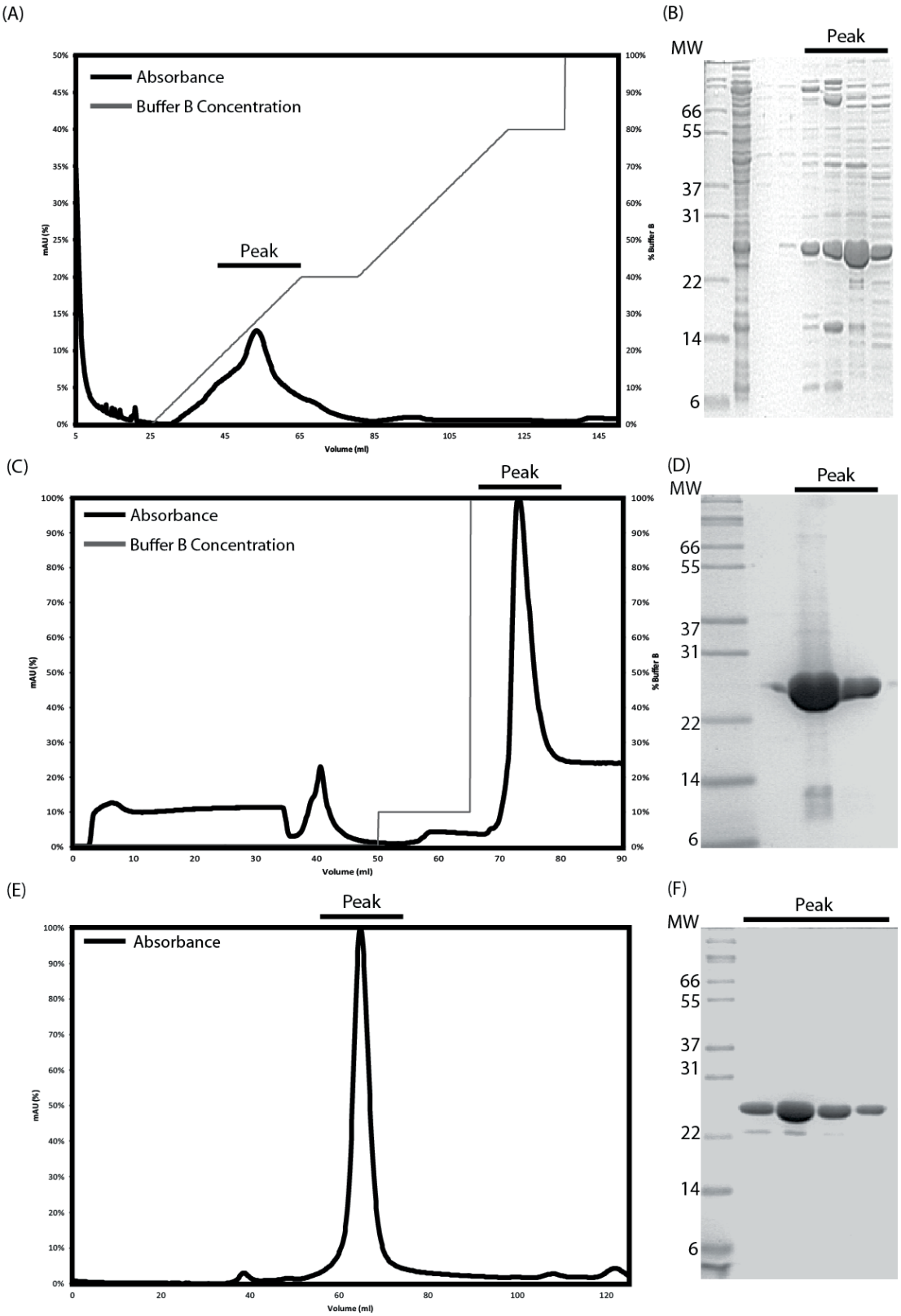


Figure 3.3: Purification of his-tagged TFL1. Purification was divided into three steps. **(A)** Ion exchange chromatography of his-TFL1. **(B)** Nickel-affinity chromatography of his-TFL1. **(C)** Gel Filtration of TFL1**.** In these purification chromatograms the normalised absorbance at 280nm (mAU, left axis) is plotted against the elution volume. The Ion Exchange and the Nickel affinity chromatogram also shows the percentage of elution buffer (right axis). Samples were assessed by SDS Page **(D) (E) (F)**.

3.2.2.1 Purification of untagged TFL1

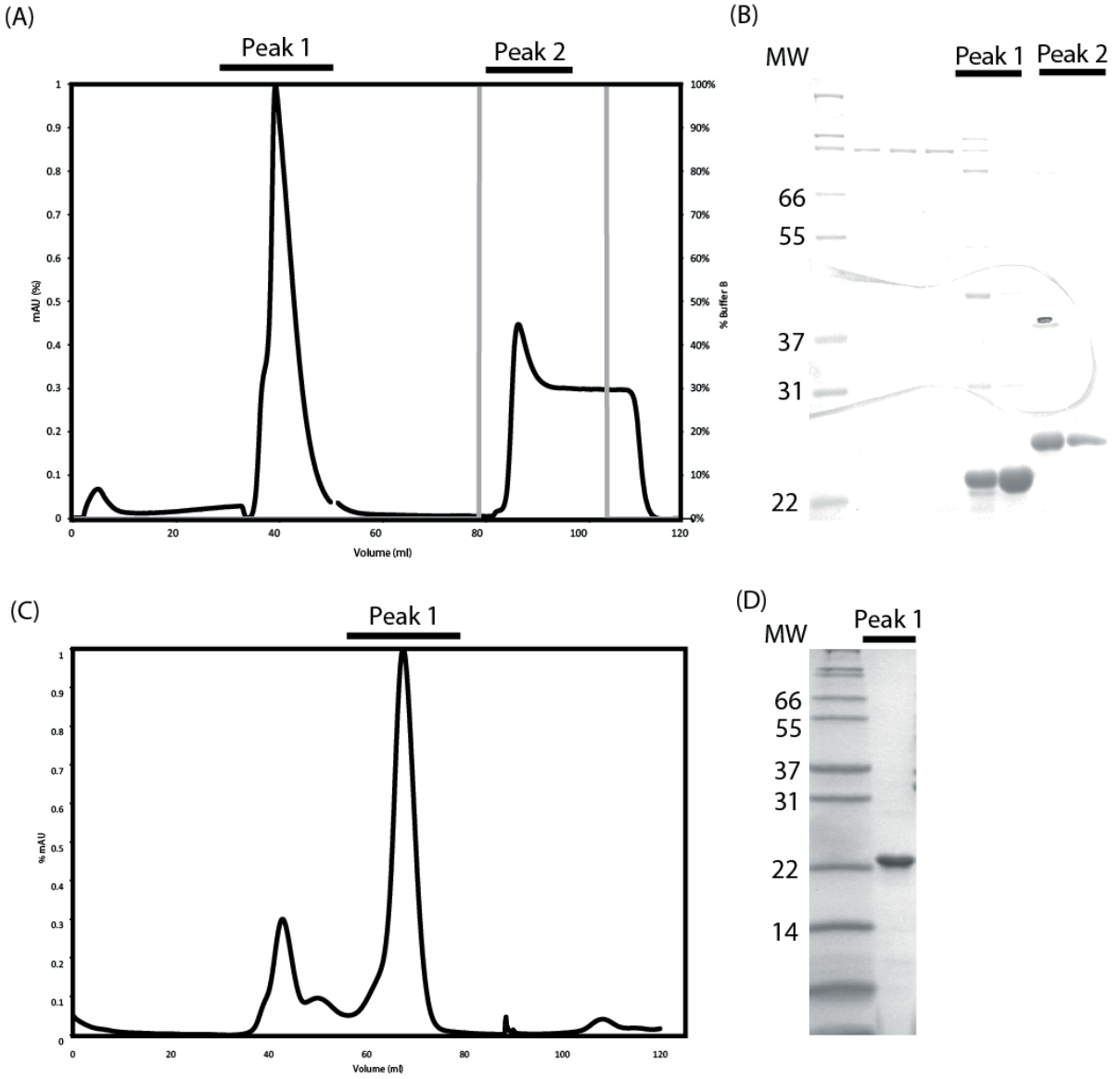


Figure 3.4: Purification of untagged TFL1. After TFL1 was purified by Nickel affinity the protein was dialysed into His Wash Buffer without imidazole, incubated with thrombin overnight and subject to a further two step purification. **(A)** Nickel-affinity chromatography removal of uncleaved protein. **(B)** Gel Filtration of TFL1. Pooled sample assessed by SDS page **(C and D)**. In these purification chromatograms the normalised absorbance at 280nm (mAU, left axis) is plotted against the elution volume. The Nickel affinity chromatogram also shows the percentage of elution buffer (right axis).

To produce untagged TFL1, his-tagged TFL1 was purified from lysate by ion exchange and Ni-affinity chromatography, as described previously. Purified protein was incubated with thrombin at 4°C overnight and purified as described in the materials and methods. Purification via Ni-affinity resulted in a sharp peak of TFL1 during the wash step (Figure 3.4a; Figure 3.4b). Fractions of TFL1 were concentrated and gel filtrated to remove aggregation resulting in an elution profile comparable to purification of his-TFL1 (Figure 3.4c; Figure 3.4d).

3.2.2.2 Expression and Purification of FT

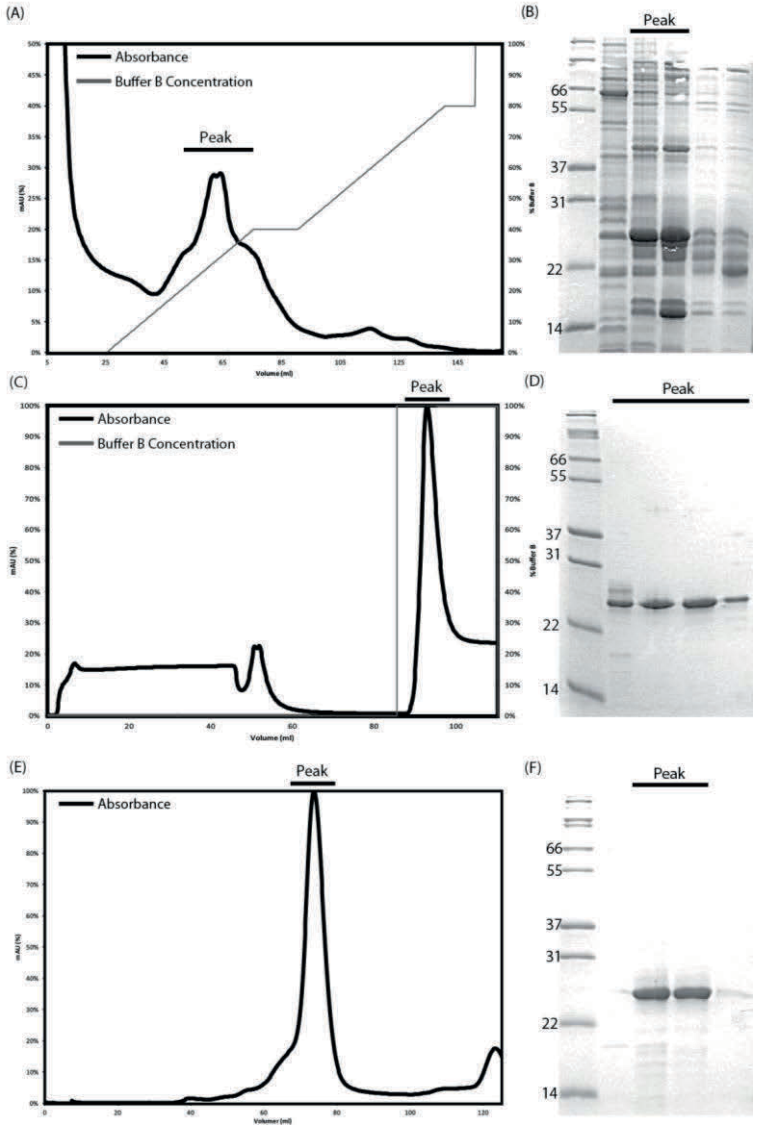


Figure 3.5: **Purification of His tagged FT.** Purification was divided into three steps. **(A)** Ion exchange chromatography of His-FT. **(B)** Nickel-affinity Chromatography of His-FT. **(C)** Gel Filtration of FT**.** In these purification chromatograms the elution volume is plotted gas the normalised absorbance at 280nm (mAU) on the primary axis. In the Ion Exchange step and the Nickel affinity step the secondary axis shows the elution volume plotted against the percentage of elution buffer. Samples were assessed by SDS Page **(D) (E) (F)**.

FT was cloned into the vectors PET28 and PET26. Constructs were confirmed by sequencing. His-tagged FT was used throughout this study. Protein expression methodology is detailed in section 2.5. FT was purified by ion exchange (Figure 3.5a; Figure 3.5b) and Ni-affinity (Figure 3.5c; Figure 3.5d). The resulting protein was further purified by gel filtration using an SD75 column resulting in a sharp peak at approximately 68 ml which contained pure monomeric his-FT (Figure 3.5e; Figure 3.5f).

3.2.3 Mass Spectrometry of PEBPs

Table 3.1: Peptide identified by mass spectrometry from samples of his-TFL1. The sequence of the peptide is given alongside the confidence scores, the name of protein and accession number that the peptide is associated with. Peptides derived from TFL1 were detected indicating that the sample contains pure TFL1.

Sequence	Names	Accessions	Confidence
EHLHWIVTNIPGTTDATFGK	TFL1	AT5G03840.1	99.0
KQVSNGHELFPSSVSSKPR	TFL1	AT5G03840.1	99.0
QVSNGHELFPSSVSSKPR	TFL1	AT5G03840.1	99.0
RVIFPNIPSR	TFL1	AT5G03840.1	99.0
RVIFPNIPSRDHFNTR	TFL1	AT5G03840.1	99.0
RVVGDVLDFFTPTTK	TFL1	AT5G03840.1	99.0
VEIHGGDLR	TFL1	AT5G03840.1	99.0
VVGDVLDFFTPTTK	TFL1	AT5G03840.1	99.0

Table 3.2: Peptides identified by mass spectrometry from samples of his-FT. The sequence of the peptide is given alongside the confidence score, the name of protein and accession number that the peptide is associated with. Peptides derived from FT were detected indicating that the sample contains pure FT.

Sequence	Name	Accessions	Confidence
EFAEIYNLGLPVAAVFYNCQR	FT	AT1G65480.1	99.0
EVTNGLDLRPSQVQNKPR	FT	AT1G65480.1	99.0
MSINIRDPLIVSR	FT	AT1G65480.1	99.0
NFYTLVMVDPDVPSPSNPHLR	FT	AT1G65480.1	99.0
VEIGGEDLRNFYTLVMVDPDV PSPSNPHLR	FT	AT1G65480.1	99.0
DPLIVSR	FT	AT1G65480.1	98.3
TNGLDLRPSQVQNKPR	FT	AT1G65480.1	99.0

To confirm that samples contained TFL1 or FT. Protein samples were subjected to a tryptic digest and analysed via mass spectrometry. Peptides originating from TFL1 were detected in the samples derived from TFL1 purifications. Several peptides unique to TFL1 were identified with >95% confidence (Table 3.1). Likewise, peptides associated with FT were detected in the sample derived from FT purifications. Several peptides unique to FT and close FT-homologs were identified with >95% confidence (Table 3.2). A MRM methodology was developed based upon this to identify specific unique peptides to achieve a sensitive method for screening *ex vivo* samples to enable future localization of TFL1 and FT *in vivo* (Appendix 4).

3.2.41D NMR of PEBPs

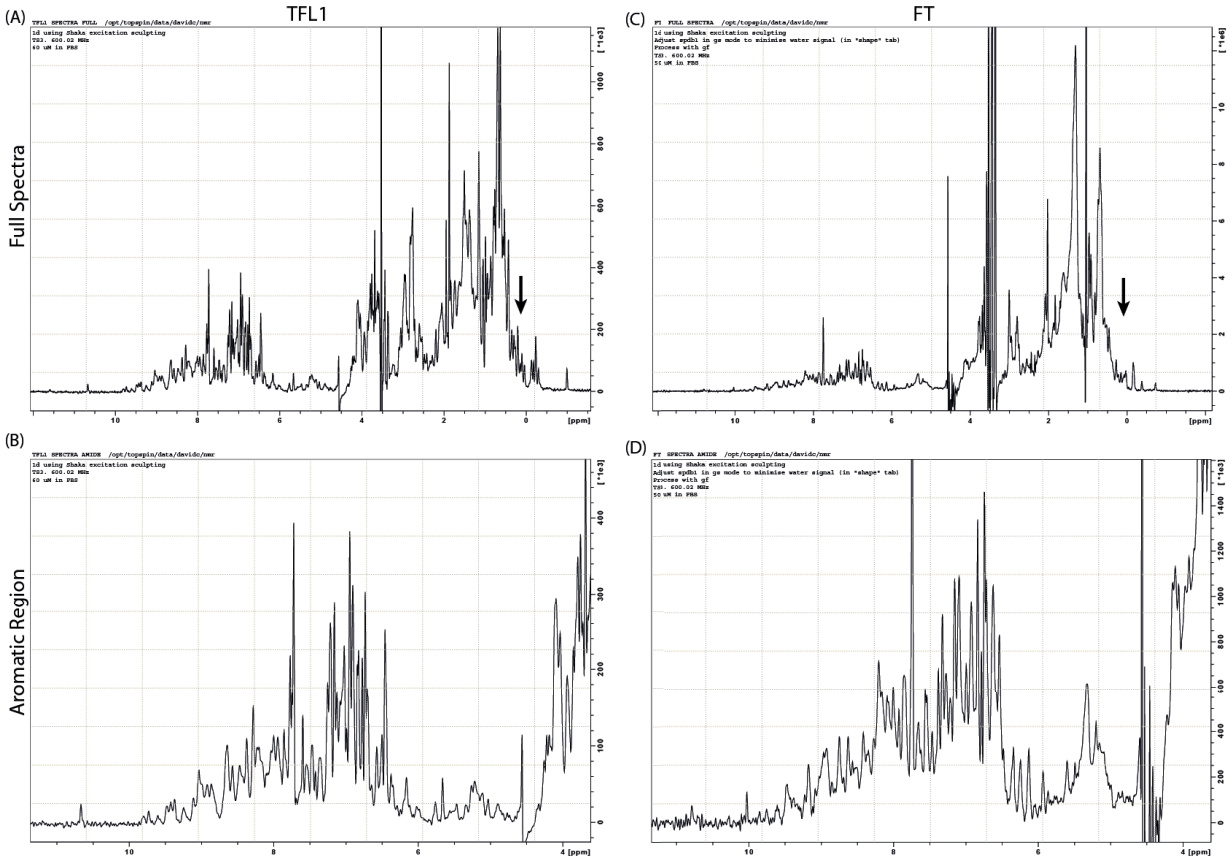


Figure 3.6: **1D NMR Spectra of TFL1 and FT after purification.** Chemical shift (ppm) is plotted against signal amplitude. **(A)** Peaks observed across the his-TFL1 NMR spectra feature several points of interest including peaks around 1 ppm which indicated folded protein **(B)** Detailed NMR spectra of his-TFL1 between 5 and 11 ppm. Several clear peaks were distributed between 8.5 and 6.5 indicating proper folding. **(C)** Peaks observed across the his-FT NMR spectra around 1 ppm indicate that his-FT is folded **(D)** Detailed NMR spectra between 5 and 11 ppm with several clear peaks between 8.5 and 6.5.

1D ^{1}H-NMR has been shown to be a suitable method for assessing whether proteins are correctly folded. his-TFL1 and his-FT were analysed by this method. Signals found between 8.5 and 11 ppm, within the aromatic region are indicative of folded proteins (Figure 3.6b; Figure 3.6d), as are peaks found around 1 ppm and below 0 ppm (Figure 3.6a; Figure 3.6c). Both his-TFL1 and his-FT had strong peaks between 8.5 and 11 ppm and peaks below 0 ppm, both of which were indicative of properly folded proteins.

3.3 Characterising the 14-3-3 Protein Family

3.3.1 Bioinformatics Analysis of the Arabidopsis 14-3-3 Protein Family

3.3.1.1 Sequences Similarity between 14-3-3s

14-3-3 proteins play an important role in mediating the activities of PEBPs. They are thought to facilitate interactions between PEBPs and other developmental regulators (Taoka et al., 2011). Phylogenetic analysis of the 14 members of the *Arabidopsis* 14-3-3 protein sequences suggests that an early duplication event divided the isoforms into four major groups and one outgroup containing the 14-3-3 Pi isoform alone. A secondary duplication event led to a split resulting in the epsilon isoform and non-epsilon isoforms. The non-epsilon isoforms underwent several duplication events resulting in the other major groups (Figure 3.7a). Sequences were compared by a multiple sequence alignment; significant sequence similarity can be observed between 14-3-3 isoforms particularly within regions predicted to form alpha helices (Figure 3.7b). The third, fifth, seventh and ninth alpha helices are highly conserved. These helices are predicted to be involved in the dimerization interface and the central ligand binding sites. The other alpha helices share large amounts of conservation (Figure 3.7b).

3.3.1.2 Selection of 14-3-3s

To explore the interactions between PEBPs and members of the 14-3-3 protein family, a model 14-3-3 was selected. Members of the Psi-Nu-Upsilon clade were selected because of their homology with GRF14c from Rice, a 14-3-3 that has been linked to floral activation and repression (Purwestri et al., 2009, Taoka et al., 2011). On average members of the Psi-Nu-Upsilon clade share approximately 87% sequence identity with GFR14c. In contrast, 14-3-3 Epsilon shares 71% sequence identity and 14-3-3 Psi shares 48% sequence identity. Of the members of the Psi-Nu-Upsilon clade, 14-3-3 Nu is most similar to GRF14c (approximately 88% sequence identity). Given the high sequence identity and the redundancy between 14-3-3 protein family; 14-3-3 Nu was used as a model 14-3-3 (Figure 3.7b).

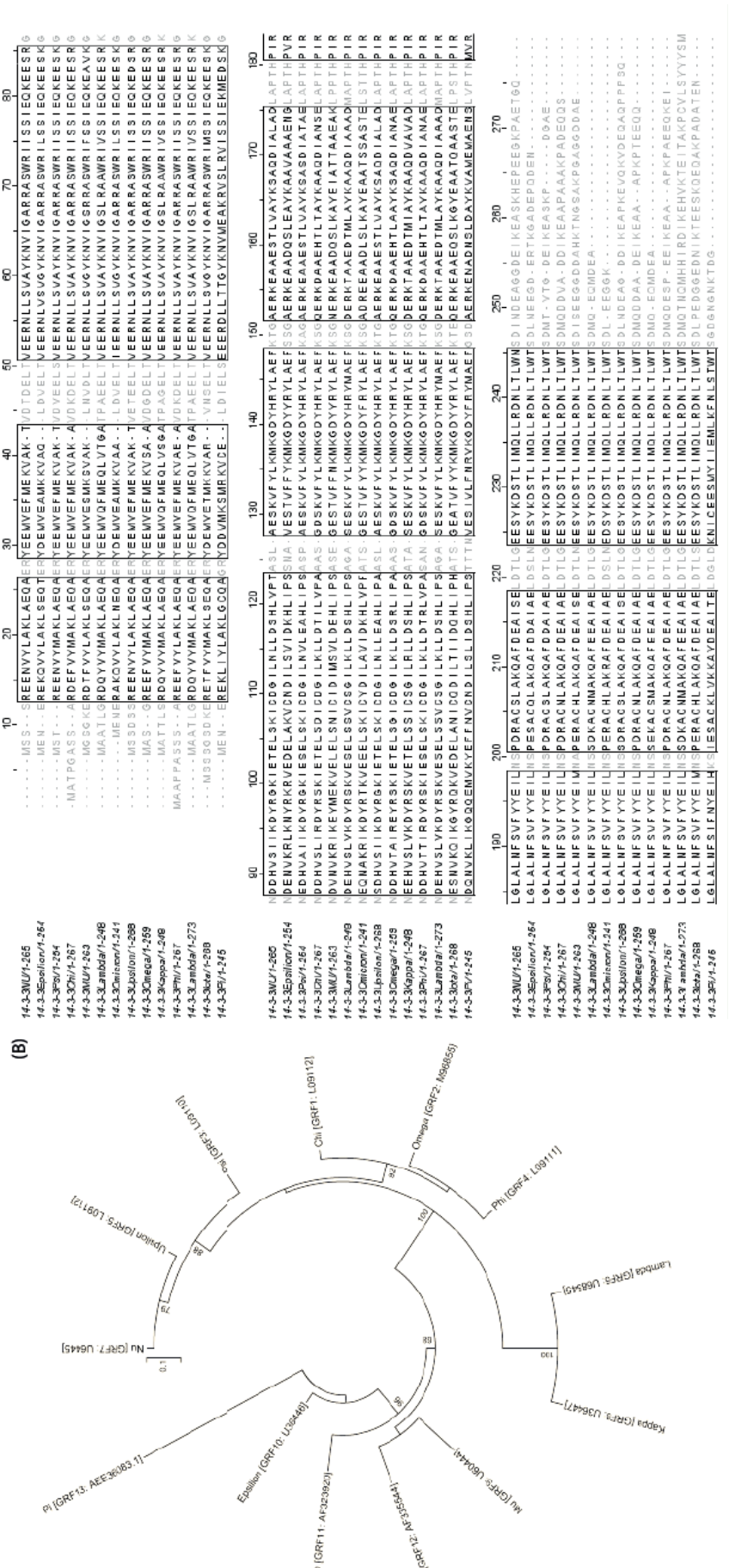


Figure 3.7: Analysis of Sequence Conservation amongst 14-3-3 Genes in Arabidopsis. (A) Inferred phylogeny of *Arabidopsis* 14-3-3 genes using the maximum likelihood method. There were a total 14 sequences in the final dataset. Phylogenetic analyses were conducted in MEGA4 (Tamura et al., 2007). **(B)** Multiple sequence alignment of *Arabidopsis* 14-3-3s aligned using the clustalW algorithm. Predicted structured α-helical elements are boxed.

3.3.2 Design of 14-3-3 Nu Constructs

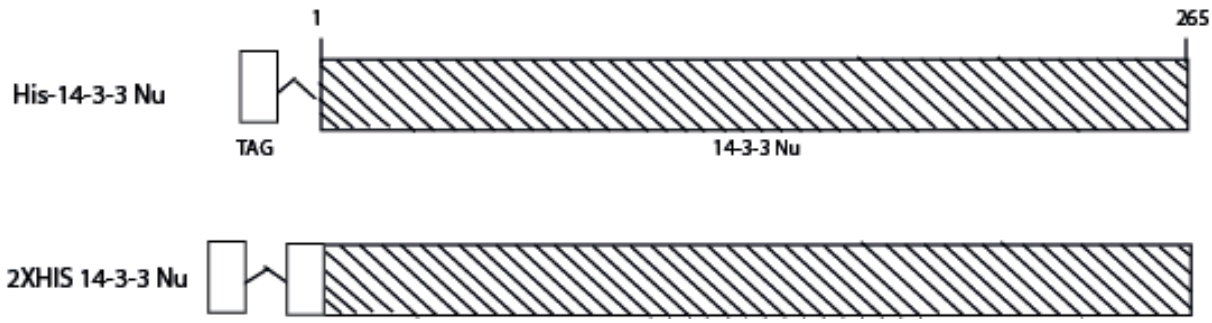


Figure 3.8: Design of 14-3-3 Nu Constructs. A series of construct were designed to encompass full length 14-3-3 Nu. A single construct cloned into pET53.

14-3-3 Nu was cloned into pET53 with a cleavable hexa-histidine tag and with an noncleavable dual hexa-histine tag (Figure 3.8). Double hexa-histine tags have been shown to enhance binding to nickel conjugated surfaces enabling stable immobilization on affinity columns allowing greater concentrations of imidazole to be used to remove contaminants from the target protein (Khan et al., 2006). However, long affinity tags have been shown to adversely affect crystallization and diffraction (Bucher et al., 2002). Consequently, two constructs were created.

3.3.3 Purification and Characterisation of 14-3-3 Nu

3.3.3.1 Purification of 2xHis 14-3-3 Nu

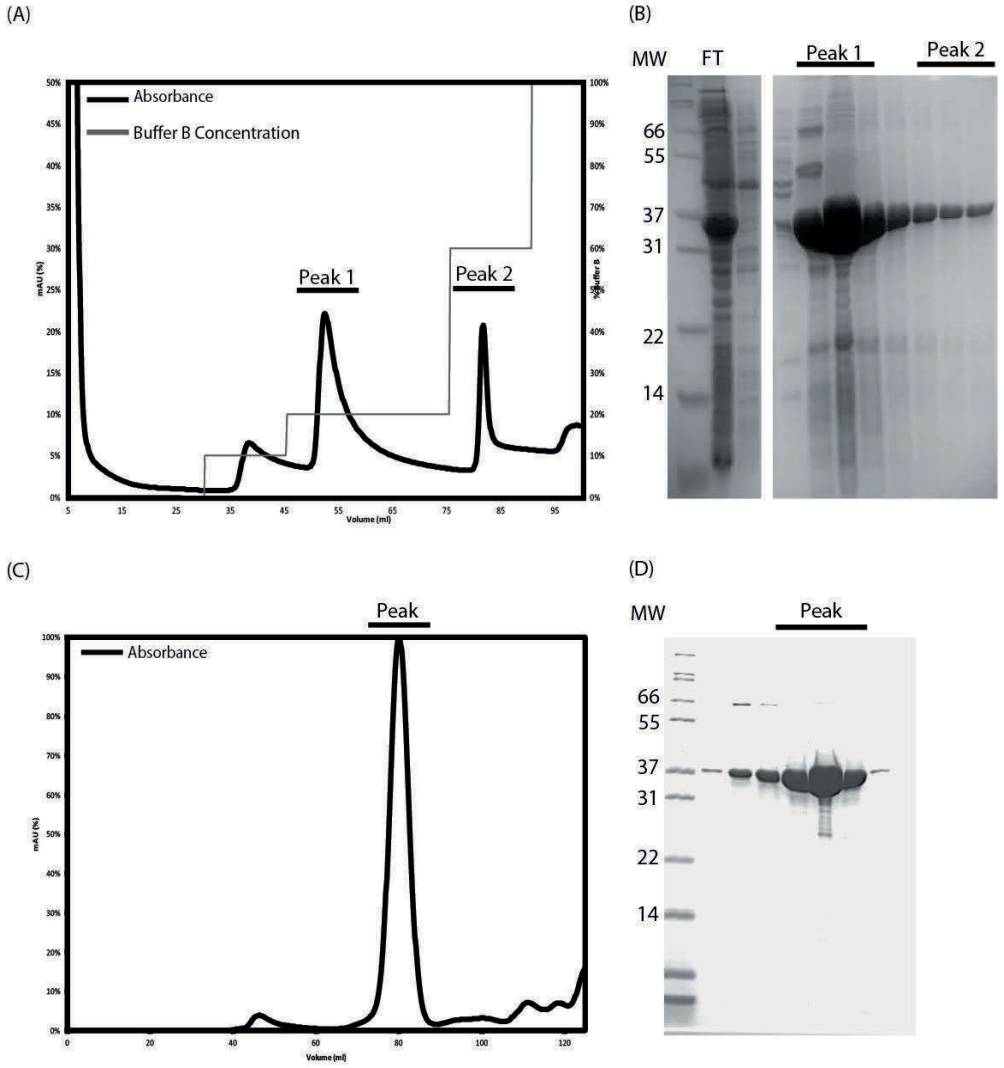


Figure 3.9: Purification of 2Xhis-14-3-3 Nu. Purification was conducted in two steps. **(A)** Nickel affinity purification of 14-3-3 Nu. **(C)** Gel Filtration of 2xhis-14-3-3 Nu. In these purification chromatograms the elution volume is plotted as the normalised absorbance at 280nm (mAU) on the primary axis. In the Nickel affinity step the secondary axis shows the elution volume plotted against the percentage of elution buffer. Samples were assessed by SDS Page **(B) (D)**.

Dual hexa-histidine tagged 14-3-3 Nu was purified as described in the materials and methods. Samples were initially subjected to Ni-Affinity. Fractions from the 40% and 60% washes were pooled (Figure 3.9a; Figure 3.9b), concentrated and further purified by gel filtration on an SD200 to separate any aggregated protein from the sample. A sharp protein peak was observed at approximately 80 ml (Figure 3.9c). The sample was assessed by SDS-PAGE and a band corresponding to 14-3-3 Nu (at approximately 30 KDa) was observed (Figure 3.9d). This was pure enough to be used for further work.

3.3.3.2 Purification of His 14-3-3 Nu

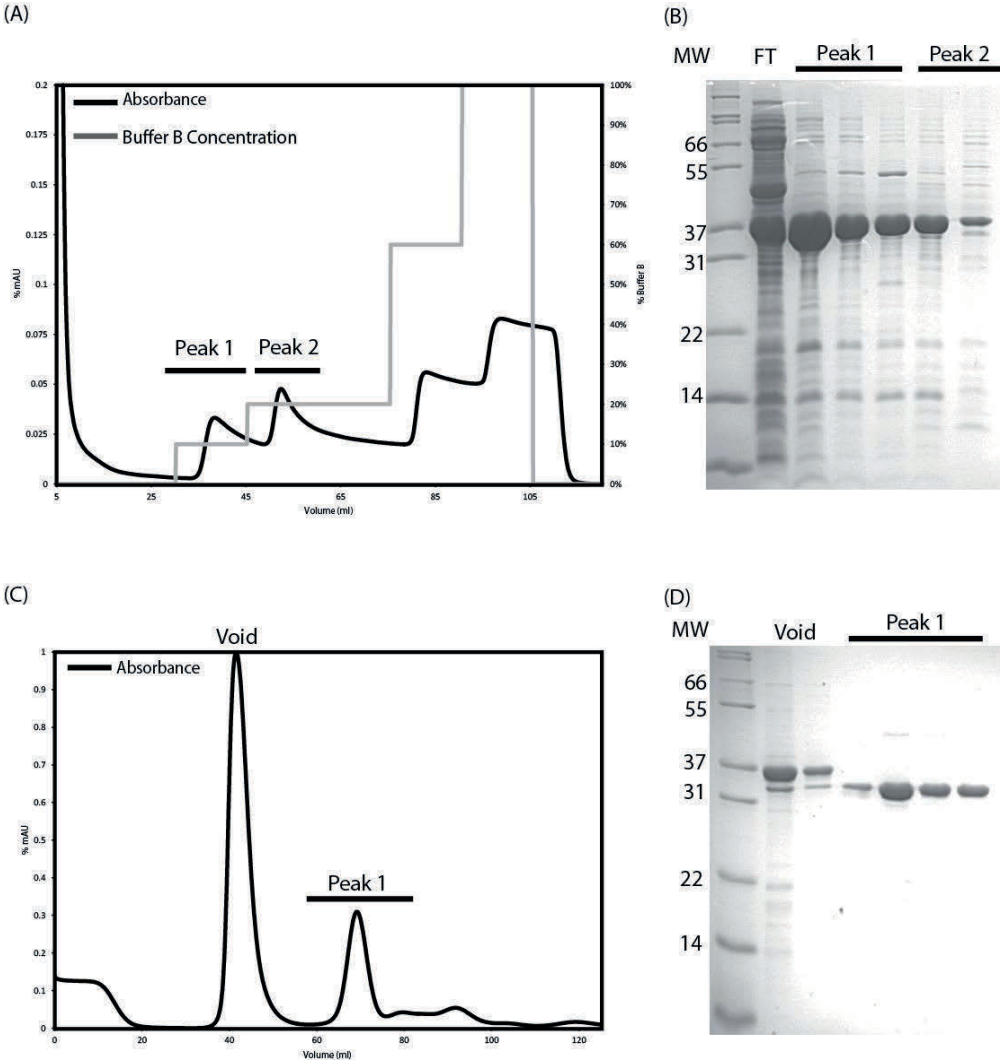


Figure 3.10: Purification of his-14-3-3 Nu. Purification was conducted in two steps. **(A)** Nickel affinity purification of 14-3-3 Nu. **(B)** Gel Filtration of his-14-3-3 Nu. In these purification chromatograms the elution volume is plotted as the normalised absorbance at 280nm (mAU) on the primary axis. In the Nickel affinity step the secondary axis shows the elution volume plotted against the percentage of elution buffer. Samples were assessed by SDS Page **(C) (D)**.

His-14-3-3 Nu was purified by a two step purification method as described in the materials and methods. Fractions from the Ni-affinity taken after the 10% and 20% wash were pooled (Figure 3.10a; Figure 3.10b). Protein was incubated with PreScission protease (GE Healthcare) left overnight at 4°C whilst being dialysed into gel filtration buffer. Protein was concentrated and further purified by gel filtration on an SD200 column. A void volume peak at 40ml containing aggregated uncleaved and cleaved 14-3-3 Nu was observed. Subsequently, a second peak at 80 ml was observed (Figure 3.10c). This peak contained a pure sample of cleaved 14-3-3 Nu (Figure 3.10d).

3.3.4 Mass Spectrometry of 14-3-3 NU

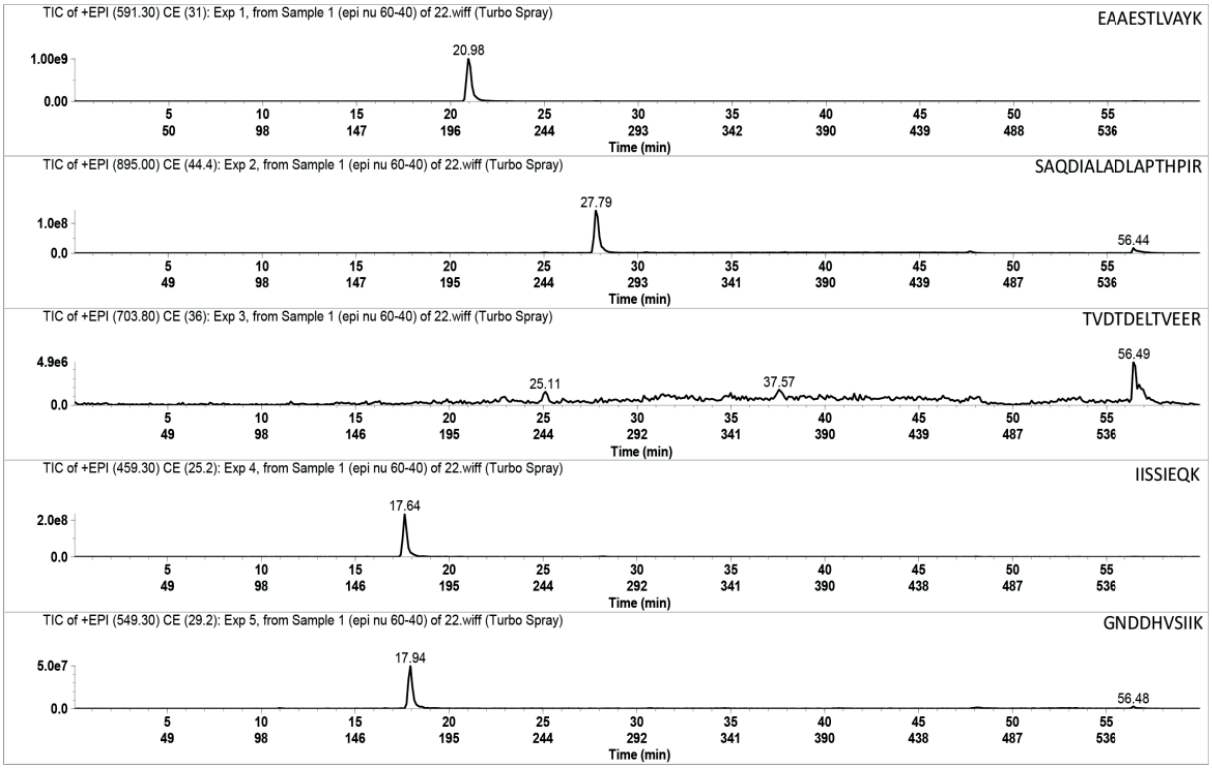


Figure 3.11: Peptides identified by mass spectrometry from samples of 14-3-3. Peptides from 14-3-3 Nu were identified. The sequence of the peptide is given alongside the chromatogram. Peptides derived from specifically 14-3-3 Nu were found indicating that the sample contains pure 14-3-3 Nu.

Given the sequence similarity between the members of the 14-3-3 protein family, a targeted method was created to detect peptides specific to 14-3-3 Nu to ensure that the correct protein had been purified. Five peptides were targeted. Two were specific to 14-3-3 Nu (GNDDHVSIIK and TVDTDELTVEER). One peptide (SAQDIALADLAPTHPIR) was common to 14-3-3 Nu and Upsilon. The peptide EAAESTLVAYK was common to all members of the Psi-Nu-Upsilon clade. The peptide ISSIEQK was found in several members of *Arabidopsis* 14-3-3 family. Four peptides (GNDDHVSIIK, SAQDIALADLAPTHPIR, ISSIEQK, EAAESTLVAYK) were identified in purified protein samples confirming the presence of 14-3-3 Nu (Figure 3.11).

3.4 Purification and Characterisation of FD

3.4.1 Bioinformatics Analysis of FD

Proper protein folding is a prerequisite for structural characterization. An initial assessment of the topology of FD was conducted using the PSIPRED secondary structure prediction method. This information was used to design appropriate expression constructs (Jones, 1999). FD is predicted to be composed of five α-helices connected by several unstructured regions. The largest structured region is an α-helix found towards the C-terminus. The C-terminal helix contains a bZIP domain beginning at residue 216 and ending at residue 267 (though the α-helix begins at residue 209).

A putative phosphorylation site at position 282 was well conserved amongst bZIP family members. All members had either a serine or threonine in that position. Phosphorylation has been shown to play an important role in the formation of a FT-FD complex (Abe et al., 2005). To replicate the physiologically important phosphorylation at position 282, phosphorylation mimics were constructed. Thr^{282} was replaced with either aspartic acid or glutamic acid to mimic a phosphorylated amino acid (Maciejewski et al., 1995).

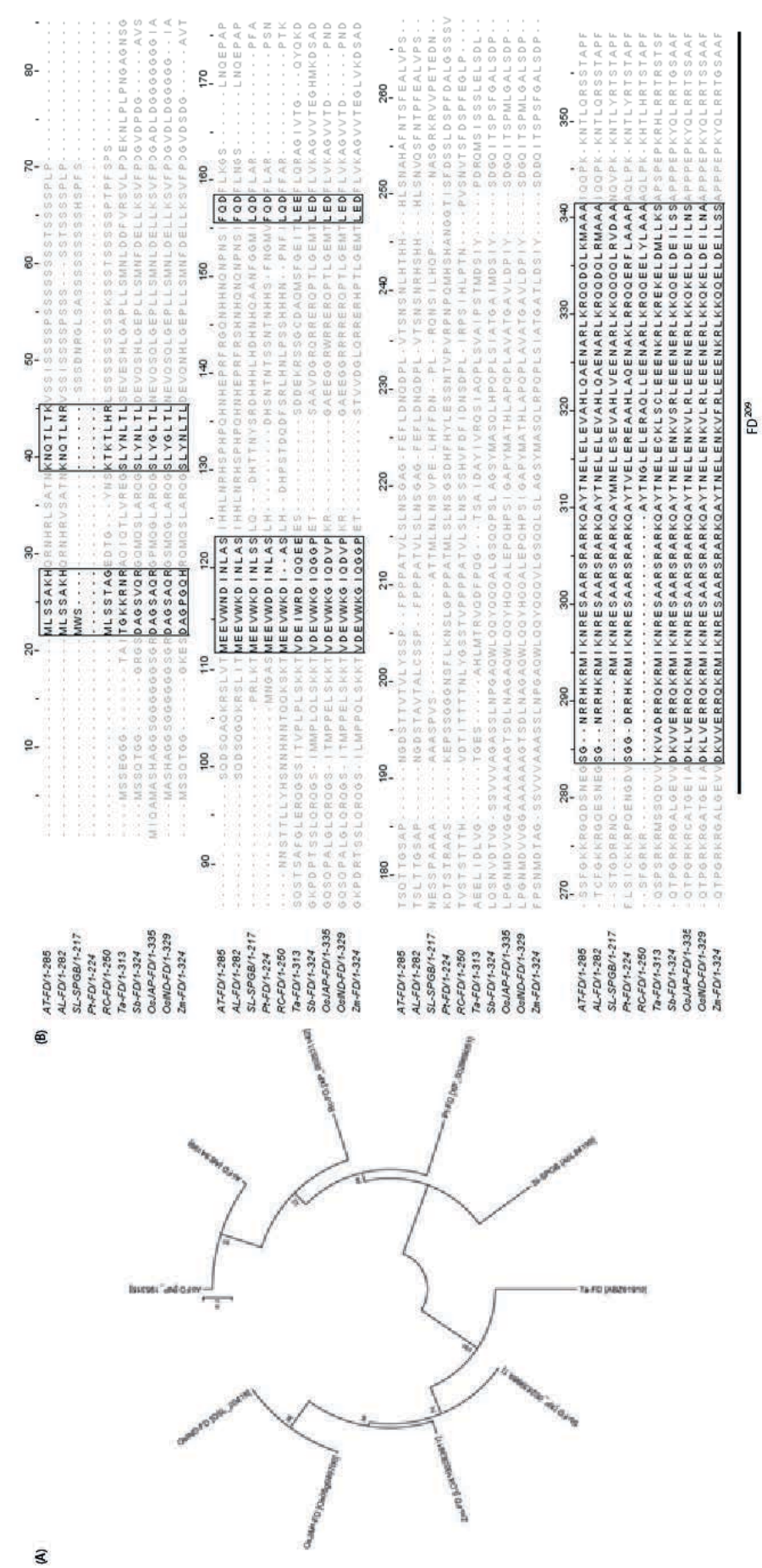


Figure 3.12: Analysis of Sequence Conservation amongst FD Homologs. (A) Inferred phylogeny of FD-Like genes using the maximum likelihood method. There were a total 10 sequences in the final dataset. Phylogenetic analyses were conducted in MEGA4 (Tamura et al., 2007). **(B)** Multiple sequence alignment of FD genes aligned using the clustalW algorithm. Predicted structured α-helical elements are boxed. Regions outside of boxed area have no predicted structure. Asterisk marks position 282 which was converted by mutagenesis into an aspartic acid (T282D) or a glutamic acid (T282E).

3.4.2 Designing FD Constructs

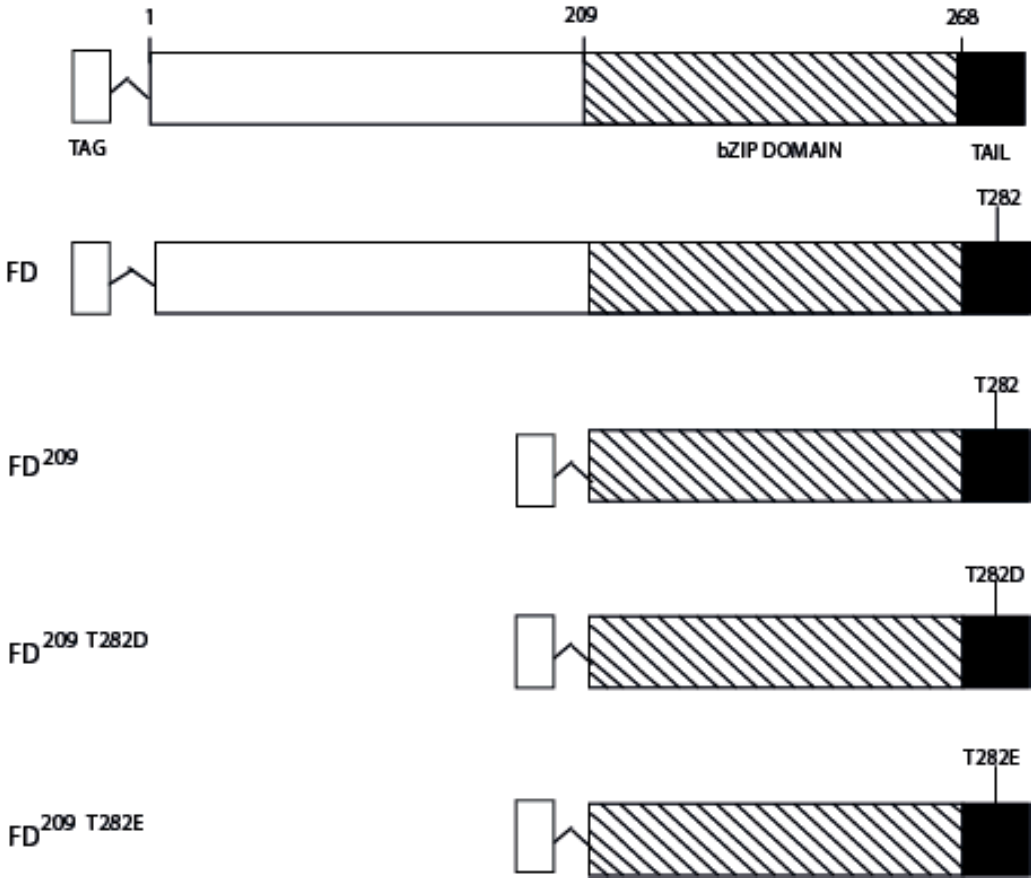


Figure 3.13: Design of FD Constructs. A series of constructs were designed based upon the predicted secondary structure of FD. Alongside the full length protein a series of C-terminal constructs were produced including C-terminal phosphorylation mimic including FD209 ^{T282D} and FD209 ^{T282E}. GST and his-tag constructs were built for truncated constructs. All constructs were built with a cleavable linker.

Based on bioinformatics several FD constructs were created (Figure 3.13). Full length FD was cloned into the vectors pET26 and pET28, enabling expression of untagged and his-tagged FD. In addition, a series of truncated constructs starting at the 209th amino acid were created. Truncated FD$^{209\text{-}285}$, FD$^{209\text{-}285\ T282E}$ and FD$^{209\text{-}285\ T282D}$ were also cloned into the vectors, pET26 and pET28. These truncated constructs were subsequently cloned into a pGEX vector, pGEX-6P-1, to enable expression of truncated FD with an N-terminal GST tag, which has been shown to enhance protein solubility (Khan et al., 2006). All constructs were confirmed by sequencing.

3.4.3 Purification of FD209 T282E

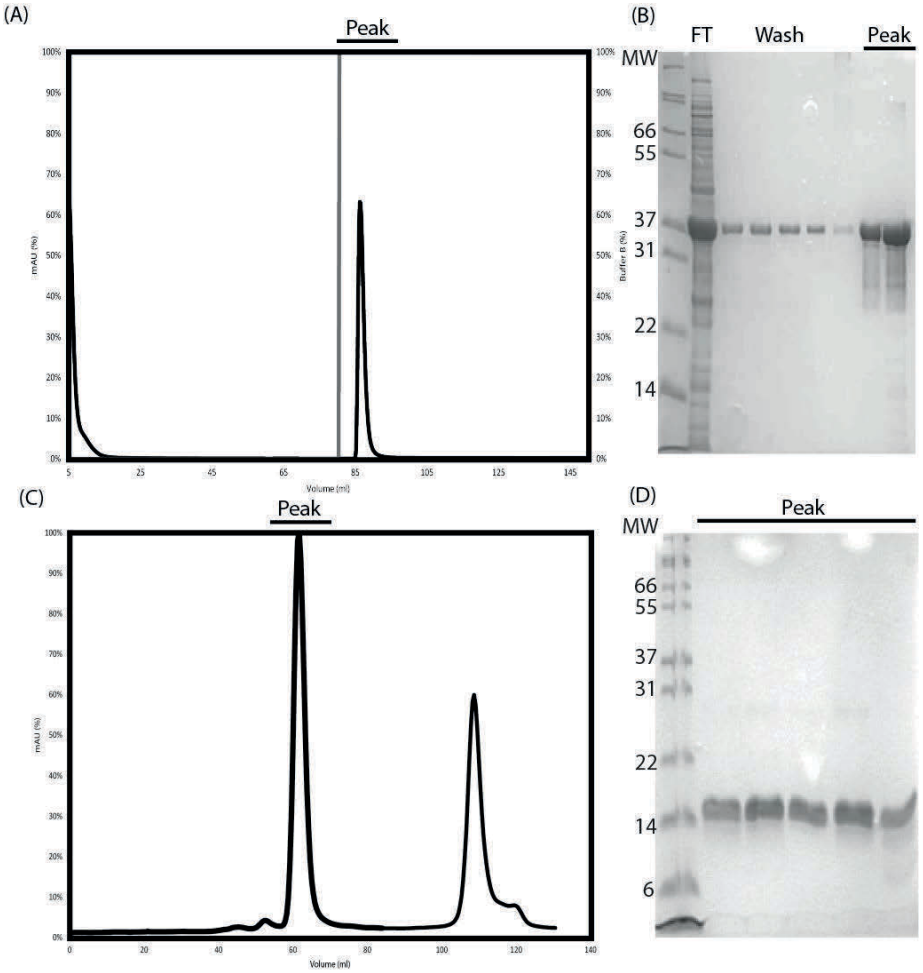


Figure 3.14: Two step purification of FD209 ^{T282E}. (A) GST affinity purification of GST-FD209. **(B)** Gel filtration of cleaved FD209 ^{T282E}. In these purification chromatograms the elution volume is plotted as the normalised absorbance at 280nm (mAU) on the primary axis. In the GST affinity step the secondary axis shows the elution volume plotted against the percentage of elution buffer. Samples were assessed by SDS Page **(C) (D)**.

GST-tagged proteins were purified using a 5 ml GST-trap column (GE Healthcare). Cleared lysate was loaded onto the column using a peristaltic pump and protein was eluted using a pre-prepared ÄKTA system. A sharp peak containing a protein with an approximate molecular weight of 36 KDa was observed during the elution step (Figure 3.14a; Figure 3.14). The GST-tag was removed by enzymatic cleavage with prescission protease (GE Healthcare). The GST-tag was then separated from cleaved FD by passing the solution through a GST-column. The flow-through was concentrated and subjected to further purification by gel filtration with an SD75 column. A peak at 61.9 ml was observed corresponding to FD$^{209\ T282E}$ (Figure 3.14b Figure 3.14d). This sample was >95% pure and consequently was used in biochemical assays.

3.4.4 Mass Spectrometry of FD209 T282E

Table 3.3: Peptides identified by Mass Spectrometry from Samples of his-FD. The sequence of the peptide is given alongside the confidence score, the name of protein and accession number that the peptide is associated with. Peptides derived from FD were identified indicating that the sample contains pure FT.

Sequence	Names	Annotation	Confidence
KQAYTNELELEVAHLQAENAR	FD	AT4G35900.1	99
QAYTNELELEVAHLQAENAR	FD	AT4G35900.1	99
MAAAIQQPK	FD	AT4G35900.1	93.0

Mass spectrometry was employed to confirm that samples contained $FD^{209\ T282E}$. Purified $FD^{209\ T282E}$ was subjected to tryptic digest but because of the limited size of $FD^{209\ T282E}$ resulted in only a limited number of peptides being identified. Thought the peptides fragments were sufficient to enable identification of FD209; the peptides identified did not cover the glutamic acid at position 282. Two related peptides, KQAYTNELELEVAHLQAENAR and QAYTNELELEVAHLQAENAR, which were unique to FD were identified with >95% confidence.

3.4.5 1D NMR of FD209 T282E

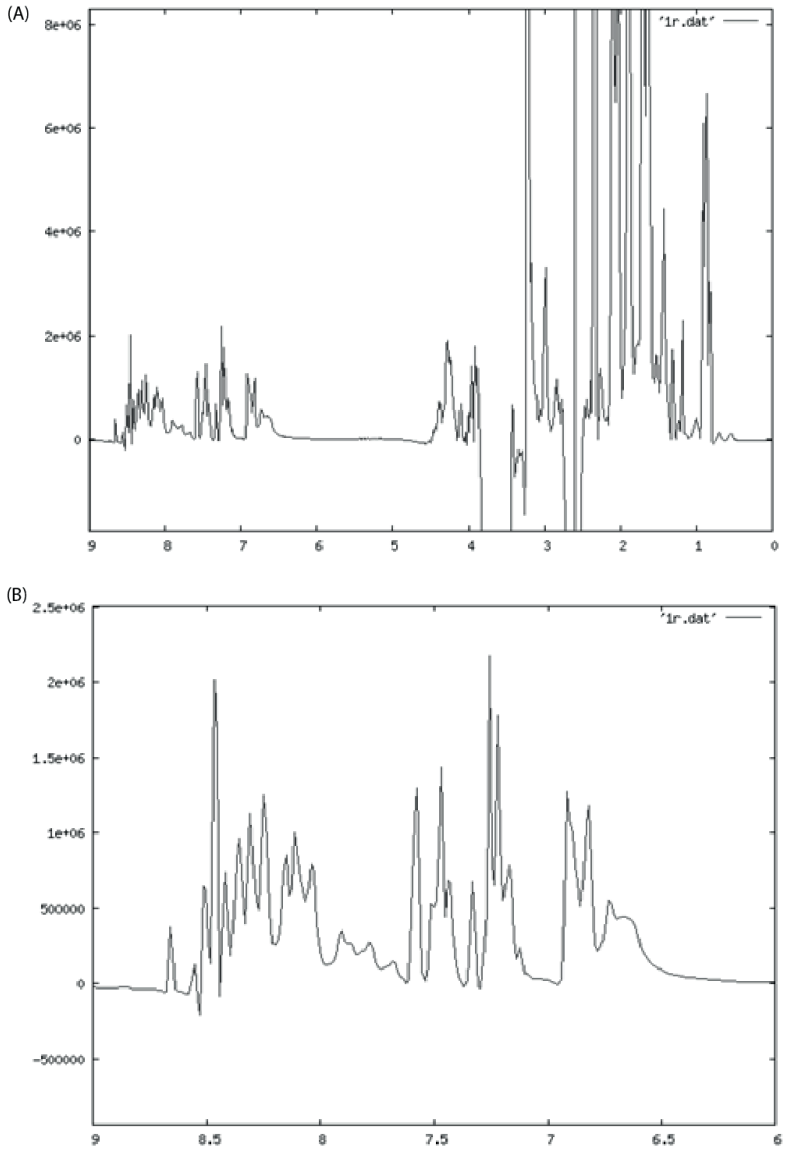


Figure 3.15: 1D 1H-NMR of FD209 ^{T282E} (A) Peaks observed across the NMR spectra feature several points of interest including peaks around 1 ppm within the aliphatic region of the spectrum. **(B)** Detailed NMR spectra between 6 and 9 ppm show several clear peaks distributed between 8.5 and 6.5.

Signals for FD$^{209\ T282E}$ were found beyond 8.5 ppm suggesting that protons were being exposed to a variety of shielding effects suggesting that FD$^{209\ T282E}$ was folded (Figure 3.15b). Signals around 10 ppm, normally associated with tryptophan were not found in FD$^{209\ 282E}$ because FD$^{209\ 282E}$ contains no tryptophan. Peaks found around 1 ppm were also observed (Figure 3.15a).

3.5 Discussion

3.5.1 Expression and Purification of the PEBPs

TFL1 and FT are key regulators of flowering (Ahn et al., 2006, Hanano and Goto, 2011). In this study, the two floral PEBPs were produced recombinantly in *E.coli*. Constructs enabling the expression of TFL1 and FT with and without a cleavable histidine tag were created. Although both constructs were capable of expression, the constructs producing proteins with histidine tags were used for ease of purification. FT and TFL1 were expressed as soluble proteins and at high yield. In the past the expression of plant proteins (including TFL1) in *E.coli* has been hindered by poor solubility (Nishiyama et al., 2003). Previously, similar technical challenges have been overcome by the use of chemical denaturation followed by dilution and refolding (Ahn et al., 2006). The evidence suggests that it is possible to produce soluble TFL1 after autoinduction at 22°C for 16 hours. The success of these techniques may partly be due to decreasing the temperature to 22°C during expression. The hydrophobic interactions that typically drive aggregation are reduced at low temperatures (Kiefhaber et al., 1991). In addition, to this slower expression may reduce the impact of the metabolic burden placed upon an organism during overexpression (Reviewed in Sorensen and Mortensen, 2005). This makes sense as the high yields associated with autoinduction are linked closely with high cell densities which infers that the contribution by individual cells to the overall yield may be lower (Sivashanmugam et al., 2009).

After expression and purification samples were tested by 1D NMR, which confirmed that they are folded and were suitable for further structural studies. This methodology represents a practical strategy for the production of the flowering regulators, FT and TFL1, which may facilitate further structural and functional studies.

3.5.2 Analysis, Expression and Purification of the 14-3-3s

3.5.2.1 Sequence Analysis of 14-3-3s

The 14-3-3 proteins in *Arabidopsis* are highly conserved. The most variable regions are found around the N and C termini of the proteins and though they have been implicated in protein-protein interaction they

are not involved in PEBP 14-3-3 interaction binding. In rice, the last two α-helices of GF14c have been shown to be directly involved in interacting with HD3a (Taoka et al., 2011). HD3a has been shown to interact with several rice 14-3-3s, despite the variability at the C-terminus (Taoka et al., 2011). This may be because the residues that are involved in binding are highly conserved across all 14-3-3 proteins and are found within the highly conserved α-helices. This may also explain why redundancy has been observed (Lu et al., 1994). Simply, the sequence similarities between the 14-3-3 proteins are sufficient to mediate several different interactions.

3.5.2.2 Expression and Purification

14-3-3 Nu was chosen due to the high sequence similarity with GF14c, a 14-3-3 protein that has been shown to act as both a negative and positive regulator of flowering (Purwestri et al., 2009, Taoka et al., 2011). 14-3-3 Nu was expressed and purified. No aggregation was observed after gel filtration suggesting that the protein was stable in buffer. Samples of 14-3-3 Nu were not tested by 1D NMR because the molecular weight of the protein was beyond a testable threshold; large proteins typically produce uninterpretable spectra, with extremely high numbers of amide peaks.

3.5.3 Expression and Purification of the FD

The C-terminal α-helix of FD has been shown to be important for the interaction with FT (Abe et al., 2005). To examine a functionally relevant domain of sufficient stability, a C-terminal truncation of FD was created. As phosphorylation at position 282 has been identified as important for interaction (Abe et al., 2005). Phosphorylation mimics were constructed with a glutamic acid at that position to overcome the problem associated with phosphorylation-dependent interaction (Maciejewski et al., 1995, Ahn et al., 2006).

3.6 Summary

Three critical components of the flowering pathway FT, TFL and FD were cloned and expressed in an *E.coli* expression system. The expression conditions were optimised to obtain large amounts of soluble TFL1 and FT. A C-terminal truncation of folded FD was also cloned and purified to homogeneity. A model

Arabidopsis 14-3-3, 14-3-3 Nu, was selected, cloned, expressed and purified to homogeneity. Components were tested and shown to be folded by 1D NMR.

Chapter 4 - Interaction Between TFL1 and 14-3-3s

4.1 Introduction

TFL1 plays a key role in the onset of flowering (Kobayashi et al., 1999). TFL1 acts antagonistically to FT by repressing the transcription of genes associated with flowering (Hanano and Goto, 2011). It has been proposed that the interaction between FT and members of the 14-3-3 protein family plays an essential role in the induction of flowering (Taoka et al., 2011). However, currently there is little information regarding the interaction between TFL1 and members of the 14-3-3 family of proteins. To elucidate the precise mechanism by which TFL1 negatively regulates flowering, this study examines the interaction between the model 14-3-3 protein, 14-3-3 Nu and TFL1 to understand the structural basis for the antagonistic activities of FT and TFL1.

4.2 Results

4.2.1 Assessment of TFL1 14-3-3 Binding by NMR

To characterise the interaction between TFL1 and 14-3-3 Nu solution structural studies of TFL1 were conducted. An initial assessment of the interaction was conducted by 1D NMR. A 1D spectrum of TFL1 was taken before and after the addition of 14-3-3 Nu (at a 1:5 M equivalent ratio). The TFL1 spectra indicated that TFL1 was correctly folded (Figure 4.1a). The intensity of the TFL1 signal decreased significantly upon the addition of 14-3-3 Nu inferring that an interaction had occurred between the two proteins (Figure 4.1). The interaction was further characterised by multidimensional NMR. Upon the increasing addition of 14-3-3 Nu large chemical shifts were observed in the 2D 1H- 15N TROSY spectrum of TFL1 (Figure 4.2; Figure 4.3). Several peaks within the spectrum disappeared upon the addition of 14-3-3 Nu suggesting that TFL1 was capable of forming a complex with 14-3-3 Nu. A large disappearance of peaks was observed when labelled TFL1 was mixed with 14-3-3 Nu in 1:5 M equivalent ratio further indicating that TFL1 can interact directly with 14-3-3 Nu (Figure 4.2c).

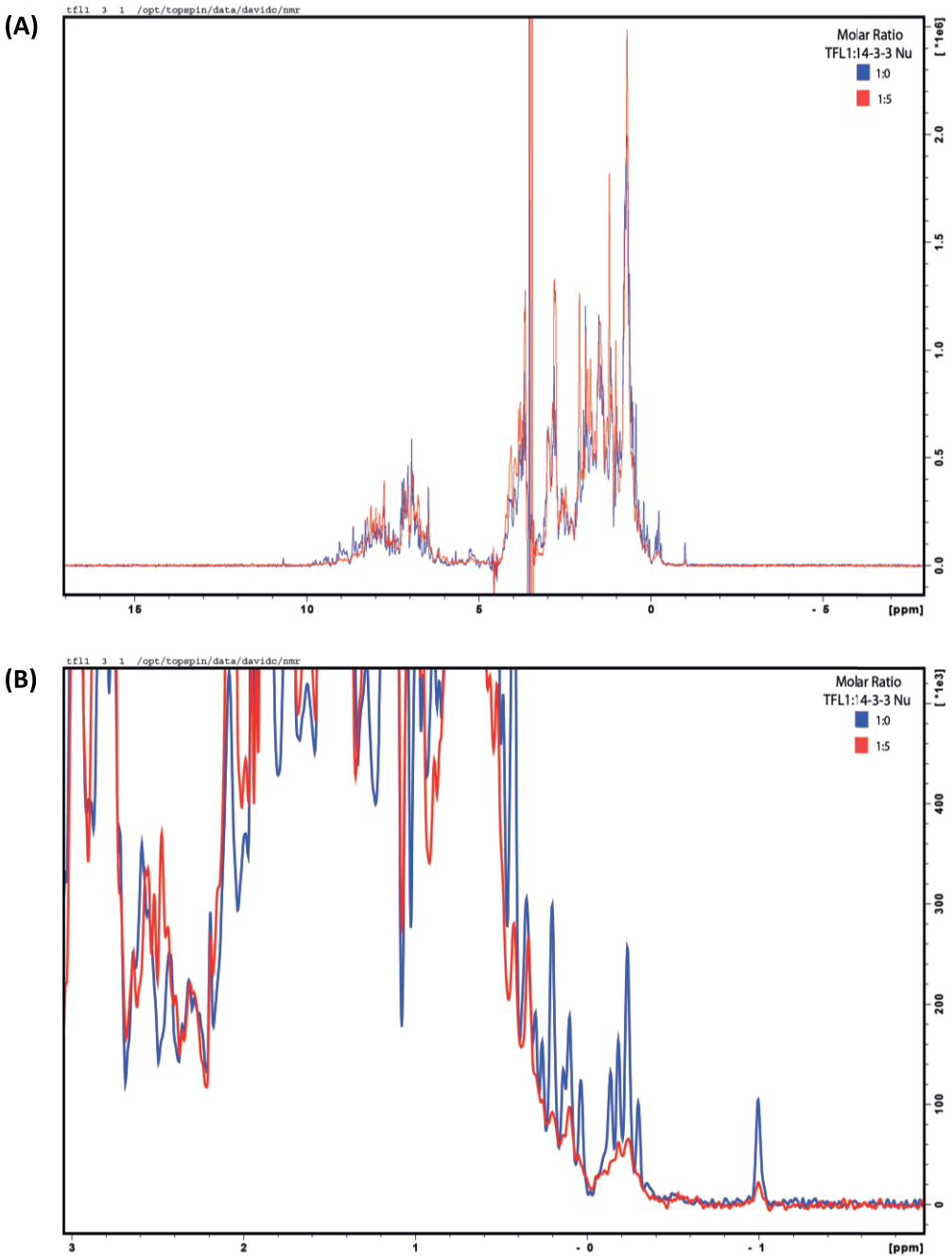


Figure 4.1: 1D NMR Spectra of recombinant full-length TFL1 with excess 14-3-3 Nu. The spectrum of TFL1 alone (Blue) overlaid with a spectrum TFL1 with 5 times molar excess of 14-3-3 (Red). High signal dispersion and strong signals was observed before addition 14-3-3 Nu. Intensity of the signal from peaks in the across the spectra decreased significantly after the addition of 14-3-3. **(A)** Full TFL1 1NMR Spectra. **(B)** Methyl region of the spectra.

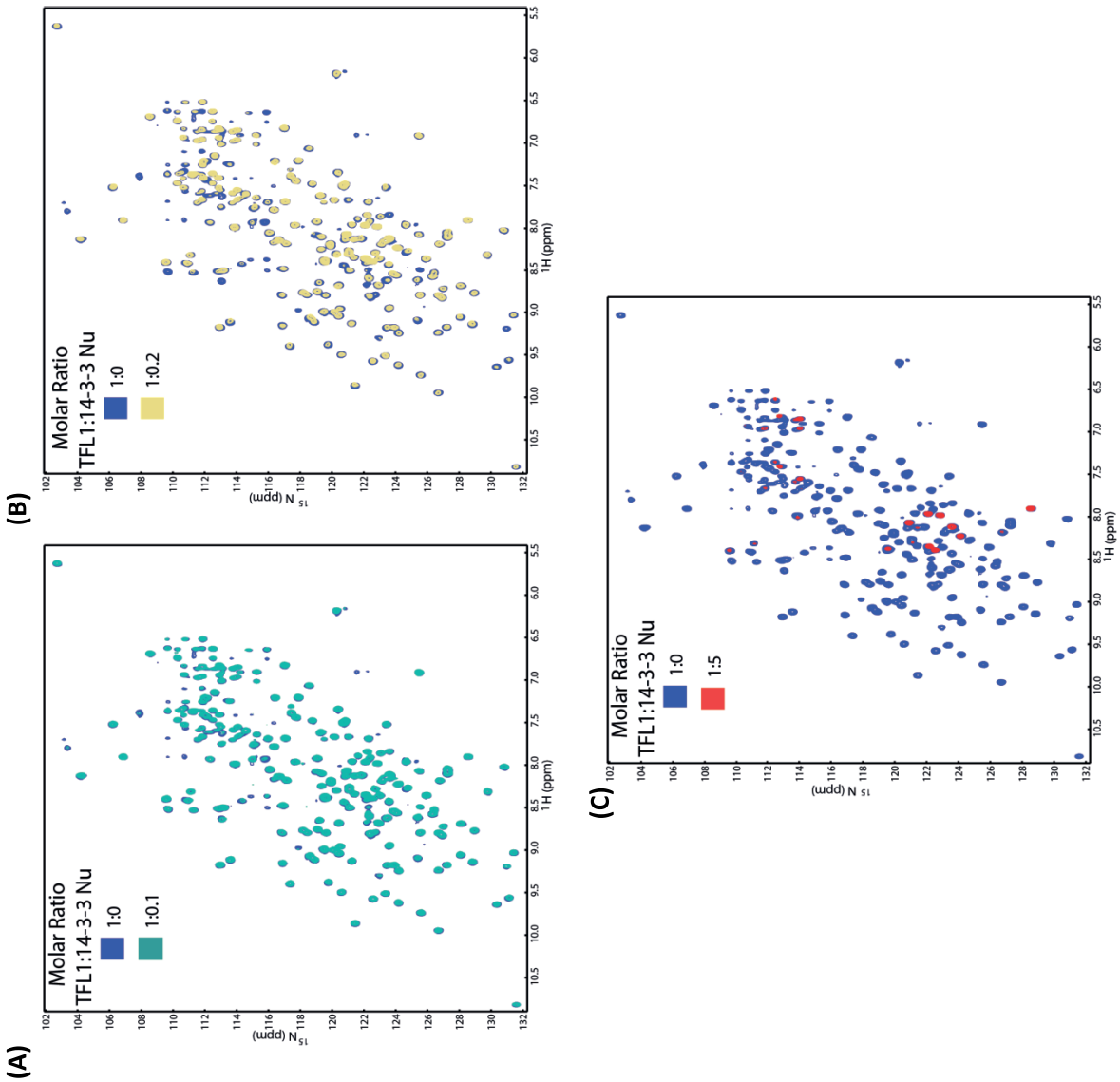


Figure 4.2: Interaction of TFL1 with 14-3-3 Nu using NMR. Spectra of ^{1}H-^{15}N TROSY spectrum of TFL1 with either 0.1, 0.2 or 5 molar equivalents of 14-3-3 Nu. The presence of dark blue peaks indicates an a chemical shift perturbance where the overlaid peaks have decreased in intensity. PPM: Parts per million.

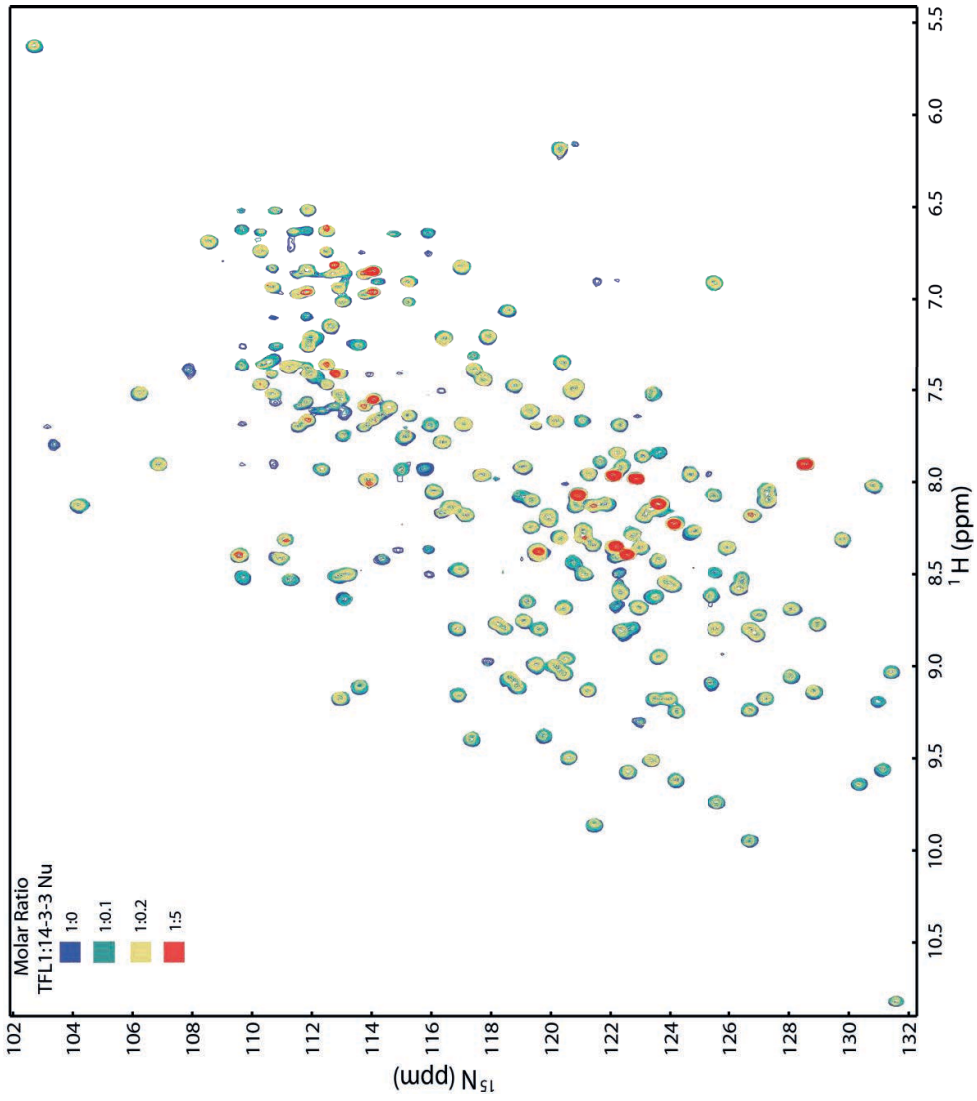


Figure 4.3: Chemical Shift perturbation of TFL1 caused by the interaction with 14-3-3 Nu using Multi dimensional NMR. Overlay showing the ^{1}H-^{15}N TROSY spectrum of TFL1 shows different peak shift changes in the presence of 14-3-3 Nu. Free TFL1 spectrum is blue. TFL1 in the presence of 1 to 0.1 (Green), 1 to 0.2 (Yellow) and 1:5 (Red) M equivalents. Increasing the concentration of 14-3-3 Nu causes a decrease in intensity of particular peaks thus dark blue, green and yellow peaks are present in the spectra. PPM: Parts per million.

4.2.2 Quantitative Assessment of TFL1 14-3-3 Binding

4.2.2.1 Assessment of TFL1 14-3-3 Binding by EMSA

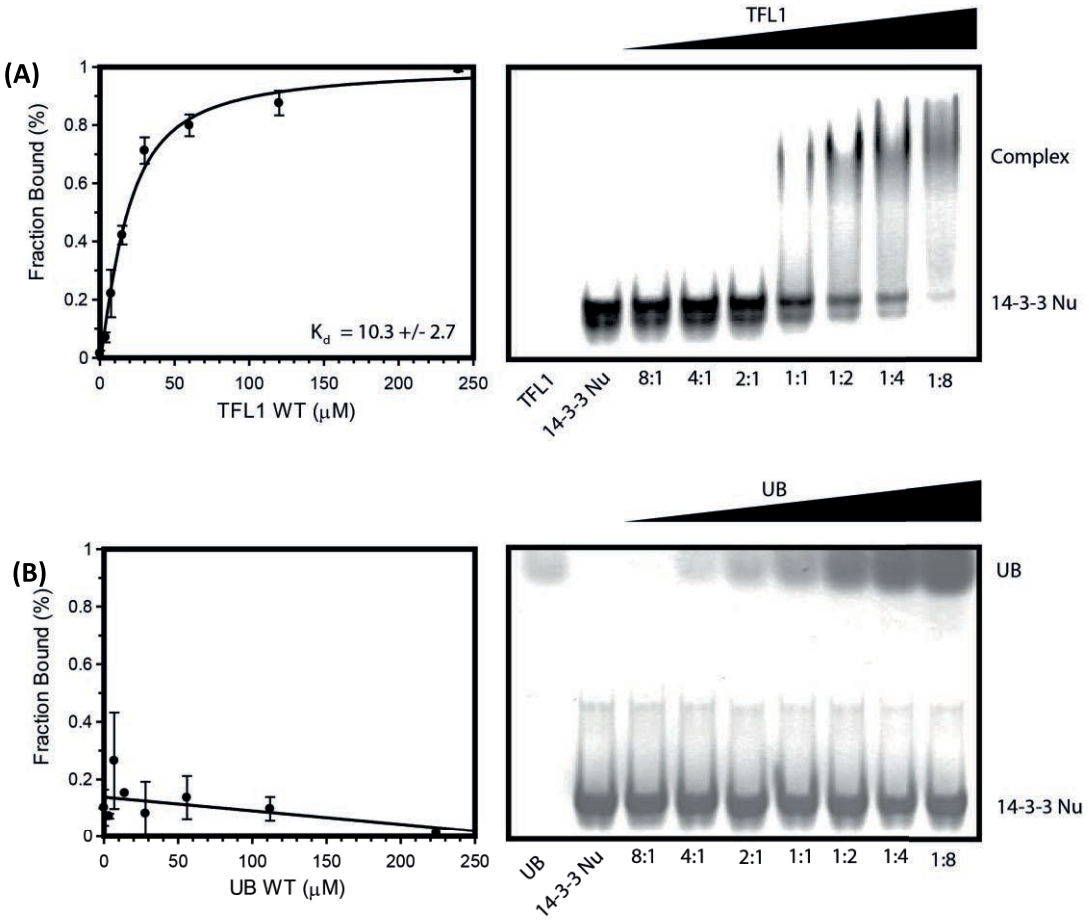


Figure 4.4: Assessment of the Specificity of Binding by Gel Mobility Shift Assay. Full-length his-TFL1 was titrated against 2xhis-14-3-3 Nu. 14-3-3 Nu is retarded by the interaction with his-TFL1 causing a shift band. **(A and B)** Binding of 14-3-3 Nu by TFL1. The fraction of free 14-3-3 is plotted as a function of the concentration of TFL1. **(C and D)** Binding of 14-3-3 Nu by Ubiquitin (UB). The fraction of free 14-3-3 is plotted as a function of the concentration of UB.

EMSAs were used to investigate the specificity of the interaction between TFL1 and 14-3-3 Nu. Full length his-tagged TFL1 was titrated against tagged 14-3-3 Nu. A decrease in the intensity of 14-3-3 Nu was observed with increasing concentrations of TFL1 (Figure 4.4a). The formation of complex was confirmed by the presence of a band shift in lanes containing both TFL1 and 14-3-3 Nu. Free TFL1 was allowed to run off the gel. Quantification of the interaction revealed a dissociation constant (Kd) of ~10.3 μM +/- 2.7 μM. No interaction was observed between ubiquitin and 14-3-3 Nu, confirming the specificity of the interaction (Figure 4.4b).

4.2.2.2 Assessment of TFL1 14-3-3 Binding by Thermophoresis

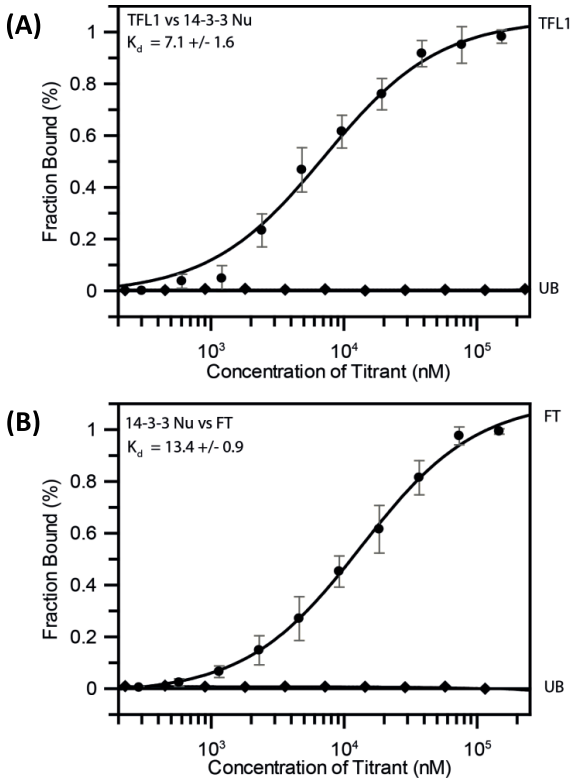


Figure 4.5: Interaction of TFL1 and FT with 14-3-3 Nu using Microscale Thermophoresis. Interaction causes a change in thermophoresis consistent with binding. Normalised fluorescence is plotted against concentration of titrated protein. **(A)** TFL1 titrated into 14-3-3 Nu. **(B)** 14-3-3 Nu titrated into FT. Control reactions conducted by titrating in UB.

The affinity of TFL1 for 14-3-3 Nu was assessed by microscale thermophoresis. Purified his-tagged TFL1 was titrated into fluorescently labelled 14-3-3 Nu. The interaction of TFL1 to 14-3-3 Nu was dose-dependent and saturable with an estimated Kd of 7.1 +/- 1.6 µM (Figure 4.5a). No binding was observed between ubiquitin and labelled 14-3-3 Nu. The reciprocal experiment was conducted to compare the interaction between FT and 14-3-3 Nu. 14-3-3 Nu was titrated into labelled FT, owing to the greater concentration of 14-3-3 Nu. Saturable, dose-dependent binding was observed and a Kd of 13.4 +/- 0.9 µM was estimated (Figure 4.5b). To ensure specificity ubiquitin was titrated into labelled FT. No interaction was detected. Taken together, this confirms that TFL1 and FT bind to 14-3-3 proteins with similar affinities. Moreover, this suggests that TFL1 can form a complex specifically with 14-3-3 Nu, hereafter known as the proto-Floral Inhibitory Complex (FIC). Likewise, FT can interact with 14-3-3 proteins to form a proto-Florigen Activation Complex.

4.2.3 Crystallization of the Proto-Floral Inhibitory Complex

4.2.3.1 Initial Crystallization Screens and Characterization of initial Hits

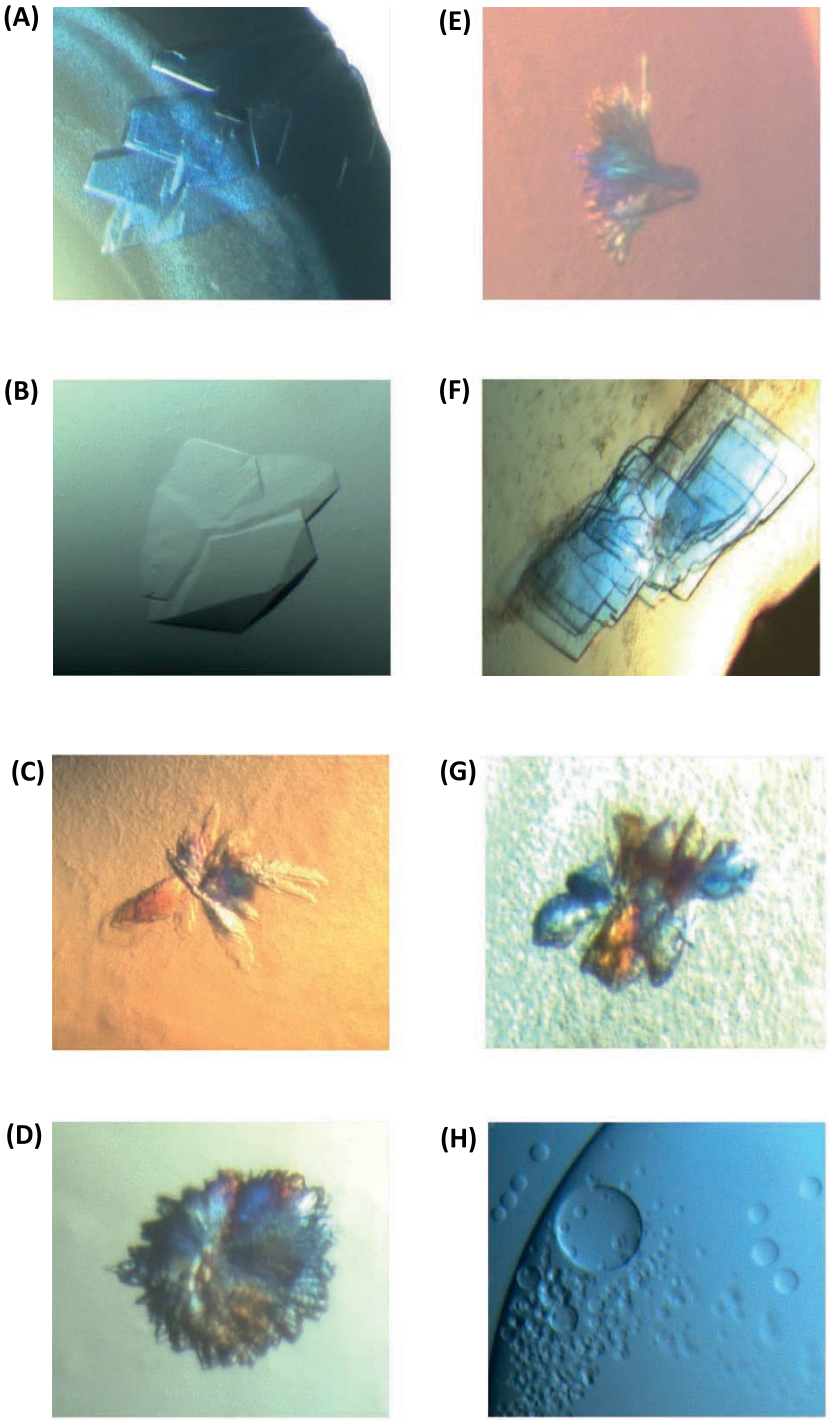


Figure 4.6: Putative initial hits in TFL1-14-3-3 Nu Crystallization Trials. Hits were evaluated visually and suitable hits **(A, B and F)** were screened by X-rays.

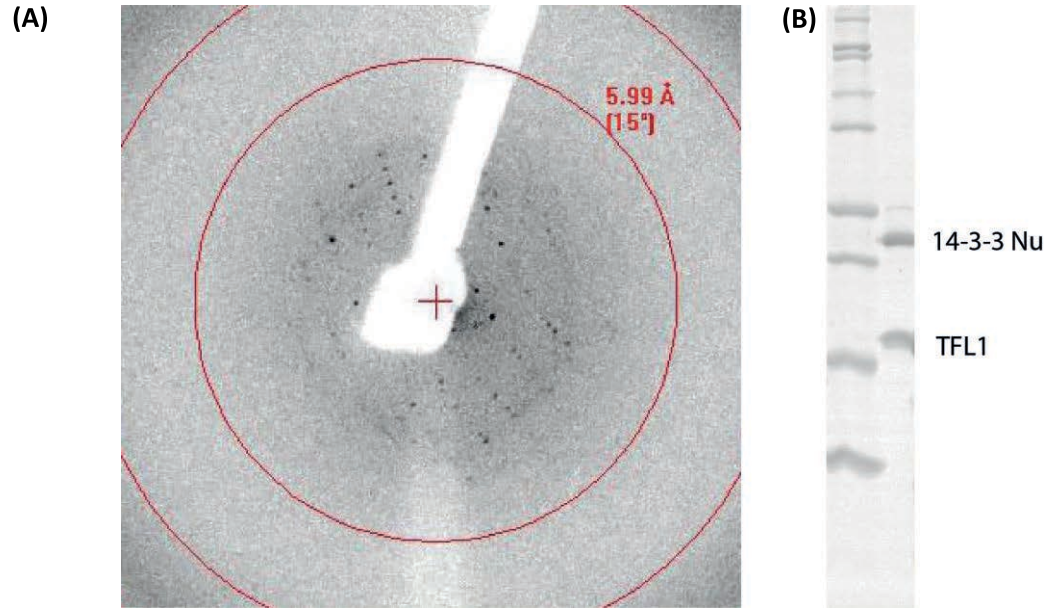


Figure 4.7: Characterisation of Initial Hits. (A) The diffraction of initial TFL1-14-3-3 Nu crystals grown in 500mMLi_2SO_4, 17.5% PEG 8000 and 17.5% Glycerol on a Rigaku Cu^{2+} X-ray source **(B)** Washed crystals run on SDS-PAGE. Two bands were observed corresponding to 14-3-3 Nu (~30 kDa) and to TFL1 (~20KDa).

The preliminary crystallization conditions of the proto-FIC were determined by sparse-matrix screening. Purified TFL1 and 14-3-3 Nu were incubated together, concentrated to ~ 12 mg/ml and distributed into trays by a crystallization robot. 140 nl of protein at 12 mg/ml was mixed with 140 nl of various commercial crystallization buffer in sitting-drop vapour diffusion plates. Drops were equilibrated against 185 µl of crystallization buffer. Trays were incubated for approximately 10 days at 4°C. In total 480 conditions were screened. Crystals suitable for mounting and screening by diffraction were harvested (Figure 4.7). Crystals in cryoprotected conditions were flash cooled in liquid nitrogen. Crystals without cryoprotectant were passed through a cryoprotecting solution prior to freezing. Several salt crystals were identified. One crystal observed in conditions containing 17.5% Glycerol, 17.5% PEG 8000 and 500 mM Li_2SO_4 diffracted to approximately 10 Å with a protein-like lattice (Figure 4.7a). The data were not sufficient to determine a space group. The crystal was replicated, harvested and washed in crystallization buffer and run out on an SDS-PAGE gel. Two bands were observed at approximately 30 kDa (representing 14-3-3 Nu) and at 20 kDa (representing TFL1) (Figure 4.7b).

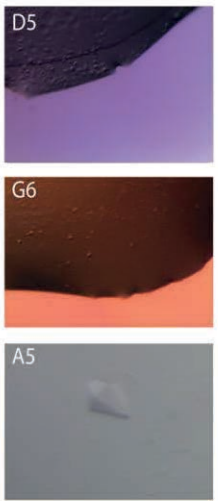
4.2.3.2 Optimization of Crystals

(A)

PEG 8000

Glycerol	7.5%	10%	12.5%	15%	17.5%	20%	Li_2SO_4
5%	Phase Seperation	Micro Crystals	Micro Crystals	Micro Crystals	Crystals	Precipitate	500mM
10%	Clear	Clear	Clear	Clear	Precipitate	Precipitate	500mM
15%	Clear	Clear	Clear	Precipitate	Micro Crystals	Crystals	500mM
20%	Clear	Phase Seperation	Clear	Precipitate	Crystals	Phase Seperation	500mM

(B)



(C)



Figure 4.8: Optimization of TFL1-14-3-3 Nu Complex Crystals. (A) Schematic of the optimization tray **(B)** TFL1-14-3-3 Nu Crystal in variations of the initial crystal condition. **(C)** Hexagonal based bi-pyramidal crystals grown in 500mM Li_2SO_4, 17.5% PEG 8000 and 5% Glycerol approximately 40 µM in diameter.

Crystallization hits were manually optimized by the sitting drop methodology (Figure 4.8a). 2 µl of complex solution was mixed with 2 µl of reservoir solution. The resulting drop was equilibrated against 200 µl of reservoir solution. Crystals suitable for harvesting were observed in conditions containing more than 17.5% PEG 8000. Increased concentrations of glycerol were typically associated with clear drops and with small crystals (Figure 4.8b). Three conditions produced crystals suitable for mounting for diffraction experiments; the largest crystals were found in conditions with 500 mM Li_2SO_4, 17.5% PEG 8000 and 5% glycerol (Figure 4.8c). Tests showed that this buffer was suitable for freezing. These crystals were clear, hexagonal bi-pyramidal structures with sharp edges approximately 40 µM in diameter (Figure 4.8Figure 4.8c).

4.2.3.3 Testing, Diffraction and Data Collection

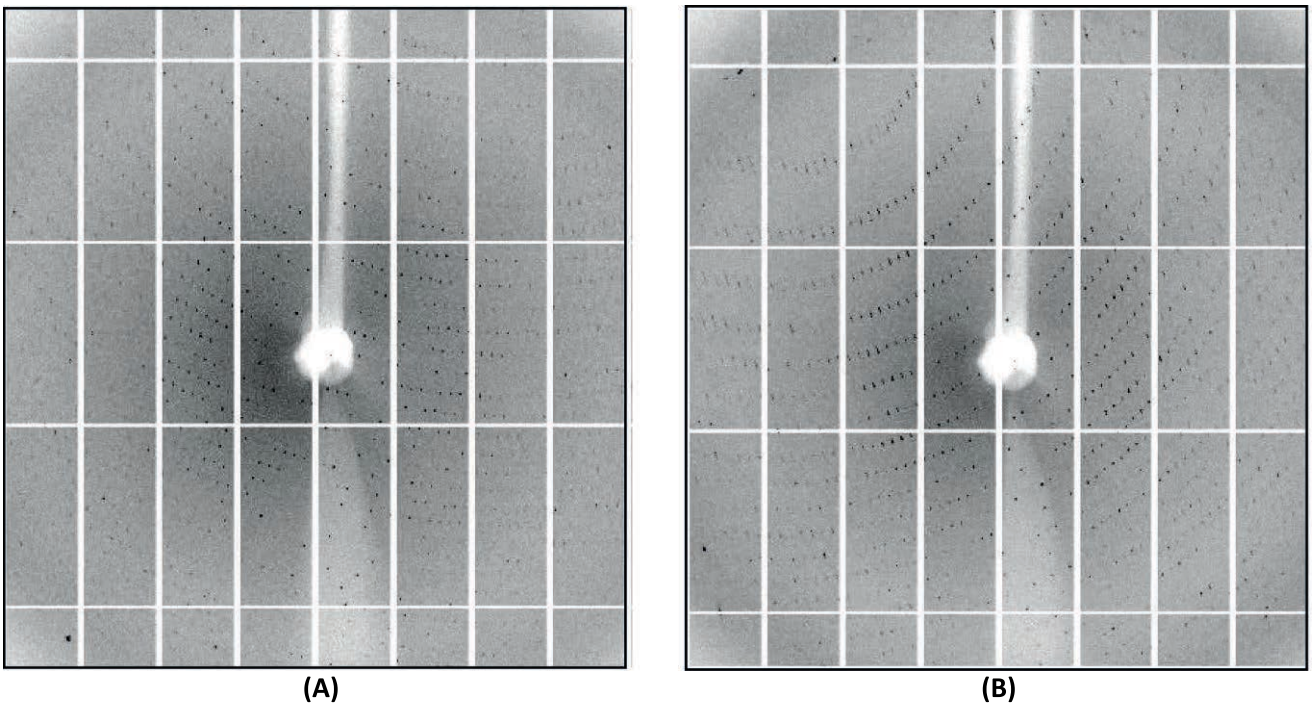


Figure 4.9: Diffraction of TFL1 14-3-3 Nu complex grown in 500mM Li_2SO_4, 17.5% PEG 8000 and 5% Glycerol. (A) Initial diffraction images showing a lattice-like pattern. **(B)** Diffraction of the crystal when rotated by 90°.

A native dataset for the proto-FIC crystals was collected on the MX-I24 beamline at Diamond Light Source and was processed with iMOSFLM (Leslie and Powell, 2007) (Figure 4.9). Data processing revealed that the crystal belonged to either the primitive hexagonal space group $P6_522$ or $P6_122$ with unit cell parameters, a = 154 Å, b = 154 Å, c = 488 Å (α = 90°, β = 90°, γ =120°). The number of molecules in the unit cell was estimated by way of the Matthews' coefficient. A cell containing two tetramers (four TFL1 and four 14-3-3 Nu) was considered the most probable scenario and was associated with Matthews' coefficient of 4.18 $Å^3$ Da^{-1} and an estimated solvent content of 70.55%, similar to the high solvent content observed in the related floral activation complex structure (Matthews, 1968, Kantardjieff and Rupp, 2003; Server: http://www.ruppweb.org/mattprob/, Taoka et al., 2011). A summary of the statistics for the data set is given in Table 4.1.

Table 4.1: Data collection statistics. Values in parentheses are the highest resolution shell.

	Overall (Highest Resolution Shell)
Wavelength (Å)	0.9686
Resolution (Å)	3.8
Space Group	$P6_522$
Unit Cell Parameters (Å)	
a	154.4
b	154.4
c	488.0
No of Observed Reflections	119750
No of Unique Reflections	32819
Multiplicity	3.6 (3.6)
Completeness (%)	95.3 (99.3)
Mean I/σ	6.0 (1.9)
R_{merge}	0.20 (0.82)
R_{fact}/R_{free}	0.23 / 0.28

4.2.3.4 Crystal Structure of proto-Floral Inhibitory Complex

The crystal structure of the TFL1-14-3-3 Nu complex was solved by molecular replacement at 3.8 Å. The refined complex ($P6_522$, R_{fact} = 23%, R_{free} = 28%) showed striking similarity to the Hd3a-14-3-3 complex with an r.m.s.d of 4.12 Å over 791 equivalent Cα positions, confirming the conserved nature of the 14-3-3-PEBP architecture. The complex is a tetramer composed of a dimer of 14-3-3 Nu and two TFL1s as suggested by the electrophoretic mobility shift assay, forming a W-shaped complex 80 Å by 100 Å and 60 Å deep (Figure 4.10).

TFL1 interacts with two α-helices at the C-terminus of the 14-3-3 protomer. Specifically, TFL1 binds between two acidic patches found on the C-terminal helices. These helices form a hydrophobic cleft, Phe^{104} and Leu^{64} of TFL1 are likely to reside between these helices (Figure 4.12). Residues found early in the variable loop were found close to the 14-3-3 binding side adjacent to the acidic lobe including Arg^{133} which exists close to one of the acidic patches (Figure 4.12b). Residues later in the loop face away from the binding site and point towards the exterior of the complex. Likewise, the ligand binding pocket is found to the exterior of the structure.

In the 14-3-3 portion of the structure, the interface between the 14-3-3 protomers is formed by the first four α-helices in manner commonly observed amongst the 14-3-3 family of proteins and contains a number of hydrophobic residues. Helix one packs against helix three, with Tyr^{10} and Leu^{14} from helix one and Iso^{65} and Iso^{66} from helix three likely to be held in the interface. Within the 14-3-3 dimer there are two large positively charged pockets, in homologous 14-3-3 molecules have been shown to be involved in the interaction with phosphorylated peptide and proteins (Rittinger et al., 1999, Taoka et al., 2011). In the crystal structure, a density which could be modelled as a sulphate moiety is found residing within these clefts which may expose a propensity for the region to interact with negatively charged chemical groups including phosphorylated peptides and proteins. The negatively charged SO_4^- appears to lie close to three positively charged residues; Lys^{53}, Arg^{60} and Arg^{133} (Figure 4.11). The side chain of Arg^{133} is approximately 2.6 Å from the sulphate ion and may be involved in interaction. Tyr^{134} also may help to coordinate the sulphate ion by possibly forming a hydrogen bond with the moiety as it is 2.5 Å away.

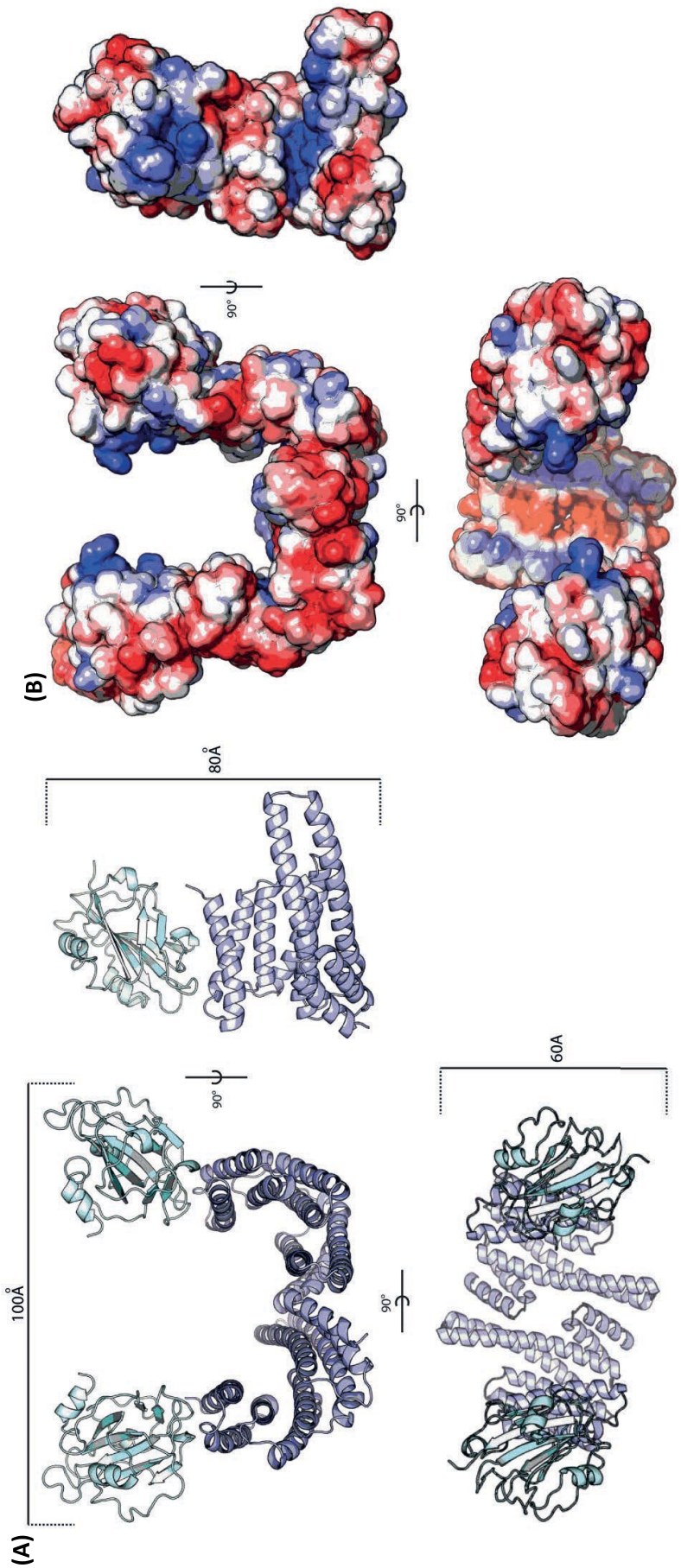


Figure 4.10: Structure of the Proto-Floral Inhibitory Complex. The hetero tetrameric structure of the FIC with two TFL1 (cyan) complexed with a 14-3-3 Nu dimer (blue). (A) The cartoon diagram of the FIC (B) Surface charge representation of the complex. Blue positive charge. Red negative charge.

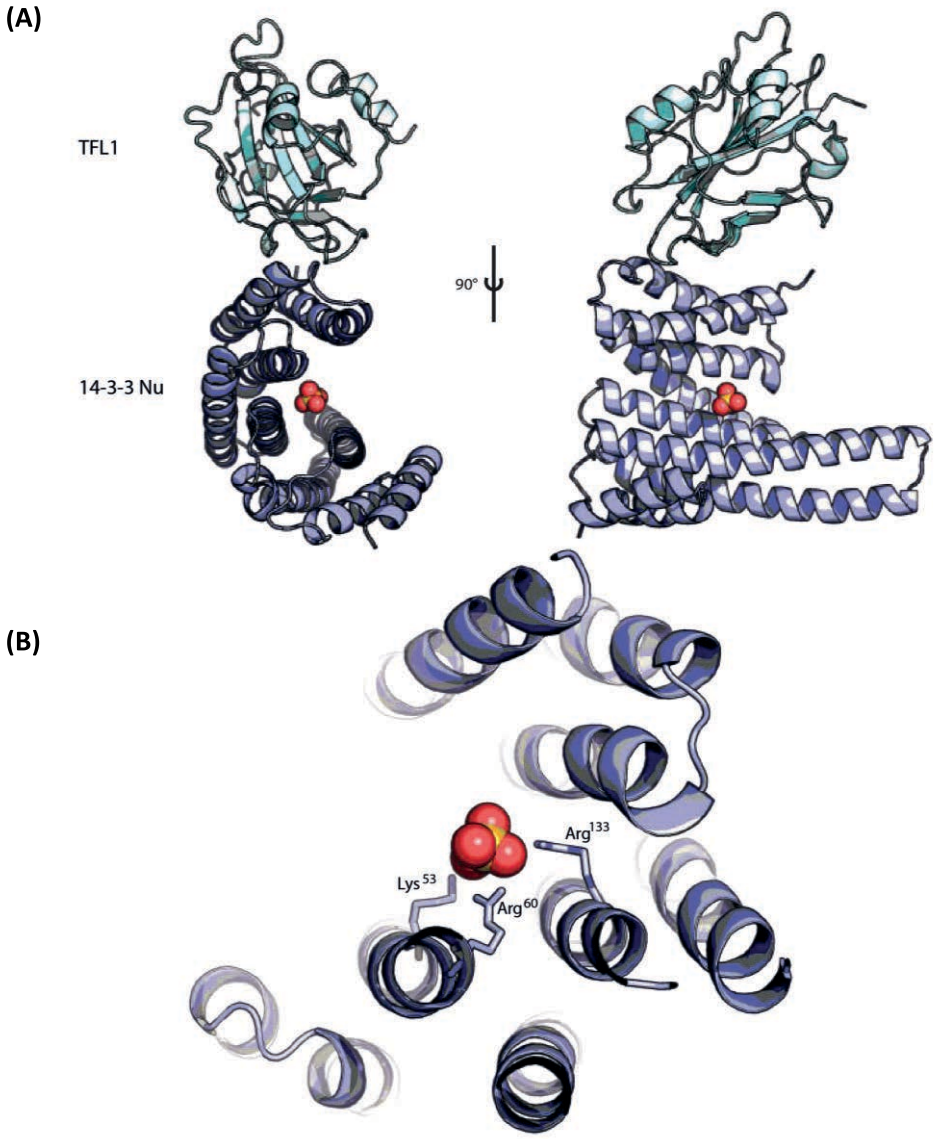


Figure 4.11: A sulphate moiety bound to 14-3-3 Nu. (A) The sulphate interacts with binding cleft found in 14-3-3 Nu in the same positions as phosphorylated peptides. **(B)** Three positively charged residues are found in the vicinity which may coordinated the negatively charged sulphate.

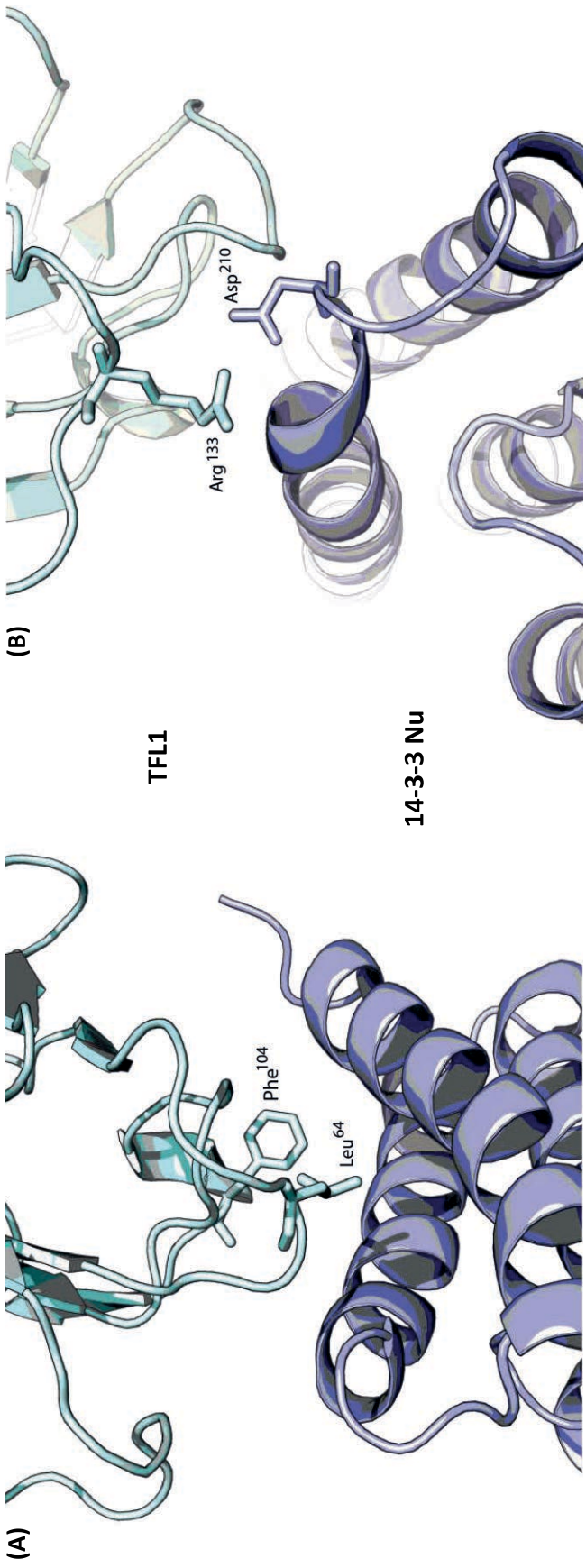


Figure 4.12: Key residues involved in the interaction between TFL1 (cyan) and 14-3-3 Nu (blue). (A) Two hydrophobic residues (Leu^{64} and Phe^{104}) insert into the hydrophobic pocket created by two C-terminal α-helices. **(B)** Residues towards the N-terminus of the loop are close to the 14-3-3 Nu binding site. Arg^{133} is close to the acidic lobe of 14-3-3 Nu which contains Asp^{210}.

4.2.4 Biochemical Assessment TFL1 14-3-3 Interaction

4.2.4.1 Characterisation of the TFL1 Extended Loop Mutants

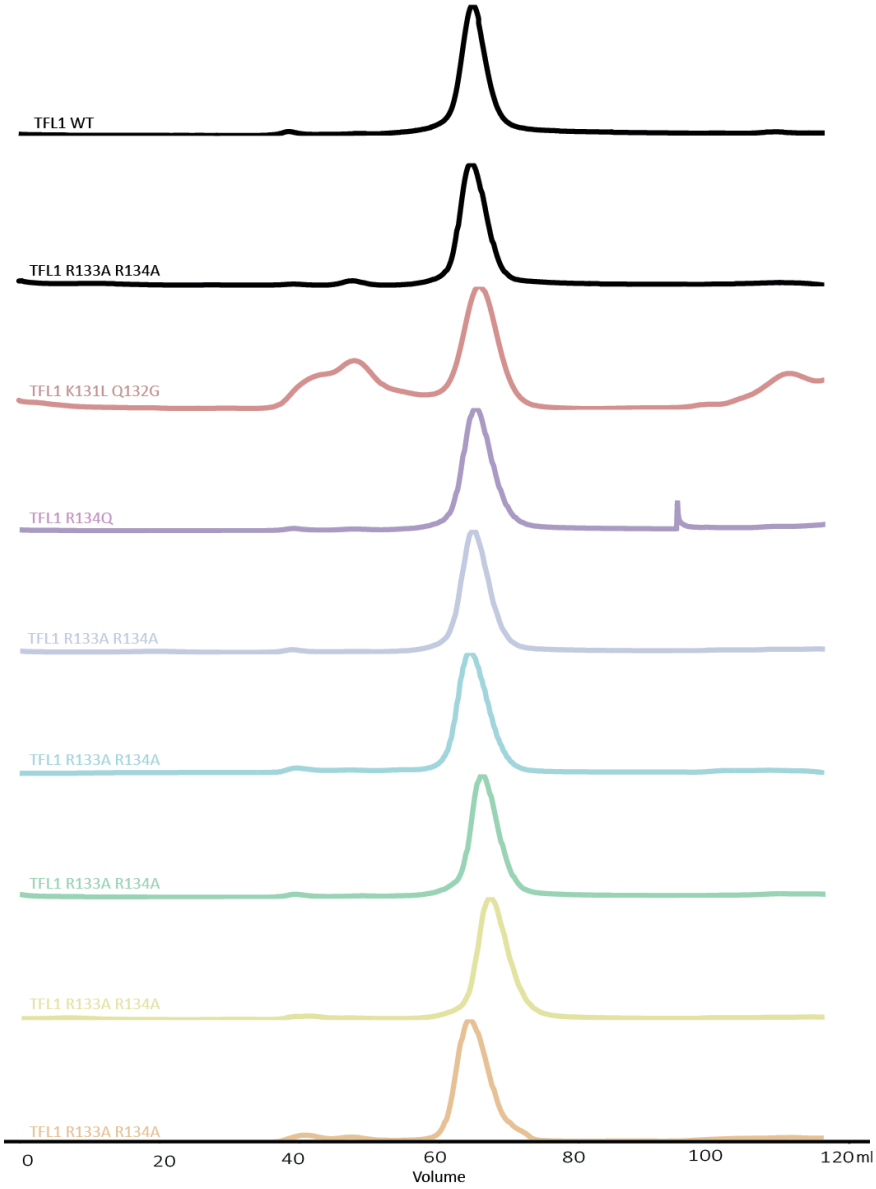


Figure 4.13: Comparison of TFL1 and a series of TFL1 mutants Gel Filtration Profiles. The chromatograms of the TFL1 mutants illustrate the similarity between samples. All samples eluted between approximately 60 and 70 ml. All samples were run on a Superdex 75 gel filtration column. The void volume of the column is approximately 4 Elution volume (ml) is plotted against normalized absorbance at 280 nm.

To probe the role of the extended loop in the interaction of TFL1 and 14-3-3 Nu a series of loop mutants were derived. Residues in the loop of TFL1 were mutated pair wise to their counter parts in FT. Mutants were purified using the same protocol applied to TFL1 (described in section 2.5) . The gel filtration profile of TFL1 mutants was similar to the profile wild-type TFL1 (Figure 4.13).

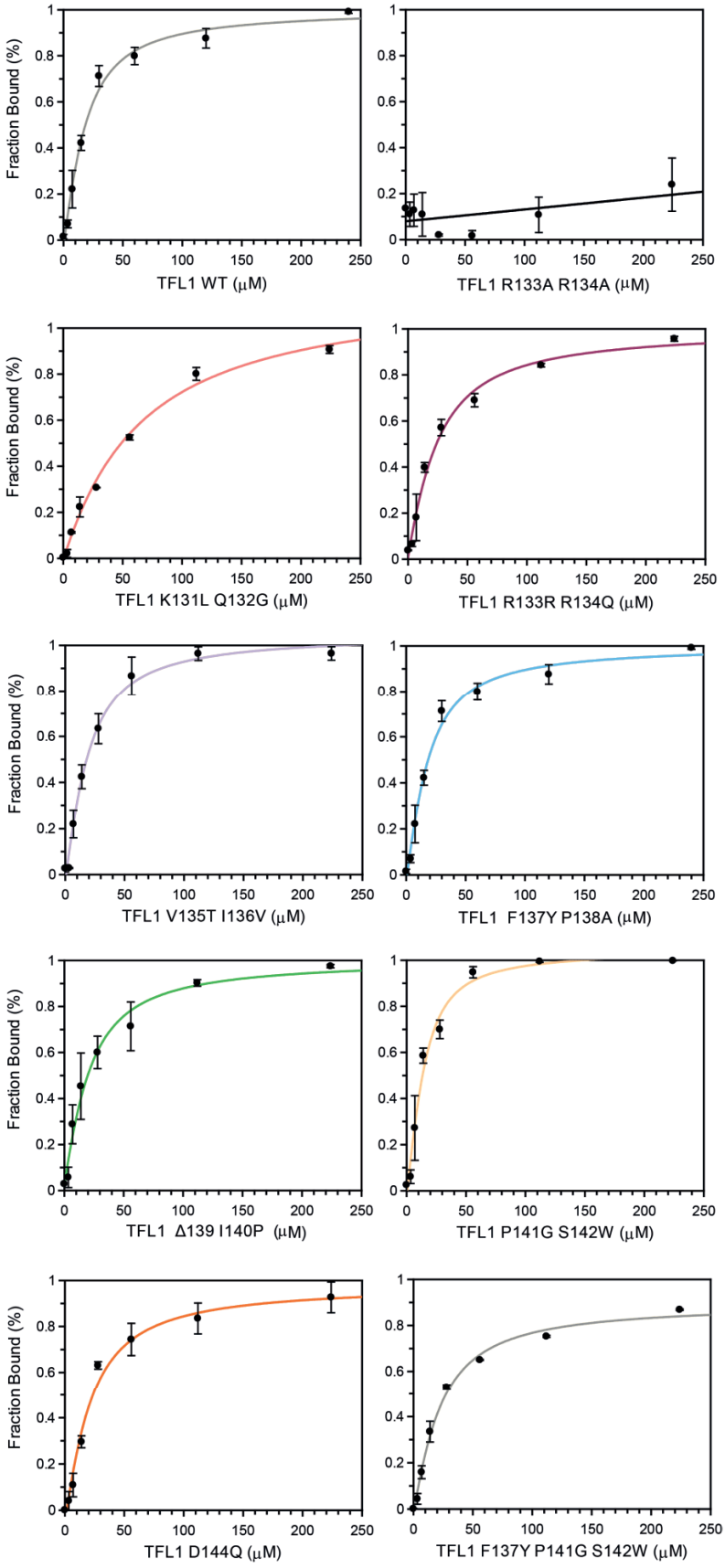
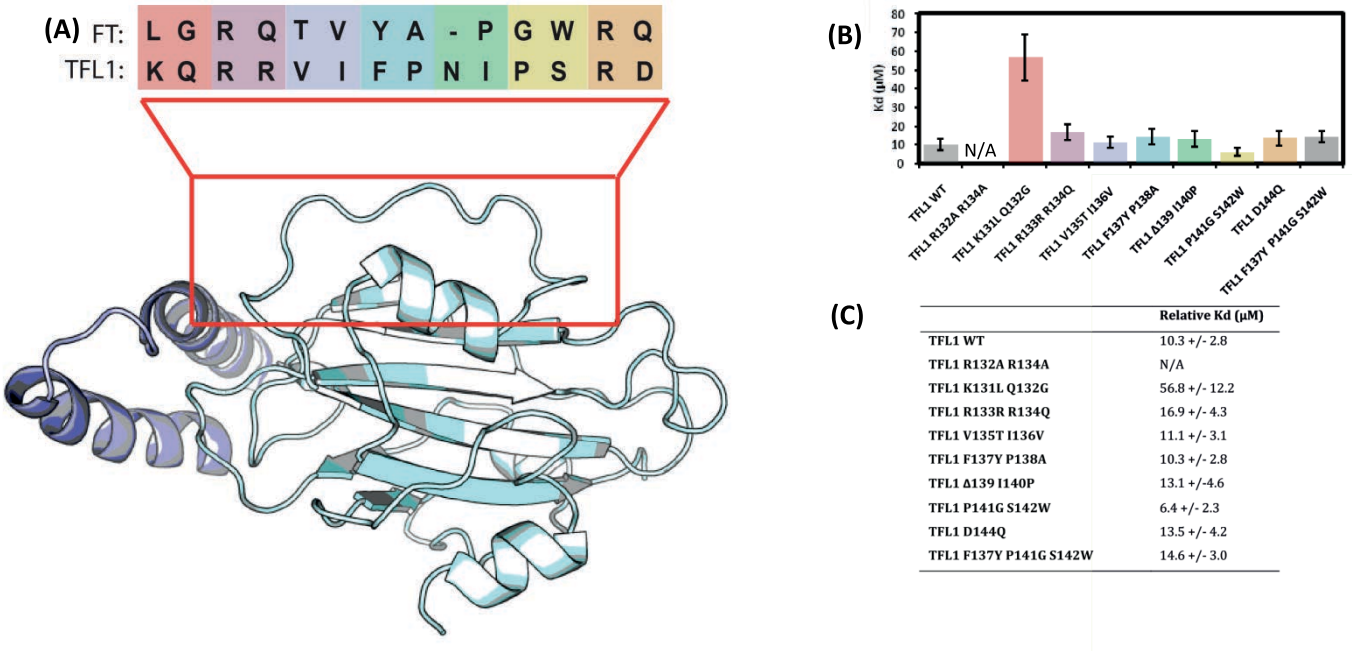


Figure 4.14: Assessment of the role of the loop in the interaction between TFL1 and 14-3-3 Nu. Interaction as measured by electrophoretic mobility shift assay. Loop mutants were titrated in increasing amounts against 14-3-3 Nu. The fraction of free 14-3-3 was plotted against the concentration TFL1. The relative dissociation constant (Kd) is given.



(C)

	Relative Kd (μM)
TFL1 WT	10.3 +/- 2.8
TFL1 R132A R134A	N/A
TFL1 K131L Q132G	56.8 +/- 12.2
TFL1 R133R R134Q	16.9 +/- 4.3
TFL1 V135T I136V	11.1 +/- 3.1
TFL1 F137Y P138A	10.3 +/- 2.8
TFL1 Δ139 I140P	13.1 +/-4.6
TFL1 P141G S142W	6.4 +/- 2.3
TFL1 D144Q	13.5 +/- 4.2
TFL1 F137Y P141G S142W	14.6 +/- 3.0

Figure 4.15: A summary of the assessment of the role of the loop in the interaction between TFL1 and 14-3-3 Nu. Interaction as measured by electrophoretic mobility shift assay. Loop mutants were titrated increasing amounts against 14-3-3 Nu. The relative dissociation constant (Kd) is given. N/A: No binding detected.

4.2.4.2 Biochemical Assessment of the Role of the Extended Loop in 14-3-3 Interaction

To provide additional biochemical information about the interface a series of loop mutants were analysed by electrophoretic mobility shift assays. Mutations to residues early in the loop reduced the strength of interaction. Switching Leu^{131} and Gly^{132} to lysine and glutamine respectively, caused a 6-fold decrease in affinity. Quantification revealed an approximate relative Kd of 56.8 μM (+/- 12.2 μM). Mutating Arg^{133} and Arg^{134} to two alanine residues abolished the interaction between 14-3-3 Nu and TFL1. However, changing Arg^{134} to a glutamine had no significant effect on relative Kd (16.6 μM +/- 4.3 μM) suggesting that Arg^{134} is not directly involved in the interaction. Mutations further along the loop did not affect relative Kd. Constructs containing TFL1 $^{V135T\ I136V}$, TFL1 $^{F137Y\ P138A}$, TFL1 $^{F137Y\ P138A}$, TFL1 $^{P141G\ S138W}$ and TFL1 ^{D144Q} were examined. These TFL1 constructs were found to interact with similar strength (Figure 4.15b; Figure 4.15c). The data, alongside the crystal structure, clearly supports the notion that residues 134 to 144 are unlikely to be involved in the interaction with 14-3-3 whilst residues 131 to 134 are likely to be involved in interaction.

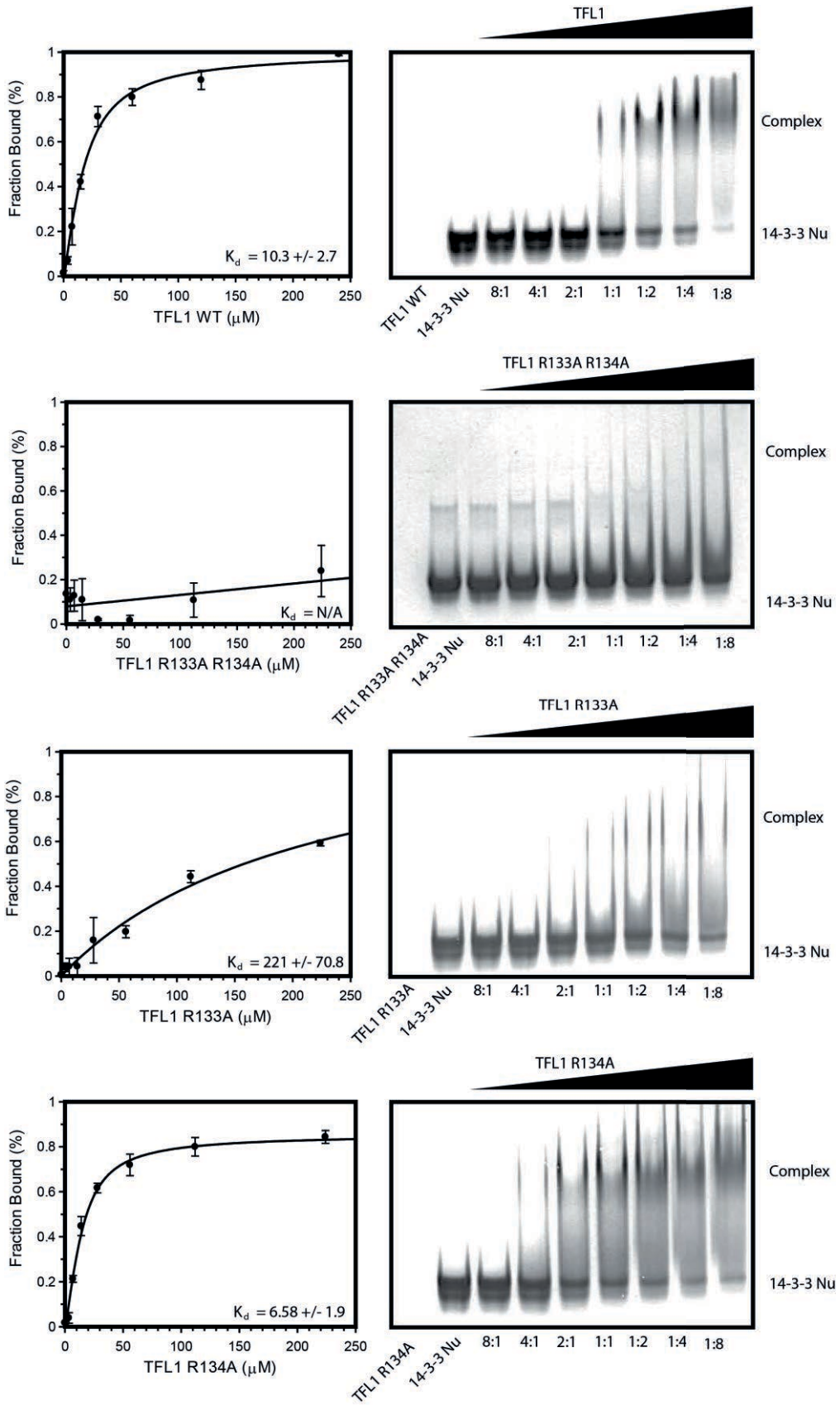


Figure 4.16: Assessment of the role of Arg^{133} and Arg^{134} in the interaction between TFL1 and 14-3-3 Nu. Interaction as measured by electrophoretic mobility shift assay. Alanine mutants were titrated in increasing amounts against 14-3-3 Nu. The fraction of free 14-3-3 was plotted against the concentration TFL1. The relative dissociation constant (Kd) is given.

4.2.4.3 Biochemical Assessment of the Arg^{133} in 14-3-3 Interaction

Owing to the strong effect of Arg^{133} and Arg^{134}, further mutations were derived. Conversion of Arg^{133} to alanine, caused a 20-fold increase in relative Kd (Figure 4.16). TFL1 ^{R133A} mutants bound to 14-3-3 Nu with approximate relative Kd of 221 µM (+/- 70 µM) compared to wild-type TFL1 which bound with a relative Kd of 10.3 µM (+/- 2.8 µM). Conversely, protein where Arg^{134} was mutated to alanine bound to 14-3-3 Nu with an approximate relative Kd of 6.58 µM (+/- 1.9 µM), similar to the estimated relative Kd for wild-type TFL1. Taken together this strongly implies that Arg^{133} is involved in the interaction between TFL1 and 14-3-3 Nu. This is consistent with the crystal structure where Arg^{133} is close to the acidic lobe found in the 14-3-3 Nu binding site (Figure 4.12).

4.2.4.4 Biochemical Assessment of the Phe^{104} in 14-3-3 Interaction

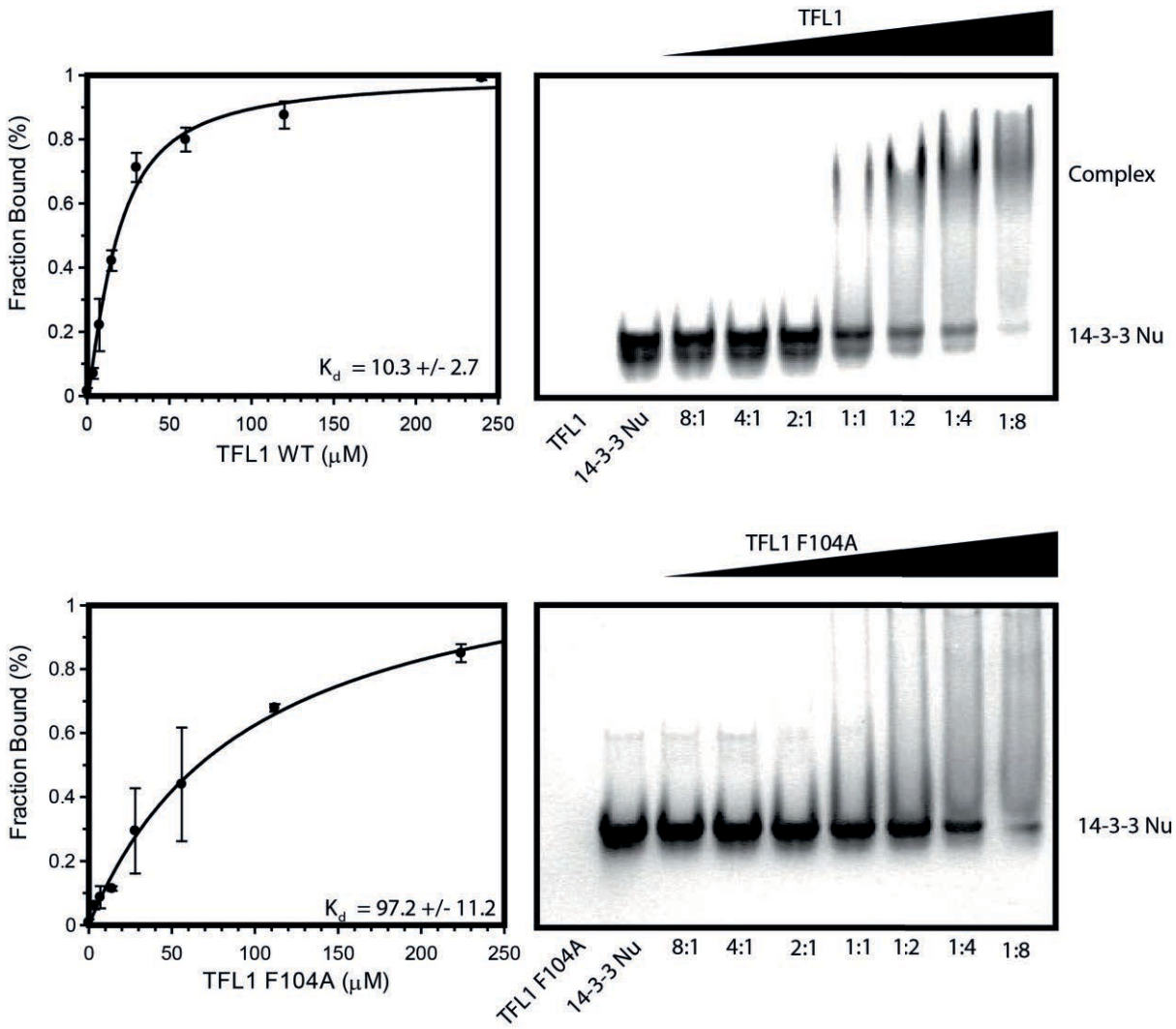


Figure 4.17: Assessment of the role of Phe^{104} in the interaction between TFL1 and 14-3-3 Nu. Interaction as measured by electrophoretic mobility shift assay. The alanine mutant was titrated in increasing amounts against 14-3-3 Nu. The fraction of free 14-3-3 was plotted against the concentration TFL1. The relative dissociation constant (Kd) is given.

Given the location of Phe^{104} at the centre of the binding interface, a further TFL1 mutant was derived. Although TFL1 can still interact with 14-3-3 Nu changing Phe^{104} to alanine causes a 10-fold increase in relative Kd to 97.2 μM. This is consistent with the crystal structure where Phe^{104} is buried within a hydrophobic cleft created by the two C-terminal α-helices found in the 14-3-3 Nu binding site (Figure 4.12).

4.3 Discussion

4.3.1 The Significance of the TFL1-14-3-3 Complex

4.3.1.1 PEBP-14-3-3 Complex Formation

Members of the 14-3-3 protein family play a pivotal role in regulating the transition to flowering. In rice, mutations to GF14c have been linked to delayed flowering and accelerated flowering phenotypes (Purwestri et al., 2009, Taoka et al., 2011). Although interactions between PEBPs and members of the 14-3-3 protein family have been identified previously, this study shows for the first time that TFL1 and FT can bind directly to the same 14-3-3 protein. Moreover, quantification of these interactions has revealed these two proteins bind to 14-3-3 Nu with similar strength. The interaction between TFL1 and members of the 14-3-3 protein family has important implications, as binding to 14-3-3 proteins is thought to be essential for proper biological activity (Taoka et al., 2011).

4.3.1.2 Structure of TFL1-14-3-3 Complex

TFL1 binds to the C-terminus of 14-3-3 protein via the two C-terminal α-helices and forms a W-shaped complex via a non-canonical 14-3-3 interaction. This interaction is extremely similar to the interaction found between Hd3a and GF14c suggesting that this interaction is conserved between TFL1 and FT homologs across plants. This observation has validity given the sequence and structural similarity between TFL1 and FT (Ahn et al., 2006). This conservation may be indicative of an important aspect of biological function; the interaction between the floral PEBPs and 14-3-3 proteins may preclude a nuclear export signal found on the C-terminal helix of 14-3-3 proteins (Taoka et al., 2011). In the absence of floral PEBPs 14-3-3 proteins are actively exported from the nucleus (Taoka et al., 2011). The interaction may enable 14-3-3 proteins to become localised to the nucleus where they act to regulate the expression of genes. This hypothesis would suggest that the 14-3-3 proteins have a secondary function within the nucleus but does not in itself explain the biological differences associated with TFL1 and FT. In this scenario one of the functions of FT and TFL1 might be to inhibit the export of 14-3-3 proteins thus

controlling their subcellular localization. Though plausible this scenario would depend upon the relative abundances of the PEBPs and 14-3-3 proteins. These proteins have not yet been quantified *in vivo*.

4.3.2 A Section of the Loop Mediates Binding

The structure suggests that the N-terminal portion of the loop of TFL1 may help to mediate the interaction with members of the 14-3-3 protein family. One residue in particular Arg^{133} faces into the binding interface. Mutation of this residue causes a 20-fold decrease in the strength of interaction. This residue may be comparable to Arg^{132} in FT. Mutation of Arg^{132} inhibits the interaction between Hd3a and 14-3-3 proteins in yeast-two hybrid assays (Taoka et al., 2011). In rice, plants overexpressing HD3a $^{R64G\ R132A}$ flower later than plants overexpressing wild-type Hd3a demonstrating that these residues are important, *in vivo* (Taoka et al., 2011). Mutations to residues before Arg^{132} also affect binding. TFL1 $^{K131L\ Q132G}$ interacts significantly weaker with 14-3-3 Nu than wild-type TFL1 suggesting that these residues are involved in the interaction. However, it is unclear whether the effect upon binding is indirect or direct. The C-terminal portion of the loop is not in involved in the interaction between 14-3-3 Nu and TFL1. In binding assays mutations between residues 135 and 144 had no significant affect on Kd. Despite this in FT there is high conservation of the residues which implies that they may play an important functional role (Ahn et al., 2006). However, the crystal structure does not provide enough evidence to conclude what role they play or whether residues from the C-terminus alone could mediate the activity of FT or TFL1. Given their position it is possible that these residues are involved in binding another partner which acts to facilitate the activation or inhibition of flowering.

4.3.3 Interface Mutations

Several hydrophobic residues from TFL1 insert between the two C-terminal helices of 14-3-3 Nu. One residue, Phe^{104} is critical to the interaction between TFL1 and 14-3-3s. Mutation of Phe^{104} stops binding. The strength of interaction for TFL1 ^{F104A} mutants was approximately 10-fold less than wild-type mutations. A similar mutation, in the FT homology HD3a ^{F103A} was unable to bind to 14-3-3s in yeast-two hybrid assays highlighting the similarities in the binding mechanism between TFL1 and FT-like proteins (Taoka et al., 2011).

4.4 Summary

TFL1 plays a key role in the onset of flowering (Kobayashi et al., 1999). A direct interaction between the PEBPs, TFL1 and FT, with a 14-3-3 protein has been demonstrated. Both floral regulators interact with 14-3-3 proteins with similar affinity (both interactions have low μM dissociation constants). To further dissect this interaction the crystal structure of TFL-14-3-3 complex was solved. TFL1 binds to 14-3-3 Nu forming a W-shaped complex, which is possibly due to a non-canonical interaction between TFL1 and the C-terminus α-helices of in a manner similar to the interaction between HD3a, an FT-like protein, and GRF14c. Several hydrophobic residues insert between the two C-terminal helices including Phe^{104} which, when mutated to alanine significantly affects binding, highlighting the central role that this residue plays. The loop of the PEBPs which has previously been shown to play a critical role in their activity, face outwards (Ahn et al., 2006, Taoka et al., 2011). A small section of the loop, towards the N-terminus centred about Arg^{133}, is involved directly in the interaction. Mutations to these residues significantly decrease binding affinity, implicating that these residues are involved in binding.

Chapter 5 - The Interaction between FD and 14-3-3s

5.1 Introduction

The activity of TFL1 is suppressed *in vivo* by mutations to FD, a bZIP transcription factor (Hanano and Goto, 2011). TFL1 and FT have been shown to associate with FD *in vivo,* via bimolecular fluorescence complementation and by yeast-two hybrid assays, but these results do not necessarily imply a direct interaction (Hanano and Goto, 2011). These interactions occur in the nucleus and are dependent upon 7 amino acids found at the C-terminus of FD (Hanano and Goto, 2011, Abe et al., 2005). In yeast-two hybrid assays, mutants without the C-terminus are unable to interact with FT (Abe et al., 2005). The C-terminus of FD contains a 14-3-3 binding site enabling interaction with 14-3-3s (Muslin et al., 1996, Taoka et al., 2011). This interaction has been observed within the crystal structure of the FAC (Taoka et al., 2011). However, it is unclear whether a different process occurs in the presence of TFL1. To determine whether the interaction between FD and TFL1 occurs directly or indirectly via members of the 14-3-3 protein family, this study examines the interaction of the C-terminus of FD with 14-3-3 Nu, a model 14-3-3, and TFL1.

5.2 Results

5.2.1 Qualitative Assessment of FD 14-3-3 Interaction

To establish whether FD binds directly to TFL1 or associates indirectly using a 14-3-3 intermediate, differential scanning fluorimetry (DSF) was employed (Figure 5.1). A phosphorylated 7 amino acid C-terminal peptide, was added in increasing concentration to 14-3-3 Nu. A 10° K increase in the melting temperature of 14-3-3 Nu was observed upon the addition of the FD C-terminal peptide (Figure 5.1a; Figure 5.1b). This increase in stability may be caused by binding of the C-terminal peptide to 14-3-3 Nu. This shift was not observed when 14-3-3 Nu was tested with a control peptide (Figure 5.1c; Figure 5.1d). The addition of either peptide to TFL1 had no effect upon the stability of TFL1 suggesting that C-terminus FD does not interact with TFL1 (Figure 5.1f; Figure 5.1h).

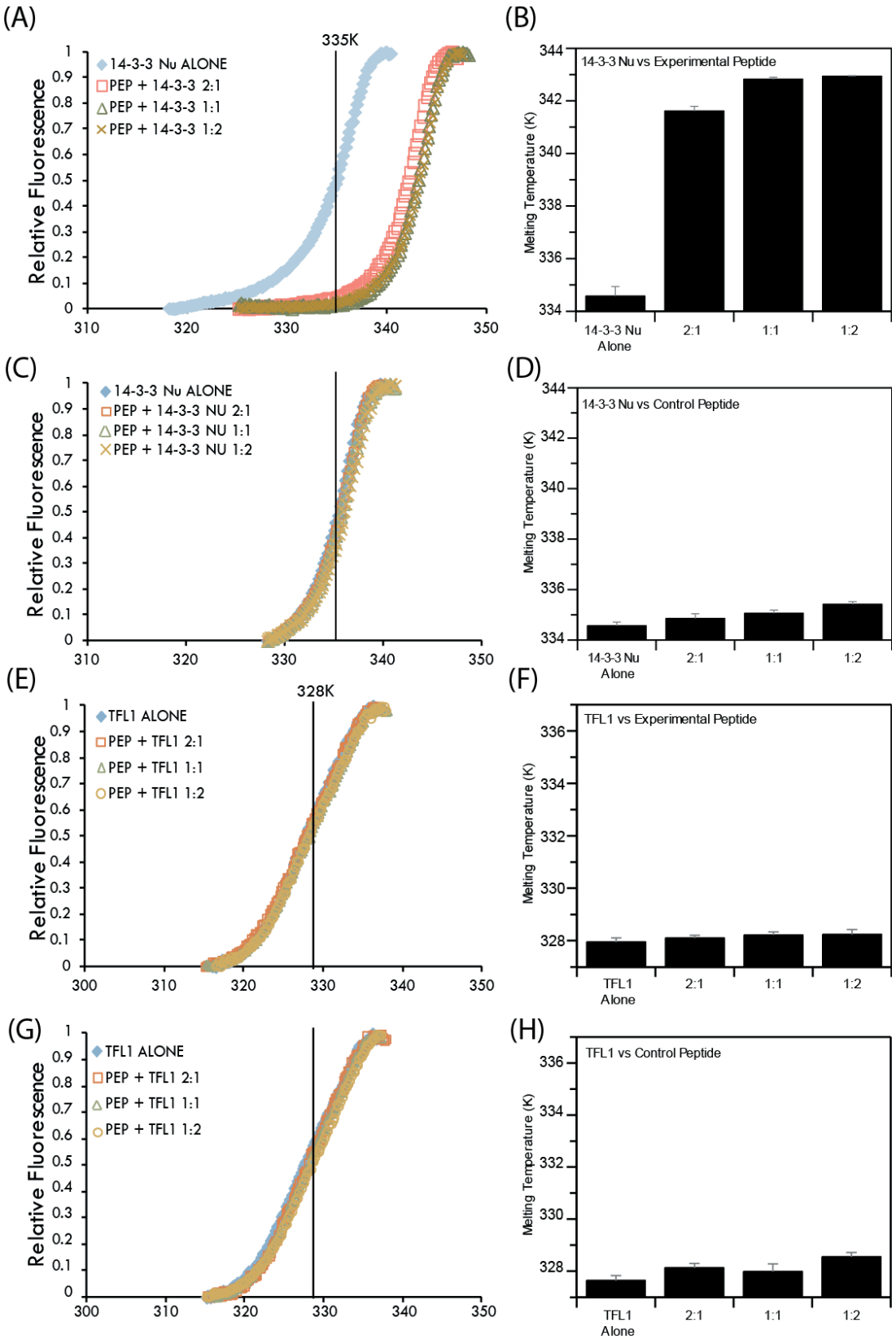


Figure 5.1: Interaction of TFL1 and 14-3-3 Nu with a 7 amino acid C-terminal peptide of FD. Increasing concentrations of experimental peptide FD peptide and control peptide were added to proteins. **(A - B)** An increase in melting temperature was observed upon the addition of FD peptide to 14-3-3 Nu. **(C - D)** No change in melting temperature was observed upon the addition of control peptide to 14-3-3 Nu. **(E - F)** No change in melting temperature was observed upon the addition of FD peptide to TFL1. **(G - H)** No change in melting temperature was observed upon the addition of control peptide to TFL1.

5.2.2 Initial Quantitative Assessment of FD 14-3-3 Interaction

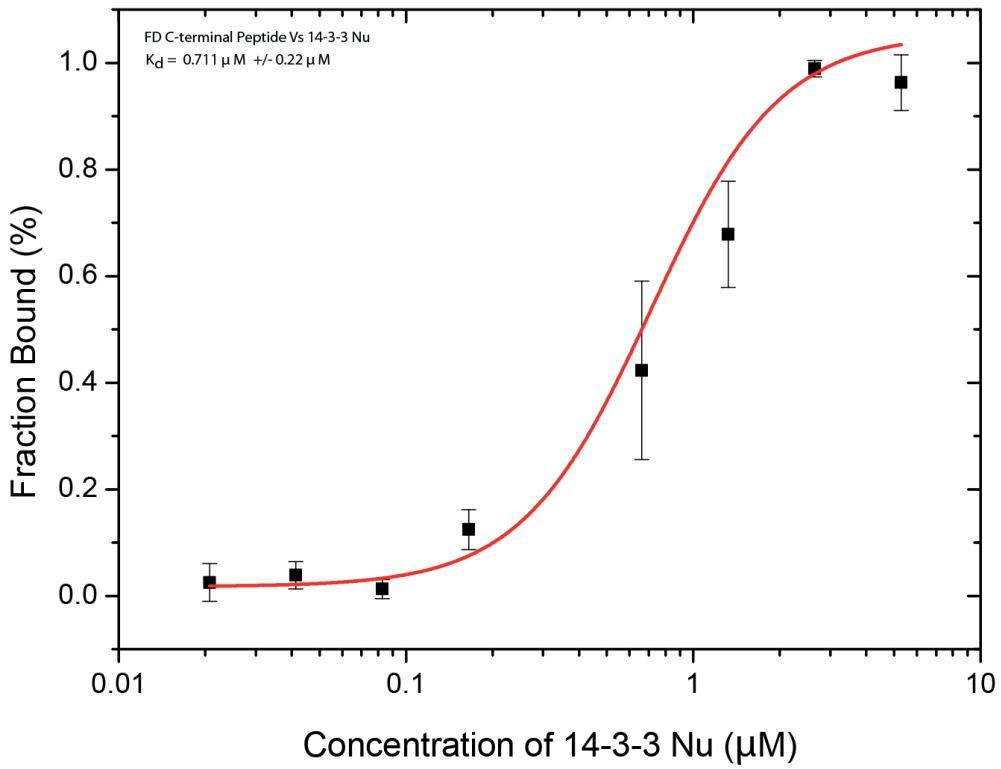


Figure 5.2: Interaction of a 7 amino acid C-terminal peptide of FD with 14-3-3 Nu using Microscale Thermophoresis. Interaction causes a change in thermophoresis consistent with binding. Normalised thermophoresis is plotted against concentration of titrated protein.

The affinity of the interaction between 14-3-3 Nu and the C-terminus of FD was determined by microscale thermophoresis. Purified dual his-tagged 14-3-3 Nu was titrated against a synthesised fluorescently labelled phosphorylated FD peptide (Cambridge Peptide). The interaction of the FD peptide with 14-3-3 Nu was dose-dependent and saturable. The fraction bound was plotted against the concentration of 14-3-3 Nu and a Kd of 0.711 +/- 0.22 µM was estimated after the data was fitted with a one site binding model (Figure 5.2). Taken together this suggests that 14-3-3 proteins can interact with TFL1 and the C-terminus of FD to form a ternary complex, hereafter described as the Floral Inhibitory Complex.

5.2.3 Crystallization of the Floral Inhibitory Complex

5.2.3.1 Initial Crystallization Screens

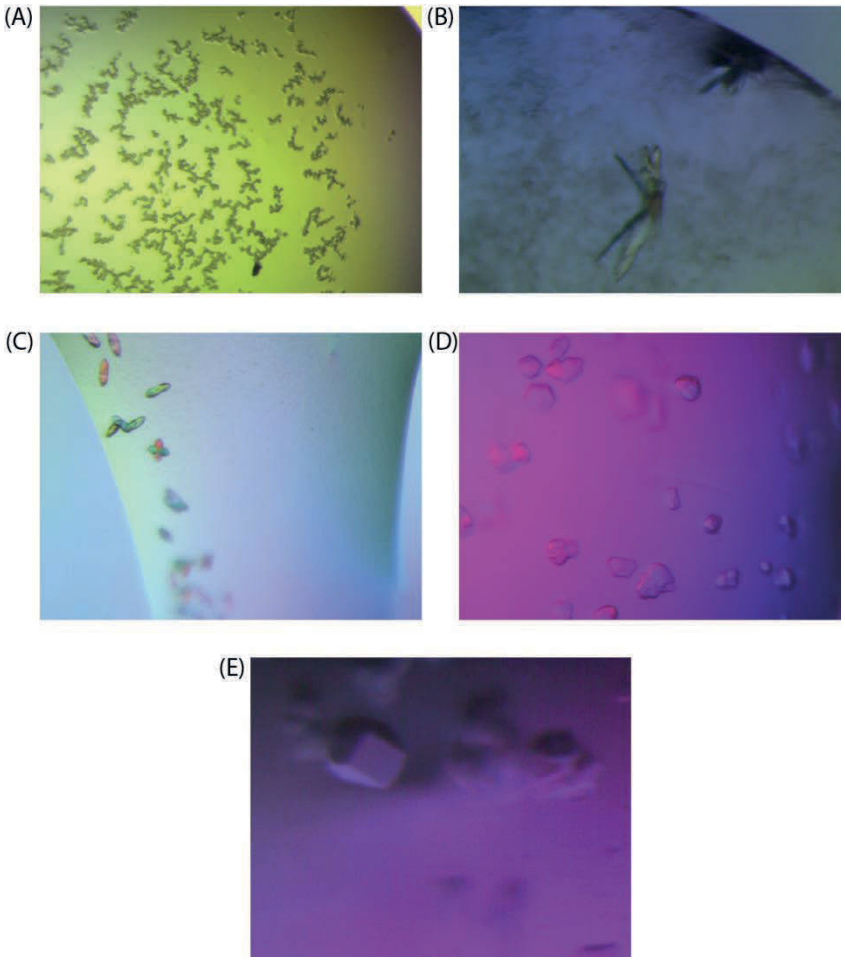


Figure 5.3: Putative initial hits in TFL1-14-3-3 Nu-FD peptide Crystallization Trials. Hits were evaluated visually and suitable hits **(D and E)** were screened by X-rays.

Sparse-matrix plates were setup to determine the preliminary crystallization conditions of the Floral Inhibitory Complex. Purified TFL1 and 14-3-3 Nu were incubated with approximately 5 molar equivalents of FD peptide and concentrated to ~ 12mg/ml and distributed into tray by a crystallization robot. Trays were incubated for approximately 10 days at 4°C. Approximately 288 conditions were screened. Crystallization hits were observed in 17.5% Glycerol, 17.5% PEG 8000 and 500 mM Li_2SO_4 were further optimised (Figure 5.3d; Figure 5.3e).

5.2.3.2 Replication and Optimization of Crystals

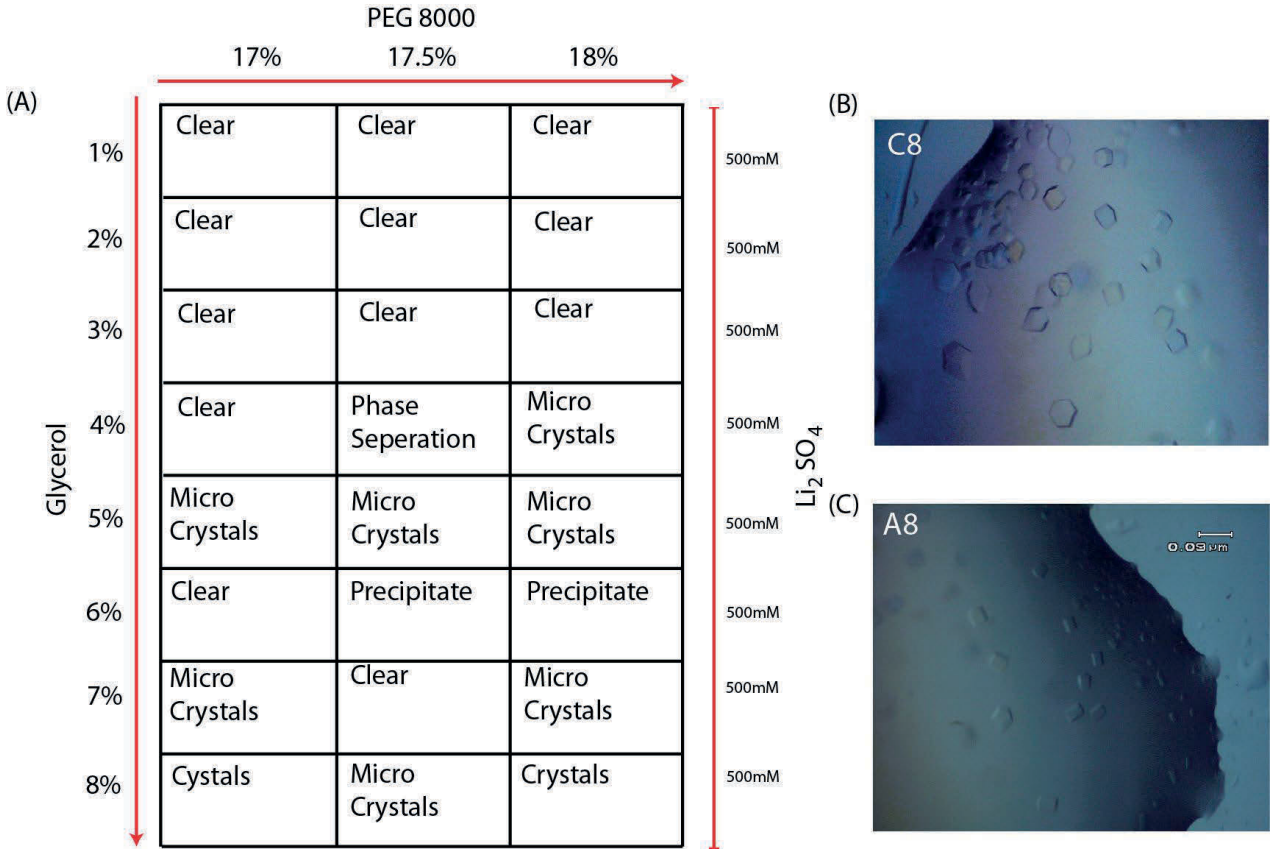


Figure 5.4: Optimization of Floral Inhibitory Complex Crystals. (A) Schematic of the optimization tray **(B)** Floral Inhibitory Complex Crystal in grown in 500mM Li_2SO_4, 17% PEG 8000 and 8% Glycerol. Hexagonal prism crystals were observed in the drop. **(C)** Floral Inhibitory Complex Crystal in grown in 500mM Li_2SO_4, 18% PEG 8000 and 8% Glycerol. Hexagonal prism crystals were observed in the drop.

Crystallization hits were manually optimized using the sitting drop methodology (Figure 5.4a). 2 µl of mixed complex solution with 5 M equivalents of FD peptide was mixed with 2 µl of reservoir solution. The drop was equilibrated against 200 µl of reservoir solution. Crystals suitable for harvesting were observed in conditions with 8% glycerol. Two conditions produce crystals suitable for mounting for diffraction; the largest were found in conditions with 500 mM Li_2SO_4, with either 17% or 18% PEG 8000 and 8% glycerol (Figure 5.4a). Tests showed that this buffer was suitable for freezing so no addition cryoprotectant solution was use. These crystals were clear, hexagonal prism structures with distinct faces (Figure 5.4b; Figure 5.4c).

5.2.3.3 Testing, Diffraction and Data Collection

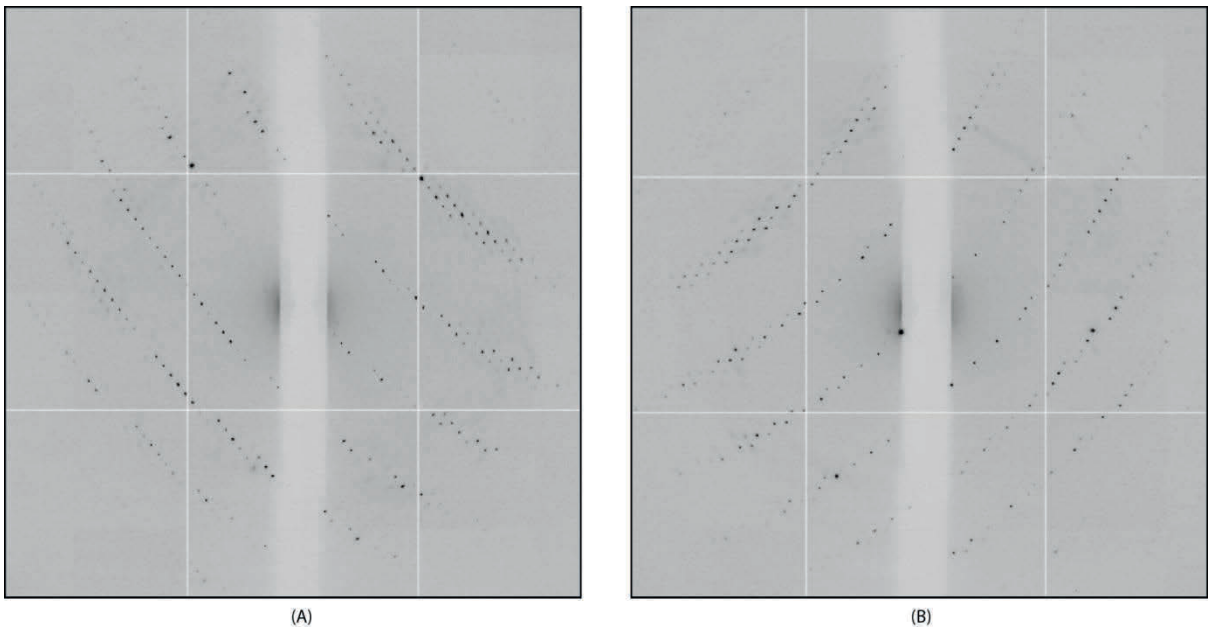


Figure 5.5: Diffraction of TFL1 14-3-3 Nu complex grown in 500mM Li_2SO_4, 18% PEG 8000 and 8% Glycerol (A) Initial diffraction images showing a lattice-like pattern **(B)** diffraction of the crystal when rotated.

A native data set for the crystals of the complex of TFL1-4-3-3 Nu with the FD peptide (described in section 5.2.3.2) was collected on the MX-I03 beamline at the Diamond Light Source and was processed using the iMOSFLM software (Figure 5.5). Data processing revealed that the crystal belonged to the primitive trigonal space group P3 2 1 with unit cell parameters, a = 185 Å, b = 185 Å, c = 65.19 Å (α = 90°, β = 90°, γ =120°). To estimate the number of molecules within the unit cell the Matthews' coefficient was calculated. A one tetramer solution (two TFL1 and a 14-3-3 Nu dimer) with a Matthews' coefficient of 3.22 Å3 Da-1 and an estimated solvent content of 61.81% was considered most probable. The estimated solvent content was similar to the high solvent content observed in the related floral activation complex structure (Matthews, 1968, Kantardjieff and Rupp, 2003; Server: http://www.ruppweb.org/mattprob/, Taoka et al., 2011). A summary of the statistics for the data set is given in Table 4.1.

Table 5.1: Data collection statistics. Values in parentheses are the highest resolution shell.

	Overall (Highest Resolution Shell)
Wavelength (Å)	0.9686
Resolution (Å)	5
Space Group	P3 2 1
Unit Cell Parameters (Å)	
A	185
B	185
C	65
No of Observed Reflections	25890
No of Unique Reflections	5090
Multiplicity	5.1 (4.7)
Completeness (%)	93.7 (94.3)
Mean I/σ	20.6 (2.3)
R_{merge}	0.10 (0.69)
R_{fact}/R_{free}	0.35/0.36

5.2.3.4 Crystal Structure of Floral Inhibitory Complex

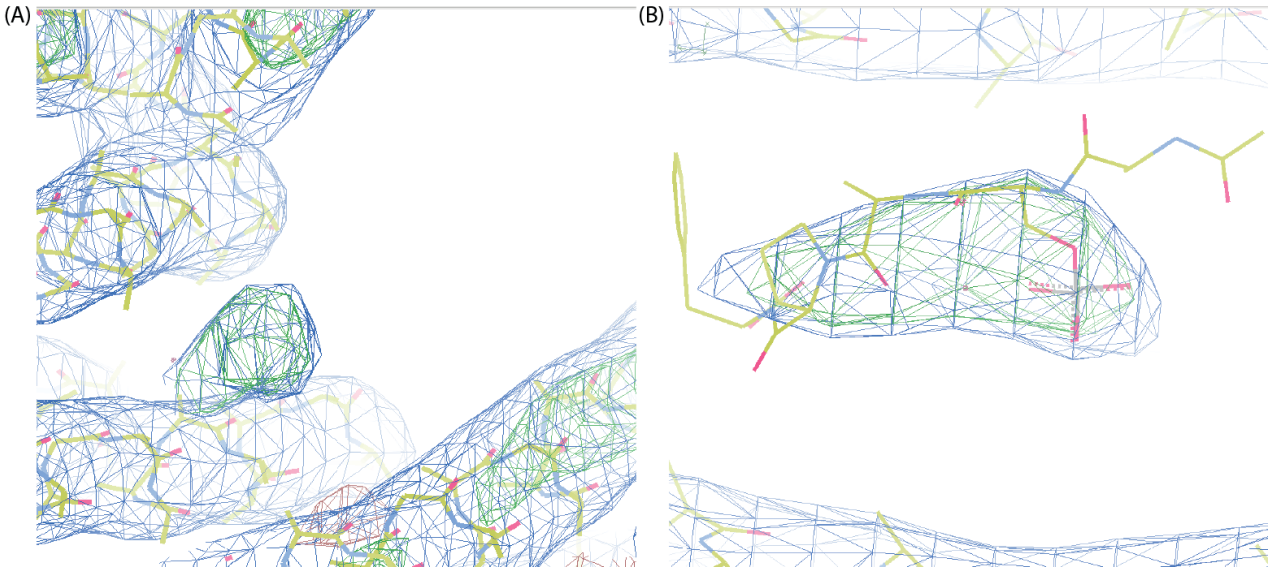


Figure 5.6: Electron density observed from the structural determination of Floral Inhibitory Complex.(A) Density is observed between the α-helices of 14-3-3 Nu. **(B)** A model of the FD C-terminal peptide within the electron density found between the α-helices of 14-3-3 Nu. 2Fo-Fc map shown in blue with contour levels set to 1.5 sigma. Fo-FC shown in green and red with contour levels set to 3 sigma.

The crystal structure of the floral inhibitory complex was solved using molecular replacement. The complex has a similar arrangement to the proto-floral inhibitory complex with two TFL1 protomers interacting with the C-terminal helices of the 14-3-3 (Figure 5.6). Electron density was observed in the two large positively charged pockets found in the 14-3-3 dimer (Rittinger et al., 1999, Taoka et al., 2011). To determine if this density could belong to the peptide, the FAC crystal structure (3AXY) was overlaid on to the FIC structure. The 14-3-3 and HD3a models were removed leaving the peptide in place. A large section of the peptide fitted the electron density; with significant difference density observed around the region of the phosphorylated residue (Figure 5.6; Figure 5.7). This suggests that the C-terminus of FD associates indirectly with TFL1 via members of the 14-3-3 protein family and suggests that the arrangement of the interaction between FD and TFL1/FT is highly conserved.

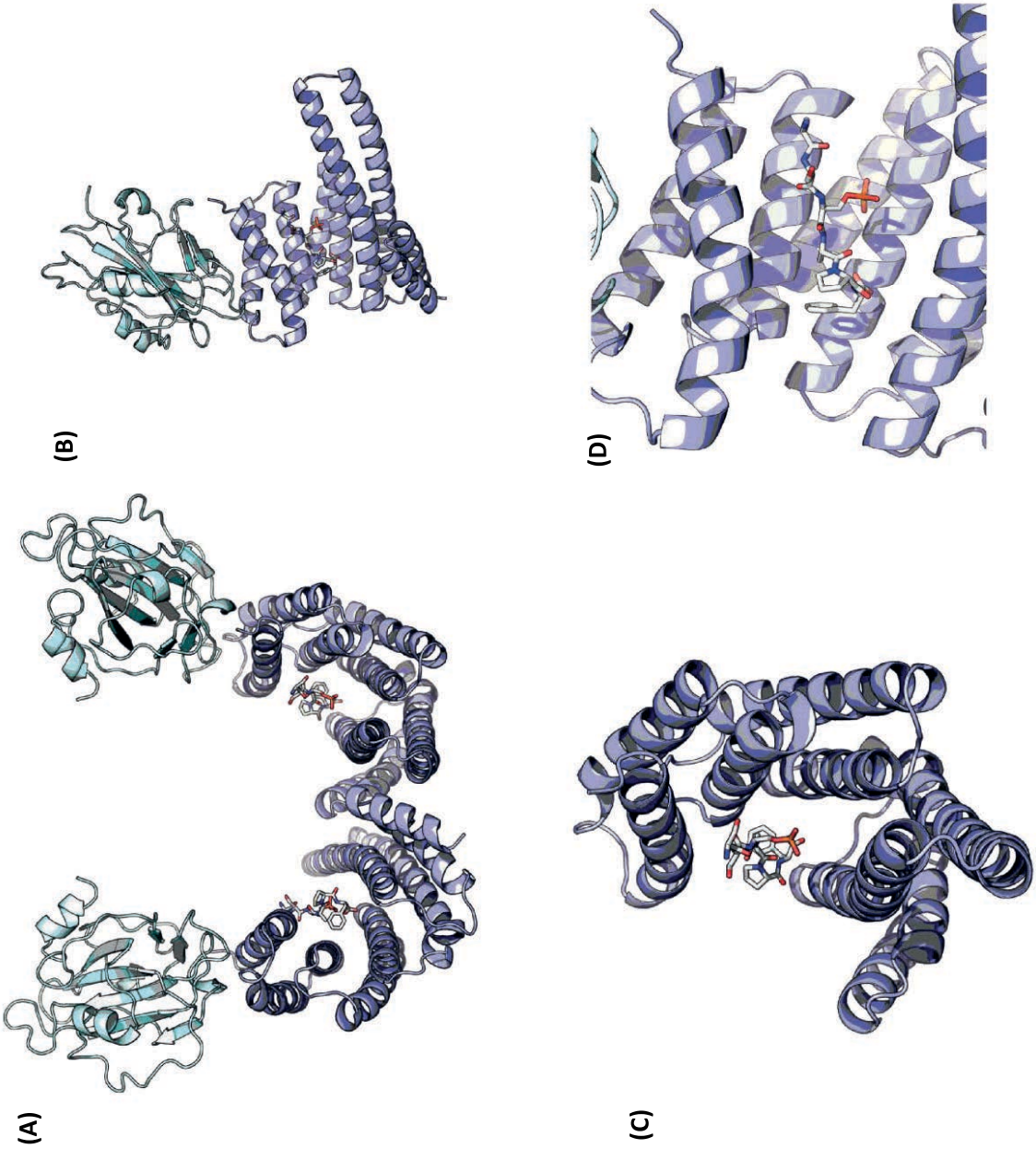


Figure 5.7: Structure of the Floral Inhibitory Complex. The hetero-tetrameric structure of the FIC with two TFL1 (cyan) complexed with a 14-3-3 Nu dimer (blue). **(A)** The cartoon diagram of the FIC. **(B)** Surface charge representation of the complex. Blue positive charge. Red negative charge.

5.3 Discussion

5.3.1 The Floral Inhibitory Complex

5.3.1.1 FD interacts with 14-3-3 Nu

FD plays a pivotal role in regulating the transcription of genes involved in flowering (Hanano and Goto, 2011, Wigge et al., 2005). TFL1's activity is dependent on FD (Hanano and Goto, 2011). However, it has not been clear whether FD and TFL1 interact directly. In this study, the arrangement of TFL1 and 14-3-3 Nu with the C-terminus of FD was elucidated. This interaction has been shown to been essential for the association between FT and FD (Abe et al., 2005). In this study, the C-terminus of FD is shown to interact with and stabilise 14-3-3 Nu, but not TFL1. Despite the limited resolution of the crystal structure, difference density could be observed in the region where peptide was observed in the FAC complex.

5.3.1.2 The Phosphorylation of FD

Phosphorylation of FD is essential for the transduction of floral signals (Abe et al., 2005). Mutations converting a threonine at position 282 to alanine prevents binding between floral PEBP and FD in yeast-two hybrid assays (Abe et al., 2005). Moreover, the mutation of the equivalent residue in rice FD abrogates the effect of FD overexpression (Taoka et al., 2011). Binding studies have demonstrated that phosphorylation is critical for the interaction between 14-3-3 proteins and their targets (Muslin et al., 1996).

Typically, 14-3-3 proteins are capable of binding their phosphorylated target proteins with typical dissociation constants in range of 200-600 nM (Muslin et al., 1996, Yaffe et al., 1997). In this study, the phosphorylated C-terminus of FD was show to bind to 14-3-3 Nu with a dissociation constant of approximately 700 nM which suggests strongly that the mechanism involved in the creation of the FIC are similar to those previously observed between 14-3-3 proteins and their targets. In the FAC, the phosphate moiety is coordinated by two arginines and a tyrosine (Taoka et al., 2011). Given the similarities between the FIC and the FAC, and in particular the similarities between 14-3-3 Nu and GF14c,

and given that the FD peptide in the FIC structure appears to be in same location it is possible that binding might be mediated in a similar way.

However, it is not clear what regulates or effects the phosphorylation of FD although it is clear that phosphorylation does not directly affect the sub-cellular localization of FD homologs (Tsuji et al., 2013). Mutations to the C-terminal phosphorylation site in FD homologs in rice from serine to alanine do not affect presence of FD in the nucleus. Consequently the kinase responsible must be able to travel into the nucleus. FD may play a role in trapping floral complexes within the nucleus. After the floral PEBPs interact with 14-3-3 proteins they can be trafficked into the nucleus. Phosphorylated FD may then recruit, bind and trap the complexes within the vicinity of the associated floral promoters.

5.4 Summary

FD, a bZIP transcription factor, critical for the biological inhibition of flowering forms a complex with TFL1. Here it is shown that the phosphorylated C-terminus interacts with 14-3-3 Nu but not with TFL1. The interaction between FD and 14-3-3 Nu is comparable in strength to previously characterised interaction between 14-3-3 proteins and their targets. Structurally, this interaction is likely to occur at the electropositive cleft away from the TFL1 binding site in a similar manner to the arrangement found in the FAC.

Chapter 6 - Assessment of the Interaction between DNA and The Floral Complexes

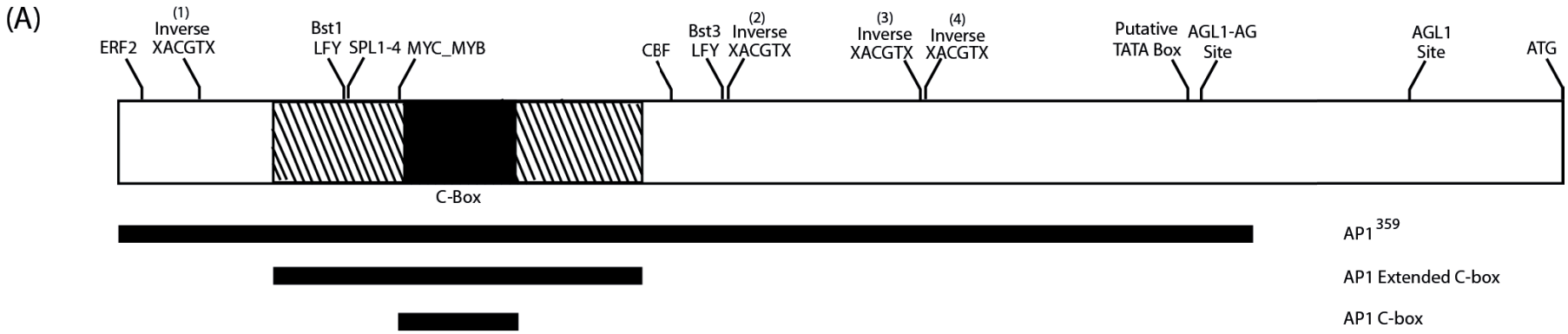
6.1 Introduction

Expression of the transcription factor AP1 is an early step in floral development in *Arabidopsis* (Mandel et al., 1992). FT promotes the transcription of AP1 through FD (Abe et al., 2005). A 500 bp core promoter has been shown to be essential for transcription *in vivo*, suggesting that the FAC binds within this region (Wigge et al., 2005). A C-box motif, often associated with bZIP transcription factors, has been bioinformatically predicted within the core promoter (Wigge et al., 2005). However, no direct interaction between *Arabidopsis* FD and the *Arabidopsis* C-box has been observed (Benlloch et al., 2011). Moreover, the overexpression of FD can drive the expression of GUS, under the control of the AP1 promoter with a mutated C-box, in plants (Benlloch et al., 2011). Collectively, this suggests that the C-box is not the FAC binding site, *in vivo*. To elucidate the precise mechanisms by which TFL1 negatively regulates AP1, this study examines the interaction between the FIC and the FAC with the AP1 promoter to understand the structural basis for the antagonistic activities of FT and TFL1.

6.2 Results

6.2.1 Bioinformatics and Design of the AP1 Promoter Fragments

The 500 bp region identified as the core promoter was assessed computationally via AthaMap for transcription factor binding sites (Steffens et al., 2004) (Figure 6.1). The 500 bp region contained LFY (Bst1), SQUAMOSA PROMOTER BINDING PROTEIN-LIKE (SPL) and MYC_MYB binding sites, in close proximity to the C-box. A second LFY binding site (Bst3) was observed approximately 113 base pairs from the C-box. A motif with characteristics of a TATA box was observed 140 bp upstream of the start codon immediately preceding several binding sites for the AGAMOUS (AG) family of MADS box transcription factors. Throughout the region several inverse ACGT motifs were identified. A 359 bp section of DNA was created, based on the 500 bp minimum promoter that but excluding the region beyond the TATA box (Figure 6.1). Given the significant focus on the C-box, two regions centred around the C-box were also created; a 22 bp section and a 71 bp extended section.



(B)

Extended C-box: TAC AAT GTT ACT TAC CCA TTT CTC TTC ACG AG**A CGT** CGA TAA TCA AAT TGT TTA TTT TCA TAT TTT TAA GT

C-box: C TTC ACG AG**A CGT** CGA TAA TCA

(C) Inverse XACGTX:

1: AA TGCA AA
TT ACGT TT

2: TT TGCA AA
AA ACGT TT

3: CC TGCA AA
GG ACGT TT

4: AA ACGT AA
TT TGCA TT

Figure 6.1: Schematic of the AP1 Core promoter region. (A) DNA from the AP1 promoter was assessed bioinformatically. Transcription factor binding sites and key features are noted. Construct in experiments are used are noted below. **(B)** Sequence of the C-box constructs C-box core highlighted. **(C)** Sequences of unusual A/G/C-box like features.

6.2.2 Assessment of FIC and FAC Interaction with AP1 Promoter DNA

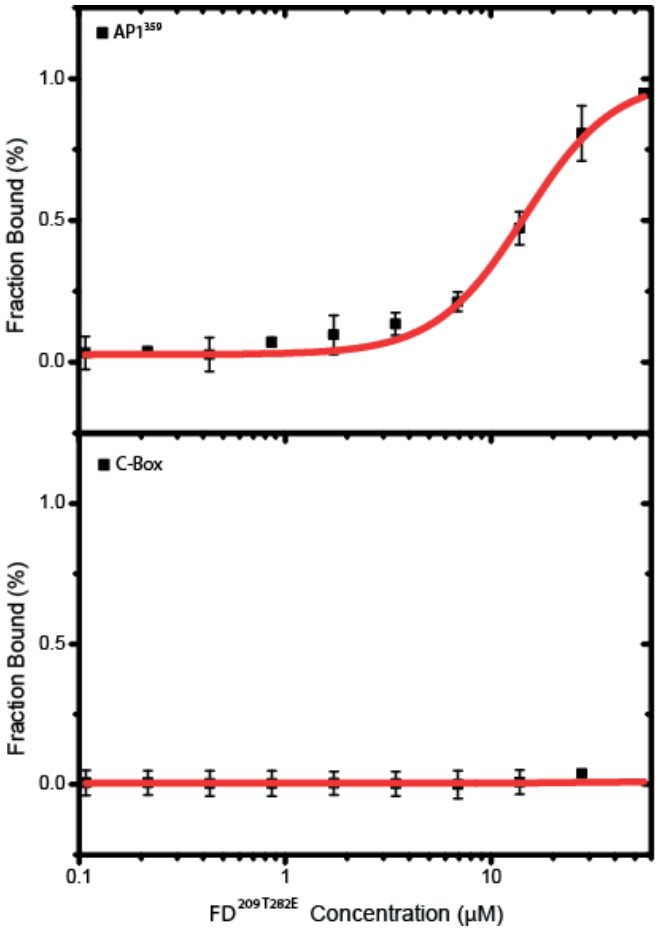


Figure 6.2: The interaction between FD209 ^{T282E} and elements of the AP1 promoter. Interaction as measured by using microscale thermophoresis. FD209 ^{T282E} was titrated against a fluorescently labelled 359 bp section of the AP1 promoter containing the C-box region and a short fluorescently labelled 22 bp section representing the C-box. The fraction bound was plotted against the concentration FD209 ^{T282E}.

To establish whether a binding site for FD existed within the 359 bp oligomer, FD$^{209\ T282E}$ was titrated into labelled AP1^{359} (Figure 6.2). A change in thermophoresis was observed upon the addition of increasing concentrations of FD$^{209\ T282E}$ indicating the formation of complex. After plotting the fraction bound against the concentration of FD$^{209\ T282E}$ and fitting with a one site binding model, a low μM dissociation constant (Kd) was estimated. As a comparison, the interaction between the C-box and FD$^{209\ T282E}$ was assessed; no binding was detected between the components. Thus despite FD$^{209\ T282E}$ being capable of binding to the 359 bp region, FD$^{209\ T282E}$ alone was not sufficient to mediate a detectable interaction with the C-box.

6.2.3 Assessment of FIC and FAC Interaction with AP1 Promoter DNA

6.2.3.1 Assessment of FIC and FAC Interaction with AP1 Promoter DNA

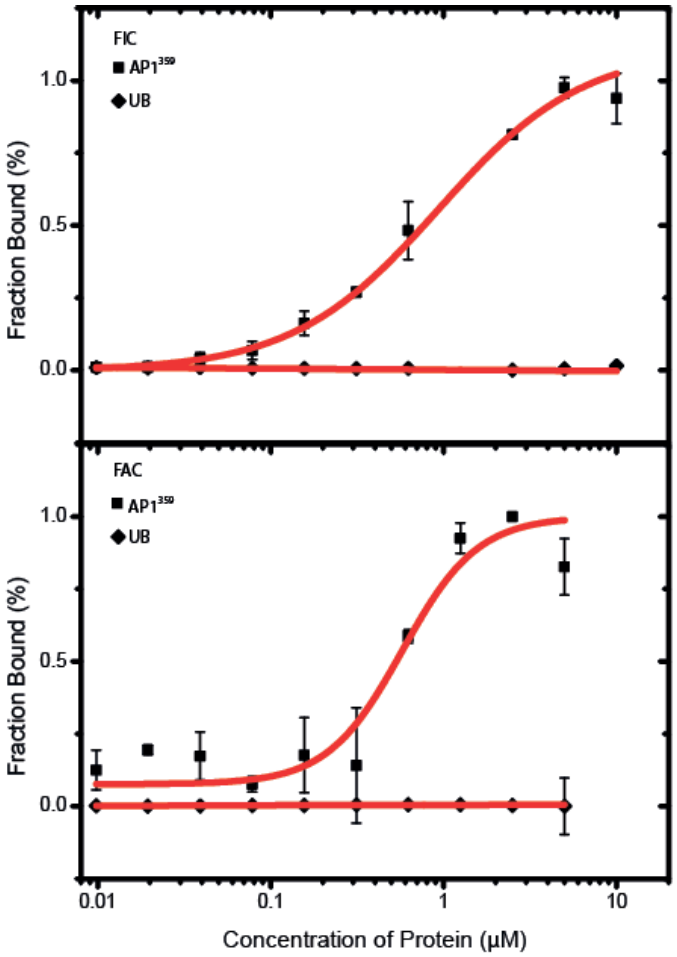


Figure 6.3: The interaction between FIC and FAC with elements of the AP1 promoter. Interaction as measured by using microscale thermophoresis. Complexes were titrated against a fluorescently labelled 359 bp section of the AP1 promoter containing the C-box or DNA from ubiquitin. The fraction bound was plotted against the concentration complex.

To assess whether the FAC or the FIC could bind to $AP1^{359}$, both complexes were titrated into labelled $AP1^{359}$ (Figure 6.3). The addition of FIC to $AP1^{359}$ caused a change in thermophoresis indicating that the FIC was capable of interacting with $AP1^{359}$. To ensure specificity the FIC was titrated against a 245 bp sequence encoding mammalian ubiquitin. No binding was observed between the FIC and ubiquitin. Complex formation was also observed when the FAC was titrated into $AP1^{359}$. No binding was observed between the FAC and ubiquitin. Both interactions were plotted and fitted with a one site binding model. A high nM Kd was estimated for both interactions.

6.2.3.2 Assessment of proto-FIC and proto-FAC Interaction with AP1 Promoter DNA

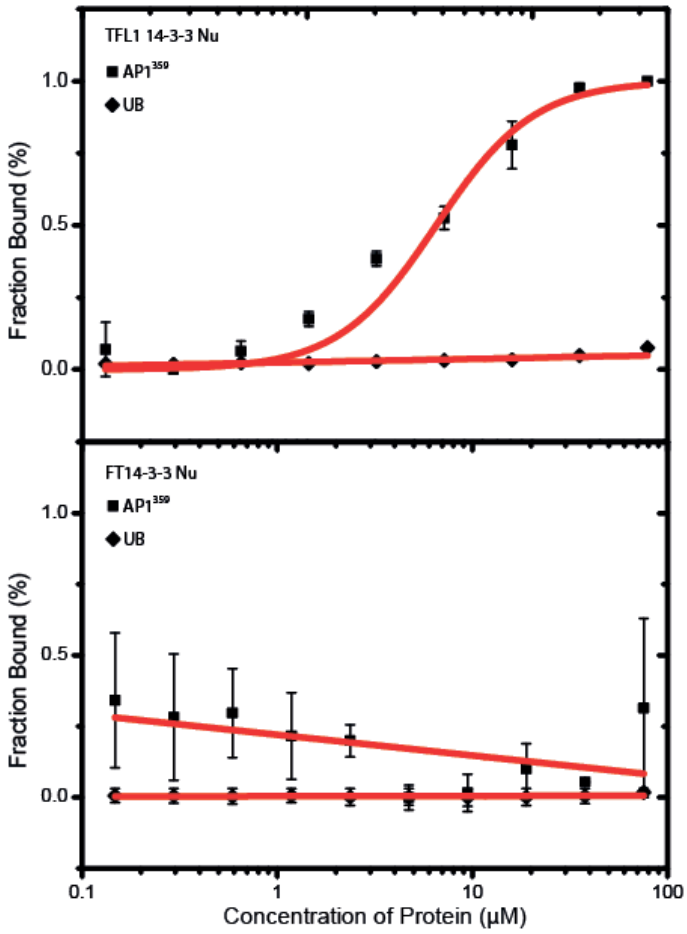
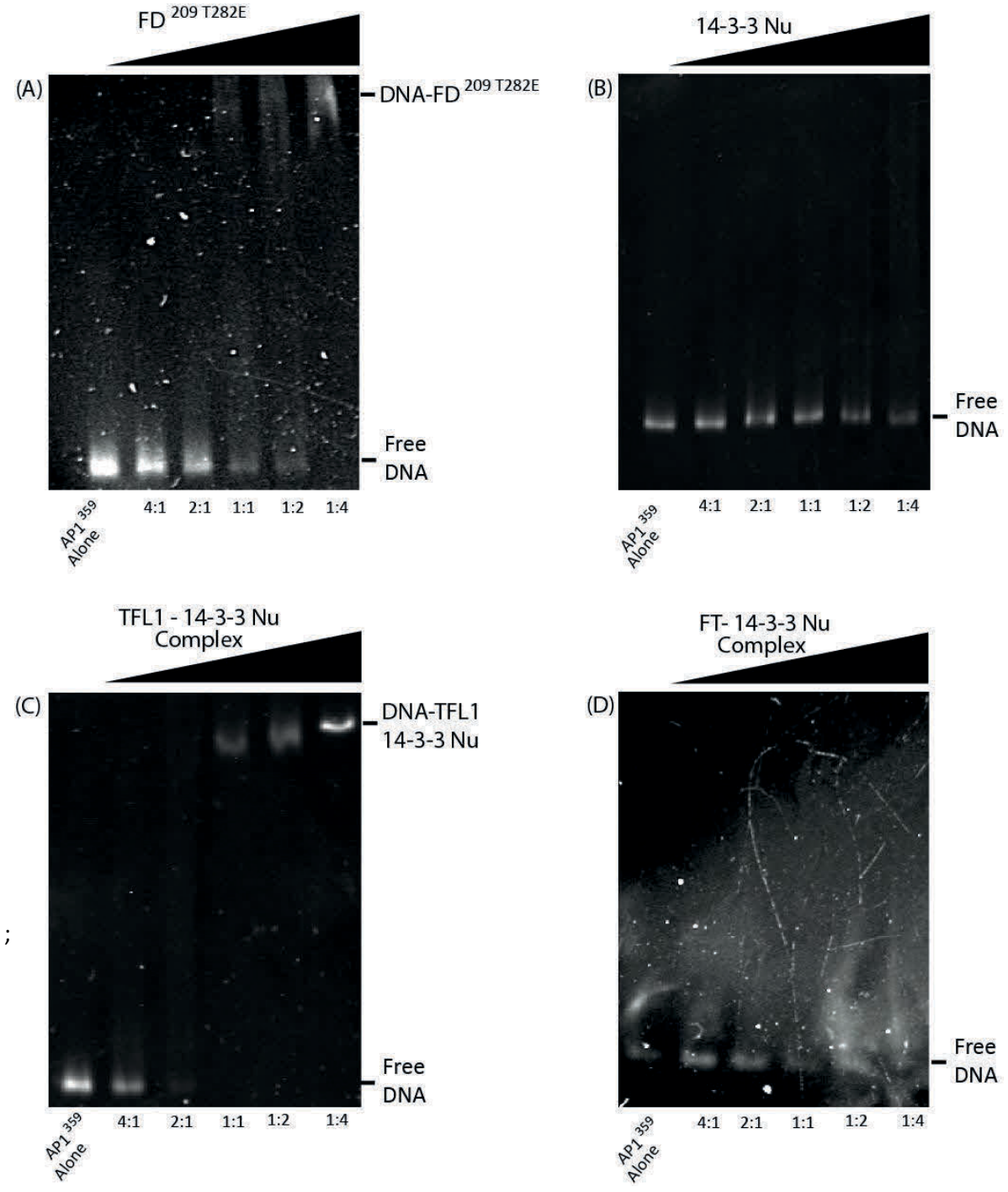


Figure 6.4: The interaction between proto-FIC and proto-FAC with elements of the AP1 promoter. Interaction as measured by using microscale thermophoresis. Complexes were titrated against a fluorescently labelled 359 bp section of the AP1 promoter containing the C-box or DNA from ubiquitin. The fraction bound was plotted against the concentration complex.

To determine whether FD was essential for the interaction between the complexes and DNA, the proto-FIC and proto-FAC were titrated into labelled $AP1^{359}$ (Figure 6.4). When the proto-FIC was titrated into $AP1^{359}$ a change in thermophoresis, indicative of binding, was observed. This interaction was fitted with a one site binding model to DNA and a low µM Kd was estimated. Comparisons of the binding demonstrated that the proto-FIC bound $AP1^{359}$ with significantly lower affinity than the FIC (Appendix 3b). In contrast, no binding was observed upon the addition of the proto-FAC complex. No change was observed upon the addition of either complex to fluorescently labelled ubiquitin DNA inferring that the interaction was specific.



;

Figure 6.5: Assessment of the interaction between proto-FIC and components by Native gel. Protein was titrated against a 359 bp section of the AP1 promoter containing the C-box. The molar ratio of DNA to protein is shown underneath each lane.

6.2.3.3 Assessment of Complex formation with AP1 Promoter DNA via Native Gel

To confirm the interaction between AP1 and the floral regulatory proteins, the purified proteins were mixed in with $AP1^{359}$ in various molar ratios and analysed by EMSAs (Figure 6.5). A shift was observed when purified $FD^{209\ T282E}$ was titrated into $AP1^{359}$, confirming that $FD^{209\ T282E}$ has a binding site in that region (Figure 6.5a). In contrast, no shift was apparent when 14-3-3 Nu was titrated into $AP1^{359}$ confirming that 14-3-3 Nu alone was not sufficient to mediate any interaction with DNA (Figure 6.5b). Both proto-FIC and proto-FAC were also tested for their ability to retard the progression of DNA. Increasing concentrations of proto-FIC resulted in a shift band; inferring that the proto-FIC can interact with DNA (Figure 6.5c). However, increasing the concentration of the proto-FAC did not cause any shift in the DNA (Figure 6.5d). These observations were fully consistent with those obtained through thermophoresis.

6.2.4 Assessment of FIC and FAC Interaction with C-Box DNA

To establish whether the C-box was the site for interaction between the complexes and DNA, two fluorescently labelled C-box oligonucleotides were prepared; a 22 bp C-box oligonucleotide and a 71 bp extended C-box oligonucleotide (Figure 6.6). When the FIC was titrated into the C-box no interaction was observed however when the FIC was titrated into the extended C-box a change in thermophoresis was observed indicating that the FIC is capable of interaction with the extended C-box. In contrast, no interaction was observed when the FAC was titrated into either the 22 bp C-box oligonucleotide or the 71 bp extended C-box. Likewise, no binding was detected when complex of FD-14-3-3 Nu was titrated to the C-box or to the extended C-box. Collectively, this suggests that the FIC binds at the C-box and that TFL1 is essential in mediating this interaction.

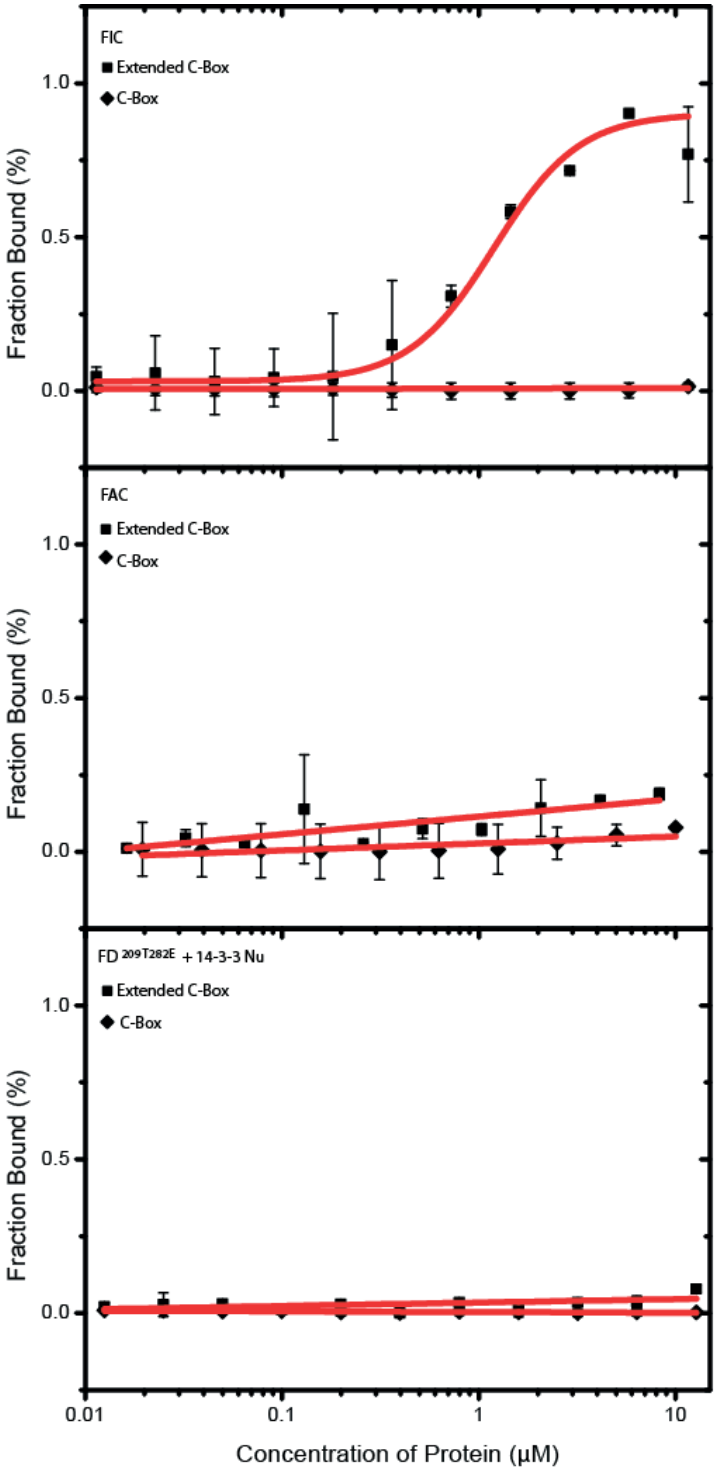


Figure 6.6: The interaction between FIC and FAC and elements of the AP1 promoter. Interaction as measured by using microscale thermophoresis. Complexes were titrated against a fluorescently labelled 71 bp extended C-box or the 22 bp C-box. The fraction bound was plotted against the concentration complex.

6.2.5 Electron Microscopy of FIC and DNA

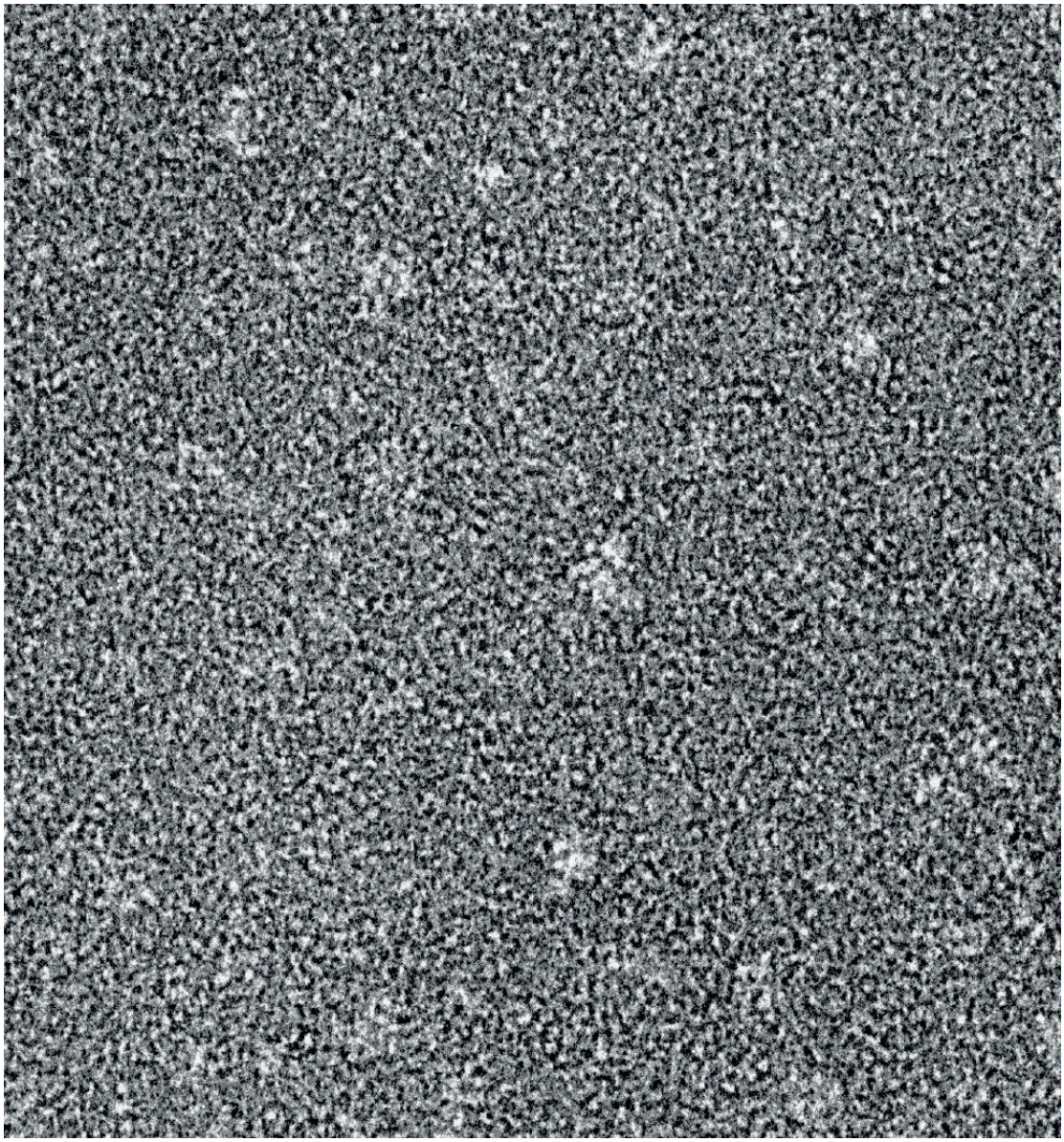


Figure 6.7: Images of Micrographs collected for the negative stain structural analysis of the FIC. Complex incubated with Extended C-box DNA imaged under and electron microscope.

To elucidate the structural basis of the interaction with DNA structural characterization by electron microscopy was initiated (Figure 6.7). Data was collected on a Philips CM200 electron microscope, operating at 200 kV with a 50,000x magnification. Images were taken on a CCD camera. Micrographs were checked for drift and astigmatism. Micrographs were then assessed visually, and those that showed good contrast, with a good distribution of clearly visible particles were used for further processing.

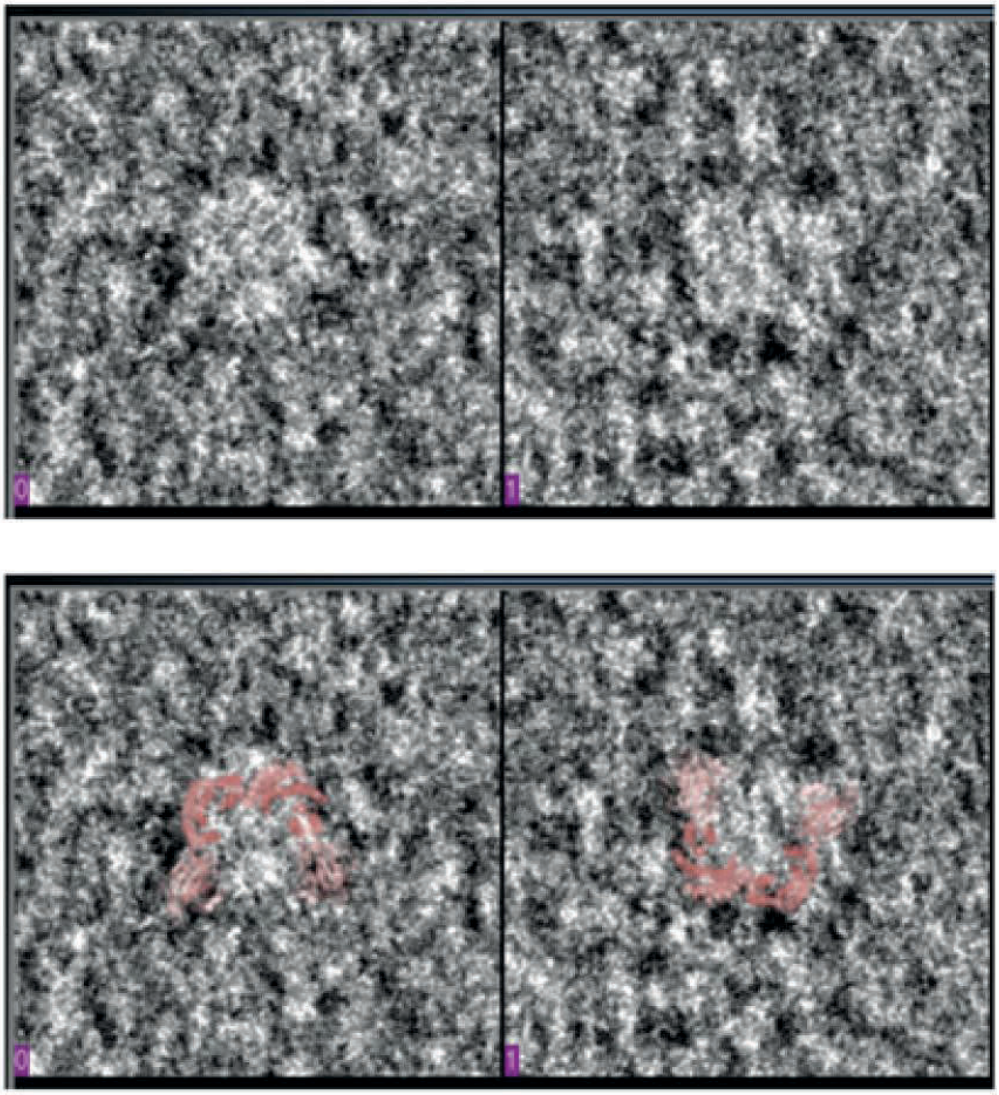


Figure 6.8: Structural assessment of the particles found on the micrograph. Putative particles were boxed with a 200 by 200 pixel box. Particles were shown to have a similar shape to the complex after assessment against the crystal structure of the proto-FIC.

To determine the structure of the complex with DNA particles were picked interactively from micrographs using a 200 by 200 pixel box (Figure 6.8). Particles appeared to have the same dimensions and overall shape as the crystal structure. It was not possible to determine the location of DNA in images of single particles, though DNA may be present in the sample.

6.3 Discussion

6.3.1 The Interaction of FD with DNA

6.3.1.1 FD binds to the Minimal Promoter but not at the C-box

Previously, it has been suggested that FD binds to the AP1 promoter at the C-box although a direct interaction has not been established with *Arabidopsis* FD (Wigge et al., 2005, Benlloch et al., 2011). The data suggests that FD alone does not bind to C-box, but instead binds to an alternative FD binding site within $AP1^{359}$. Several ACGT-like motifs exist across the promoter which may facilitate binding. Importantly, in the AP1 homolog in rice (OsMADS15) no perfect C-box exists within the area analogous to the core promoter suggesting that FD and FD-like proteins may have the ability to bind non-canonical sequence motifs (Taoka et al., 2011).

6.3.2 The Floral Complexes Differentially Interact with DNA

6.3.2.1 The Extended C-box Contains the FIC Binding Site

Both the FIC and the FAC are capable of interacting with $AP1^{359}$. This infers that both complexes have binding sites within the core promoter. It was previously assumed that the FIC and FAC would bind to a single site determined by FD, in this study, the possibility of two or more binding sites is highlighted. TFL1 and FT appear to determine the location at which the complexes bind. This is possible because the proto-FIC appears to have properties that enable it to associate weakly with DNA which the proto-FAC lacks (Benlloch et al., 2011). This may partially explain why no interaction has been detected between the *Arabidopsis* C-box and Arabidopsis FD in previous electrophoretic mobility shift assays (Benlloch et al., 2011). It is possible that TFL1 mediates the indirect interaction of FD to the C-box.

6.3.2.2 The Role of the FIC-DNA Interaction

The presence of TFL1 and the nucleotides around the C-box appears to be required to enable the FIC to bind to DNA. This implies that TFL1 may associate with the AT rich region around the C-box. However, it is unclear if the interaction with DNA has any other effects. It is possible that the interaction between the

TFL1 and DNA acts to obscure the binding sites for LFY and SPL family of proteins which are found in close proximity to the binding site (Figure 6.1). Both the SPL family of proteins and LFY are important for the correct initiation of flowering. The SPL family of proteins are a group of transcription factors that bind to DNA via a SBP domain (Klein et al., 1996). SPL3 and SPL4 are known to accelerate flowering when over expressed in *Arabidopsis* (Cardon et al., 1997). SPL3 is known to increase the expression of FUL and AP1 without altering the levels of FT (Yamaguchi et al., 2009). This suggests that SPL3 works directly upon the expression of AP1. Consequently, one possible mechanism of TFL1 based floral inhibition is the inhibition of SPL protein-DNA binding by steric hindrance around the SPL proteins' binding site. Likewise, mutations to LFY affect the development of flowers (Schultz and Haughn, 1991). The LFY binding site (bst1) in the AP1 promoter is within the extended C-Box (Benlloch et al., 2011). Inhibiting binding could be a mechanism by which TFL1 delays the development of flowers.

Alternatively, the association with DNA may affect the conformation of DNA which may alter gene transcription. DNA bending has been shown to be one mechanism by which gene regulation is mediated (TenHarmsel and Biggin, 1995). It can operate by preventing the interaction of Transcription Factor II D ($TF_{II}D$) with DNA (TenHarmsel and Biggin, 1995). The region around the C-Box is high AT rich and it is feasible that this region is flexible. This would enable the proto-FIC to indirectly influence the binding of additional factors. In this case, TFL1's role would be to guide additional factors to specific regions of DNA to enable gene repression.

6.3.2.3 The FAC Binding Site

In this study, no interaction was observed between the FAC and the extended C-box region; this implies that the FAC binds to a different location. Given that there is no observable interaction between $AP1^{359}$ and the proto-FAC but there is an interaction between $AP1^{359}$ and the FAC it is possible that FD mediates an interaction between the FAC and the FAC binding site. Simply, the binding between the FAC and DNA may be FD driven. It is possible that the FAC binds to the alternative FD binding site whilst the FIC binds to the extended C-box region.

6.3.2.4 The FIC and FAC may bind Several Sites

Though an interaction has been established between the floral complexes and AP1[359] this does not preclude the possibility that the proto-FAC can bind outside of the core promoter region. It is possible that several binding sites are occupied by the FIC and the FAC simultaneously across the length of the full promoter. However, currently the number and nature of binding sites still requires confirmation using techniques like DNA footprinting.

6.4 Summary

TFL1 is thought to regulate the expression of the floral identity gene AP1 (Hanano and Goto, 2011). A 500 bp core promoter is essential for the activity, *in vivo* (Wigge et al., 2005). Here it is demonstrated that the both the FIC and the FAC can bind to the core promoter region. Moreover, the FIC can bind weakly even in the absence of FD. The FIC is capable of binding to the region around the C-box whilst the FAC binds in a different location. No direct interaction was observed between the bZIP region of FD and the C-box implying that FD requires TFL1 and a 14-3-3 protein to interact. The FD bZIP was also shown to interact with a longer stretch of DNA implying that an alternative FD binding site might be present within the core promoter.

Chapter 7 - Assessment of the Extended Loop *in vivo*

7.1 Introduction

The opposing activities of TFL1 and FT have been linked to the extended loop, *in vivo* (Ahn et al., 2006). In TFL1, the loop is composed of 14 amino acids. Plants overexpressing chimeric FT with the loop of TFL1 flower late, implying that some of the residues responsible for TFL1's activity lie within the loop (Ahn et al., 2006). Similar experiments have demonstrated that the loops of FT-like and TFL1-like proteins in other species are responsible for mediating their antagonistic activity. In *Beta vulgaris*, two proteins with high sequence similarity to FT, regulate flowering; BvFT2 a protein that has FT-Like activity and BvFT1 that has TFL1-like activity (Pin et al., 2010). Plants overexpressing in BvFT1 have a delayed flowering phenotype (Pin et al., 2010). Importantly, the loops of these proteins differ by three amino acids found toward the C-terminal portion of the loop. BvFT2 shares Tyr^{134}, Gly^{137} and Typ^{138} with *Arabidopsis* FT whilst BvFT1 has an asparagine and two glutamines in those positions (Pin et al., 2010). However, currently there is little information regarding whether these residues are critical for the biological activity of *Arabidopsis* FT. To provide further information regarding TFL1's mechanism of action, this study examines the effects of mutations to the loop of FT, with the goal of converting FT into a TFL1-like protein.

7.2 Results

7.2.1 Construct Design and Transformation of FT-NQQ-GFP

An FT plasmid was modified by sequential site directed mutagenesis so that Tyr^{134}, Gly^{137} and Trp^{138} were converted to their equivalent residues in BvFT1 (Figure 7.1a). The modified insert was amplified, cloned without a stop codon into the vector PGWB5 (Nakagawa et al., 2007) (Figure 7.1a; Figure 7.1b). The plasmid was transformed into *Agrobacterium* and subsequently into *Arabidopsis*. T1 plants were grown on MS plates with antibiotics for 11 days and healthy plants were transplanted onto soil. Leaves from T1 plants were imaged with confocal microscopy as transformed plants could be identified by the presence of GFP fluorescence by exciting GFP with laser light at 488nm and observing signals within a detection

window around the maximal emission of GFP (Figure 7.1c). DNA was taken from plants and amplified using gene specific primers, the band was then confirmed by sequencing as the belonging to FT-NQQ-GFP (Figure 7.1d).

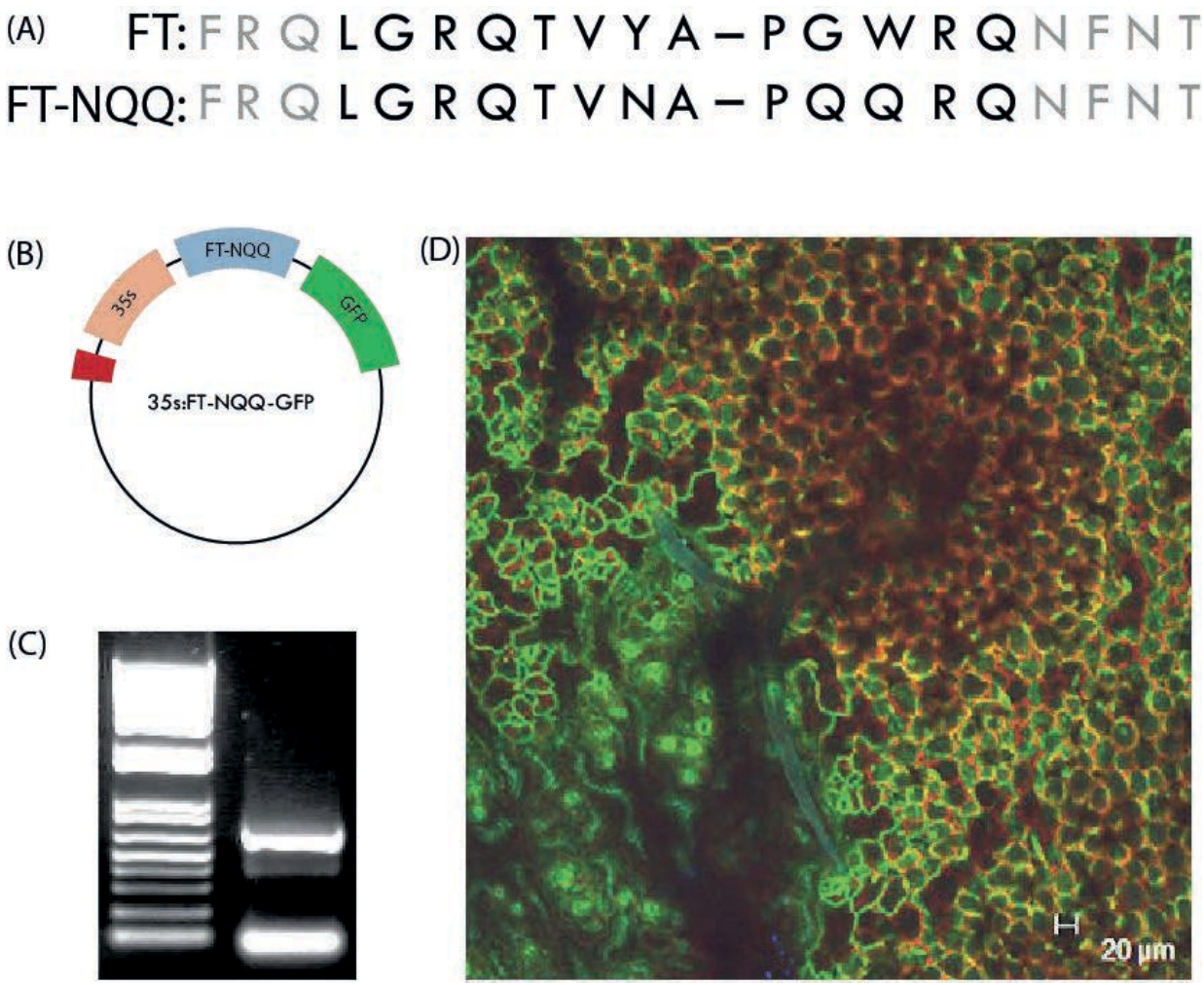


Figure 7.1:Design, construction and testing of FT-NQQ-GFP. (A) Sequence alignment of the regions of wild-type FT which were mutated to FT-NQQ-GFP shaded and boxed. **(B)** Schematic of the vector used in this study. The fusion protein FT-NQQ-GFP shown under the control of the **(C)** Genotyping transformants via the amplification of the FT-NQQ transgene by PCR. **(D)** Confocal microscopy of the leaves of T1 plants transformed with FT-NQQ-GFP. In all images GFP was excited by light at 488 nm and emissions were observed using a detection window between 490 to 570 nm. Background autofluorescence was excited using a 405 nm laser with a 410 - 480 nm detection band. The 633 laser line was also used as was a detection window set at 580 – 625 nm

7.2.2 Phenotypic Characterisation of FT-NQQ-GFP Plants

7.2.3 Assessment of the Early Development of FT-NQQ-GFP Plants

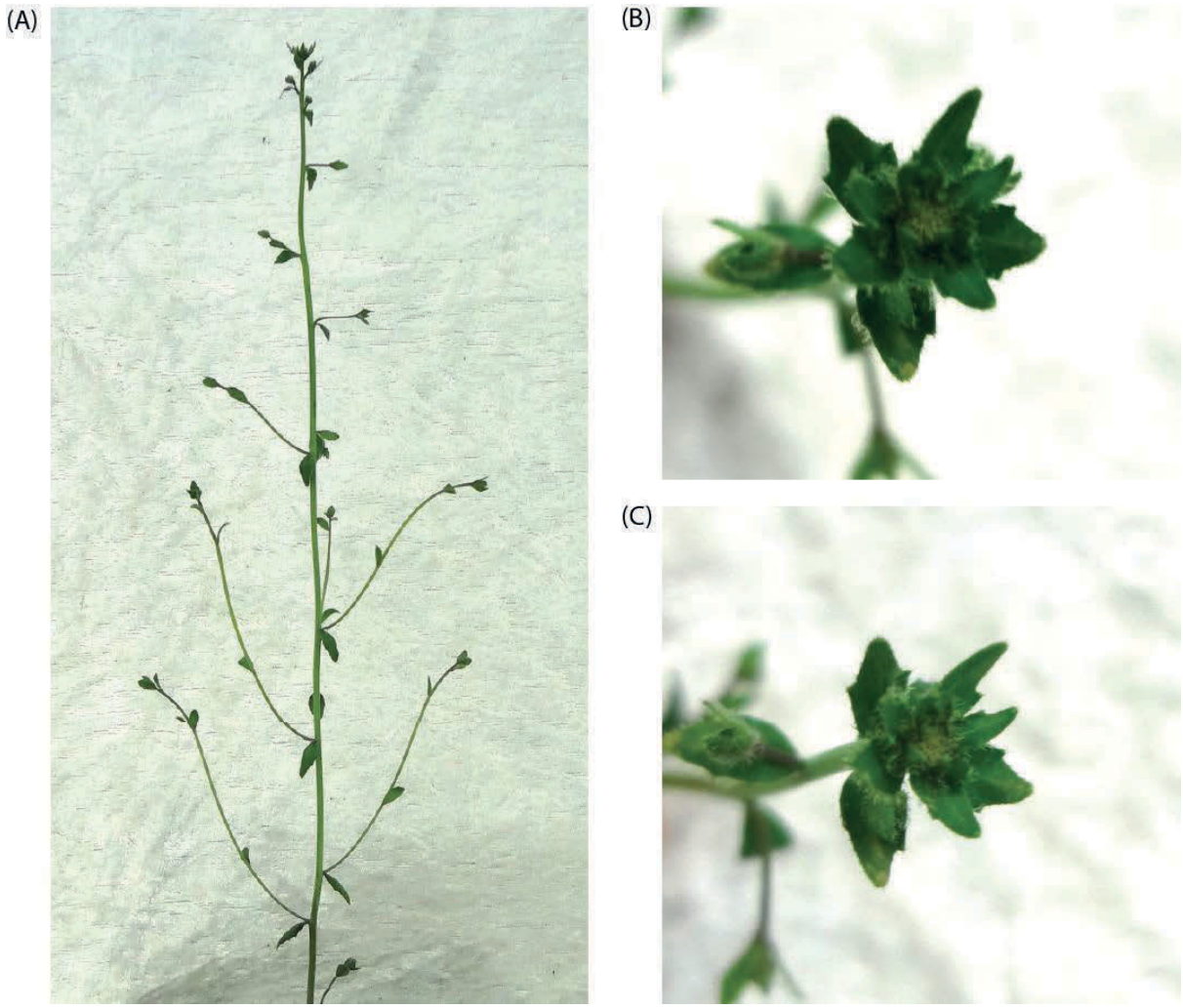


Figure 7.2: Early developmental phenotype of FT-NQQ-GFP plants at approximately 6 weeks. (A) Overall structure of the FT-NQQ-GFP plants after bolting. A series of secondary shoot are apparent. **(B - C)** The aberrant structure found at the tip of the primary inflorescence shoot.

T1 generation plants were phenotypically characterised after being transferred onto soil. T1 plants did not flower after bolting instead the primary inflorescences shoot produced an aberrant structure containing several leaf-like organs rather than floral organs (Figure 7.2). In the axils of the cauline leaves, secondary shoot developed. These structures gave rise to aberrant inflorescence-like structures at the tip. These secondary shoots continued to grow throughout the life of the plant creating a bushy phenotype (Figure 7.3).

7.2.3.1 Assessment of the Late Development of FT-NQQ-GFP Plants

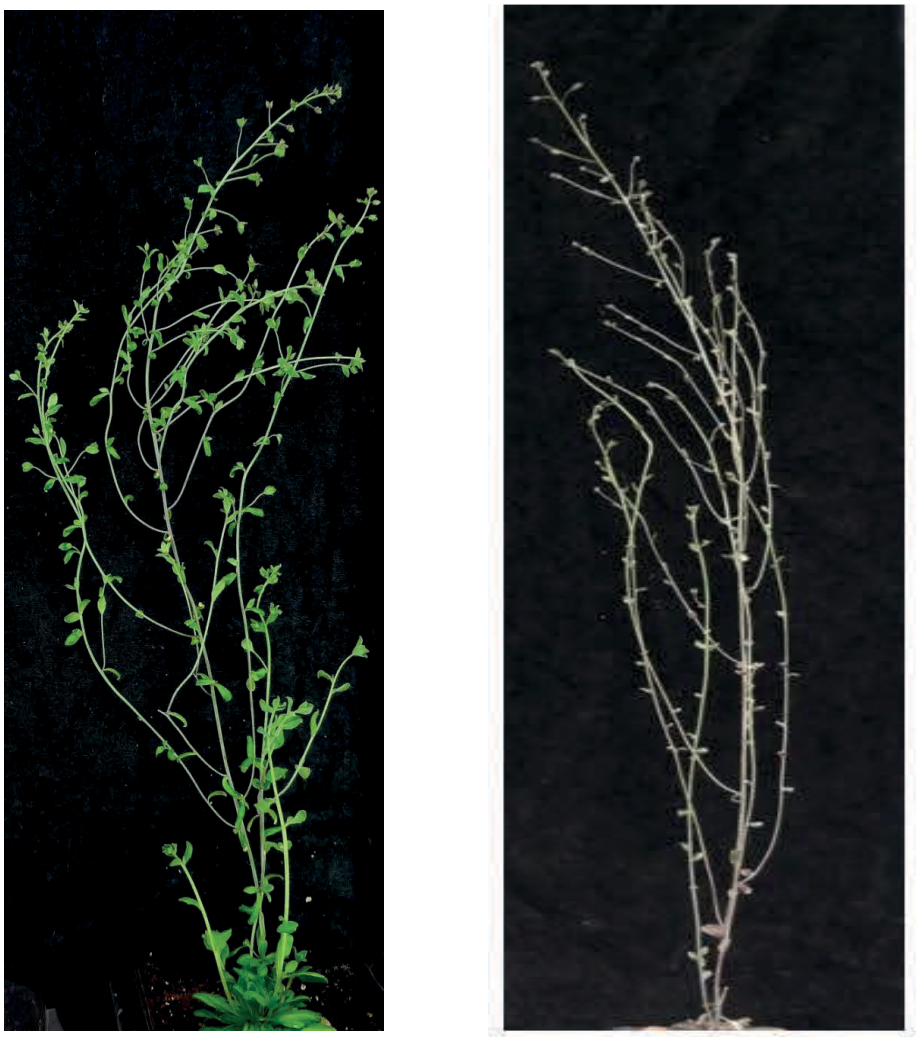


Figure 7.3: Late developmental phenotype of FT-NQQ-GFP plants at approximately 12 weeks. (A) Overall structure of a FT-NQQ-GFP plant. A series of elongated secondary shoot are apparent creating bushy appearance. **(B)** Overall structure of a second FT-NQQ-GFP plant. **(A-B)** Plants are approximately 60 cm in length.

Mutant plants grew to approximately 60 cm in length. Mutant plants initially developed a series of aberrant inflorescences which lacked the structures typically associated with flowers but after approximately 15 weeks flowers with typical structures appeared and the plants bore seed. Wild-type plants typically complete their life cycle in six weeks and were consequently not used for comparison at this stage (Figure 7.3). Two independent transformants with similar phenotypes were identified and characterised. Seed was collected from mutant plants and used to generate lines for further characterisation.

7.2.3.2 Assessment of Aberrant Inflorescences by Light Microscopy

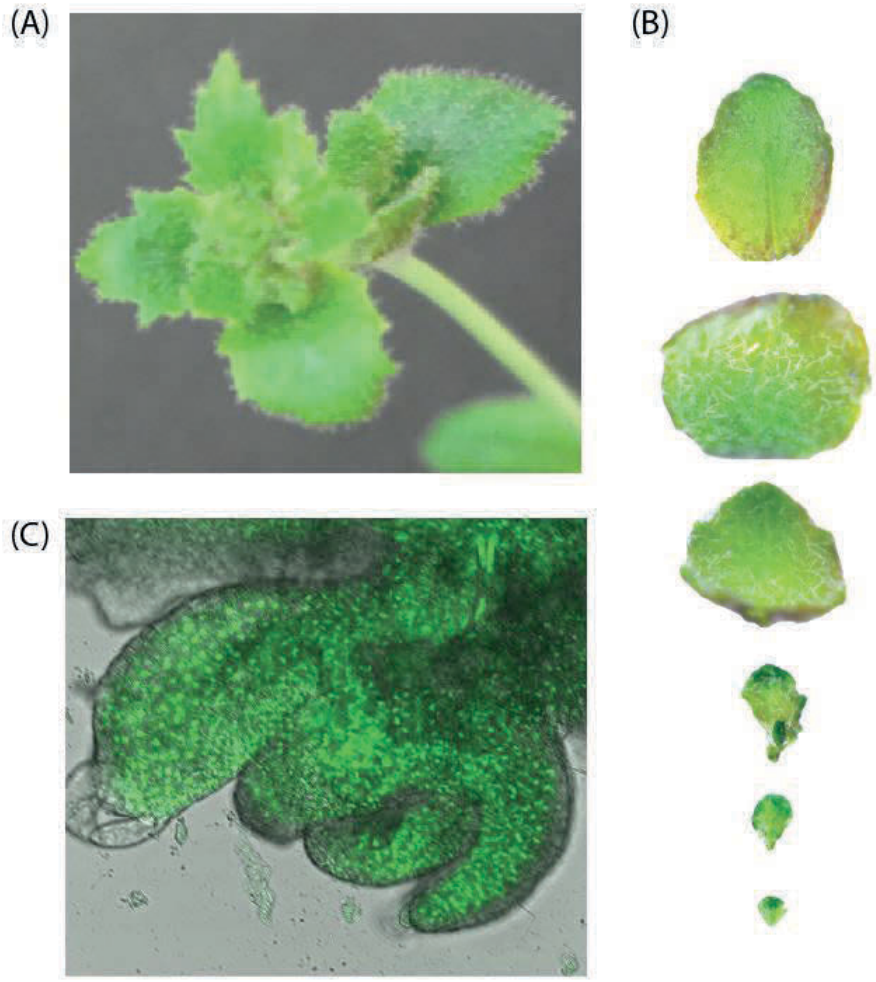


Figure 7.4: Assessment of aberrant inflorescences of FT-NQQ-GFP plants at approximately 12 weeks. (A) Aberrant inflorescences under a dissecting microscope. **(B)** Removal of the leaf-like structures found around the aberrant inflorescences. **(C)** Aberrant inflorescences after dissection under confocal microscope with bright field illumination. GFP was excited by light at 488 nm and emissions were observed using a detection window between 490 to 570 nm.

The inflorescences were assessed in further detail by a combination of light and confocal microscopy. The aberrant inflorescences were devoid of sepals, petals, carpels and stamens instead consisting of a series of leaf-like sepaloids (Figure 7.4a). These organs bore trichomes, similar to those found on cauline leaves. Removal of the outer layer of leaf-like sepaloids confirmed the absence of floral structures (Figure 7.4c). The dissected inflorescences were further examined by confocal microscopy (Figure 7.4). Under higher magnification no floral structures were evident in mutants though floral organs were observed in wild-type plants. GFP was excited by light from the 488 nm laser confirming the expression of FT-NQQ-GFP.

7.2.3.3 Assessment of Abhorrent Inflorescences by Scanning Electron Microscopy

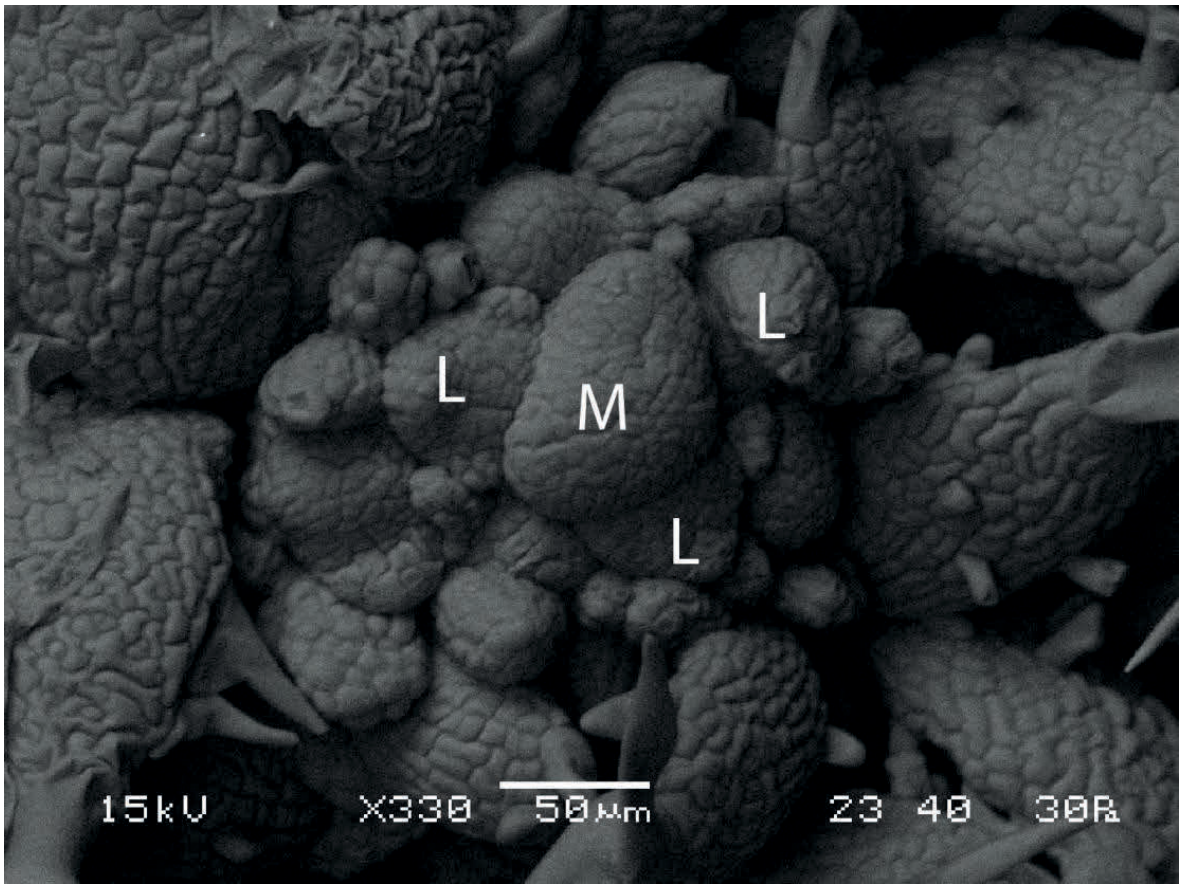


Figure 7.5: Assessment of aberrant inflorescences of FT-NQQ-GFP plants at approximately 12 weeks by Scanning Electron Microscopy. L - Leaf-like sepaloids. M - Meristem. Scale bar and magnification shown.

The ultrastructure of the meristem of the aberrant inflorescence samples were examined by scanning electron microscopy (Figure 7.5). Aberrant inflorescences examined after 10 weeks of growth were mounted and assessed in a variable pressure scanning electron microscope. Close inspection of the meristem did not reveal any mature or aborted floral organs; no carpels or gynoecium-like structures were present about the meristem confirming that the inflorescences could not contribute to the reproductive success of the plant. High magnification confirmed that the leaf-like organs bore satellite trichomes (Figure 7.6a). Moreover, electron microscopy revealed that the leaf-like sepaloids arose around the meristem in a phyllotactic-like spiral (Figure 7.6b).

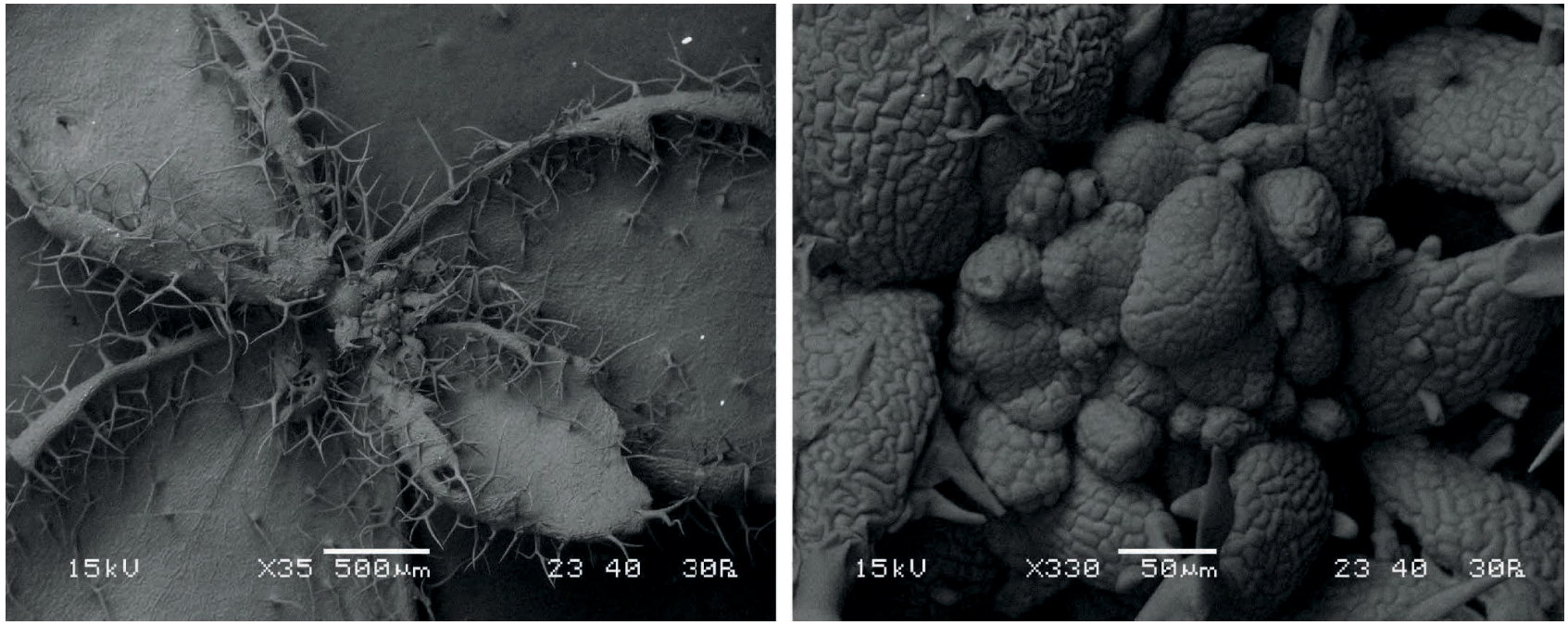


Figure 7.6: Assessment of aberrant inflorescences of FT-NQQ-GFP plants at approximately 12 weeks by Scanning Electron Microscopy. (A) Micrograph providing an overview of the aberrant inflorescence. **(B)** Micrograph of the Meristem of the aberrant inflorescence. Scale bar and magnification

7.2.4 Segregation and Development of FT-NQQ-GFP lines

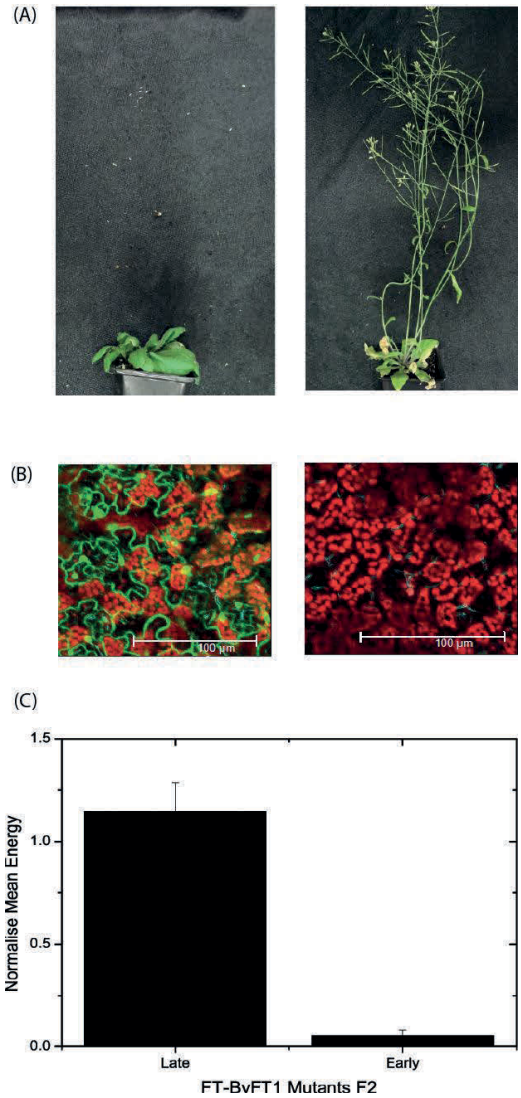


Figure 7.7: The Development of T2 Generation FT-NQQ-GFP. (A) Plants display two phenotype; an early flowering phenotype and a late flowering phenotype. **(B)** Leaves from plants displaying the two phenotypes were analysed by confocal microscopy. Late flowering plants (left) showed evidence of GFP expression. In all images GFP was excited by light at 488 nm and emissions were observed using a detection window between 490 to 570 nm. Background autofluorescence was excited using a 405 nm laser with a 410 - 480 nm detection band. The 633 laser line was also used as was a detection window set at 580 – 625 nm. **(C)** Quantification of the florescence in the 495 to 550 nm window relative to the mean fluorescence in the 580 – 625 nm window. n = 5. Standard Error of the mean shown.

Seeds taken from T1 plants were planted on soil. Plants were assessed visually under broad-spectrum UV excitation. Two populations of plants were evident; those with visible GFP and those without visible GFP. 41 GFP expressing and 18 non-expressing plants were identified (Table 7.1). The presence of GFP was confirmed by confocal microscopy and quantified by normalizing mean energy caused by the excitation of GFP against autofluorescent signal from excited chlorophyll (Figure 7.7c). Significantly higher GFP signal was observed in late flowering mutants than in early flowering plants.

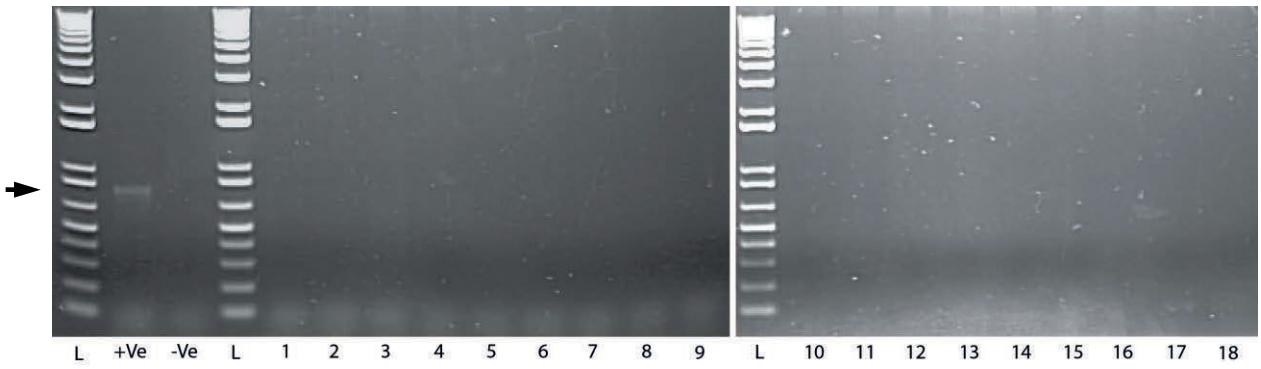


Figure 7.8: Genotyping of the early flowering F2 Mutant Plants. DNA was extracted from the 18 early flowering plants. DNA was extracted from the late flowering plants as a positive control. A band can be seen at approximately ~700 bp. Water was used instead of DNA in the negative control. Lanes numbers correspond to plant number. Lanes marked with L contain marker.

Table 7.1: The X^2 test assuming one transgene insertion. Given Mendelian inheritance if one transgene was present, a ratio of 3 mutant plants to 1 wild-type would be expected. The X^2 (0.95) number is less than the critical value (3.841) so the hypothesis is not significantly different from expected model.

	Observed (O)	**Expected (E)**	**$(O - E)^2$**	**$(O - E)^2/E$**
Early	18	14.75	10.56	0.71
Late	41	44.25	10.56	0.24

$X^2 = 0.95$

Cut off value = 3.8

Analysis of the expression of GFP suggested that the T2 plants were a segregating population. To confirm that the T2 mutant plants were a segregating population genomic DNA was extracted and plants were analysed by genotyping. The insertions were amplified using a primer complementary to a region before the gene of interest and a reverse primer within the GFP sequence. The insert was amplified from a bulk sample of DNA from late flowering plants but it was not possible to amplify the insert from the 18 early flowering plants indicating that these plants did not have the construct. To determine whether the observed data are compatible with a theoretical model where the T1 plant contained one transgene insertion, a statistical test was conducted (Table 7.1). In the model 75% of the offspring would be expected to contain the transgene. A chi squared statistical test showed no statistical difference between the observed and expected values ($X^2 < 3.841$). This implies the T1 generation had a single copy of the transgene.

7.2.4.1 Assessment of Bolting

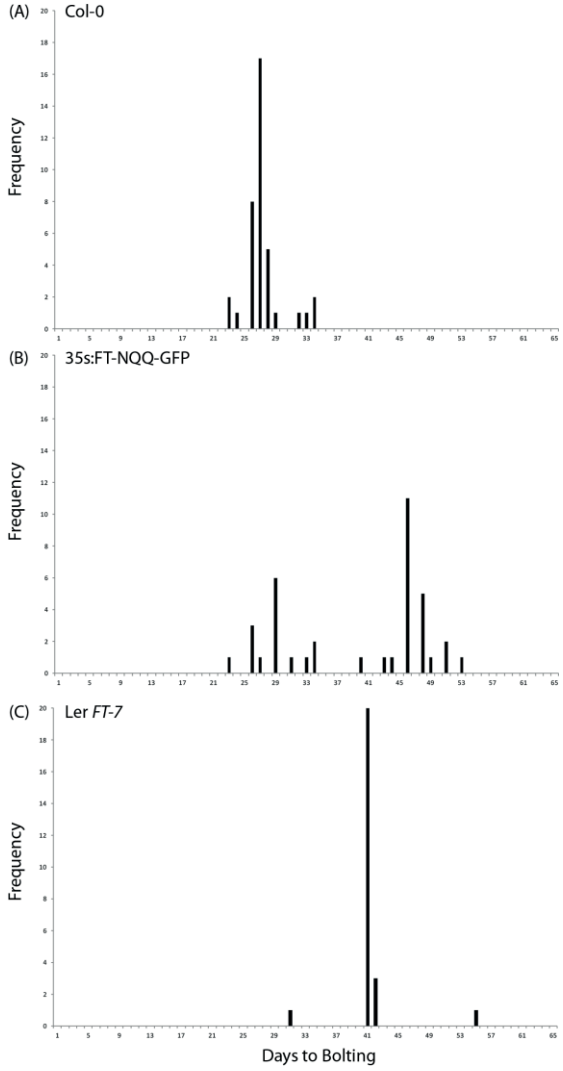


Figure 7.9: Distribution of the time to bolting in T2 transformants over expressing FT-NQQ-GFP under the 35s promoter compared to Col-0. (A) Histogram of the time to bolting of Col-0. **(B)** Histogram of the time to bolting of T2 lines transformed with 35s:FT-NQQ-GFP.

To ascertain whether the expression of FT-NQQ-GFP affected bolting T2 generation transformants were characterised. The number of days to bolting was recorded for each plant. The T2 plant population showed a bi-nominal distribution with one population of plants bolting at the same time as wild type plants (peaking at approximately 27 days in wild-type plant and 29 days in the early mutants) and a second population flowering significantly later (peaking at approximately 46 days). The early bolting group contained only plants lacking GFP expression whilst the late bolting plants were shown to be expressing the GFP fused transgene.

7.2.4.2 Assessment of Flowering Time

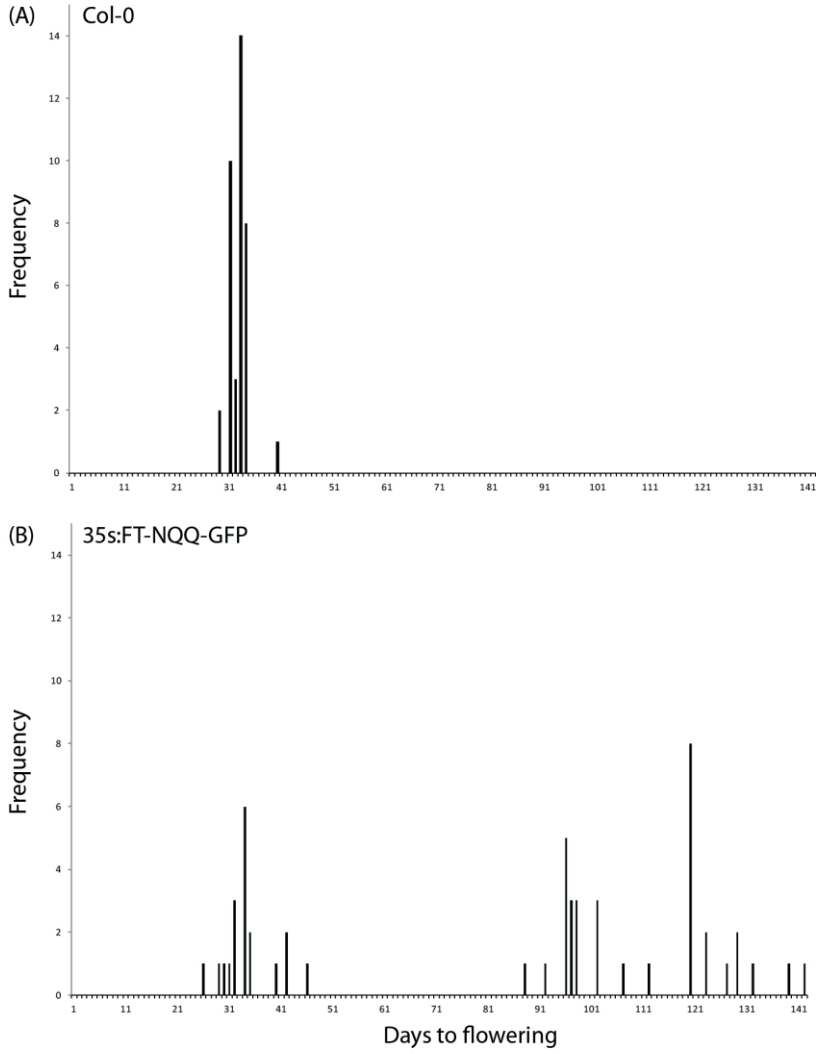


Figure 7.10: Distribution of flowering times in T2 transformants overexpressing FT-NQQ-GFP under the 35s promoter compared to Col-0. (A) Histogram of the flowering time Col-0. **(B)** Histogram of the flowering time of T2 lines transformed with 35s:FT-NQQ-GFP.

The flowering time of T2 generation transformants was recorded. Flowering time was analysed in terms of number of days-to-flower. The T2 plant population showed a bi-nominal distribution with one population of plants flowering at the same time as wild-type plants (peaking at approximately 33 days) and second population flowering significantly later (peaking at approximately 130 days). The early flowering group contained only plants lacking GFP expression whilst the late flowering plants expressed GFP.

The late population could be separated into two distinct groups with the modal average of the two groups separated by 35 days, which may correspond to the heterozygotic and homozygotic offspring of the original T1 generation plant. Owing to the difficulty of resolving these two groups, at this stage, the populations were considered as a single late population for further analysis.

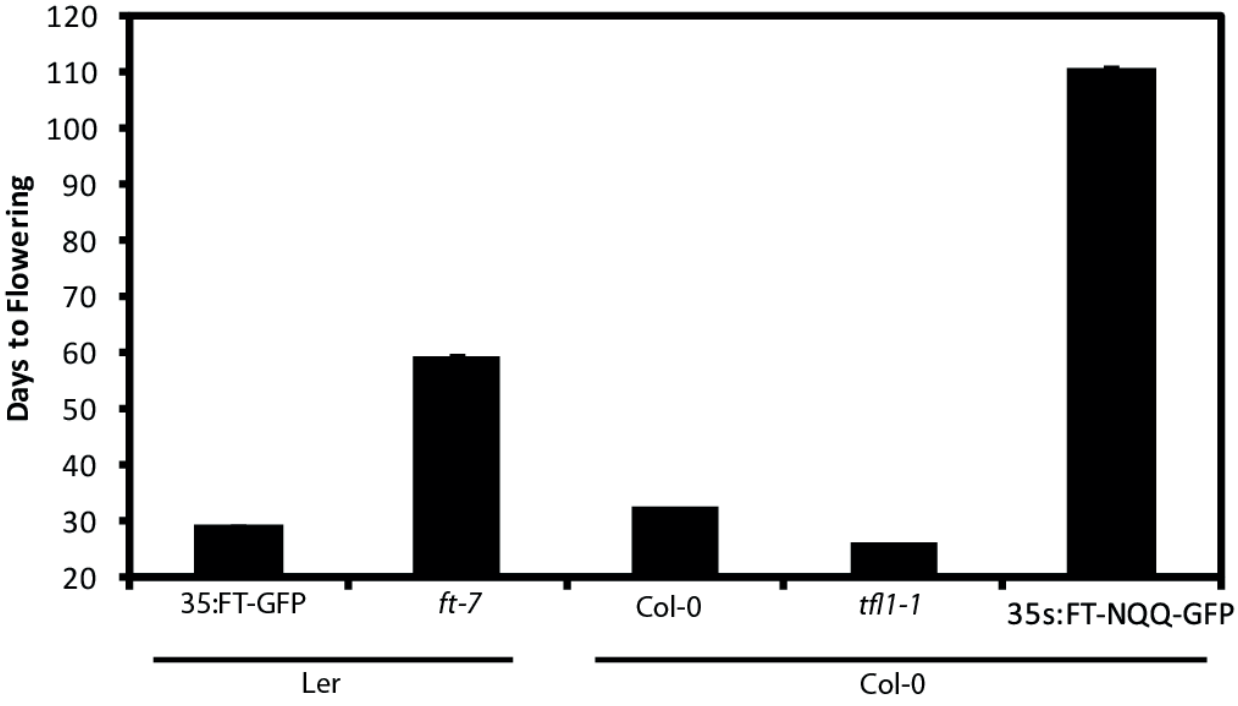


Figure 7.11: Assessment of Flowering Time of Mutant Plants (days-to-flower). The mean number of days-to-flowering is shown. The standard error is shown. n = 34.

To further characterise the effect of over expression of FT-NQQ-GFP. T2 mutant plants which had been confirmed as expressing GFP were assessed for flowering time abnormalities against several other mutant genotypes. Overexpression of FT-GFP is correlated with faster time between sowing and flowering whilst lost of FT is associated with delays in flowering time (Figure 7.11). Plants expressing FT-NQQ-GFP took on average three times as long to flower as wild-type plants (Figure 7.11) and flowered much later than other mutants (Figure 7.12; Figure 7.13). FT-NQQ-GFP plants flowered later than *ft-7* mutants which are deficient in the expression of *FT*. This suggests mutations to residues 134, 137 and 138 are critical for the regulation of flowering. Seeds were collected from T2 plants to identify and propagate homozygous lines.



Figure 7.12: Phenotypic Characterisation of Mutant Plants at after ~ 4 Weeks. Phenotype of mutant plants compared to a series of mutants plants grown alongside control plants in long day conditions.Col-0, 35s:FT-GFP (Ler) and tfl1-1 have flowered. FT-10 (Col-0) and 35s:FT-NQQ-GFP have not flowered.

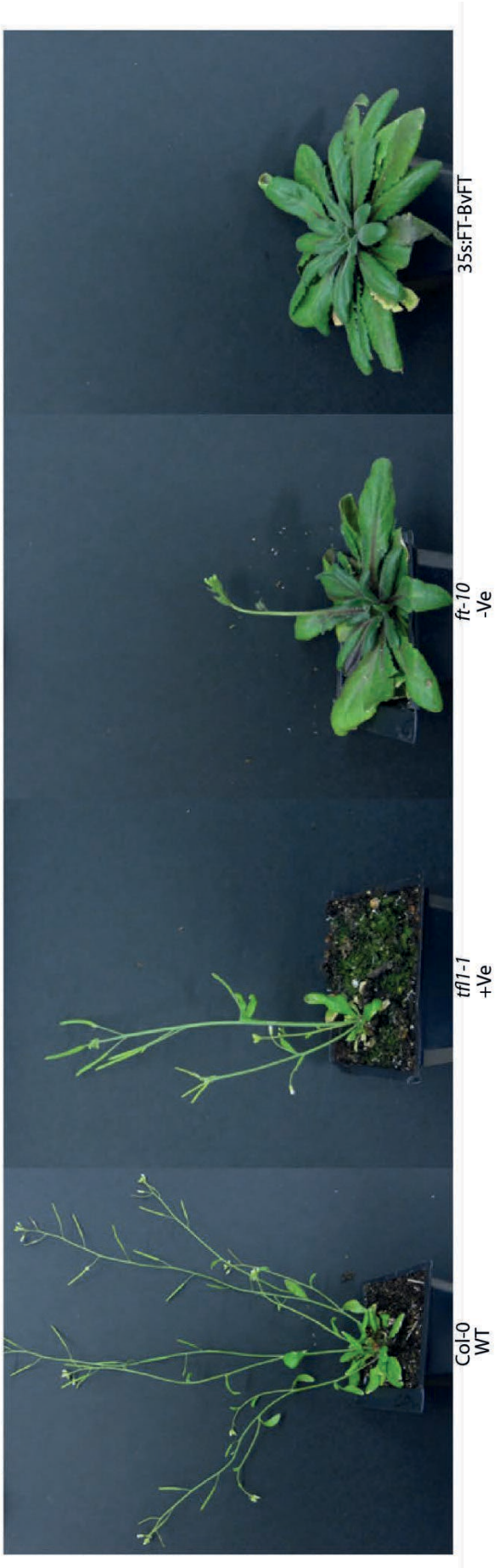


Figure 7.13: Phenotypic Characterisation of Mutant Plants after ~ 5 Weeks of Development. Phenotype of mutant plants compared to a series of mutants plants grown alongside control plant in long day conditions.Col-0, 35s:FT-GFP (ler), tfl1-1 and FT-10 (Col-0) have flowered but 35s:FT-NQQ-GFP plants have not.

7.3 Discussion

7.3.1TFL1 may be involved in Bolting and the Conversion of Leaves to Flowers

7.3.1.1.1 TFL1 involvement in Flowering

The loop has been previously shown to be essential for the biological activity of TFL1 and FT; plants expressing FT with loop of TFL1 typically flower later than wild-type plants (Ahn et al., 2006). In this study, FT has been converted to a repressor of flowering by mutating three amino acids. Flowering occurs after the shoot apical meristem develops a floral meristem. This process is involves the expression of numerous identify genes like *AP1*, *LFY* and *CAULIFLOWER* (*CAL*) (Smith, 2010). One possibility for this delay is that that mutation prevents the expression of floral meristem identity genes like AP1 and LFY preventing the transition from the early stages to the later stages of development where flowers are produced. However, it is significant that these mutations do not completely suppress reproductive development; plants overexpressing the FT-NQQ microchimeria flower and produce seeds but after a delay. This delay is more extreme than would be expected from mutant plants overexpressing TFL1 from another species; overexpression of the *Citrus senesis* TFL1 in *Arabidopsis* delay flowering by approximately 20 days (Pillitteri et al., 2004). In contrast, in this study, mutating three residues caused a 97 day delay in flowering which was significantly greater than the 27.3 day delay observed between *ft-7* mutant plants and wild-type plants.

7.3.1.1.2 TFL1 Involvement in Bolting

The late bolting phenotype observed in mutant plants may partially be involved in the late flowering phenotype. Specifically, some of the delay in flowering can be attributed to a to the increased time spent in vegetative development. During this period of time the meristem is not capable of producing reproductive structures regardless of the conditions the plant is exposed to (Reviewed in Levy and Dean, 1998). This suggests that TFL1-like proteins may have a role in the commitment to reproductive development. However, it is unclear whether the TFL1 operates directly by the inhibition of gene like LFY and AP1 or whether it may operate at other loci to reduce the competence of the shoot to inductive

floral signals (Mandel et al., 1992). Alternatively, these functions could be unique to the FT-NQQ microchimeria which arise because of the combination of biological activity from elements of the microchimeria that are from FT alongside the biological effects of the elements from BvFT1.

7.3.1.1.3 TFL1 involvement in the Conversion of Leaves to Flowers

In addition to the delayed bolting and delayed flowering phenotype that arose, transformed plants also had aberrant inflorescences. This is consistent with the view that TFL1-like proteins have a role both in flowering time and meristem identity. Proteins known be involved in determining floral organs include AP1 and LFY, thus it may be possible that this FT mutant acted to downregulate these genes either direct or indirectly. Alternatively, they could work by inhibiting the activity of these genes. Indeed, plants deficient in LFY, produce leafy buds composed which contained whorls of sepaloid and sometimes carples (Schultz and Haughn, 1991). Consequently, some *lfy* mutant plants are female fertile. In contrast, plants overexpressing FT-NQQ-GFP microchimeria initially produced no recognisable floral organs. Instead these plants produced inflorescences with a series of leaf-like structures which lacked the organs to contribute to the reproductive success of the plant which suggests that the FT-NQQ-GFP microchimeria does not simply repress the expression of *lfy*. Interestingly, the same phenotype is not observed with mutants overexpressing TFL1 which do not produce leafy inflorescences which suggests that FT-NQQ-GFP is not simply an analogue of TFL1 (Shannon and Meeks-Wagner, 1991). However, TFL1 overexpression is associated delayed flower suggesting that FT-NQQ-GFP may have some TFL1-like activity (Mimida et al., 2001).

7.4 Summary

The loops of the floral PEBPs have been implicated in mediating their biological function (Ahn et al., 2006). Mutating three residues towards the C-terminus of the loop can convert FT in to a potent repressor of flowering. Plants expressing the FT-NQQ-GFP construct bolted and flowered significantly later than wild-type controls. These plants also initially developed aberrant inflorescences which were composed of phyllotactic spirals of leaves with no evidence of reproductive floral organs. Subsequently, these plants went on to develop functional flowers and produce seeds.

Chapter 8 - Artificial Inhibition of TFL1 Activity

8.1 Introduction

Identifying new molecules that reversibly modulate biological function is a long term goal of chemical biology. Attempts have been made to artificially modulate flowering time using a variety of molecules, including gibberellins (GAs), benzyladenine (BA) and indoleacetic acid (IAA) (Liverman and Lang, 1956, Goldberg-Moeller et al., 2013, Ogawa and King, 1979). To identify methodologies to artificially modulate flowering, this study examines the effects of small molecules upon interaction the model 14-3-3 protein, 14-3-3 Nu, and TFL1.

8.2 Results

8.2.1 Molecule Identification

8.2.1.1 Screening Small Molecules

Fragment-based screening methods involves testing weakly interacting small molecules, that can act as a frame for the development of larger molecules that may be used as inhibitors or activators of biochemical pathways. Fragments in this study conformed to the rule of three; all compounds have a molecular mass of <300 Da, 3 hydrogen bond donors, 3 hydrogen bond acceptors and a lipophilicity of less than LogP 3. Fragments were tested using differential scanning fluorimetry. 50 fragments, solubilised in DMSO, were initially screened in a proof-of-principle trial. Stocks were diluted in assay buffer till the compound was at 2 mM and the concentration of DMSO was at 2%. TFL1 was kept at a concentration of 4 µM. The change in the Tm of TFL1 was measured by differential scanning fluorimetry (Figure 8.1). A threshold change of 1.9° K was used as a cut-off value for identifying useful compounds (Neki Patel, personal communication). The introduction of 2% DMSO did not significantly affect the melting temperature of TFL1. Three compounds caused a shift of greater than 1.9° and were deemed suitable for further investigation. Two compounds CD1000 and TL00908 increased the thermal stability of TFL1; CD1000 caused an increase of 2.6° K while TL00908 caused an increase of 3.0° K. Compound CC40909 caused decrease thermal stability by 1.9° K.

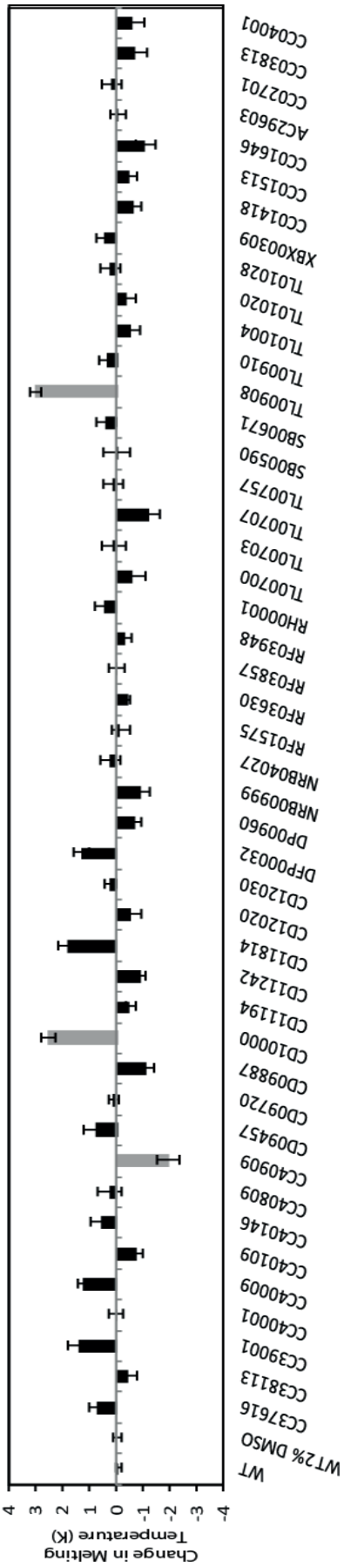


Figure 8.1: Stabilization of TFL1 by Compounds in the fragment library. Compounds that cause a increase or decrease in Tm of **≥** 1.9° K relative to control samples with 2% DMSO are coloured in grey. Standard error of the mean shown. N = 3.

8.2.1.2 Dose Dependent Effects of Small Molecules *in Vitro*

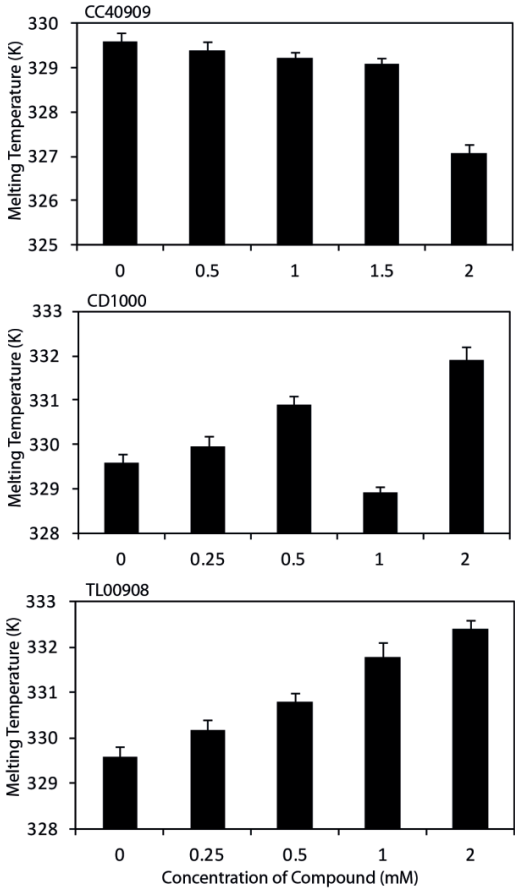


Figure 8.2: Concentration-dependent stabilization and destabilization of TFL1 by a Series of fragments. The Tm for 4 μM of TFL1 was measured by DSF with a series of different compound concentration. Standard error of the mean shown. N = 3.

The positive hits were re-screened (Figure 8.2). A series of different concentrations were examined to establish whether the stabilization caused by the compound was reproducible. As the concentration of TL00908 was increased the stability of the protein was increased, which indicates that thermal stability of TFL1 is proportional to the concentration of the ligand. TL00908 stabilised TFL1, increasing the Tm by more than 2.8° K at the highest concentrations but only by approximately 0.6° K at the lowest concentration. Increasing the concentration of CC40909 had the effect of decreasing the Tm at high concentrations but not at low concentrations. At 2 mM a 2.5° K decrease was observed whereas at 1.5 mM CC40909 a 0.5° K decrease was observed. No dose dependent relationship between Tm and concentration of CD1000 was observed. As a result CD1000 was eliminated from further trials.

8.2.1.3 Effect of Compounds on TFL1 14-3-3 Interaction

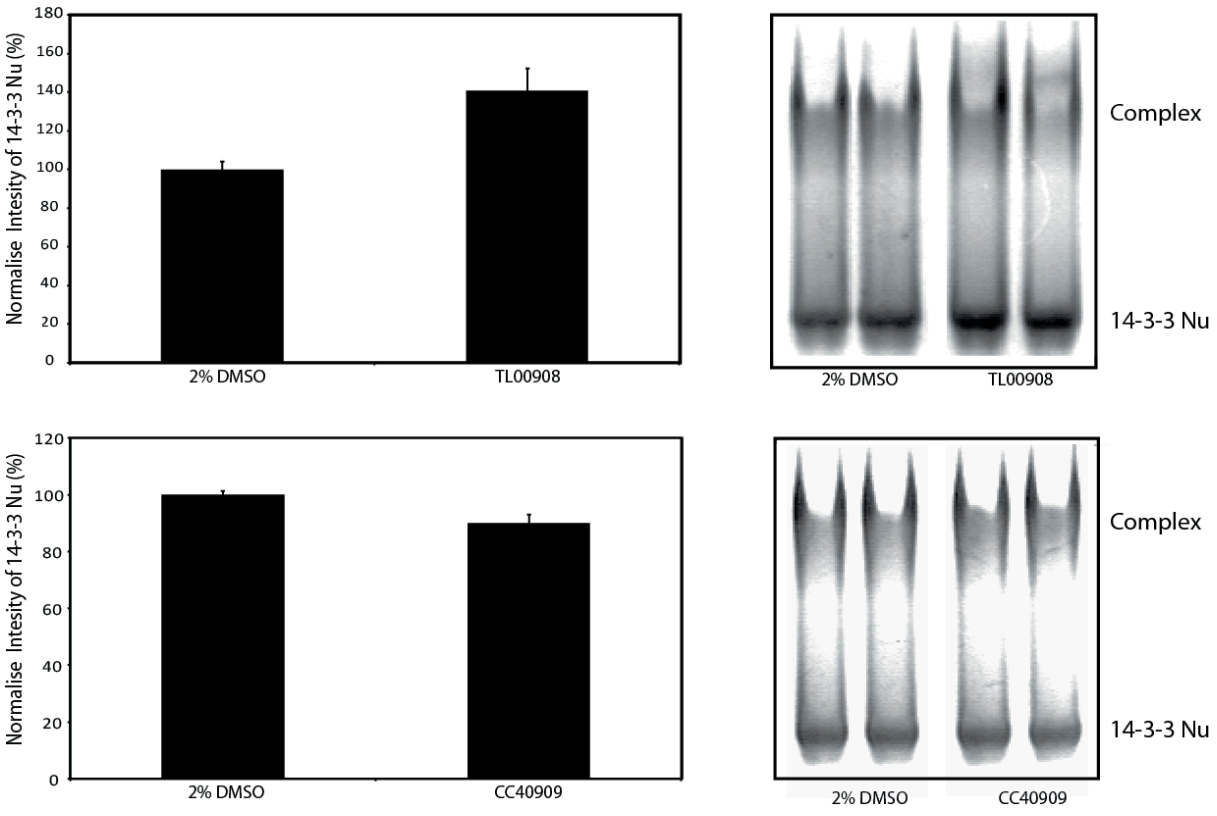


Figure 8.3: The change in Affinity between TFL1 and 14-3-3 Nu in the presence of Compound. The interaction of TFL1 and 14-3-3 Nu was assessed by gel shift. The intensity of the 14-3-3 Nu band was assessed. Samples with compound were normalised against samples with 2% DMSO.

To establish whether these compounds had an effect on the interaction between 14-3-3 Nu and TFL1; a binding assay was conducted using native PAGE. TFL1 and 14-3-3 Nu were mixed in 1:1 ratio with 2% DMSO or with compound in DMSO. The intensity of the 14-3-3 Nu band was measured and compared with samples containing DMSO alone and samples with compound. Incubation of TFL1 and 14-3-3 Nu with TL00908 resulted in a small increase in the intensity of 14-3-3 Nu indicating a slight inhibition of interaction ($P = 0.0294$). Incubation of TFL1 and 14-3-3 Nu with CC40909 resulted in no significant change in the intensity of 14-3-3 Nu ($P = 0.0924$). As a result TL00908 demonstrated to be a plausible lead compound.

8.3 Discussion

8.3.1 Small Molecule Inhibition of Protein-Protein Interaction

The protein-protein interaction between the components of the proto-FIC is central to the regulation of flowering time. Plants lacking TFL1 flower early (Shannon and Meeks-Wagner, 1991). As mutations that prevent binding between FT and 14-3-3 proteins abrogate the biological activity of FT in rice, it is likely that similar mutations would affect the biological activity of TFL1 (Taoka et al., 2011). A compound developed to inhibit the interaction between these proteins could also abrogate the biological activity. However, identifying a small molecule that is capable of interacting with a protein-protein interface is difficult because the two surfaces are often flexible and adaptive and are not well defined (Reviewed in Sundberg and Mariuzza, 2000). Moreover, it is difficult to predict which compound might interact with a particular surface. To interrupt an interaction the compound has to be able to interrupt a subset of interactions, which contribute significantly to the overall binding affinity. It is difficult to predict which compound will be capable of disrupting these interactions (Bogan and Thorn, 1998).

In this study, a methodology for screening fragments capable of interacting with TFL1 was developed. Differential scanning fluorimetry is a medium throughput methodology for screening. Compounds that caused a significant shift in the observed thermal stability were considered to bind to the protein. However, the changes in melting temperature do not truly reflect the affinity of the compound for the protein (Niesen et al., 2007). Thus some compounds that may bind may have been omitted from the pool of lead compounds. Other compounds may also interact with TFL1 but not sufficiently enhance thermal stability (Niesen et al., 2007). Alternatively these compounds could affect the test by affecting the fluorescence of the dye or detection of the signal and influence the observed result rather than the proteins stability. Consequently, further tests are required to confirm the interaction utilizing alternate methodologies. However, given the large number of possible compounds to test, fast screening methods are essential. Moreover, two compounds demonstrated stabilization in a concentration dependent manner which suggests that the thermal stability of the protein for those compounds is dependent upon the concentration of the compound and provides a strong indication that the effects of these two

compounds are reliable. Compounds could be re-screened with more robust techniques like NMR or Isothermal Titration Calorimetry.

8.3.2 Inhibiting the Interaction between TFL1 and Macromolecules

As blocking the formation of the proto-FIC would likely disrupt the inhibitory activity of TFL1, inhibitors to TFL1-14-3-3 binding could act as activators of flowering. This is feasible, as previously work has been able to demonstrated that it is possible to modulate 14-3-3 protein-protein interactions (Zhao et al., 2011). FOBISIN, a small molecule inhibitor, mimicking a phosphorylated target protein, that binds to 14-3-3s within the electropositive cleft blocks interactions between 14-3-3 proteins and binding partners (Zhao et al., 2011). However, in the context of a plant interaction global inhibition of 14-3-3 proteins would be inappropriate given the number of processes that 14-3-3 proteins are involved in. Thus TFL1 was chosen as a target. In this study, the presence of excess TL00908 was able to slightly reduce the amount of complex formed suggesting that it could act as an inhibitor. However, further tests are required to determine whether TL00908 would be an appropriate lead compound. Structural characterization of the complex with TL00908 may help further elucidate future strategies. Importantly, TFL1 is likely to interact with a variety of macromolecules; thus compounds that bind may not affect the interaction with 14-3-3 Nu but may alter biological activity.

8.4 Summary

Artificially modulating flowering by chemical interference is a long term goal in plant chemical biology (Liverman and Lang, 1956, Goldberg-Moeller et al., 2013, Ogawa and King, 1979). Several compounds were screened for their ability to interact with TFL1 using differential scanning fluorimetry. Three compounds were identified as being capable of making significant perturbations to the melting temperature of TFL1; TL00908, CD1000 and CC40909. Whilst TL00908 and CD1000 increased melting temperature, CC40909 decreased melting temperature. However, only TL00908 and CC40909 were shown to have a dose dependent effect upon melting temperature. These two compounds were screened for their ability to affect the formation of complexes with 14-3-3, TL00908 was shown to marginally decrease the amount of complex formed suggesting that it may act as a weak inhibitor.

Chapter 9 - Discussion

9.1 The Structure of the TFL1-14-3-3 reveals a Common Architecture amongst the Floral Complexes

The similarity between the crystal structures of the proto-FIC and the HD3a-based proto-FAC confirms the role of members of the 14-3-3 protein family in the regulation of flowering time. The 14-3-3 protein family plays a critical role in the activities of floral regulatory complexes, enabling both activation and repression of flowering (Taoka et al., 2011). Moreover, the existence of TFL1(FT-like)-14-3-3 complexes suggests the possibility of a standardised functional platform for the action of PEBPs *in planta*.

9.2 Structural and Functional Comparison of the FIC and the FAC

9.2.1 Structural Comparison

Analysis of the proto-FIC and proto-FAC structures shows that the proto-FIC forms a slightly wider W-shaped complex (Figure 9.1). However, this could be due to crystal packing as 14-3-3 dimers have been previously shown to form at a range of angles (Yang et al., 2006). Importantly, TFL1 interacts with the 14-3-3 proteins via the same non-canonical interaction as observed previously in the HD3a-GF14c interaction. The interaction surface between 14-3-3 proteins and the PEBPs is almost identical with a ~528.1 $Å^2$ buried interface between each TFL1 and the corresponding 14-3-3 which is comparable to the 653.8 $Å^2$ interface between HD3a and its corresponding 14-3-3. The residues that are involved in the interaction are largely conserved (Taoka et al., 2011). This suggests the possibility that 14-3-3 proteins act as a universal platform in the formation of floral complexes, with different 14-3-3 proteins capable of mediating repression or activation (Taoka et al., 2011).

Significant similarities were observed in the electrostatic surfaces of 14-3-3 Nu and GF14c. Both proteins are largely negatively charged toward the outer surface with a large positively charged cleft within the interior of the protomer that may act as a binding surface capable of mediating the canonical interaction where a phosphorylated segment of the target protein binds with the positively charged cleft. In the FIC and the FAC structures, the PEBPs bind with their loops facing towards the exterior of the structure (Taoka et al., 2011). This orientation exposes a strong electropositive region to the interior of the

structure which may be important in the function of TFL1 (Figure 9.2). This lies close to the region predicted to contain the bZIP region of FD and DNA but it is unclear whether it is involved in DNA binding or other processes.

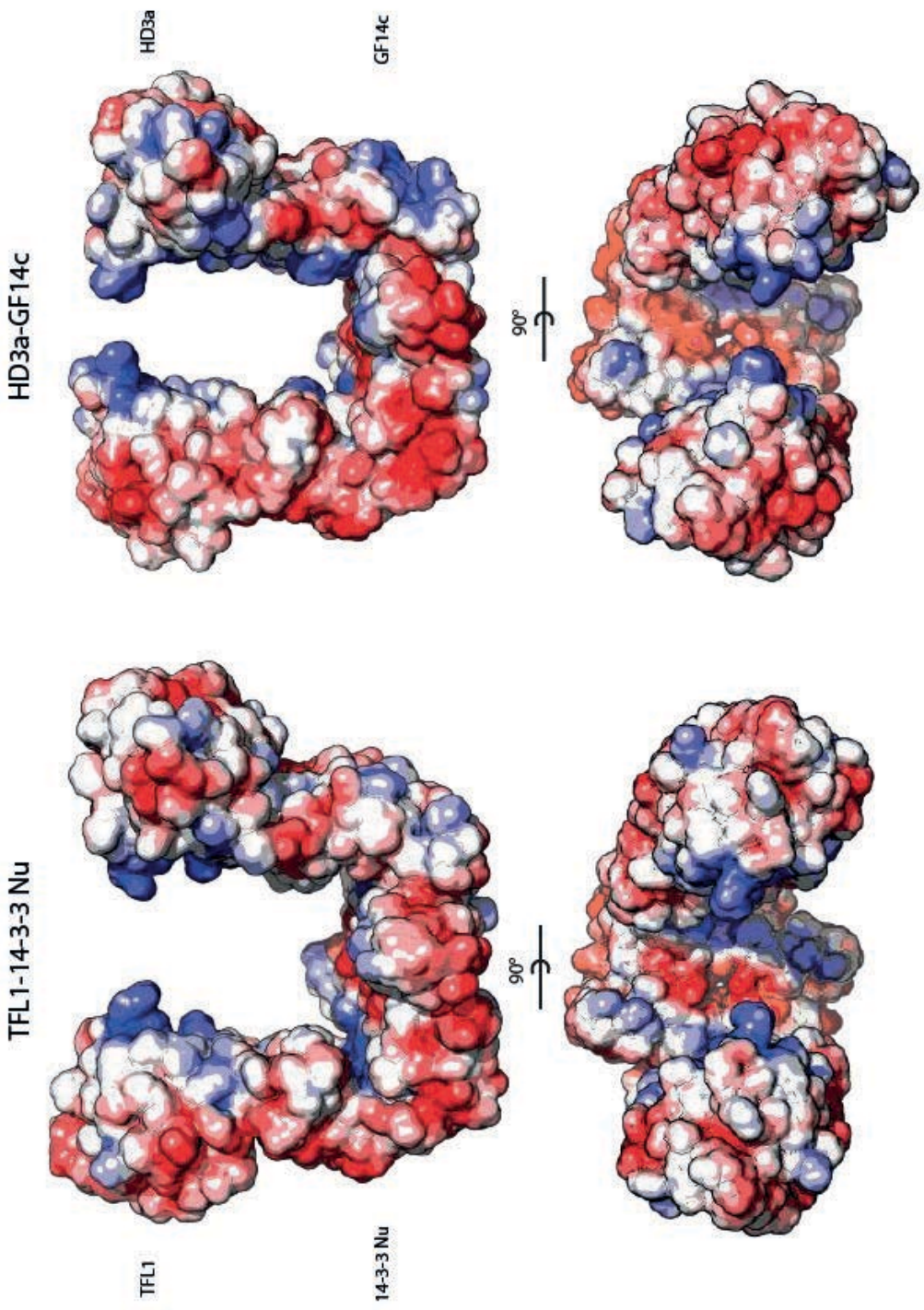


Figure 9.1: Comparisons of the electrostatic surface of the FIC and the FAC. (A) The complex of TFL1 and 14-3-3 Nu .**(B)** The complex of HD3a and GF14c. Red areas are negatively charged. Blue areas are positively charged.

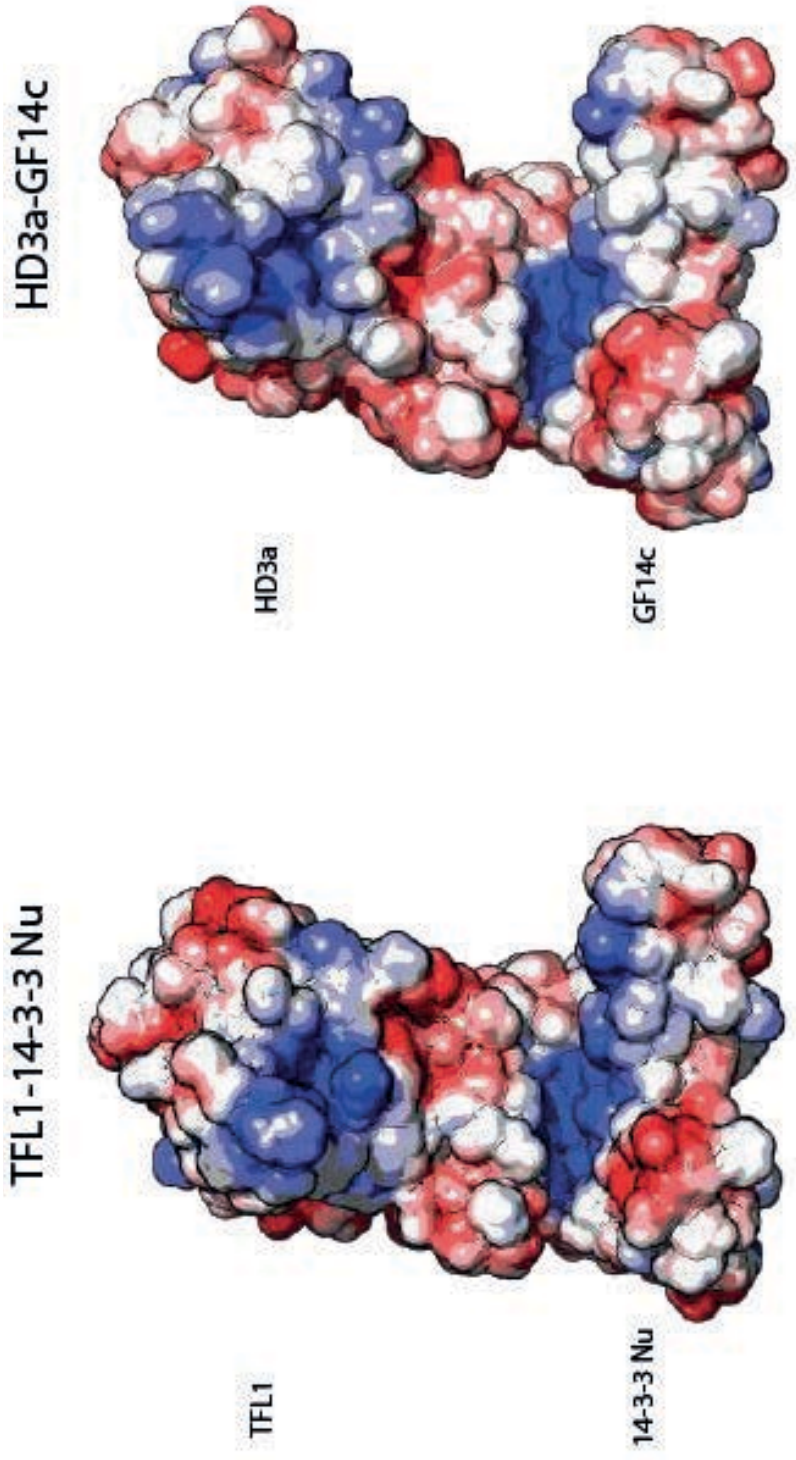


Figure 9.2: Comparisons of the electrostatic surface of the interior of the FIC and the FAC. **(A)** The complex of TFL1 and 14-3-3 Nu. **(B)** The complex of HD3a and GF14c. Red areas are negatively charged. Blue areas are positively charged.

9.2.2 The Role of the Extended Loop

9.2.2.1 Conformations of the Extended Loop

Previous analysis of the PEBPs has suggested that the external loops of FT and TFL1 may take on different conformations relative to each other (Ahn et al., 2006). In the crystal structure of TFL1 (1wko) two distinct loop conformations were observed; one was significantly extended with respect to the loop of the other (Figure 9.3c). However, the loop conformations of FT and TFL1 in the complexes were comparable. One possibility is that the loop of TFL1 is flexible and changes conformation upon binding to 14-3-3 proteins. It is also possible the differences in loop conformations in the crystal structure could be due to crystal contacts. Regardless, the comparability of the loop once bound suggests that the structure of the loops is not responsible for the functional antagonism between FT and TFL1 (Figure 9.3c).

9.2.2.2 The N-terminus of the Loop is involved in the Interaction with 14-3-3s

The N-terminus of the loop of TFL1 is involved in the interaction with 14-3-3 proteins. Arg^{133} plays a particularly important role which appears to be conserved between FT and TFL1. Arg^{132}, the equivalent residue in HD3a, interacts with residues within the acidic lobes of 14-3-3 proteins via salt bridges (Taoka et al., 2011). As a result mutations to Arg^{133} causes a decrease in binding affinity. Moreover, mutations to residues preceding this (Leu^{131} and Gly^{132}) cause a decrease in affinity. These residues may be involved in positioning critical residues close to the site of interaction. This is significant as a part of the loop can be ascribed a role in the formation of complexes with 14-3-3 proteins. Mutations that affect FT-14-3-3 binding are known to have a phenotypic effect (Taoka et al., 2011), so it is possible that these mutations that affect TFL1 binding may also have a phenotypic effect. Interaction between the floral PEBPs and 14-3-3 proteins occurs in a largely analogous fashion and consequently does not explain the antagonistic activities.

9.2.2.3 The C-terminus of the Loop Plays a Critical Role in Mediating Biological Activity

Plants expressing FT with the loop of TFL1 flower later than wild-type plants (Ahn et al., 2006). A similar exchange has been shown to reverse the activities of BvFT1 and BvFT2, in *Beta vulgaris in vivo* suggesting that the loops of PEBPs are essential for the function of FT across the plant kingdom (Pin et al., 2010).

This study has demonstrated that three residues, found in the C-terminal portion of the loop are essential for the floral promoting activity associated with *Arabidopsis* FT. In this study, FT was converted to a repressor of flowering by mutating Tyr^{134}, Gly^{137} and Trp^{138} to an asparagine and two glutamines. Further experiments to check the stability of the mutated protein *in vivo* are required. Previously it has been demonstrated converting Tyr^{134} or Trp^{138} to alanine abrogates the biological function of FT when expressed *in vivo* (Yoo et al., 2013). This confirms that the C-terminus of the loop is critical for the biological function of FT. However, plants overexpressing TFL1 with the loops of FT do not flower early, suggesting that the C-terminus of TFL1's loop may not be sufficient to mediate the biological activity of TFL1 or that residues outside of the loop are important in TFL1's function (Ahn et al., 2006). These regions adjacent to the extended loop (designated section C) differ at three positions between TFL1 and FT; Lys^{150} which in FT is glutamic acid, Val^{153} which in FT is a glutamic acid and Glu^{153} which in FT is a isoleucine (residue 150) (Ahn et al., 2006).

The exact role of the three mutated amino acids remains unclear as in this study no biochemical function was attributed to this region. These residues face towards the exterior of the complex and are not involved in binding to 14-3-3 proteins (Taoka et al., 2011). The exposed nature and the importance of this loop suggests that these residues could be involved in interacting with other regulators, other than 14-3-3 proteins, that can affect flowering time.

Given that these residues are within a highly acidic region it is unlikely that they are directly involved in any form of interaction with negatively charged molecules like DNA. Thus it is possible that they are involved in recruiting additional proteins to the complex. Mutations to these residues may prevent FT specific proteins from binding via steric hindrance or may enable interaction with regulators that normally associate with TFL1-like proteins. As of yet the identities of these proteins is unclear but a series

of other proteins have been linked with the floral PEBPs including the NIMA-related kinase (NEK) family of proteins and transcription factors including homologs of KANADI (Pnueli et al., 2001b, Taoka et al., 2011). One candidate which has been characterised is BRANCHED1 (BRC1), a binding partner of FT which interacts with FT via residues in section B and section C. Specifically, it has been shown to interact via Tyr^{134} and with the Ile^{150} in FT. Both residues are unique to FT homologs and essential for binding (Niwa et al., 2013). This might partly explain why TFL1 cannot be converted to an FT-like protein (Ahn et al., 2006). Residues in segment C might enable interaction with specific FT binding proteins. This would explain why in this study a small number of mutation to the loop abrogates and reverses FT's activity as both FT specific residues from segment B and segment C are required to interact with BRC1-like transcription factors. This suggests that additional factors that bind TFL1 interact with the loop of TFL1 alone enabling conversion via loop mutagenesis.

BRC1 is a member of the TCP transcription factor family of proteins which is predicted to form a non-canonical basic-Helix-Loop-Helix (Cubas et al., 1999). These proteins may function by directly interacting with DNA in the presence of FT. However, BRC1 is confined to auxiliary meristems, as a result these proteins are not responsible floral development at the shoot apical meristem (Niwa et al., 2013). Indeed, although there are currently more than 20 members of the TCP transcription factor family and several of these have been linked to development, none of these proteins have been confirmed to operate in the shoot apical meristem (Martin-Trillo and Cubas, 2010). It possible that similar basic-Helix-Loop-Helix transcription factors outside of the TCP family could interact with FT in the shoot apical meristem whilst a different class of protein could be involved in the action of TFL1. However, the identity of these proteins has not been resolved.

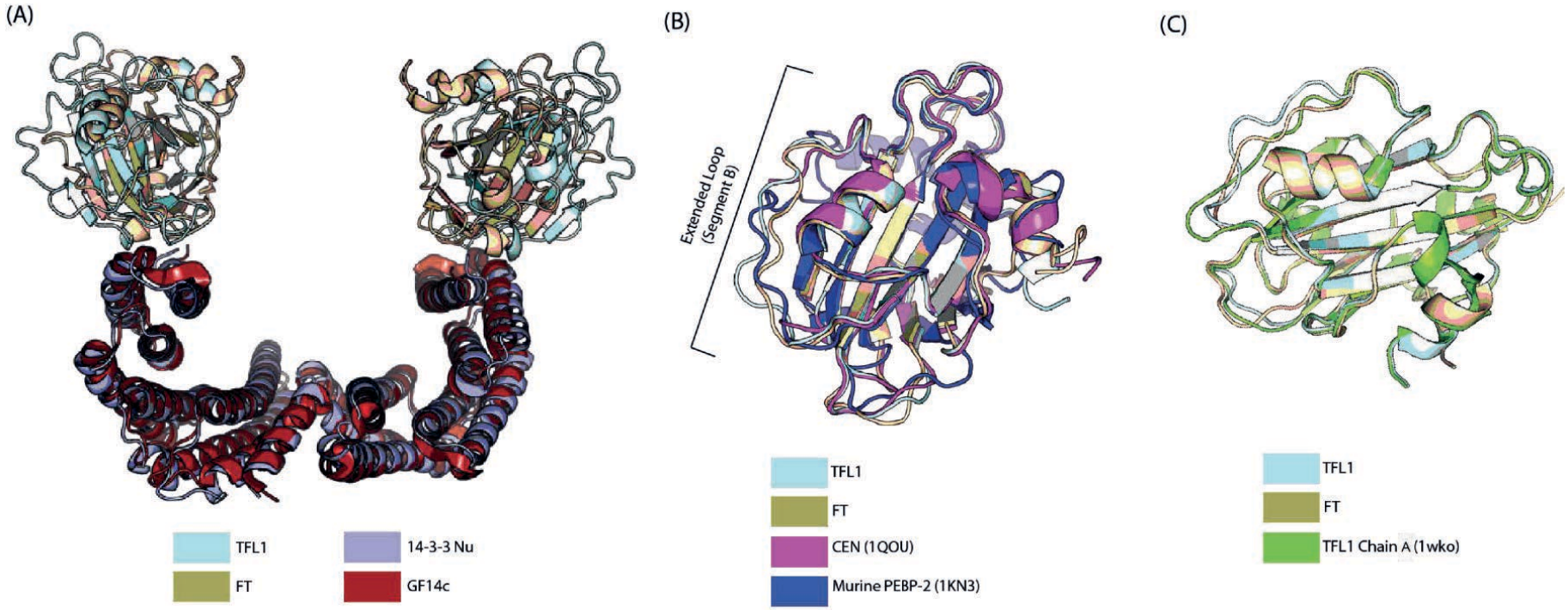


Figure 9.3: Crystal structures of FIC and the FAC. (A) Cartoon representation of FIC and FAC. **(B)** Close-up showing an overlay of segment B and surrounding regions of FT, TFL1, CEN and Murine PEBP-2. **(C)** Comparison of the loops of TFL1 and FT. The structure of TFL1 is compared against chain A of TFL1 in 1wko and chain A of FT in 1wkp.

9.2.3 The Role of the Putative Binding Pocket

Previously, it was shown that mutations to His^{88} in TFL1 or the equivalent residue in FT, Tyr^{85}, affects the biological activity of the floral PEBPs (Hanzawa et al., 2005). These residues are at the entrance of a pocket that may be involved in PEBP-regulator interactions. Intriguingly, residues around the C-terminal portion of the loop are in close proximity to the binding pocket (Ahn et al., 2006). Given the strong effects of mutations around the putative binding pocket, it is possible that the binding pocket plays a role in mediating biological activity. The binding pocket has been shown to interact with phosphotyrosine suggesting that the binding pocket may play a role in the interaction with phosphorylated proteins (Simister et al., 2011).

9.2.4 The Role of Other Biological Important Residues

Several other residues have been shown to be important in mediating the activities of TFL1 and FT. In, this study, Phe^{104} was demonstrated to be involved in the interaction between TFL1 and 14-3-3 Nu. Interestingly, plants expressing TFL1 ^{G105N} (*tfl1-1* mutants) flower early relative to wild-type plants suggesting that the protein is defective *in vivo* (Shannon and Meeks-Wagner, 1991). Though no biochemical evidence has established the effect of the mutations to Gly^{105} it is possible that this mutation affects the positioning of Phe^{104}. In HD3a, a similar residue Phe^{103} abolishes the interaction with 14-3-3 in yeast-two hybrid assays. *In vivo*, these mutants flower later than plants overexpressing wild-type HD3a (Taoka et al., 2011). Consequently, it is possible that mutations to Phe^{104} in TFL1 could disrupt the biological activity of TFL1.

The C-terminus of TFL1 and FT is another region that is divergent between the two groups of PEBPs but highly conserved within each group. These residues were not observed in the crystal structure of the FIC or in the structure of TFL1 alone (Ahn et al., 2006). The structure of FT was solved with truncated FT without the C-terminus (Ahn et al., 2006). Consequently, it is impossible to ascertain the position of the C-terminus within the FIC and the FAC. Mutating Gly^{171}, a residue within the C-terminus, in *Arabidopsis* FT to alanine abolishes biological function inferring that this residue may be involved in the function of FT (Yoo et al., 2013). Given the lack of structural information it is difficult to determine what role these

residues might play. However, flexible termini have been shown to be involved in binding interactions and this may be the case with the floral PEBPs (May et al., 2010).

9.3 The Indirect Interaction between FD and TFL1

FD is a key regulator of flowering, as the activity of both FT and TFL1 are dependent upon the presence of FD (Abe et al., 2005, Hanano and Goto, 2011). FD interacts with FT via a 14-3-3 protein (Taoka et al., 2011). The data demonstrates that 14-3-3 proteins act to bridge the interaction between FD and TFL1, further confirming that PEBP-14-3-3 complexes act as a platform for binding partner interactions. The C-terminus is essential for the interaction between FT and FD (Abe et al., 2005). Importantly, the C-terminal region of rice and *Arabidopsis* FD contains a 14-3-3 binding site as do several other proteins associated with the floral PEBPs (Taoka et al., 2011). Proteins with homology to the transcription factor KANDI contain canonical 14-3-3 binding site toward their C-terminus. FIC crystals grown with FD peptide had additional density found in the region of the 14-3-3 Nu electropositive cleft associated with the peptide in a similar manner to the peptide observed in the FAC (Taoka et al., 2011). It is possible that the phosphorylated C-termini of these protein can bind to 14-3-3 proteins in a similar fashion to FD.

9.4 PEBP-14-3-3 Complex is a Universal Platform which may Interact with Several Targets

One possibility is that the PEBPs interacts with 14-3-3 proteins to form a variety of floral complexes including variant transcriptional complexes. One candidate that might form a complex with PEBP-14-3-3 platforms is ABA-Responsive Element Binding protein 3 (AREB3), a protein which shares significant sequence similarity with FD and has 14-3-3 binding site in the C-terminus (Jaspert et al., 2011). AREB3 is expressed in maturing embryos (Bensmihen et al., 2005). Mature embryos are also associated with the expression of MOTHER OF FT (MFT) (Karlgren et al., 2011). It is possible that MFT forms a complex with 14-3-3 proteins and with transcription factors like AREB3 to regulate gene expression in developing embryos. Future studies should be directed at such an interaction. It is possible that the interaction between PEBPs and 14-3-3 proteins is a general mechanism in plant development, with the complexes acting as master regulatory switches acquiring specific transcription factors and regulating specific transcriptional events.

The PEBP-14-3-3 platform may be an adaptable complex, interacting with several different targets enabling non-transcriptional related activity. In tomato, SP, a homolog of TFL1, interacts with a kinase known as SPAK. SPAK has been found to interact with 14-3-3 proteins and SP (Pnueli et al., 2001b). This interaction is dependent upon the presence of a 14-3-3 binding site found in SPAK. Mutation in either a 14-3-3 or SP disrupt this interaction. Previously, it was assumed that SP and 14-3-3 proteins compete for this binding site (Pnueli et al., 2001b). An intriguing alternative is that the interaction between SP and SPAK is bridged by endogenous yeast 14-3-3 proteins instead. This may mean that a kinase-based PEBP-14-3-3 complex may form in tomato. This suggests that non-transcriptional floral complexes may also exist increasing the range of biological activities the PEBPs can perform, *in vivo*. In this case it would be expected that floral PEBPs are able to mediate a variety of different biological effects.

9.5 Floral Complexes as Master Developmental Regulators

There is increasing evidence to suggest that the floral PEBPs act as global developmental regulators, mediating a variety of events *in vivo*; influencing the expression of genes involved in controlling the length of developmental phases and the morphology of plants (Navarro et al., 2011, Shalit et al., 2009).

9.5.1 Floral Complexes Determine the Timing of Bolting and Flowering

There is genetic and molecular evidence to suggest that the floral regulators TFL1 and FT determine the onset of flowering. Loss of function mutations to *TFL1* result in early flowering and early bolting which demonstrates the involvement of the floral PEBP in determining the length of these stages (Bradley et al., 1996). This function appears to be universal, as overexpression of BvFT1, a TFL1-like protein with high sequence similarly, in sugar beet results in delayed bolting (Pin et al., 2010). An extended vegetative growth phase was observed even in the presence of inductive conditions (Pin et al., 2010). This was also observed when BvFT1 was expressed in *Arabidopsis* (Pin et al., 2010). In rice, overexpression of RCN1 and RCN2, TFL1-homologs, caused the delayed transition between shoot and floral meristems (Nakagawa et al., 2002). This ability has been linked to the extended loop as plants overexpressing FT-NQQ-GFP appeared to bolt and flower later than wild-type plants. This result has two significant implications. Firstly, it demonstrates that the loop functions in both bolting and flowering, confirming the loop is a

functional region. Secondly, it suggests that a very small number of residues determine the ability of interaction partners to bind.

9.5.2 The Floral Complexes May Determine Morphology

Increasingly it appears that the floral regulators TFL1 and FT may be capable of determining the morphology of plants. In this study, plants overexpressing FT-NQQ-GFP produced aberrant inflorescences. Moreover, FT-NQQ-GFP plants appeared to branch more often than wild-type controls leading to a bushy phenotype. This suggests that components of the FAC and the FIC have some role in determining morphology rather than just determining the timing of flowering. If these proteins were involved in determining the morphology, then it could be predicted that the overexpression of FT and TFL1 homologs *in vivo* might lead to unusual morphologies. Indeed, in rice the overexpression of RCN1 and RC2 has been linked to an increased branching phenotype (Nakagawa et al., 2002). Overexpression of BvFT1 in *ft-10* mutant plants has been shown to be associated with floral abnormalities. Plants overexpressing BvFT1 were found to produce flowers lacking petals (Pin et al., 2010). FT and FT-orthologs have also been linked to altered floral architecture (Lifschitz et al., 2006). One possibility explanation is that TFL1 is a master regulator controlling the growth of vegetative tissues whilst FT inhibits vegetative growth and promotes cell differentiation (Lifschitz et al., 2006). As such the changes in morphology occur because cells that differentiate into specialised structures have an altered ratio of enhancing and inhibitory signals. The significance of this is that the floral PEBPs control both the timing of developmental stages and the output of those stages.

9.5.3 PEBP in Other Aspects of Plant Development

In *Arabidopsis*, there are several PEBPs expressed in different locales. These could contribute to the regulation of developmental events. In tomato, local balances between SFT, a FT-homolog, and SP, a TFL1 homolog are thought to determine the complexity of leaves (Shalit et al., 2009). Increasing the levels of SFT or decreasing the levels of SP in trifoliate plants reduces the number of leaflets whilst increasing the levels of SP or decreasing the levels of SFT causes the opposite effect (Shalit et al., 2009). This suggests that FT and TFL1 are capable of mediating several pleiotropic effects. It is likely that these effects are

mediated by interacting with 14-3-3 proteins. A notion which is consistent with the idea of a PEBP-14-3-3 universal platform involved in several aspects of plant development (discussed in section 9.4). In this study, the extended loop has been demonstrated to be extremely important for the morphological activity mediated by floral PEBPs.

9.6 DNA binding in Floral Regulation

9.6.1 The role of FD in Floral Regulation

9.6.1.1 FD may interact with C-box-like elements found across the AP1 Promoter

It has been previously speculated that floral complexes may interact with DNA. The core elements for this interaction are believed exist within the first 500 bp of the AP1 promoter. The C-box has been bioinformatically predicted as the FD binding site (Taoka et al., 2011, Wigge et al., 2005). The data indicates that the DNA-binding bZIP region of FD can interact with relatively low affinity with DNA from the core promoter region without other proteins but is not capable of interacting with the C-box region alone. This collectively suggests that FD has a binding site within the core promoter that is distinct from the C-box. This interpretation is broadly consistent with previous results (Benlloch et al., 2011). The data suggests that FD-bZIP on its own could interact with another region within the AP1 promoter. This potential alternate binding site may explain why FD can drive the expression of GUS, under the control of AP1 with a mutated C-box, in plants (Benlloch et al., 2011). However, there currently is no indication of where the alternate binding site is within the AP1 core promoter. There are several possible binding sites within the AP1 promoter including several imperfect or inverted A/C/G-boxes. In rice, which is believed to work in an analogous way, there are no perfect C-boxes immediately upstream of the gene; instead several imperfect and inverted C-boxes can be found (Taoka et al., 2011). This suggests that these imperfect C-boxes may be important in the activity of FD.

The observation that bZIP transcription factors may bind to sites other than those with typical ACGT core motifs is not without precedent. Several plant bZIP transcription factors have been shown to bind to DNA without a typical ACGT core. In pea, the bZIP transcription factor Opaque-2 (O2) binds to the non-

canonical sequence ATGAGTCAT (de Pater et al., 1994). The yeast bZIP transcription factor GCN4 binds to the pseudo-palindromic non-canonical sequence ATGACTCAT (Koldin et al., 1995). These sites are related to the ACGT core motif, but lack a nucleotide with their central ACGT-like region; these binding sites still enable high affinity binding with an apparent Kd the nM range. Some bZIP transcription factors bind sequences lacking an ACGT-like core; the transcription factor VSF-1 in tomato, binds to pseudo palindromic sequence which does not have a central AGCT core (CAACGGTTG) (Ringli and Keller, 1998). Thus it is possible that FD and FD-homologs bind to a novel sequences in the AP1 core promoter.

9.6.1.2 Floral Complexes interact with DNA with greater strength than FD Alone

Interestingly, both the FAC and FIC bind with high affinity to DNA whilst FD-bZIP alone binds a lower affinity. This opens up the possibility that either other components within the FAC or FIC could contribute to the binding directly or these components can induce changes in FD that facilitates a strengthened interaction with DNA. FD is thought to act as a weak positive regulator of flowering enabling activation of flowering genes in the absence of activating PEBPs as; sextuplet mutants deficient in the expression of all floral PEBPs still flower (Kim et al., 2013, Ahn et al., 2006). This ability to form both low strength and high strength interactions may be responsible for this weak/strong activity. It may also help to explain why mutations to the conserved phosphorylated residue in OsFD1 reduce but do not abolish the expression of the AP1 homolog OsMADS15 (Taoka et al., 2011).

9.6.2 DNA Binding may be Important for TFL1 Activity

The FIC can interact strongly with the 359 bp AP1 promoter fragment as well as the extended C-box region fragment. This interaction was not observed with the 22 bp C-box suggesting that DNA outside the C-box is involved in binding. Moreover, FIC binding did not occur with control DNA eliminating the possibility of non-specific binding or end-binding. These experiments have demonstrated that the proto-FIC can interact with relatively low affinity with internal sites within DNA in the absence of FD. This is surprising, as no prior studies have categorised either TFL1 or 14-3-3 proteins as DNA binding proteins. Their postulated effects as gene regulators have been associated with the activity of FD, a known transcription factor (Hanano and Goto, 2011). The fact that the proto-FIC does not interact with C-box

elements but interacts weakly with an extended AT rich region surrounding the C-box suggests that DNA the extended C-box might be involved in the interaction or the extended region is important for the correct conformation of the C-box for productive interactions. These interactions are not conserved in the proto-FAC. Indeed electrostatic analysis of the surface of TFL1 shows that there are two positively charged patches on the surface. One is inside the W-shaped complex towards the tip, formed by Arg^{7}, Lys^{30}, Lys^{37} and Lys^{38}. Interestingly, Lys^{30} is highly conserved among the TFL1 proteins while is poorly conserved among the FT proteins. Lys^{37} is either Arg/Lys or a Asn in TFL1 proteins while highly variable among FT proteins. Lys^{38} is either Arg or Lys in FT and TFL1 proteins. The other positively charged patch is at the tip of the W shape forming a positively charged path along a ridge on the protein surface. This patch is formed by Arg^{7}, Arg^{16} and Lys^{150}. Arg^{16} is conserved in both TFL1 and FT while Lys^{150} is relatively conserved in TFL1 but is a highly conserved negatively charged residue (Asp or Glu) in FT proteins. These subtle differences could potentially contribute to the ability of complexes containing TFL1, but not FT, to interact with DNA directly. Further investigations are required to dissect the exact roles of these amino acids.

9.6.3 The Floral Inhibitory Complex interacts with the C-box

Although the proto-FIC can weakly interact with DNA in the absence of FD, the interaction is significantly enhanced in the presence of FD even though FD alone does not bind to this region. This synergetic relationship between the proto-FIC and FD in DNA binding ensures multiple signals (including the presence of TFL1 and phosphorylation of FD) are integrated in the inhibition of flowering. The proto-FIC may play a major role in recruiting FD to the region around the C-box; explaining why FD on its own does not bind to this region while the FIC does. No interaction was detected between the FAC and the extended C-box DNA which suggests that the FAC and FIC have different binding sites, potentially providing a mechanism for the opposing action of the floral PEBPs.

9.6.4 Low Affinity DNA Binding Proteins

The proto-FIC interacts with DNA from the AP1 promoter with low μM affinity. Bacteriophage T7 gene 4 primase is another example of a low μM affinity DNA binding protein. T7 Primase interacts with its

recognition motif with an affinity of 10 µM (Frick and Richardson, 1999). In the crystal structure of DNAG, an *E.coli* primase, the backbone of DNA is loosely coordinated by a positively charged surface patch containing arginines (Corn et al., 2008). Only a few hydrophobic residues form van der Waals contacts with a small number of nucleotides (Corn et al., 2008). It is possible that similar interactions are made between TFL1 and DNA; these interactions could be made by the electropositive or hydrophobic patches on the surface of TFL1. High affinity binding is only possible in the presence of FD and is mediated by specific interactions between residues FD and DNA.

9.7 The Molecular Basis of Flowering

9.7.1 Nuclear localization of the Floral Inhibitory Complex

Members of the 14-3-3 protein family have a nuclear export signal, found at the C-terminus close to the PEBP binding site. Residues found within the nuclear export signal are involved in the interaction between PEBPs and 14-3-3 proteins. Potentially in the presence of PEBPs, the nuclear export signal is obscured, enabling PEBP-14-3-3 complexes to travel into the nucleus without being exported (Taoka et al., 2011). Though no nuclear import signal has been identified in 14-3-3 Nu, homologous 14-3-3 proteins in rice are found distributed throughout the cell including within the nucleus (Taoka et al., 2011). In the absence of PEBPs, 14-3-3 proteins are exported. Another possibility is that both the PEBPs and 14-3-3 proteins can enter the nucleus but only PEBP-14-3-3 protein complexes can remain. In either case only the PEBP-14-3-3 complex would be available to interact with phosphorylated FD. The interaction of FD with the complex may trap the complex within the nucleus which may explain why in BiFC experiments, signals from labelled 14-3-3 proteins and HD3a are located in the nucleus when OsFD is simultaneously overexpressed but found more widely across the cell in the absence of FD (Taoka et al., 2011). The interaction between 14-3-3 and FD may enhance the interaction between FD and DNA. However, this interaction can only occur in the presence of TFL1 and FT.

9.7.2 Differential binding as a Key Mechanism for Regulation

One possible model to explain the differences between the activity of the FAC and the FIC is that the FAC is preferentially recruited to the alternative FD binding site by FD, which promotes flowering whilst the proto-FIC recruits FD to the C-box region, hence preventing the formation of the FAC at the activating region by sequestration of FD (Figure 9.4). FD alone would weakly interact with the AP1 promoter and weakly promote the expression of AP1. Once in the nucleus the proto-FIC could recruit FD to the C-box region, away from its activation site potentially even competing with the proto-FAC for FD. At the C-box the complex would act to reduce expression of AP1. FICz might therefore inhibit flowering both by competing with FAC for FD at the activation site, hence reducing the activation directly, and by recruiting FD towards sites including the C-box where it may trigger downregulation of AP1 either by altering the conformation of DNA or by interfering with the action of other regulators like LFY (Hou and Yang, 2009, Hanano and Goto, 2011). It is likely that increasing concentrzations of the FAC could recruit FD away from the C-box to positive cis-acting elements which could provide a mechanistic basis for the antagonistic action of TFL1 and FT, *in vivo*.

9.8 Future Work

9.8.1 The effect of the FIC upon DNA

One unanswered question is whether the FIC has the potential to directly influence the conformation of DNA. Deformation of DNA can be monitored by fluorescent resonance energy transfer (FRET) in situations where florescent probes are placed at the end of DNA duplexes (Reviewed in Dragan and Privalov, 2008). In FRET assays, a donor probe is excited whilst the florescence of an acceptor probe is monitored. In the simplest case, when in close proximity energy can be transferred between the donor probe and the acceptor probe, resulting emission from the acceptor probe. Typically, probes can be no more than 10 nm away from each other(Didenko, 2001). When DNA is bent, the probes attached to each end may enter the necessary proximity to FRET enabling direct assessment of DNA bending. In this case probes attached to the duplex around the FIC binding site might be sufficient to monitor the effect. Upon the titration of protein a change in the fluorescent signal would be detectable and would infer binding.

An alternative method would be to use pBEND family of plasmids which contain a duplicated set of restriction sites which are repeated in the same order around the region of interest. Digestion creates a series of fragments of different size. The position of the region of interest differs in different fragments. Fragments which are incubated with the protein of interest can be assessed by EMSA as the mobility of DNA is less when DNA is bent centrally than when it is bent on either end. By measuring the mobility of different complexes the angle of the bend can be estimated allowing examination of the DNA bending.

9.8.2 The effect of FIC upon LFY

It is possible that the interaction of the FIC with DNA affects the binding of other regulators. Within the AP1 core promoter there are several LFY binding sites. *In vivo* the FIC may directly or indirectly influence the interaction of LFY with promoter DNA. This could be tested by examining the interaction of LFY and the AP1 core promoter region in the presence of the of the FIC and the FAC. Using microscale thermophoresis the interaction between GFP tagged LFY and AP1 core promoter should be detectable. If LFY and the FIC compete for a binding site, then it should be possible to detect the dissociation of LFY from AP1 in the presence of increasing concentrations of FIC.

9.8.3 Identifying Novel Regulators

The floral PEBPs may act through a variety of other proteins. Other transcription factors like FDP have been shown to bind to PEBPs (Hanano and Goto, 2011). One possibility is that TFL1 and FT mediate there effects through different transcription factors. To test this hypothesis, it would be necessary to over express alternative transcription factors in the presence or absence of functional TFL1 and examine the resulting phenotype. If the phenotypes differ in different background that would indicate that FDP's activity is dependent upon TFL1. Other proteins may also bind to TFL1 and FT, by the loop region, which may enhance the flowering phenotypes associated with the PEBPs. To identify which regulators might bind to TFL1 and FT, tagged PEBPs could be used as bait to pull-down proteins acquired from *Arabidopsis* cell extract. Proteins capable of binding to TFL1 could be identified via mass spectrometry.

9.8.4 Identifying New Binding Site *in Vivo*

In this study, DNA binding has been conducted upon synthesised DNA. Binding *in vivo* is determined by the accessibility of DNA within chromatin. To assess whether sites identified by *in vitro* studies are relevant *in vivo* chromatin immunoprecipitation sequencing (ChIP SEQ) could be employed. ChIP SEQ involves cross linking proteins in the nucleus to DNA, extracting DNA-protein complex via an antibody to the target protein, unlinking and purifying DNA before identifying the binding motif by sequencing. These motifs could then be used to identify genes under the control of the FIC or the FAC.

9.8.5 Testing the Differential Binding Model

In this study, it has been propose that the FIC and the FAC control flowering by binding to different regions of DNA. To assess whether this model is correct an *in vitro* transcription assay could be conducted to compare the wild-type core promoter to modified core promoters lacking either FAC binding site or FIC binding site. The effect of increasing concentrations of FAC and FIC could then be tested by measuring the expression of a reporter gene by qRT-PCR. The effect of competition between the complexes could also be tested in this way.

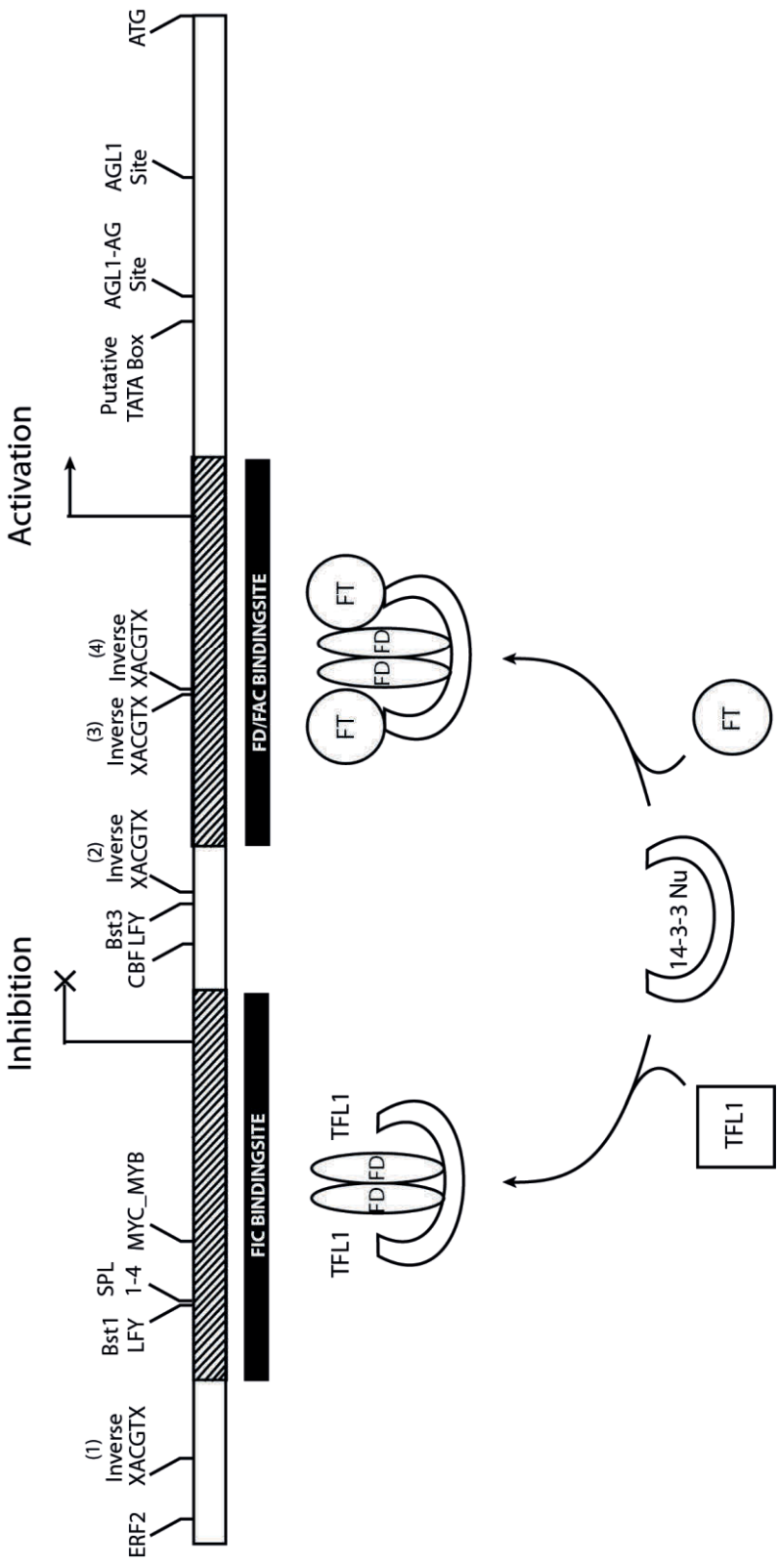


Figure 9.4: Model for interaction of floral complexes with AP1. FT converts FD into a strong activator while TFL1 converts FD into a strong repressor by recruiting FD to different locations within the AP1 core promoter. This interaction is mediated by 14-3-3 proteins.

9.8.6 Expression of FT-NQQ-GFP in different backgrounds

In this study, FT-NQQ-GFP was expressed in wild-type Col-0 plants. The phenotypes observed could be complicated by the presence of endogenous FT and TFL1. Expressing the construct in a background deficient in *FT* and *TFL1* could result in different phenotypes. In the current system, it is possible that the unusual phenotype observed occurred because of competition between the endogenous PEBPs and FT-NQQ-GFP. More refined expression using the phloem companion cell-specific SUC2 promoter could also enable the examination of whether FT-NQQ and similar constructs are capable of moving through the phloem which could allow examination of whether the extended loop is involved in transport (Truernit and Sauer, 1995). Additionally, in the current set of *in vivo* experiments it is possible the effect of the current constructs could be partially mediated through another complex. expressing the construct in plants deficient in *FD* would disambiguate these possibilities. If the protein were acting via FD, rather than other bZIP transcription factor like FD paralog, it would be expected that the phenotypes of FD deficient plants and plants expressing FT-NQQ-GFP in FD deficient plants would be different from the phenotype of wild-type plants expressing FT-NQQ-GFP.

9.8.7 Screening Compounds

This study has presented methodology to examine the interaction of small molecules with TFL1. The compounds identified in this study as potential inhibitor candidates require further characterisation via other techniques like NMR and crystallography to establish how the compounds bind. This would enable rational development of the compounds. These derivatives could be tested to see whether they improved or disrupted binding using ITC or microscale thermophoresis. Moreover, only a small subset of compounds has been examined, a large library of compounds and peptides could be screened to identify more effective inhibitory compounds.

Chapter 10 - Summary

In this study, four components of the floral regulatory network FT, TFL, 14-3-3 and FD were characterised. A direct interaction has been demonstrated between the 14-3-3 proteins and the PEBPs, TFL1 and FT. Both floral regulators interact with 14-3-3 proteins with similar affinity. The structure of the proto-FIC was solved, demonstrating that TFL1 binds to 14-3-3 Nu via a non-canonical interaction between TFL1 and the C-terminal α-helices of 14-3-3 Nu forming a W-shaped complex which is similar to the interaction between HD3a, an FT-like protein, and GRF14c, a complex collectively known as the Florigen Activation Complex (FAC).

The loops of TFL1 which have previously been shown to play a critical role in its activity are only partially involved in the interaction with 14-3-3 proteins (Ahn et al., 2006, Taoka et al., 2011). In TFL1 a small section of the loop, towards the N-terminus centred about Arg^{133}, is involved directly in the interaction. Mutations to residues in the N-terminus of the loop significantly decrease binding affinity, implying that these residues essential role in the interaction. Mutating three residues towards the C-terminus of the loop facing the exterior of the structure, converts FT into a potent repressor of flowering. Plants expressing the FT-NQQ-GFP construct bolted and flowered significantly later than wild-type controls and also produced aberrant flowers.

FD, a bZIP transcription factor, critical for the biological inhibition of flowering forms a complex with TFL1. Here it is shown that the phosphorylated C-terminus interacts with 14-3-3 Nu but not with TFL1, confirming the existence of the complex of TFL1, 14-3-3 Nu and FD designated here as the Floral Inhibitory Complex (FIC). Both the FIC and the FAC can bind to the core promoter region of AP1. The FIC can bind weakly to the core promoter of AP1 even in the absence of FD. The FIC is capable of binding to the region around the C-box whilst the FAC binds in a different location. No direct interaction was observed between the bZIP region of FD and the C-box implying that FD requires TFL1 and a 14-3-3 protein to interact with the C-box. However, the FD bZIP was also shown to interact with a longer stretch of DNA implying that an alternative site might be present within the AP1 core promoter. Collectively, the data suggests a mechanistic model for the antagonistic functions of TFL1 and FT in regulating flowering.

References

ABE, M., KOBAYASHI, Y., YAMAMOTO, S., DAIMON, Y., YAMAGUCHI, A., IKEDA, Y., ICHINOKI, H., NOTAGUCHI, M., GOTO, K. & ARAKI, T. 2005. FD, a bZIP protein mediating signals from the floral pathway integrator FT at the shoot apex. *Science,* 309**,** 1052-6.

ADAMS, P. D., AFONINE, P. V., BUNKOCZI, G., CHEN, V. B., DAVIS, I. W., ECHOLS, N., HEADD, J. J., HUNG, L. W., KAPRAL, G. J., GROSSE-KUNSTLEVE, R. W., MCCOY, A. J., MORIARTY, N. W., OEFFNER, R., READ, R. J., RICHARDSON, D. C., RICHARDSON, J. S., TERWILLIGER, T. C. & ZWART, P. H. 2010. PHENIX: a comprehensive Python-based system for macromolecular structure solution. *Acta Crystallogr D Biol Crystallogr,* 66**,** 213-21.

AHN, J. H., MILLER, D., WINTER, V. J., BANFIELD, M. J., LEE, J. H., YOO, S. Y., HENZ, S. R., BRADY, R. L. & WEIGEL, D. 2006. A divergent external loop confers antagonistic activity on floral regulators FT and TFL1. *EMBO J,* 25**,** 605-14.

AITKEN, A., COLLINGE, D. B., VAN HEUSDEN, B. P., ISOBE, T., ROSEBOOM, P. H., ROSENFELD, G. & SOLL, J. 1992. 14-3-3 proteins: a highly conserved, widespread family of eukaryotic proteins. *Trends in biochemical sciences,* 17**,** 498-501.

ALABADI, D., YANOVSKY, M. J., MAS, P., HARMER, S. L. & KAY, S. A. 2002. Critical role for CCA1 and LHY in maintaining circadian rhythmicity in Arabidopsis. *Curr Biol,* 12**,** 757-61.

ALTSCHUL, S. F., GISH, W., MILLER, W., MYERS, E. W. & LIPMAN, D. J. 1990. Basic local alignment search tool. *J Mol Biol,* 215**,** 403-10.

ANDRES, F. & COUPLAND, G. 2012. The genetic basis of flowering responses to seasonal cues. *Nature reviews Genetics,* 13**,** 627-39.

BAGNALL, D. J., KING, R. W. & HANGARTER, R. P. 1996. Blue-light promotion of flowering is absent in hy4 mutants of Arabidopsis. *Planta,* 200**,** 278-80.

BANFIELD, M. J. & BRADY, R. L. 2000. The structure of Antirrhinum centroradialis protein (CEN) suggests a role as a kinase regulator. *J Mol Biol,* 297**,** 1159-70.

BENLLOCH, R., KIM, M. C., SAYOU, C., THEVENON, E., PARCY, F. & NILSSON, O. 2011. Integrating long-day flowering signals: a LEAFY binding site is essential for proper photoperiodic activation of APETALA1. *Plant J,* 67**,** 1094-102.

BENSMIHEN, S., GIRAUDAT, J. & PARCY, F. 2005. Characterization of three homologous basic leucine zipper transcription factors (bZIP) of the ABI5 family during Arabidopsis thaliana embryo maturation. *Journal of experimental botany,* 56**,** 597-603.

BENZINGER, A., POPOWICZ, G. M., JOY, J. K., MAJUMDAR, S., HOLAK, T. A. & HERMEKING, H. 2005. The crystal structure of the non-liganded 14-3-3sigma protein: insights into determinants of isoform specific ligand binding and dimerization. *Cell research,* 15**,** 219-27.

BIHN, E. A., PAUL, A. L., WANG, S. W., ERDOS, G. W. & FERL, R. J. 1997. Localization of 14-3-3 proteins in the nuclei of arabidopsis and maize. *The Plant journal : for cell and molecular biology,* 12**,** 1439-45.

BOGAN, A. A. & THORN, K. S. 1998. Anatomy of hot spots in protein interfaces. *J Mol Biol,* 280**,** 1-9.

BOSS, P. K., BASTOW, R. M., MYLNE, J. S. & DEAN, C. 2004. Multiple pathways in the decision to flower: enabling, promoting, and resetting. *Plant Cell,* 16 Suppl**,** S18-31.

BRADLEY, D., CARPENTER, R., COPSEY, L., VINCENT, C., ROTHSTEIN, S. & COEN, E. 1996. Control of inflorescence architecture in Antirrhinum. *Nature,* 379**,** 791-7.

BRADLEY, D., RATCLIFFE, O., VINCENT, C., CARPENTER, R. & COEN, E. 1997. Inflorescence Commitment and Architecture in Arabidopsis. *Science,* 275**,** 80-83.

BRYSON, K., MCGUFFIN, L. J., MARSDEN, R. L., WARD, J. J., SODHI, J. S. & JONES, D. T. 1999. Protein structure prediction servers at University College London. *Nucleic Acids Research,* 33**,** W36-W38.

BUCHER, M. H., EVDOKIMOV, A. G. & WAUGH, D. S. 2002. Differential effects of short affinity tags on the crystallization of Pyrococcus furiosus maltodextrin-binding protein. *Acta Crystallogr D Biol Crystallogr,* 58**,** 392-7.

CARDON, G. H., HOHMANN, S., NETTESHEIM, K., SAEDLER, H. & HUIJSER, P. 1997. Functional analysis of the Arabidopsis thaliana SBP-box gene SPL3: a novel gene involved in the floral transition. *Plant J,* 12**,** 367-77.

CASTILLON, A., SHEN, H. & HUQ, E. 2007. Phytochrome Interacting Factors: central players in phytochrome-mediated light signaling networks. *Trends in plant science,* 12**,** 514-21.

COHEN, P. 2002. The origins of protein phosphorylation. *Nat Cell Biol,* 4**,** E127-30.

CONTI, L. & BRADLEY, D. 2007. TERMINAL FLOWER1 is a mobile signal controlling Arabidopsis architecture. *The Plant cell,* 19**,** 767-78.

CORBESIER, L., VINCENT, C., JANG, S., FORNARA, F., FAN, Q., SEARLE, I., GIAKOUNTIS, A., FARRONA, S., GISSOT, L., TURNBULL, C. & COUPLAND, G. 2007. FT Protein Movement Contributes to Long-Distance Signaling in Floral Induction of Arabidopsis. *Science,* 316**,** 1030-1033.

CORN, J. E., PELTON, J. G. & BERGER, J. M. 2008. Identification of a DNA primase template tracking site redefines the geometry of primer synthesis. *Nat Struct Mol Biol,* 15**,** 163-9.

CUBAS, P., LAUTER, N., DOEBLEY, J. & COEN, E. 1999. The TCP domain: a motif found in proteins regulating plant growth and development. *Plant J,* 18**,** 215-22.

CUTLER, S. & MCCOURT, P. 2005. Dude, where's my phenotype? Dealing with redundancy in signaling networks. *Plant Physiol,* 138**,** 558-9.

CZARNOTA, G. J., BAZETT-JONES, D. P., MENDEZ, E., ALLFREY, V. G. & OTTENSMYER, F. P. 1997. High resolution microanalysis and three-dimensional nucleosome structure associated with transcribing chromatin. *Micron,* 28**,** 419-431.

DANILEVSKAYA, O. N., MENG, X., HOU, Z., ANANIEV, E. V. & SIMMONS, C. R. 2008. A genomic and expression compendium of the expanded PEBP gene family from maize. *Plant Physiol,* 146**,** 250-64.

DAUGHERTY, C. J., ROONEY, M. F., MILLER, P. W. & FERL, R. J. 1996. Molecular organization and tissue-specific expression of an Arabidopsis 14-3-3 gene. *The Plant cell,* 8**,** 1239-48.

DE PATER, S., KATAGIRI, F., KIJNE, J. & CHUA, N. H. 1994. bZIP proteins bind to a palindromic sequence without an ACGT core located in a seed-specific element of the pea lectin promoter. *Plant J,* 6**,** 133-40.

DIDENKO, V. V. 2001. DNA probes using fluorescence resonance energy transfer (FRET): designs and applications. *Biotechniques,* 31**,** 1106-16, 1118, 1120-1.

DING, Z., DOYLE, M. R., AMASINO, R. M. & DAVIS, S. J. 2007. A complex genetic interaction between Arabidopsis thaliana TOC1 and CCA1/LHY in driving the circadian clock and in output regulation. *Genetics,* 176**,** 1501-10.

DRAGAN, A. I. & PRIVALOV, P. L. 2008. Use of fluorescence resonance energy transfer (FRET) in studying protein-induced DNA bending. *Methods Enzymol,* 450**,** 185-99.

DUHR, S. & BRAUN, D. 2006. Why molecules move along a temperature gradient. *Proceedings of the National Academy of Sciences of the United States of America,* 103**,** 19678-19682.

DUNLAP, J. C. 1999. Molecular Bases for Circadian Clocks. *Cell,* 96**,** 271-290.

EMSLEY, P., LOHKAMP, B., SCOTT, W. G. & COWTAN, K. 2010. Features and development of Coot. *Acta Crystallogr D Biol Crystallogr,* 66**,** 486-501.

ESSEN, L.-O., MAILLIET, J. & HUGHES, J. 2008. The structure of a complete phytochrome sensory module in the Pr ground state. *Proceedings of the National Academy of Sciences of the United States of America,* 105**,** 14709-14.

FENNER, M. 1998. The phenology of growth and reproduction in plants. *Perspectives in Plant Ecology, Evolution and Systematics,* 1**,** 78-91.

FRICK, D. N. & RICHARDSON, C. C. 1999. Interaction of bacteriophage T7 gene 4 primase with its template recognition site. *The Journal of biological chemistry,* 274**,** 35889-98.

FUJIWARA, S., ODA, A., YOSHIDA, R., NIINUMA, K., MIYATA, K., TOMOZOE, Y., TAJIMA, T., NAKAGAWA, M., HAYASHI, K., COUPLAND, G. & MIZOGUCHI, T. 2008. Circadian clock proteins LHY and CCA1 regulate SVP protein accumulation to control flowering in Arabidopsis. *Plant Cell,* 20**,** 2960-71.

GOLDBERG-MOELLER, R., SHALOM, L., SHLIZERMAN, L., SAMUELS, S., ZUR, N., OPHIR, R., BLUMWALD, E. & SADKA, A. 2013. Effects of gibberellin treatment during flowering induction period on global gene expression and the transcription of flowering-control genes in Citrus buds. *Plant Sci,* 198**,** 46-57.

GUAN, C. M., ZHU, S. S., LI, X. G. & ZHANG, X. S. 2006. Hormone-regulated inflorescence induction and TFL1 expression in Arabidopsis callus in vitro. *Plant Cell Rep,* 25**,** 1133-7.

GUO, H., YANG, H., MOCKLER, T. C. & LIN, C. 1998. Regulation of flowering time by Arabidopsis photoreceptors. *Science (New York, N Y),* 279**,** 1360-3.

GUSTAFSON-BROWN, C., SAVIDGE, B. & YANOFSKY, M. F. 1994. Regulation of the arabidopsis floral homeotic gene APETALA1. *Cell,* 76**,** 131-43.

HANANO, S. & GOTO, K. 2011. Arabidopsis TERMINAL FLOWER1 is involved in the regulation of flowering time and inflorescence development through transcriptional repression. *The Plant cell,* 23**,** 3172-84.

HANZAWA, Y., MONEY, T. & BRADLEY, D. 2005. A single amino acid converts a repressor to an activator of flowering. *Proc Natl Acad Sci U S A,* 102**,** 7748-53.

HECHT, V., KNOWLES, C. L., VANDER SCHOOR, J. K., LIEW, L. C., JONES, S. E., LAMBERT, M. J. M. & WELLER, J. L. 2007. Pea LATE BLOOMER1 Is a GIGANTEA Ortholog with Roles in Photoperiodic Flowering,

Deetiolation, and Transcriptional Regulation of Circadian Clock Gene Homologs. *Plant Physiol.,* 144**,** 648-661.

HEMPEL, F. D., WEIGEL, D., MANDEL, M. A., DITTA, G., ZAMBRYSKI, P. C., FELDMAN, L. J. & YANOFSKY, M. F. 1997. Floral determination and expression of floral regulatory genes in Arabidopsis. *Development,* 124**,** 3845-3853.

HEPWORTH, S. R., VALVERDE, F., RAVENSCROFT, D., MOURADOV, A. & COUPLAND, G. 2002. Antagonistic regulation of flowering-time gene SOC1 by CONSTANS and FLC via separate promoter motifs. *EMBO J,* 21**,** 4327-4337.

HOPE, H. 1990. Crystallography of biological macromolecules at ultra-low temperature. *Annu Rev Biophys Biophys Chem,* 19**,** 107-26.

HOPE, H., FROLOW, F., VON BOHLEN, K., MAKOWSKI, I., KRATKY, C., HALFON, Y., DANZ, H., WEBSTER, P., BARTELS, K. S., WITTMANN, H. G. & ET AL. 1989. Cryocrystallography of ribosomal particles. *Acta Crystallogr B,* 45 (Pt 2)**,** 190-9.

HOU, C. J. & YANG, C. H. 2009. Functional analysis of FT and TFL1 orthologs from orchid (Oncidium Gower Ramsey) that regulate the vegetative to reproductive transition. *Plant Cell Physiol,* 50**,** 1544-57.

HUQ, E., TEPPERMAN, J. M. & QUAIL, P. H. 2000. GIGANTEA is a nuclear protein involved in phytochrome signaling in Arabidopsis. *Proc Natl Acad Sci U S A,* 97**,** 9789-94.

IRISH, V. F. 2010. The flowering of Arabidopsis flower development. *The Plant journal : for cell and molecular biology,* 61**,** 1014-28.

ISHIKAWA, R., TAMAKI, S., YOKOI, S., INAGAKI, N., SHINOMURA, T., TAKANO, M. & SHIMAMOTO, K. 2005. Suppression of the floral activator Hd3a is the principal cause of the night break effect in rice. *Plant Cell,* 17**,** 3326-36.

IZAWA, T., FOSTER, R. & CHUA, N. H. 1993. Plant bZIP protein DNA binding specificity. *J Mol Biol,* 230**,** 1131-44.

JAKOBY, M., WEISSHAAR, B., DROGE-LASER, W., VICENTE-CARBAJOSA, J., TIEDEMANN, J., KROJ, T. & PARCY, F. 2002. bZIP transcription factors in Arabidopsis. *Trends Plant Sci,* 7**,** 106-11.

JASPERT, N., THROM, C. & OECKING, C. 2011. Arabidopsis 14-3-3 proteins: fascinating and less fascinating aspects. *Front Plant Sci,* 2**,** 96.

JOHNSON, E., BRADLEY, M., HARBERD, N. P. & WHITELAM, G. C. 1994. Photoresponses of Light-Grown phyA Mutants of Arabidopsis (Phytochrome A Is Required for the Perception of Daylength Extensions). *Plant Physiol,* 105**,** 141-149.

JONES, D. H., LEY, S. & AITKEN, A. 1995. Isoforms of 14-3-3 protein can form homo- and heterodimers in vivo and in vitro: implications for function as adapter proteins. *FEBS letters,* 368**,** 55-8.

JONES, D. T. 1999. Protein secondary structure prediction based on position-specific scoring matrices. *J Mol Biol,* 292**,** 195-202.

JUNG, C. & MULLER, A. E. 2009. Flowering time control and applications in plant breeding. *Trends Plant Sci,* 14**,** 563-73.

KANTARDJIEFF, K. A. & RUPP, B. 2003. Matthews coefficient probabilities: Improved estimates for unit cell contents of proteins, DNA, and protein-nucleic acid complex crystals. *Protein Science,* 12**,** 1865-71.

KARDAILSKY, I., SHUKLA, V. K., AHN, J. H., DAGENAIS, N., CHRISTENSEN, S. K., NGUYEN, J. T., CHORY, J., HARRISON, M. J. & WEIGEL, D. 1999. Activation Tagging of the Floral Inducer FT. *Science,* 286**,** 1962-1965.

KARLGREN, A., GYLLENSTRAND, N., KALLMAN, T., SUNDSTROM, J. F., MOORE, D., LASCOUX, M. & LAGERCRANTZ, U. 2011. Evolution of the PEBP gene family in plants: functional diversification in seed plant evolution. *Plant Physiol,* 156**,** 1967-77.

KELLEY, L. A. & STERNBERG, M. J. 2009. Protein structure prediction on the Web: a case study using the Phyre server. *Nature Protocols,* 4**,** 363-71.

KEMMER, G. & KELLER, S. 2010. Nonlinear least-squares data fitting in Excel spreadsheets. *Nature Protocols,* 5**,** 267-81.

KHAN, F., HE, M. & TAUSSIG, M. J. 2006. Double-hexahistidine tag with high-affinity binding for protein immobilization, purification, and detection on ni-nitrilotriacetic acid surfaces. *Analytical chemistry,* 78**,** 3072-9.

KIEFHABER, T., RUDOLPH, R., KOHLER, H. H. & BUCHNER, J. 1991. Protein aggregation in vitro and in vivo: a quantitative model of the kinetic competition between folding and aggregation. *Biotechnology (N Y),* 9**,** 825-9.

KIM, W., PARK, T. I., YOO, S. J., JUN, A. R. & AHN, J. H. 2013. Generation and analysis of a complete mutant set for the Arabidopsis FT/TFL1 family shows specific effects on thermo-sensitive flowering regulation. *Journal of experimental botany,* 64**,** 1715-29.

KING, R. W., EVANS, L.T., AND WARDLAW, I.F. 1968. Translocation of the floral stimulus in Pharbitis nil in relation to that of assimilates. *Zeitschrift fur Pflanzenphysiologie,* 59**,** 377–388.

KLEIN, J., SAEDLER, H. & HUIJSER, P. 1996. A new family of DNA binding proteins includes putative transcriptional regulators of the Antirrhinum majus floral meristem identity gene SQUAMOSA. *Molecular & general genetics : MGG,* 250**,** 7-16.

KOBAYASHI, Y., KAYA, H., GOTO, K., IWABUCHI, M. & ARAKI, T. 1999. A Pair of Related Genes with Antagonistic Roles in Mediating Flowering Signals. *Science,* 286**,** 1960-1962.

KOLDIN, B., SUCKOW, M., SEYDEL, A., VON WILCKEN-BERGMANN, B. & MULLER-HILL, B. 1995. A comparison of the different DNA binding specificities of the bZip proteins C/EBP and GCN4. *Nucleic Acids Res,* 23**,** 4162-9.

KOMIYA, R., IKEGAMI, A., TAMAKI, S., YOKOI, S. & SHIMAMOTO, K. 2008. Hd3a and RFT1 are essential for flowering in rice. *Development,* 135**,** 767-74.

KRIZEK, B. A. & FLETCHER, J. C. 2005. Molecular mechanisms of flower development: an armchair guide. *Nature reviews Genetics,* 6**,** 688-98.

KRYSAN, P. J., YOUNG, J. C., TAX, F. & SUSSMAN, M. R. 1996. Identification of transferred DNA insertions within Arabidopsis genes involved in signal transduction and ion transport. *Proceedings of the National Academy of Sciences,* 93**,** 8145-8150.

KUMAGAI, A. & DUNPHY, W. G. 1999. Binding of 14-3-3 proteins and nuclear export control the intracellular localization of the mitotic inducer Cdc25. *Genes & development,* 13**,** 1067-72.

LEE, J. H., YOO, S. J., PARK, S. H., HWANG, I., LEE, J. S. & AHN, J. H. 2007. Role of SVP in the control of flowering time by ambient temperature in Arabidopsis. *Genes Dev,* 21**,** 397-402.

LEMPE, J., BALASUBRAMANIAN, S., SURESHKUMAR, S., SINGH, A., SCHMID, M. & WEIGEL, D. 2005. Diversity of Flowering Responses in Wild <italic>Arabidopsis thaliana</italic> Strains. *PLoS Genet,* 1**,** e6.

LESLIE, A. W. & POWELL, H. 2007. Processing diffraction data with mosflm. *In:* READ, R. & SUSSMAN, J. (eds.) *Evolving Methods for Macromolecular Crystallography.* Springer Netherlands.

LEVY, A., PALEVITCH, D., MILO, J. & LAVIE, D. 1986. Effect of gibberellic acid on flowering and the thebaine yield of different clones of Papaver bracteatum. *Plant Growth Regulation,* 4**,** 153-157.

LEVY, Y. Y. & DEAN, C. 1998. The transition to flowering. *Plant Cell,* 10**,** 1973-90.

LICHTY, J. J., MALECKI, J. L., AGNEW, H. D., MICHELSON-HOROWITZ, D. J. & TAN, S. 2005. Comparison of affinity tags for protein purification. *Protein Expression and Purification,* 41**,** 98-105.

LIFSCHITZ, E., EVIATAR, T., ROZMAN, A., SHALIT, A., GOLDSHMIDT, A., AMSELLEM, Z., ALVAREZ, J. P. & ESHED, Y. 2006. The tomato FT ortholog triggers systemic signals that regulate growth and flowering and substitute for diverse environmental stimuli. *Proc Natl Acad Sci U S A,* 103**,** 6398-403.

LILJEGREN, S. J., GUSTAFSON-BROWN, C., PINYOPICH, A., DITTA, G. S. & YANOFSKY, M. F. 1999. Interactions among APETALA1, LEAFY, and TERMINAL FLOWER1 specify meristem fate. *The Plant cell,* 11**,** 1007-18.

LIN, I. G., TOMZYNSKI, T. J., OU, Q. & HSIEH, C. L. 2000. Modulation of DNA binding protein affinity directly affects target site demethylation. *Molecular and cellular biology,* 20**,** 2343-9.

LIU, D., BIENKOWSKA, J., PETOSA, C., COLLIER, R. J., FU, H. & LIDDINGTON, R. 1995. Crystal structure of the zeta isoform of the 14-3-3 protein. *Nature,* 376**,** 191-4.

LIVERMAN, J. L. & LANG, A. 1956. Induction of Flowering in Long Day Plants by Applied Indoleacetic Acid. *Plant Physiol,* 31**,** 147-50.

LOCKE, J. C., SOUTHERN, M. M., KOZMA-BOGNAR, L., HIBBERD, V., BROWN, P. E., TURNER, M. S. & MILLAR, A. J. 2005. Extension of a genetic network model by iterative experimentation and mathematical analysis. *Mol Syst Biol,* 1**,** 2005 0013.

LOVELL, S. C., WORD, J. M., RICHARDSON, J. S. & RICHARDSON, D. C. 2000. The penultimate rotamer library. *Proteins,* 40**,** 389-408.

LU, G., DE VETTEN, N. C., SEHNKE, P. C., ISOBE, T., ICHIMURA, T., FU, H., VAN HEUSDEN, G. P. & FERL, R. J. 1994. A single Arabidopsis GF14 isoform possesses biochemical characteristics of diverse 14-3-3 homologues. *Plant Mol Biol,* 25**,** 659-67.

LU, G., DELISLE, A. J., DE VETTEN, N. C. & FERL, R. J. 1992. Brain proteins in plants: an Arabidopsis homolog to neurotransmitter pathway activators is part of a DNA binding complex. *Proc Natl Acad Sci U S A,* 89**,** 11490-4.

MACIEJEWSKI, P. M., PETERSON, F. C., ANDERSON, P. J. & BROOKS, C. L. 1995. Mutation of serine 90 to glutamic acid mimics phosphorylation of bovine prolactin. *J Biol Chem,* 270**,** 27661-5.

MANDEL, M. A., GUSTAFSON-BROWN, C., SAVIDGE, B. & YANOFSKY, M. F. 1992. Molecular characterization of the Arabidopsis floral homeotic gene APETALA1. *Nature,* 360**,** 273-7.

MARTIN-TRILLO, M. & CUBAS, P. 2010. TCP genes: a family snapshot ten years later. *Trends Plant Sci,* 15**,** 31-9.

MATHIEU, J., WARTHMANN, N., KÜTTNER, F. & SCHMID, M. 2007. Export of FT Protein from Phloem Companion Cells Is Sufficient for Floral Induction in Arabidopsis. *Current biology : CB,* 17**,** 1055-1060.

MATTHEWS, B. W. 1968. Solvent content of protein crystals. *J Mol Biol,* 33**,** 491-7.

MAY, E. R., ARMEN, R. S., MANNAN, A. M. & BROOKS, C. L., 3RD 2010. The flexible C-terminal arm of the Lassa arenavirus Z-protein mediates interactions with multiple binding partners. *Proteins,* 78**,** 2251-64.

MAYFIELD, J. D., FOLTA, K. M., PAUL, A.-L. & FERL, R. J. 2007. The 14-3-3 Proteins μ and υ Influence Transition to Flowering and Early Phytochrome Response. *Plant Physiology,* 145**,** 1692-1702.

MENG, X., MUSZYNSKI, M. G. & DANILEVSKAYA, O. N. 2011. The FT-like ZCN8 Gene Functions as a Floral Activator and Is Involved in Photoperiod Sensitivity in Maize. *Plant Cell,* 23**,** 942-60.

MIMIDA, N., GOTO, K., KOBAYASHI, Y., ARAKI, T., AHN, J. H., WEIGEL, D., MURATA, M., MOTOYOSHI, F. & SAKAMOTO, W. 2001. Functional divergence of the TFL1-like gene family in Arabidopsis revealed by characterization of a novel homologue. *Genes Cells,* 6**,** 327-36.

MIYATA, K., CALVINO, M., ODA, A. O., SUGIYAMA, H. & MIZOGUCHI, T. 2011. Suppression of late-flowering and semi-dwarf phenotypes in the Arabidopsis clock mutant lhy-12;cca1-101 by phyB under continuous light. *Plant signaling & behavior,* 6**,** 1162-71.

MIZOGUCHI, T., WRIGHT, L., FUJIWARA, S., CREMER, F., LEE, K., ONOUCHI, H., MOURADOV, A., FOWLER, S., KAMADA, H., PUTTERILL, J. & COUPLAND, G. 2005. Distinct roles of GIGANTEA in promoting flowering and regulating circadian rhythms in Arabidopsis. *Plant Cell,* 17**,** 2255-70.

MOURADOV, A., CREMER, F. & COUPLAND, G. 2002. Control of flowering time: interacting pathways as a basis for diversity. *The Plant cell,* 14 Suppl**,** S111-30.

MUNOZ-FONTELA, C., MARCOS-VILLAR, L., GALLEGO, P., ARROYO, J., DA COSTA, M., POMERANZ, K. M., LAM, E. W. F. & RIVAS, C. 2007. Latent protein LANA2 from Kaposi's sarcoma-associated herpesvirus interacts with 14-3-3 proteins and inhibits FOXO3a transcription factor. *Journal of virology,* 81**,** 1511-6.

MURASHIGE, T. & SKOOG, F. 1962. A Revised Medium for Rapid Growth and Bio Assays with Tobacco Tissue Cultures. *Physiologia Plantarum,* 15**,** 473-497.

MURSHUDOV, G. N., SKUBAK, P., LEBEDEV, A. A., PANNU, N. S., STEINER, R. A., NICHOLLS, R. A., WINN, M. D., LONG, F. & VAGIN, A. A. 2011. REFMAC5 for the refinement of macromolecular crystal structures. *Acta Crystallogr D Biol Crystallogr,* 67**,** 355-67.

MUSLIN, A. J., TANNER, J. W., ALLEN, P. M. & SHAW, A. S. 1996. Interaction of 14-3-3 with signaling proteins is mediated by the recognition of phosphoserine. *Cell,* 84**,** 889-97.

MUSZYNSKI, M. G., DAM, T., LI, B., SHIRBROUN, D. M., HOU, Z., BRUGGEMANN, E., ARCHIBALD, R., ANANIEV, E. V. & DANILEVSKAYA, O. N. 2006. delayed flowering1 Encodes a basic leucine zipper protein that mediates floral inductive signals at the shoot apex in maize. *Plant Physiol,* 142**,** 1523-36.

NAKAGAWA, M., SHIMAMOTO, K. & KYOZUKA, J. 2002. Overexpression of RCN1 and RCN2, rice TERMINAL FLOWER 1/CENTRORADIALIS homologs, confers delay of phase transition and altered panicle morphology in rice. *Plant J,* 29**,** 743-50.

NAKAGAWA, T., KUROSE, T., HINO, T., TANAKA, K., KAWAMUKAI, M., NIWA, Y., TOYOOKA, K., MATSUOKA, K., JINBO, T. & KIMURA, T. 2007. Development of series of gateway binary vectors, pGWBs, for realizing efficient construction of fusion genes for plant transformation. *J Biosci Bioeng,* 104**,** 34-41.

NAVARRO, C., ABELENDA, J. A., CRUZ-ORO, E., CUELLAR, C. A., TAMAKI, S., SILVA, J., SHIMAMOTO, K. & PRAT, S. 2011. Control of flowering and storage organ formation in potato by FLOWERING LOCUS T. *Nature,* 478**,** 119-22.

NIESEN, F. H., BERGLUND, H. & VEDADI, M. 2007. The use of differential scanning fluorimetry to detect ligand interactions that promote protein stability. *Nature Protocols,* 2**,** 2212-21.

NISHIYAMA, Y., HARDRE-LIENARD, H., MIRAS, S., MIEGE, C., BLOCK, M. A., REVAH, F., JOYARD, J. & MARECHAL, E. 2003. Refolding from denatured inclusion bodies, purification to homogeneity and simplified assay of MGDG synthases from land plants. *Protein Expr Purif,* 31**,** 79-87.

NIWA, M., DAIMON, Y., KUROTANI, K., HIGO, A., PRUNEDA-PAZ, J. L., BRETON, G., MITSUDA, N., KAY, S. A., OHME-TAKAGI, M., ENDO, M. & ARAKI, T. 2013. BRANCHED1 interacts with FLOWERING LOCUS T to repress the floral transition of the axillary meristems in Arabidopsis. *Plant Cell,* 25**,** 1228-42.

OBSIL, T., GHIRLANDO, R., KLEIN, D. C., GANGULY, S. & DYDA, F. 2001. Crystal structure of the 14-3-3zeta:serotonin N-acetyltransferase complex. a role for scaffolding in enzyme regulation. *Cell,* 105**,** 257-67.

OGAWA, Y. & KING, R. W. 1979. Indirect Action of Benzyladenine and Other Chemicals on Flowering of Pharbitis nil Chois: Action by Interference with Assimilate Translocation from Induced Cotyledons. *Plant Physiol,* 63**,** 643-9.

PARCY, F., NILSSON, O., BUSCH, M. A., LEE, I. & WEIGEL, D. 1998. A genetic framework for floral patterning. *Nature,* 395**,** 561-6.

PAUL, A.-L., SEHNKE, P. C., FERL, R. J. & FERL, R. J. 2005. Isoform-specific subcellular localization among 14-3-3 proteins in Arabidopsis seems to be driven by client interactions. *Molecular biology of the cell,* 16**,** 1735-43.

PILLITTERI, L. J., LOVATT, C. J. & WALLING, L. L. 2004. Isolation and characterization of a TERMINAL FLOWER homolog and its correlation with juvenility in citrus. *Plant Physiol,* 135**,** 1540-51.

PIN, P. A., BENLLOCH, R., BONNET, D., WREMERTH-WEICH, E., KRAFT, T., GIELEN, J. J. & NILSSON, O. 2010. An antagonistic pair of FT homologs mediates the control of flowering time in sugar beet. *Science,* 330**,** 1397-400.

PNUELI, L., CARMEL-GOREN, L., HAREVEN, D., GUTFINGER, T., ALVAREZ, J., GANAL, M., ZAMIR, D. & LIFSCHITZ, E. 1998. The SELF-PRUNING gene of tomato regulates vegetative to reproductive switching of sympodial meristems and is the ortholog of CEN and TFL1. *Development,* 125**,** 1979-89.

PNUELI, L., GUTFINGER, T., HAREVEN, D., BEN-NAIM, O., RON, N., ADIR, N. & LIFSCHITZ, E. 2001a. Tomato SP-interacting proteins define a conserved signaling system that regulates shoot architecture and flowering. *Plant Cell,* 13**,** 2687-702.

PNUELI, L., GUTFINGER, T., HAREVEN, D., BEN-NAIM, O., RON, N., ADIR, N. & LIFSCHITZ, E. 2001b. Tomato SP-interacting proteins define a conserved signaling system that regulates shoot architecture and flowering. *The Plant cell,* 13**,** 2687-702.

POCKROS, P. J., SCHIFF, E. R., SHIFFMAN, M. L., MCHUTCHISON, J. G., GISH, R. G., AFDHAL, N. H., MAKHVILADZE, M., HUYGHE, M., HECHT, D., OLTERSDORF, T. & SHAPIRO, D. A. 2007. Oral IDN-6556, an antiapoptotic caspase inhibitor, may lower aminotransferase activity in patients with chronic hepatitis C. *Hepatology,* 46**,** 324-9.

PURWESTRI, Y. A., OGAKI, Y., TAMAKI, S., TSUJI, H. & SHIMAMOTO, K. 2009. The 14-3-3 protein GF14c acts as a negative regulator of flowering in rice by interacting with the florigen Hd3a. *Plant & cell physiology,* 50**,** 429-38.

RATCLIFFE, O. J., BRADLEY, D. J. & COEN, E. S. 1999. Separation of shoot and floral identity in Arabidopsis. *Development (Cambridge, England),* 126**,** 1109-20.

RIECHMANN, J. L., HEARD, J., MARTIN, G., REUBER, L., JIANG, C., KEDDIE, J., ADAM, L., PINEDA, O., RATCLIFFE, O. J., SAMAHA, R. R., CREELMAN, R., PILGRIM, M., BROUN, P., ZHANG, J. Z., GHANDEHARI, D., SHERMAN, B. K. & YU, G. 2000. Arabidopsis transcription factors: genome-wide comparative analysis among eukaryotes. *Science,* 290**,** 2105-10.

RIECHMANN, J. L., KRIZEK, B. A. & MEYEROWITZ, E. M. 1996. Dimerization specificity of Arabidopsis MADS domain homeotic proteins APETALA1, APETALA3, PISTILLATA, and AGAMOUS. *Proceedings of the National Academy of Sciences of the United States of America,* 93**,** 4793-8.

RIEFLER, M., NOVAK, O., STRNAD, M. & SCHMÜLLING, T. 2006. Arabidopsis Cytokinin Receptor Mutants Reveal Functions in Shoot Growth, Leaf Senescence, Seed Size, Germination, Root Development, and Cytokinin Metabolism. *The Plant Cell Online,* 18**,** 40-54.

RINGLI, C. & KELLER, B. 1998. Specific interaction of the tomato bZIP transcription factor VSF-1 with a non-palindromic DNA sequence that controls vascular gene expression. *Plant Mol Biol,* 37**,** 977-88.

RISK, J., LAURIE, R., MACKNIGHT, R. & DAY, C. 2010. FRIGIDA and related proteins have a conserved central domain and family specific N- and C- terminal regions that are functionally important. *Plant Molecular Biology,* 73**,** 493-505.

RITTINGER, K., BUDMAN, J., XU, J., VOLINIA, S., CANTLEY, L. C., SMERDON, S. J., GAMBLIN, S. J. & YAFFE, M. B. 1999. Structural analysis of 14-3-3 phosphopeptide complexes identifies a dual role for the nuclear export signal of 14-3-3 in ligand binding. *Molecular cell,* 4**,** 153-66.

RONG, J., BOWERS, J., E. , SCHULZE, S., R. , WAGHMARE, V., N., ROGERS, C., J. , PIERCE, G., J., ZHANG, H., ESTILL J., C. & AND PATERSON, A., H. 2005. Comparative genomics of Gossypium and Arabidopsis: Unraveling the consequences of both ancient and recent polyploidy. *Genome Research,* 15**,** 1198–1210.

ROSENQUIST, M., ALSTERFJORD, M., LARSSON, C. & SOMMARIN, M. 2001. Data mining the Arabidopsis genome reveals fifteen 14-3-3 genes. Expression is demonstrated for two out of five novel genes. *Plant Physiology,* 127**,** 142-9.

ROSENQUIST, M., SEHNKE, P., FERL, R. J., SOMMARIN, M. & LARSSON, C. 2000. Evolution of the 14-3-3 protein family: does the large number of isoforms in multicellular organisms reflect functional specificity? *Journal of molecular evolution,* 51**,** 446-58.

SAIKI, R. K., SCHARF, S., FALOONA, F., MULLIS, K. B., HORN, G. T., ERLICH, H. A. & ARNHEIM, N. 1985. Enzymatic amplification of beta-globin genomic sequences and restriction site analysis for diagnosis of sickle cell anemia. *Science,* 230**,** 1350-4.

SALEHI, H., RANSOM, C. B., ORABY, H. F., SEDDIGHI, Z. & STICKLEN, M. B. 2005. Delay in flowering and increase in biomass of transgenic tobacco expressing the Arabidopsis floral repressor gene FLOWERING LOCUS C. *J Plant Physiol,* 162**,** 711-7.

SCHMID, M., UHLENHAUT, N. H., GODARD, F., DEMAR, M., BRESSAN, R., WEIGEL, D. & LOHMANN, J. U. 2003. Dissection of floral induction pathways using global expression analysis. *Development,* 130**,** 6001-12.

SCHOONHEIM, P. J., SINNIGE, M. P., CASARETTO, J. A., VEIGA, H., BUNNEY, T. D., QUATRANO, R. S. & DE BOER, A. H. 2007. 14-3-3 adaptor proteins are intermediates in ABA signal transduction during barley seed germination. *The Plant journal : for cell and molecular biology,* 49**,** 289-301.

SCHULTZ, E. A. & HAUGHN, G. W. 1991. LEAFY, a Homeotic Gene That Regulates Inflorescence Development in Arabidopsis. *Plant Cell,* 3**,** 771-781.

SEARLE, I., HE, Y., TURCK, F., VINCENT, C., FORNARA, F., KROBER, S., AMASINO, R. A. & COUPLAND, G. 2006. The transcription factor FLC confers a flowering response to vernalization by repressing meristem competence and systemic signaling in Arabidopsis. *Genes Dev,* 20**,** 898-912.

SEHNKE, P. C., CHUNG, H. J., WU, K. & FERL, R. J. 2001. Regulation of starch accumulation by granule-associated plant 14-3-3 proteins. *Proceedings of the National Academy of Sciences of the United States of America,* 98**,** 765-70.

SEIDEL, S. A. I., DIJKMAN, P. M., LEA, W. A., VAN DEN BOGAART, G., JERABEK-WILLEMSEN, M., LAZIC, A., JOSEPH, J. S., SRINIVASAN, P., BAASKE, P., SIMEONOV, A., KATRITCH, I., MELO, F. A., LADBURY, J. E., SCHREIBER, G., WATTS, A., BRAUN, D. & DUHR, S. 2013. Microscale thermophoresis quantifies biomolecular interactions under previously challenging conditions. *Methods,* 59**,** 301-315.

SEIMIYA, H., SAWADA, H., MURAMATSU, Y., SHIMIZU, M., OHKO, K., YAMANE, K. & TSURUO, T. 2000. Involvement of 14-3-3 proteins in nuclear localization of telomerase. *The EMBO journal,* 19**,** 2652-61.

SHALIT, A., ROZMAN, A., GOLDSHMIDT, A., ALVAREZ, J. P., BOWMAN, J. L., ESHED, Y. & LIFSCHITZ, E. 2009. The flowering hormone florigen functions as a general systemic regulator of growth and termination. *Proc Natl Acad Sci U S A,* 106**,** 8392-7.

SHANNON, S. & MEEKS-WAGNER, D. R. 1991. A Mutation in the Arabidopsis TFL1 Gene Affects Inflorescence Meristem Development. *Plant Cell,* 3**,** 877-892.

SIMISTER, P. C., BURTON, N. M. & BRADY, R. L. 2011. Phosphotyrosine Recognition by the Raf Kinase Inhibitor Protein. 2**,** 59-70.

SIVASHANMUGAM, A., MURRAY, V., CUI, C., ZHANG, Y., WANG, J. & LI, Q. 2009. Practical protocols for production of very high yields of recombinant proteins using Escherichia coli. *Protein Science,* 18**,** 936-48.

SMITH, A., COUPLAND, G., DOLAN, L., HARBERD, N., JONES, J., MARTIN, C., SABLOWKI, R. AND ABIGAIL, A. 2010. *Plant Biology,* New York, Garland Sciences.

SORENSEN, H. P. & MORTENSEN, K. K. 2005. Soluble expression of recombinant proteins in the cytoplasm of Escherichia coli. *Microb Cell Fact,* 4**,** 1.

SORRELL, D. A., MARCHBANK, A. M., CHRIMES, D. A., DICKINSON, J. R., ROGERS, H. J., FRANCIS, D., GRIERSON, C. S. & HALFORD, N. G. 2003. The Arabidopsis 14-3-3 protein, GF14omega, binds to the Schizosaccharomyces pombe Cdc25 phosphatase and rescues checkpoint defects in the rad24-mutant. *Planta,* 218**,** 50-7.

STEFFENS, N. O., GALUSCHKA, C., SCHINDLER, M., BULOW, L. & HEHL, R. 2004. AthaMap: an online resource for in silico transcription factor binding sites in the Arabidopsis thaliana genome. *Nucleic Acids Res,* 32**,** D368-72.

STUDIER, F. W. 2005. Protein production by auto-induction in high density shaking cultures. *Protein Expr Purif,* 41**,** 207-34.

SUAREZ-LOPEZ, P., WHEATLEY, K., ROBSON, F., ONOUCHI, H., VALVERDE, F. & COUPLAND, G. 2001. CONSTANS mediates between the circadian clock and the control of flowering in Arabidopsis. *Nature,* 410**,** 1116-1120.

SUNDBERG, E. J. & MARIUZZA, R. A. 2000. Luxury accommodations: the expanding role of structural plasticity in protein-protein interactions. *Structure,* 8**,** R137-42.

TAKADA, S. & GOTO, K. 2003. TERMINAL FLOWER2, an Arabidopsis Homolog of HETEROCHROMATIN PROTEIN1, Counteracts the Activation of FLOWERING LOCUS T by CONSTANS in the Vascular Tissues of Leaves to Regulate Flowering Time. *Plant Cell,* 15**,** 2856-2865.

TAMAKI, S., MATSUO, S., WONG, H. L., YOKOI, S. & SHIMAMOTO, K. 2007. Hd3a protein is a mobile flowering signal in rice. *Science,* 316**,** 1033-6.

TAMURA, K., DUDLEY, J., NEI, M. & KUMAR, S. 2007. MEGA4: Molecular Evolutionary Genetics Analysis (MEGA) software version 4.0. *Mol Biol Evol,* 24**,** 1596-9.

TAOKA, K.-I., OHKI, I., TSUJI, H., FURUITA, K., HAYASHI, K., YANASE, T., YAMAGUCHI, M., NAKASHIMA, C., PURWESTRI, Y. A., TAMAKI, S., OGAKI, Y., SHIMADA, C., NAKAGAWA, A., KOJIMA, C. & SHIMAMOTO, K. 2011. 14-3-3 proteins act as intracellular receptors for rice Hd3a florigen. *Nature,* 476**,** 332-5.

TARABAN, M., ZHAN, H., WHITTEN, A. E., LANGLEY, D. B., MATTHEWS, K. S., SWINT-KRUSE, L. & TREWHELLA, J. 2008. Ligand-induced conformational changes and conformational dynamics in the solution structure of the lactose repressor protein. *Journal of Molecular Biology,* 376**,** 466-481.

TENHARMSEL, A. & BIGGIN, M. D. 1995. Bending DNA can repress a eukaryotic basal promoter and inhibit TFIID binding. *Molecular and cellular biology,* 15**,** 5492-8.

TEPER-BAMNOLKER, P. & SAMACH, A. 2005. The flowering integrator FT regulates SEPALLATA3 and FRUITFULL accumulation in Arabidopsis leaves. *Plant Cell,* 17**,** 2661-75.

TIEMAN, D. M. & KLEE, H. J. 1999. Differential Expression of Two Novel Members of the Tomato Ethylene-Receptor Family. *Plant Physiol.,* 120**,** 165-172.

TILMAN, D., CASSMAN, K. G., MATSON, P. A., NAYLOR, R. & POLASKY, S. 2002. Agricultural sustainability and intensive production practices. *Nature,* 418**,** 671-677.

TRUERNIT, E. & SAUER, N. 1995. The promoter of the Arabidopsis thaliana SUC2 sucrose-H+ symporter gene directs expression of beta-glucuronidase to the phloem: evidence for phloem loading and unloading by SUC2. *Planta,* 196**,** 564-70.

TSUJI, H., NAKAMURA, H., TAOKA, K. & SHIMAMOTO, K. 2013. Functional diversification of FD transcription factors in rice, components of florigen activation complexes. *Plant Cell Physiol,* 54**,** 385-97.

VALVERDE, F., MOURADOV, A., SOPPE, W., RAVENSCROFT, D., SAMACH, A. & COUPLAND, G. 2004. Photoreceptor Regulation of CONSTANS Protein in Photoperiodic Flowering. *Science,* 303**,** 1003-1006.

VAN HEEL, M. 1987. Angular reconstitution: a posteriori assignment of projection directions for 3D reconstruction. *Ultramicroscopy,* 21**,** 111-23.

VAN HEUSDEN, G. P., VAN DER ZANDEN, A. L., FERL, R. J. & STEENSMA, H. Y. 1996. Four Arabidopsis thaliana 14-3-3 protein isoforms can complement the lethal yeast bmh1 bmh2 double disruption. *FEBS letters,* 391**,** 252-6.

VARADARAJ, K. & SKINNER, D. M. 1994. Denaturants or Cosolvents Improve the Specificity of Pcr Amplification of a G+C-Rich DNA Using Genetically-Engineered DNA-Polymerases. *Gene,* 140**,** 1-5.

WANG, Z. Y. & TOBIN, E. M. 1998. Constitutive expression of the CIRCADIAN CLOCK ASSOCIATED 1 (CCA1) gene disrupts circadian rhythms and suppresses its own expression. *Cell,* 93**,** 1207-17.

WATERHOUSE, A. M., PROCTER, J. B., MARTIN, D. M., CLAMP, M. & BARTON, G. J. 2009. Jalview Version 2--a multiple sequence alignment editor and analysis workbench. *Bioinformatics,* 25**,** 1189-91.

WEIGEL, D., ALVAREZ, J., SMYTH, D. R., YANOFSKY, M. F. & MEYEROWITZ, E. M. 1992. LEAFY controls floral meristem identity in Arabidopsis. *Cell,* 69**,** 843-59.

WEIGEL, D. & NILSSON, O. 1995. A developmental switch sufficient for flower initiation in diverse plants. *Nature,* 377**,** 495-500.

WIGGE, P. A., KIM, M. C., JAEGER, K. E., BUSCH, W., SCHMID, M., LOHMANN, J. U. & WEIGEL, D. 2005. Integration of spatial and temporal information during floral induction in Arabidopsis. *Science,* 309**,** 1056-9.

WINN, M. D., BALLARD, C. C., COWTAN, K. D., DODSON, E. J., EMSLEY, P., EVANS, P. R., KEEGAN, R. M., KRISSINEL, E. B., LESLIE, A. G., MCCOY, A., MCNICHOLAS, S. J., MURSHUDOV, G. N., PANNU, N. S., POTTERTON, E. A., POWELL, H. R., READ, R. J., VAGIN, A. & WILSON, K. S. 2011. Overview of the CCP4 suite and current developments. *Acta Crystallogr D Biol Crystallogr,* 67**,** 235-42.

WU, K., ROONEY, M. F. & FERL, R. J. 1997. The Arabidopsis 14-3-3 multigene family. *Plant Physiology,* 114**,** 1421-1431.

WU, S. & WOLGEMUTH, D. J. 1995. The distinct and developmentally regulated patterns of expression of members of the mouse Cdc25 gene family suggest differential functions during gametogenesis. *Developmental biology,* 170**,** 195-206.

XI, W., LIU, C., HOU, X. & YU, H. 2010. MOTHER OF FT AND TFL1 regulates seed germination through a negative feedback loop modulating ABA signaling in Arabidopsis. *Plant Cell,* 22**,** 1733-48.

XIAO, B., SMERDON, S. J., JONES, D. H., DODSON, G. G., SONEJI, Y., AITKEN, A. & GAMBLIN, S. J. 1995. Structure of a 14-3-3 protein and implications for coordination of multiple signalling pathways. *Nature,* 376**,** 188-91.

XUE, W., XING, Y., WENG, X., ZHAO, Y., TANG, W., WANG, L., ZHOU, H., YU, S., XU, C., LI, X. & ZHANG, Q. 2008. Natural variation in Ghd7 is an important regulator of heading date and yield potential in rice. *Nature genetics,* 40**,** 761-7.

YAFFE, M. B., RITTINGER, K., VOLINIA, S., CARON, P. R., AITKEN, A., LEFFERS, H., GAMBLIN, S. J., SMERDON, S. J. & CANTLEY, L. C. 1997. The structural basis for 14-3-3:phosphopeptide binding specificity. *Cell,* 91**,** 961-71.

YAMAGUCHI, A., KOBAYASHI, Y., GOTO, K., ABE, M. & ARAKI, T. 2005. TWIN SISTER OF FT (TSF) acts as a floral pathway integrator redundantly with FT. *Plant and Cell Physiology,* 46**,** 1175-1189.

YAMAGUCHI, A., WU, M. F., YANG, L., WU, G., POETHIG, R. S. & WAGNER, D. 2009. The microRNA-regulated SBP-Box transcription factor SPL3 is a direct upstream activator of LEAFY, FRUITFULL, and APETALA1. *Developmental cell,* 17**,** 268-78.

YAN, J., HE, C., WANG, J., MAO, Z., HOLADAY, S. A., ALLEN, R. D. & ZHANG, H. 2004. Overexpression of the Arabidopsis 14-3-3 protein GF14 lambda in cotton leads to a "stay-green" phenotype and improves stress tolerance under moderate drought conditions. *Plant & cell physiology,* 45**,** 1007-14.

YANG, X., LEE, W. H., SOBOTT, F., PAPAGRIGORIOU, E., ROBINSON, C. V., GROSSMANN, J. G., SUNDSTROM, M., DOYLE, D. A. & ELKINS, J. M. 2006. Structural basis for protein-protein interactions in the 14-3-3 protein family. *Proc Natl Acad Sci U S A,* 103**,** 17237-42.

YOO, S. C., CHEN, C., ROJAS, M., DAIMON, Y., HAM, B. K., ARAKI, T. & LUCAS, W. J. 2013. Phloem long-distance delivery of FLOWERING LOCUS T (FT) to the apex. *Plant J*.

YOO, S. J., CHUNG, K. S., JUNG, S. H., YOO, S. Y., LEE, J. S. & AHN, J. H. 2010. BROTHER OF FT AND TFL1 (BFT) has TFL1-like activity and functions redundantly with TFL1 in inflorescence meristem development in Arabidopsis. *Plant J,* 63**,** 241-53.

YOO, S. K., CHUNG, K. S., KIM, J., LEE, J. H., HONG, S. M., YOO, S. J., YOO, S. Y., LEE, J. S. & AHN, J. H. 2005. CONSTANS Activates SUPPRESSOR OF OVEREXPRESSION OF CONSTANS 1 through FLOWERING LOCUS T to Promote Flowering in Arabidopsis. *Plant Physiol.,* 139**,** 770-778.

YOO, S. Y., KARDAILSKY, I., LEE, J. S., WEIGEL, D. & AHN, J. H. 2004. Acceleration of flowering by overexpression of MFT (MOTHER OF FT AND TFL1). *Mol Cells,* 17**,** 95-101.

ZARTLER, E. R. & SHAPIRO, M. J. 2005. Fragonomics: fragment-based drug discovery. *Curr Opin Chem Biol,* 9**,** 366-70.

ZHA, J., HARADA, H., YANG, E., JOCKEL, J. & KORSMEYER, S. J. 1996. Serine phosphorylation of death agonist BAD in response to survival factor results in binding to 14-3-3 not BCL-X(L). *Cell,* 87**,** 619-28.

ZHAO, J., DU, Y., HORTON, J. R., UPADHYAY, A. K., LOU, B., BAI, Y., ZHANG, X., DU, L., LI, M., WANG, B., ZHANG, L., BARBIERI, J. T., KHURI, F. R., CHENG, X. & FU, H. 2011. Discovery and structural characterization of a small molecule 14-3-3 protein-protein interaction inhibitor. *Proc Natl Acad Sci U S A,* 108**,** 16212-6.

Appendix Table 1.1 : Primer Sequence – Pseudo-Restriction Sites and Restriction Sites Underlined

Primer Name	Sequence	Notes
FTSHF	**TGTCTATAAATATAAGAGACCCTCTTATAGTAAGCAGAGTTG**	**Pseudo-*Nde1***
FTLOF	**TATGTCTATAAATATAAGAGACCCTCTTATAGTAAGCAGAGTTG**	**Pseudo-*Nde1***
FTSHR	**GCTAAAGTCTTCTTCCTCCGCAGCC**	**Pseudo-*Xho1***
FTLOR	**TGCAGCTAAAGTCTTCTTCCTCCGC**	**Pseudo-*Xho1***
FT_HINDIII_F	**GCT TAT AAG CTT ATG TCT ATA AAT ATA AGA GAC**	**HindIII Site**
FT_STOP_SACI_R	**ATA AGC CTC GAG AAG TCT TCT TCC TCC GCA GCC**	**SacI Site**
FT_NOSTOP_SACI_R	**ATA AGC GAG CTC ACT CTC CCT CTG ACA ATT GTA G**	**SacI Site**
TFLSHF	**TGGAGAATATGGGAACTAGAGTGATAGAGCC**	**Pseudo-*Nde1***
TFLLOF	**TATGGAGAATATGGGAACTAGAGTGATAGAGCC**	**Pseudo-*Nde1***
TFLSHR	**GCTAGCGTTTGCGTGCAGC**	**Pseudo-*Xho1***
TFLLOR	**TGCAGCTAGCGTTTGCGTGCAG**	**Pseudo-*Xho1***
TFL1_ HINDIII_F	**GCT TAT AAG CTT ATG GAG AAT ATG GGA ACT AGA**	**HindIII Site**
TFL1_REV_STOP0_SACI_R	**ATA AGC CTC GAG GCG TTT GCG TGC AGC**	**SacI Site**
TFL1_REV_NOSTOP_SACI_R	**ATA AGC GAG CTC GCG TTT GCG TGC AGC**	**SacI Site**
FDSHF	**TGTTGTCATCAGCTAAGCATCAGAGAAACC**	**Pseudo-*Nde1***
FDLOF	**TATGTTGTCATCAGCTAAGCATCAGAGAAAC**	**Pseudo-*Nde1***
FDLOR	**TGCAGTCAAAATGGAGCTGTGGAAGAC**	**Pseudo-*Xho1***
FDSHR	**GTCAAAATGGAGCTGTGGAAGACC**	**Pseudo-*Xho1***
FD209SHF	**TGAATGAAGGTTCAGGGAATAGAAGACATAAG**	**Pseudo-*Nde1***
FD209LOF	**TATGAATGAAGGTTCAGGGAATAGAAGACATAAG**	**Pseudo-*Nde1***
FD209_GLU_ECO1_F	**GCT ATA GAA TTC AAT GAA GGT TCA GGG AAT AGA AGA CAT AAG**	**ExoR1 Site**
FD209_GLU_XHO1_REV	**GCT ATA CTC GAG TCA AAA TGG AGC TTC GGA AGA C**	**Xho1 Site**
FD209_ASP_XHO1_REV	**GCT ATA CTC GAG TCA AAA TGG AGC ATC GGA AGA CC**	**Xho1 Site**
UB_F	**A GAT ATA CAT ATG CAG ATC TTC GTC AAG ACG**	**Nde1 Site**
UB_R	**AGA AAG CTT TCAA CCA CCT CTT AGT CTT AAG AC**	**HindIII Site**
14_3_3_NU_BAMH1_F	**GCT TAT GGA TCC ATG TCG TCT TCT CGG GAA G**	**BamHI Site**
14_3_3_NU_CLEAVESITE_BAMH1_F	**GCT TAT GGA TCC GAA GTT CTG TTC CAG GGG CCC CTG ATG TCG TCT TCT CGG GAA G**	**BamHI Site + Prescission protease site**
14_3_3_NU_HINDIII_R	**GCT TAT AAG CTT TCA CTG CCC TGT CTC AGC TGG**	**HindIII Site**
2XHIS_1433_NU_F	**AGT CAT CAC CAC CAC CAT CAC ATG TCG TCT TCT CGG GAA G**	**HIS TAG**

FT_BvFT_N_F	GGC AGG CAA ACA GTG AAC GCA CCA GGG TGG CGC CAG AAC TTC AAC ACT CGC G	SDM Primer
FT_BvFT_N_R	GTT GAA GTT CTG GCG CCA CCC TGG TGC GTT CAC TGT TTG CCT GCC AAG C	SDM Primer
FT_BvFT_NQ_F	GGCAGGCAAACAGTGAACGCACCACAGTGGCGCCAGAACTTCAACAC TCGCG	SDM Primer
FT_BvFT_NQ_R	GTTGAAGTTCTGGCGCCACTGTGGTGCGTTCACTGTTTGCCTGCCAAG C	SDM Primer
FT_BvFT_NQQ_F	GGCAGGCAAACAGTGAACGCACCACAGCAGCGCCAGAACTTCAACAC TCGCG	SDM Primer
FT_BvFT_NQQ_R	GTT GAA GTT CTG GCG CTG CTG TGG TGC GTT CAC TGT TTG CCT GCC AAG C	SDM Primer
FT_TFL1_F_F	GG CAG GCA AAC AGT GTT TGC ACC AGG GTG GCG CCA GAA CTT CAA CAC TCG CG	SDM Primer
FT_TFL1_F_R	GTT GAA GT TCT GGC GCC ACC CTG GTG CAA ACA CTG TTT GCC TGC CAA GC	SDM Primer
FT_TFL1_FP_F	GGC AGG CAA ACA GTG TTT GCA CCA CCG TGG CGC CAG AAC TTC AAC ACT CGC G	SDM Primer
FT_TFL1_FP_R	GTT GAA GTT CTG GCG CCA CGG TGG TGC AAA CAC TGT TTG CCT GCC AAG C	SDM Primer
FT_TFL1_FPS_F	GG CAG GCA AAC AGT GTT TGCA CCA CCG AGC CGC CAG AAC TTC AAC ACT CGC G	SDM Primer
FT_TFL1_FPS_R	GTT GAA GTT CTG GCG GCT CGG TGG TGC AAA CAC TGT TTG CCT GCC AAG C	SDM Primer
TFL1_AA_F	GGCAGAAGCAAGCAGCTGTTATCTTTCCTAATATCC	SDM Primer
TFL1_AA_R	GGAAAGATAACAGCTGCTTGCTTCTGCCTG	SDM Primer
TFL1_AR_F	GGC AGA AGC AAG CAC GTG TTA TCT TTC CTA ATA TCC	SDM Primer
TFL1_AR_R	GGA AAG ATA ACA CGT GCT TGC TTC TGC CTG AAC	SDM Primer
TFL1_RA_F	GGC AGA AGC AAA GAG CTG TTA TCT TTC CTA ATA TCC	SDM Primer
TFL1_RA_R	GGA AAG ATA ACA GCT CTT TGC TTC TGC CTG AAC	SDM Primer
TFL1_RQ_F	GGC AGA AGC AAA GAC AGG TTA TCT TTC CTA ATA TCC	SDM Primer
TFL1_RQ_R	GGA AAG ATA ACC TGT CTT TGC TTC TGC CTG AAC	SDM Primer
TFL1_TV_F	GGC AGA AGC AAA GAC GTA CTG TCT TTC CTA ATA TCC	SDM Primer
TFL1_TV_R	GGA AAG ACA GTA CGT CTT TGC TTC TGC CTG AAC	SDM Primer
TFL1_G_F	CTA TGA ATT GCC AAG GGC AAG CAT AGG GAT ACA TAG GTT TG	SDM Primer
TFL1_G_R	CCT ATG TAT CCC TAT GCT TGC CCT TGG CAA TTC ATA GCT C	SDM Primer
TFL1_GW_F	CTA TGA ATT GCC AAG GGC ATG GAT AGG GAT ACA TAG GTT TG	SDM Primer
TFL1_GW_R	CCT ATG TATCC CTA TCC ATG CCC TTG GCA ATT CAT AG	SDM Primer

TFL1_LG_F	CTG TTC AGG CAG CTG GGA AGA CGT GTT ATC TTT CC	SDM Primer
TFL1_LG_R	GGA TAT TAG GAA AGA TAA CAC GTC TTC CCA GCT GCC TGA AC	SDM Primer
TFL1_Y_F	CTCTCGAAGGGATATTAGGATAGATAACACGTCTTTGC	SDM Primer
TFL1_Y_R	CTTTCCTAATATCGGTTGGAGAGATCACTTC	SDM Primer
TFL1_YA_F	GCA AAG ACG TGT TAT CTA TGC TAA TAT CCC TTC G	SDM Primer
TFL1_YA_R	CTC TCG AAG GGA TAT TAG CAT AGA TAA CAC GTC TTT GC	SDM Primer
TFL1_WT_Y_REMOVAL_F	GCA AAG ACG TGT TAT CTT TCC TAA TAT CCC TAA TAT CGG	SDM Primer
TFL1_WT_Y_REMOVAL_R	GGA TAT TAG GAA AGA TAA CAC GTC TTT GCT TCT GC	SDM Primer
TFL1_Q_F	CCT AAT ATC CCT TCG AGA CAG CAC TTC AAC ACT CG	SDM Primer
TFL1_Q_R	GCA AAT TTA CGA GTG TTG AAG TGC TGT CTC GAA GGG ATA TTA G	SDM Primer
TFL1_DELTA_N_F	GG CAG AAG CAA AGA CGT GTT ATC TTT CCT ATC CCT TCG AGA GAT CAC	SDM Primer
TFL1_DELTA_N_R	CGA AGG GAT AGG AAA GAT AAC ACG TCT TTG CTT CTG CCT GAA CAG	SDM Primer
TFL1_-P_F	GG CAG AAG CAA AGA CGT GTT ATC TTT CCT CCC CCT TCG AGA GAT CAC	SDM Primer
TFL1_-P_R	CGA AGG GGG AGG AAA GAT AAC ACG TCT TTG CTT CTG CCT GAA CAG	SDM Primer
TFL1_RET_STOP_F	C GCA CAA AGA GAA ACC TAG GCA CGC AAA CGC TAG	SDM Primer
TFL1_RET_STOP_R	CG TTT GCG TGC CTA GGT TTC TCT TTG TGC GTT AAA G	SDM Primer
TFL1_G105N_F	GGC ACA ACA GAT GCT ACG TTT GAC AAA GAG GTG GTG AGC	SDM Primer
TFL1_G105N_R	CAC CAC CTC TTT GTC AAA CGT AGC ATC TGT TGT GCC GGG	SDM Primer
TFL1_R7N_F	G AAT ATG GGA ACT AAT GTG ATA GAG CCA TTG	SDM Primer
TFL1_R7N_R	GGC TCT ATC AC ATT AGT TCC CAT ATT CTC C	SDM Primer
AP1_359_F	GCT TAT CAT ATG AAT TAG GAA AGT TTT TCT TTC TTT CC	SDM Primer
AP1_359_R	ATA AGC CTC GAG TAC AGG GAA ATC TCC GCC G	SDM Primer
GFP-FT_F	ACA CAT GGC ATG GAT GAA CTA TAC AAA ATG TCT ATA AAT ATA AG AGA CCC TCT TAT AGT AAG C	-
GFP_TEV_FT_F	CA CAT GGC ATG GAT GAA CTA TAC AAA GAA AAC CTG TAT TTT CAG GGC ATG TCT ATA AAT ATA AG AGA CCC TCT TAT AGT AAG C	-
FT_R9_R	GGG AGA GTG GCT GCG GAG GAA GAA GAC TTC GGA GAC GTC GCA GGC GTA GAC GGC GGT AAT GA	-
GFP_F	ATG CGT AAA GGA GAA GAA CTT TTC ACT GGA GTT GTC CCA ATT CTT G	-
T7	TAA TAC GAC TCA CTA TAG GG	Sequencing

T7 term	**CTA GTT ATT GCT CAG CGG T**	**Sequencing**
FD_DETECTOR_FOR	**ATC AAG CTT ATG TTG TCA TCA GCT AAG C**	**-**
FD_DETECTOR_REV	**TAC AGA TCT TTC GAA TCA AAA TGG AGC TGT GGA AGA CC**	**AP1 OVERLAP**
AP1_DETECTOR_PRO_FOR	**TTC GAA AGA TCT GTA CTG AAA GAG AGT AAA AAG GG**	**FD OVERLAP**
AP1_DETECTOR_PRO_Rev	**CCT ACC CCT TCC CAT TTT TGA TCC**	**-**
REPORT_GLU _QC_F	**CAC ACT TCA ACG GTC TTC CGA AGC TCC ATT TTG ATT CG**	**SDM Primer**
REPORT_GLU _QC_F	**CTT TCG AAT CAA AAT GGA GCT TCG GAA GAC CGT TGA AGT G**	**SDM Primer**
PGBW5_F	**CCCAGCTTTCTTGTACAAAGTGG**	**Analytical**
NTERM_GFP_F	**CGGCATGGACGAGCTGTAC**	**Analytical**
C_TERM_GFP_R	**CCCCGGTGAACAGCTCCTCGCCC**	**Analytical**

pET-28a-c(+) Vectors

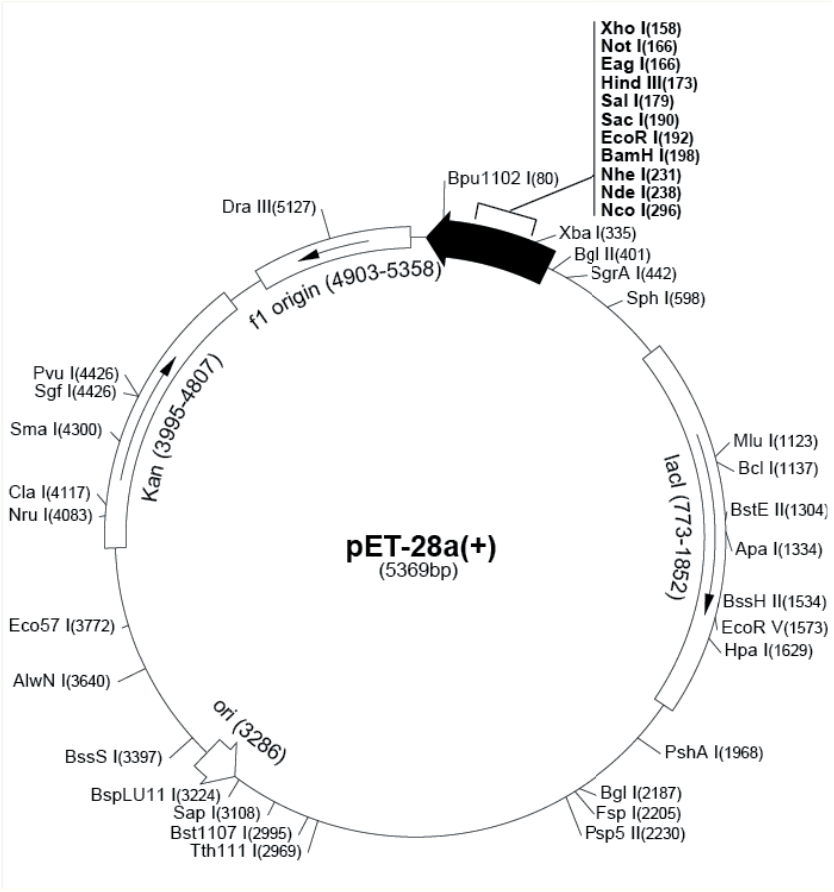
TB074 12/98

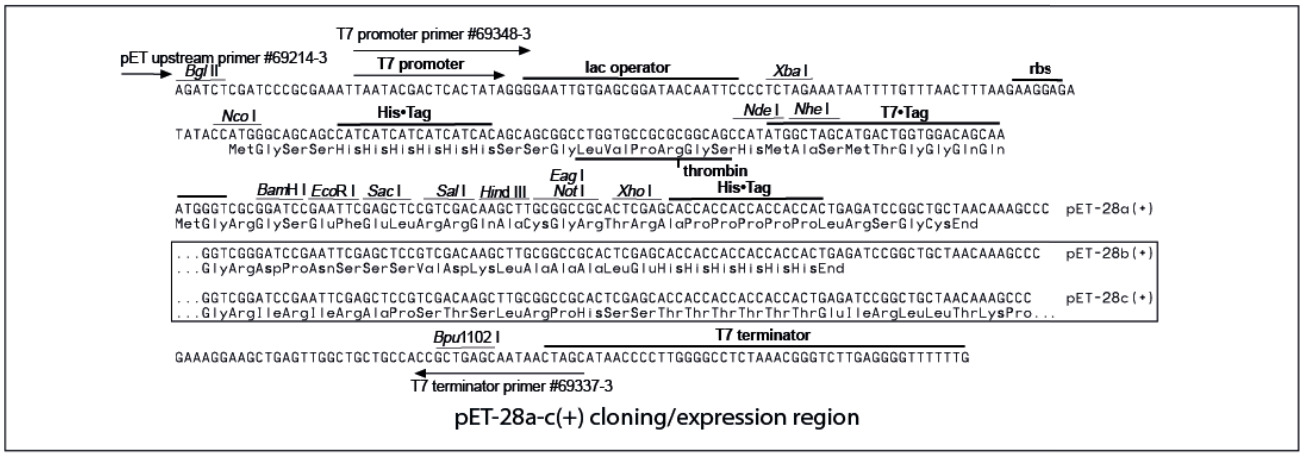
	Cat. No.
pET-28a DNA	69864-3
pET-28b DNA	69865-3
pET-28c DNA	69866-3

The pET-28a-c(+) vectors carry an N-terminal His•Tag * /thrombin/T7•Tag * configuration plus an optional C-terminal His•Tag sequence. Unique sites are shown on the circle map. Note that the sequence is numbered by the pBR322 convention, so the T7 expression region is reversed on the circular map. The cloning/expression region of the coding strand transcribed by T7 RNA polymerase is shown below. The f1 origin is oriented so that infection with helper phage will produce virions containing single-stranded DNA that corresponds to the coding strand. Therefore, single-stranded sequencing should be performed using the T7 terminator primer (Cat. No. 69337-3).

pET-28a(+) sequence landmarks	
T7 promoter	370-386
T7 transcription start	369
His•Tag coding sequence	270-287
T7•Tag coding sequence	207-239
Multiple cloning sites	
(Bam H I - Xho I)	158-203
His•Tag coding sequence	140-157
T7 terminator	26-72
lacI coding sequence	773-1852
pBR322 origin	3286
Kan coding sequence	3995-4807
f1 origin	4903-5358

The maps for pET-28b(+) and pET-28c(+) are the same as pET-28a(+) (shown) with the following exceptions: pET-28b(+) is a 5368bp plasmid; subtract 1bp from each site beyond Bam H I at 198. pET-28c(+) is a 5367bp plasmid; subtract 2bp from each site beyond Bam H I at 198.





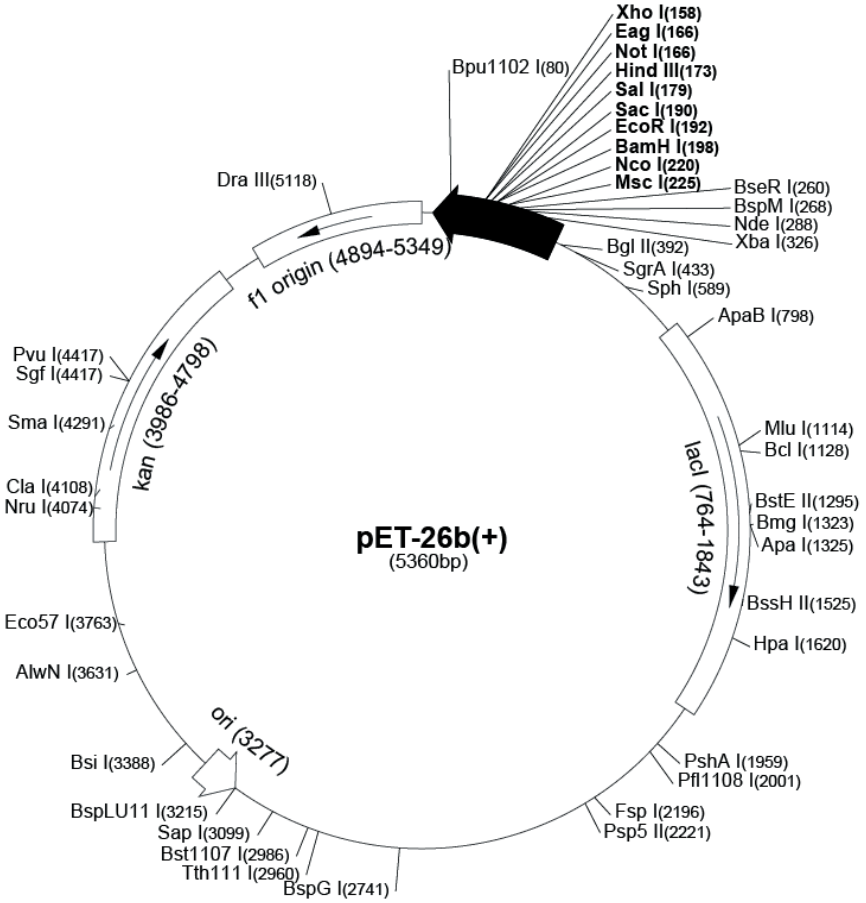
Appendix 2.1: Vector map for pET28 used for protein expression in this study. Multiple cloning suite boxed.

pET-26b(+) Vector

TB071 12/98

The pET-26b(+) vector (Cat. No. 69862-3) carries an N-terminal pelB signal sequence for potential periplasmic localization, plus optional C-terminal His•Tag * sequence. Unique sites are shown on the circle map. Note that the sequence is numbered by the pBR322 convention, so the T7 expression region is reversed on the circular map. The cloning/expression region of the coding strand transcribed by T7 RNA polymerase is shown below. The f1 origin is oriented so that infection with helper phage will produce virions containing single-stranded DNA that corresponds to the coding strand. Therefore, single-stranded sequencing should be performed using the T7 terminator primer (Cat. No. 69337-3).

pET-26b(+) sequence landmarks	
T7 promoter	361-377
T7 transcription start	360
pelB coding sequence	224-289
Multiple cloning sites	
(Nco I - Xho I)	158-225
His•Tag coding sequence	140-157
T7 terminator	26-72
lacI coding sequence	764-1843
pBR322 origin	3277
Kan coding sequence	3986-4798
f1 origin	4894-5349





pET-26b(+) cloning/expression region

Appendix 2.2: Vector map for pET26 used for protein expression in this study. Multiple cloning suite boxed.

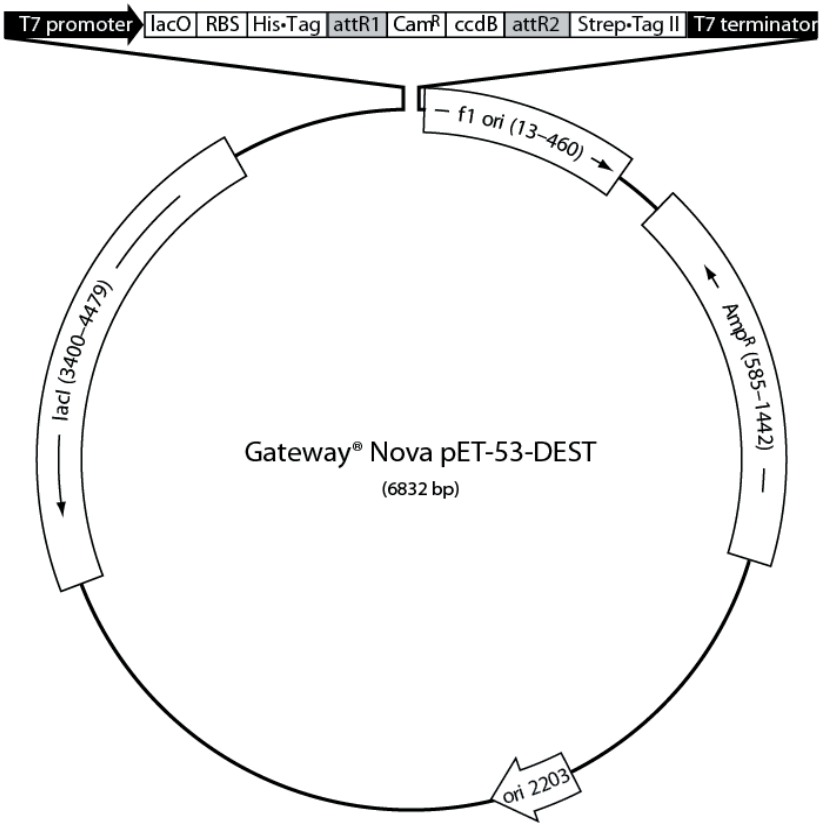
pET-53-DEST Vector

	Cat No.
Gateway® Nova pET-53-DEST™ DNA	71844-3

Feature	Location
f1 origin	13-460
Amp^R	585-1442
pBR322 ori	2203
lacI coding sequence	3400-4479
T7 promoter	4870-4886
T7 transcription start	4887
His•Tag® coding sequence	4963-4980
attR1	4984-5108
Cam^R	5217-5873
ccdB	6218-6520
attR2	6564-6688
Strep•Tag® II coding sequence	6696-6719
T7 terminator	6760-6807

The Gateway® Nova pET-53-DEST™ vector is designed to create expression clones (pEXPR) that are fused to an N-terminal His•Tag® coding sequence. If the pENTR clone lacks a stop codon and is appropriately designed for a C-terminal fusion, the target gene in the resulting pEXPR clone will also be fused to a C-terminal Strep•Tag® II coding sequence (Skerra 2000). The presence of "gentle elution" tags at both the N- and C-termini is ideal for dual purification strategies designed to isolate full-length fusion proteins (Fiedler 2002).

Fiedler, M. et al. 2002.Protein Eng.15, 931.
Skerra, A. and Schmidt, T.G.M. 2000Meth. Enzymol326, 271.



USA and Canada
Tel (800) 526-7319
novatech@novagen.com

Europe
France Freephone 0800 126 461
Germany Freecall 0800 100 3496
Ireland Toll Free 1800 409 445
United Kingdom Freephone 0800 622 935
All other European Countries +44 115 943 0840
techservice@merckbio.eu

All Other Countries
Contact Your Local Distributor
www.novagen.com
novatech@novagen.com

www.novagen.com
FOR RESEARCH USE ONLY. NOT FOR HUMAN OR DIAGNOSTIC USE .

Appendix 2.3: Vector map for pET53 used for protein expression in this study. Multiple cloning site highlighted.

GE Healthcare

pGEX Vectors, GST Gene Fusion System

Map of the glutathione S-transferase fusion vectors showing the reading frames and main features. Even though stop codons in all three frames are not depicted in this map, all thirteen vectors have stop codons in all three frames downstream from the multiple cloning site.

Do you want to learn more? Read the GST Gene Fusion System Handbook (18-1157-58). Please contact your local GE Healthcare representative for a printed copy.



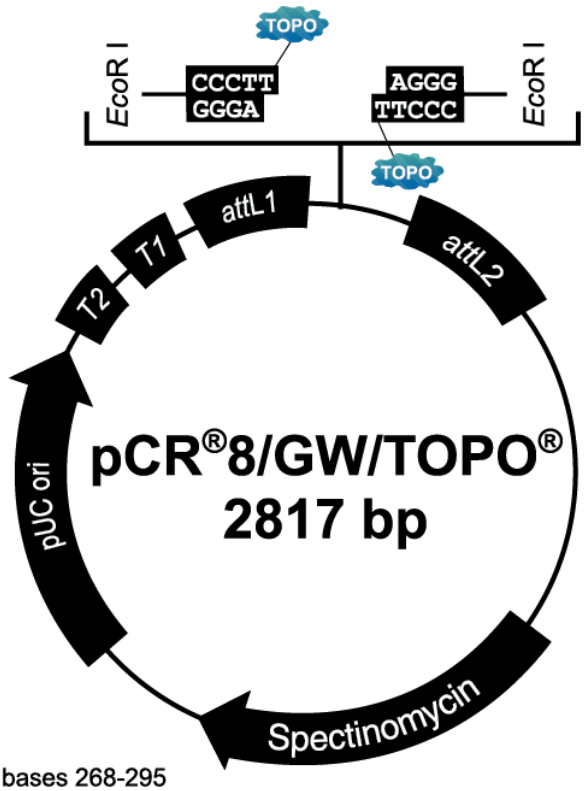
imagination at work

Appendix 2.4: Vector map for pGEX vectors including pGEX-6P-1 used for protein expression in this study. Multiple cloning site shown.

Map and Features of pCR®8/GW/TOPO®

pCR®8/GW/TOPO® Map

The figure below shows the features of the pCR ®8/GW/TOPO ® vector. The complete sequence of pCR ®8/GW/TOPO ® is available for downloading from our Web site (www.invitrogen.com) or by contacting Technical Service (see page 27).



Comments for pCR®8/GW/TOPO®
2817 nucleotides

*rrn*B T2 transcription termination sequence: bases 268-295
*rrn*B T1 transcription termination sequence: bases 427-470
M13 forward (-20) priming site: bases 537-552
*att*L1: bases 569-668
GW1 priming site: bases 607-631
TOPO® recognition site 1: bases 678-682
TOPO® recognition site 2: bases 683-687
*att*L2: bases 696-795
GW2 priming site: bases 733-757
T7 Promoter/priming site: 812-831 (c)
M13 reverse priming site: bases 836-852
Spectinomycin promoter: bases 930-1063
Spectinomycin resistance gene (Spn^R): 1064-2074
pUC origin: bases 2141-2814

(c) = complementary sequence

Appendix 2.5: Vector map for pCR8 used for cloning in this study. Multiple cloning suite highlighted.

pGWB5 : [(35S promoter, C-sGFP) (--35Spromoter–R1-ccdB-R2–sGFP--)]

(AAGCTT) -- 35S promoter --//

(TCT AA)T CAA ACA AGT TTG TAC AAA AAA --(CmR, ccdB)–TTC TTG TAC AAA GTG GTT CGA TCT AGA GGA TCC ATG --(*GFP* sequence) --(GAGCTC)

(1) The initiation codon ATG (double-underlined) is from the GFP coding sequence.

After LR reaction, the following sequence will be obtained.

35S promoter –(TCT AA)T CAA ACA AGT TTG TAC AAA AAA GCA GGC TNN (*Your Clone*) NAC CCA GCT TTC TTG TAC AAA GTG GTT CGA TCT AGA GGA TCC ATG --

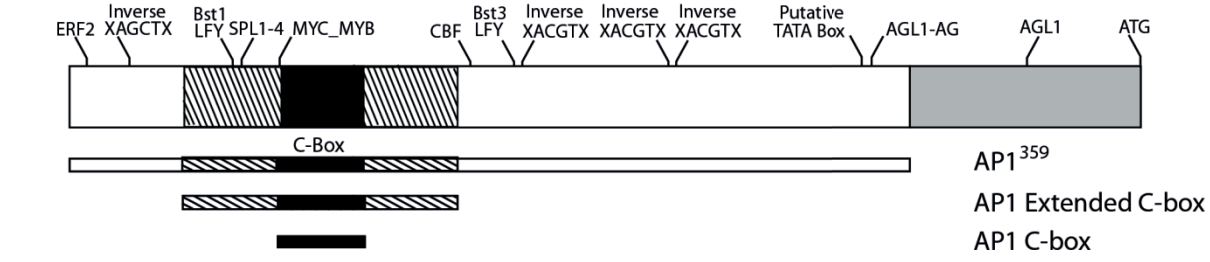
-X- -P- -A- -F- -L- -Y- -K- -V- -V- -R- -S- -R- -G- -S- -M-

(*GFP sequence*) -- (GAGCTC)

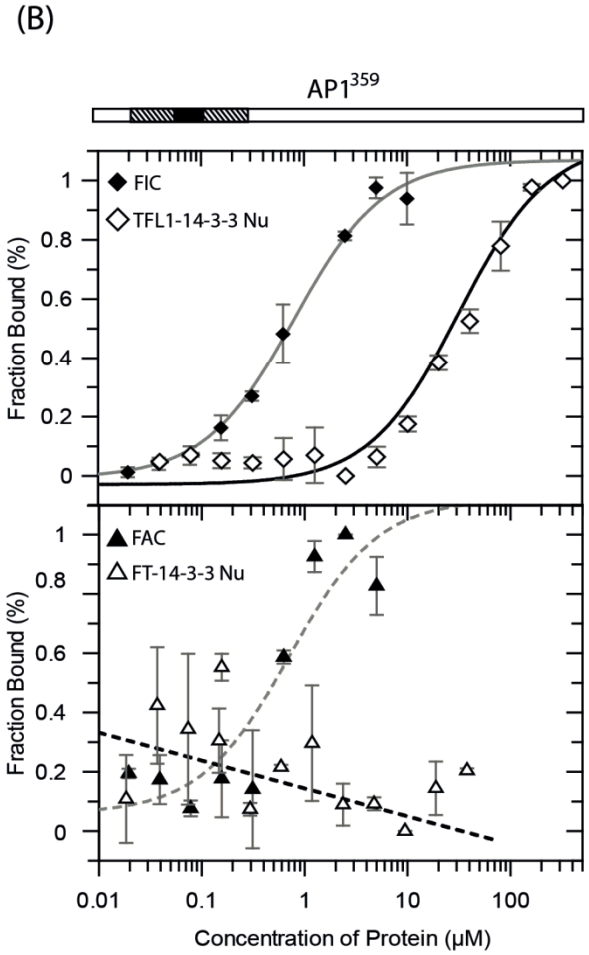
(1) Include an initiation codon ATG in Your Clone. Protein fusion with the C-terminal GFP will be linked by the peptide sequence derived from the attB2 and linker region as shown in the above sequence.
(2) N indicates the nucleotide (and X the amino acid) that is needed to be included in Your Clone.
(3) The DNA sequence downstream of GFP is the same ase in pGWB4.
(4) Hyphenations flanking the amino acid residues are used for proper spacing.

Appendix 2.6: Vector details for pGWB5 used for *in vivo* expression in this study. Multiple cloning suite highlighted.

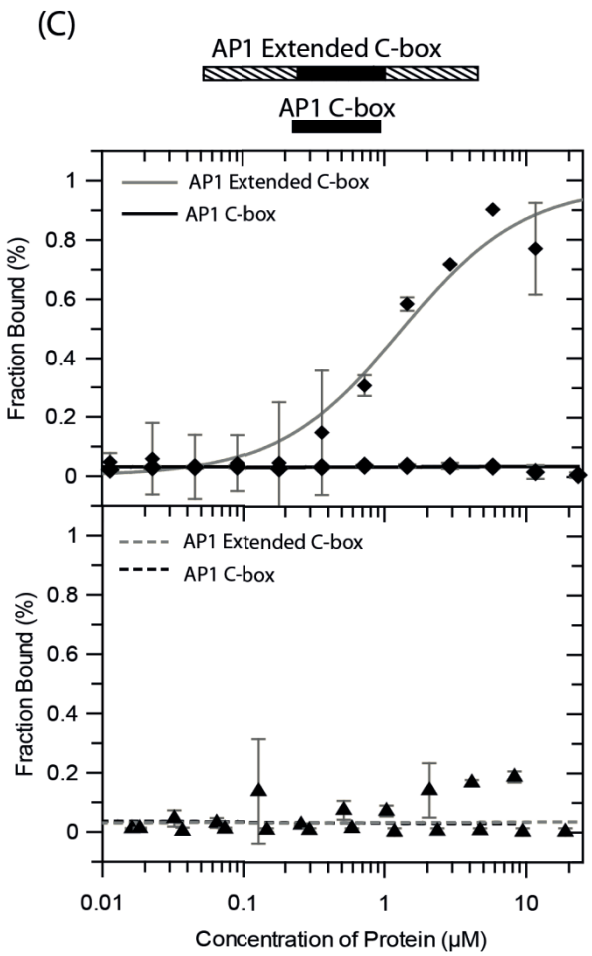
(A)



(B)



(C)



(D)

	FIC	FAC	TFL1-14-3-3 Nu	FT-14-3-3 Nu	14-3-3 Nu-FD$^{209\ T282E}$
AP1^{359}	Binding	Binding	Binding	NBD	Binding
Extended C-box	Binding	NBD	N/A	N/A	NBD
C-box	NBD	NBD	N/A	N/A	NBD
Ubiquitin	NBD	NBD	NBD	NBD	N/A

Appendix 3.1: Interaction between components of FAC and FIC and elements of the AP1 promoter. Interaction as measured by using microscale thermophoresis. **(A)** AP1 promoter region showing C-box and extended C-box. **(B)** FD$^{209\ T282E}$ was titrated against a fluorescently labelled 359 bp section of the AP1 promoter containing the C-box region and a short fluorescently labelled 22 bp section representing the C-box. The fraction bound was plotted against the concentration FD$^{209\ T282E}$. **(C)** Tabulated summary of the results.